

# **Fatigue Assessment of Large-Size Bolting Assemblies for Wind Turbine Support Structures**

- Ermüdungsbewertung  
sehr großer Schraubenverbindungen  
für Tragstrukturen von Windenergieanlagen -

Von der Fakultät für Bauingenieurwesen und Geodäsie  
der Gottfried Wilhelm Leibniz Universität Hannover  
zur Erlangung des Grades

Doktor der Ingenieurwissenschaften

- Dr.-Ing -

genehmigte Dissertation  
von

Dipl.-Ing. Rasmus Eichstädt  
geboren am 26. November 1984 in Bad Oldesloe

2019

### **Promotionskommission**

Referent:	Prof. Dr.-Ing. Peter Schaumann
Korreferentin:	Prof. Dr.-Ing. habil. Natalie Stranghöner
Kommissionsmitglied:	Prof. Dr.-Ing. Ludger Lohaus
Vorsitzender:	Prof. Dr.-Ing. Martin Achmus
Tag der Promotion:	28.06.2019

---

## Vorwort

Die vorliegende Arbeit entstand im Rahmen meiner Tätigkeit als wissenschaftlicher Mitarbeiter am Institut für Stahlbau der Gottfried Wilhelm Leibniz Universität Hannover. Mein herzlicher Dank gilt Herrn Professor Dr.-Ing. Peter Schaumann, der mich bei der Anfertigung dieser Arbeit betreut und die Erstberichterstattung übernommen hat. Die von ihm gegebenen fachlichen Impulse und bereitgestellten wissenschaftlichen Rahmenbedingungen sowie das entgegengebrachte Vertrauen haben wesentlich zum Gelingen meiner Promotion beigetragen. Frau Professorin Dr.-Ing. habil. Natalie Stranghöner danke ich sehr herzlich für die Übernahme des Korreferates. Ebenfalls herzlich bedanken möchte ich mich bei den Herren Professor Dr.-Ing. Ludger Lohaus und Professor Dr.-Ing. Martin Achmus für ihr Mitwirken in der Prüfungskommission am Tag der Promotion.

Die wesentliche Grundlage für die in dieser Dissertation dargelegte wissenschaftliche Arbeit bildete das Forschungsprojekt „Experimentelle und rechnerische Bewertung der Betriebsfestigkeit von Schrauben großer Abmessung im Stahlbau unter Berücksichtigung von Randschichteinflüssen“. Das IGF-Vorhaben 486 ZN / P925 der FOSTA - Forschungsvereinigung Stahlanwendung e.V. wurde über die AiF (Arbeitsgemeinschaft industrieller Forschungsvereinigungen „Otto von Guericke“) im Rahmen des Programms zur Förderung der industriellen Gemeinschaftsforschung (IGF) durch das Bundesministerium für Wirtschaft und Energie aufgrund eines Beschlusses des Deutschen Bundestages gefördert. Den vorgenannten Einrichtungen sei für die Betreuung und finanzielle Förderung des Vorhabens herzlich gedankt. Weiterhin bedanke ich mich bei den beteiligten Industriepartnern des projektbegleitenden Ausschusses sowie den Forschungspartnern am Zentrum für Konstruktionswerkstoffe der Technischen Universität Darmstadt, insbesondere Herrn Dr.-Ing. Fabian Simonsen, für die konstruktive Zusammenarbeit. Mein aufrichtiger Dank gilt in diesem Zusammenhang auch meiner ehemaligen Kollegin am Institut für Stahlbau Frau Professorin Dr.-Ing. Stefanie Steppeler, die in federführender Weise bei der erfolgreichen Initiierung des Forschungsprojektes mitgewirkt hat, als ich selber noch die Vorlesungen besuchte.

Einen weiteren ganz besonderen Dank richte ich an Karl-Heinz Hentschel, Christian Fricke, Dietmar Joseph und Katrin Lucher, dem technischen Personal zu meiner Zeit am Institut für Stahlbau. Ohne ihre Unterstützung wäre die Durchführung der umfangreichen Versuchsserien, dem wesentlichen Kernstück dieser Arbeit, nicht möglich gewesen. Ebenfalls bedanken möchte ich mich bei Andrea Hildebrand, Kerstin Elsmeier und Dr.-Ing. Nadja Oneschkow vom Institut für Baustoffkunde für die freundliche, kollegiale Zusammenarbeit bei der Nutzung „ihrer“ Großprüfmaschine. Herrn Dr.-Ing. Mark Alan Swider vom Institut für Werkstoffkunde danke ich für die nette Zusammenarbeit bei der Durchführung der zusätzlichen Werkstoffversuche.

Während meiner Zeit am Institut habe ich eine Reihe studentischer Arbeiten betreut, die in direktem oder indirektem Zusammenhang mit dieser Dissertation standen. Besonders erwähnen möchte ich an dieser Stelle die Herren Gerrit Gottlieb und Leon Wilms sowie die Damen Hebi Abe und Nathalie Kielbus. Ebenfalls herzlich bedanken möchte ich mich bei Franziska Müller und Christoph Kowalczyk für ihre sorgfältige Arbeit als studentische Hilfskräfte.

---

Zu großem Dank verpflichtet bin ich Herrn Dr.-Ing. Frithjof Marten für seine am Institut für Stahlbau geleisteten Vorarbeiten auf dem Gebiet der Schraubenforschung und seine stets vorhandene Unterstützungsbereitschaft auch über fachrelevante Fragestellungen hinaus. Bei meinen beiden Institutskollegen und guten Freunden Andre Stang und Dr.-Ing. Alexander Raba bedanke ich mich herzlich für die vielen Stunden der intensiven Diskussionen in unterschiedlichsten Themenbereichen und nicht zuletzt auch für ihre überaus gewissenhafte und kritische Durchsicht meines Manuskriptes. Auch allen hier nicht namentlich genannten ehemaligen Kollegen am Institut sei herzlich gedankt für das angenehme, konstruktive Arbeitsklima und viele hilfreiche Anregungen.

Zur guter Letzt bedanke ich mich vielmals bei meiner Familie und meinen Freunden für die langjährige Unterstützung und allen voran bei Laura für ihren uneingeschränkten, liebevollen Rückhalt!

Rasmus Eichstädt

---

## Kurzfassung

Hochfeste Schraubengarnituren des Systems HV mit Durchmessern M36 und größer kommen bevorzugt in Ringflanschverbindungen von Tragstrukturen von Windenergieanlagen zum Einsatz. Insbesondere an unteren Turmsektionen wird bedingt durch die auftretenden Belastungen häufig die Verwendung sehr großer Durchmesser M64 oder M72 erforderlich. Die HV-Schrauben sind hohen zyklischen Lasten mit variablen Amplituden ausgesetzt. Zur Begrenzung von Ermüdungsbeanspruchung werden die Schrauben daher auf hohe Vorspannungsniveaus angezogen. Ein zuverlässiger Schutz gegen Korrosion wird in der Regel durch Feuerverzinken sichergestellt. Es ist bekannt, dass die dabei thermisch hergestellte Zinkoberfläche die zyklische Beanspruchbarkeit stählerner Bauteile beeinträchtigt. Zudem hat auch das durch die Vorspannung erzeugte hohe Mittelspannungsniveau einen Einfluss auf die Ermüdungseigenschaften der Schrauben.

Die Durchführung von Ermüdungsversuchen an großen HV-Garnituren, insbesondere unter repräsentativer Mittelspannung, ist mit hohen Anforderungen an die verwendete Prüfeinrichtung verbunden. Bemessungswöhlerlinien normativer Regelwerke, mit besonderer praktischer Relevanz der EN 1993-1-9, sind aus diesem Grund nur begrenzt für große Schraubendurchmesser validiert. Zudem ist der quantitative Einfluss der Feuerverzinkung auf die Ermüdungsfestigkeit hochfester großer Schrauben bislang nicht abschließend untersucht.

Ergänzend zu kostspieligen Ermüdungsversuchen können mit analytischen Methoden spezifische ermüdungsrelevante Einflussfaktoren isoliert bewertet werden. Allerdings sind hierzu geeignete Verfahren noch für die Anwendung auf große HV-Garnituren anzupassen und zu validieren. Außerdem bedarf es einer geeigneten Möglichkeit zur Berücksichtigung des Einflusses der Feuerverzinkung.

Diese Dissertation beinhaltet umfangreiche, systematische Untersuchungen zum Ermüdungsverhalten großer HV-Schraubengarnituren mit experimentellen und analytischen Methoden. Die durchgeführten Ermüdungsversuche erweitern die experimentelle Validierung normativer Regelwerke erstmalig bis zum Nenndurchmesser M64. Die Anwendbarkeit des relevanten Kerbfalls 50 aus dem Eurocode 3 kann dabei bestätigt werden. Der Vergleich der erzielten Versuchsergebnisse an feuerverzinkten HV-Garnituren mit Durchmessern M36 und M64 sowie weiterführende analytische Untersuchungen zeigen für diese Schraubengrößen einen geringen Einfluss des Durchmessers. Die im Eurocode 3 berücksichtigte durchmesserabhängige Reduzierung führt darum tendenziell zu einer Unterschätzung der Ermüdungsfestigkeit. Versuche mit variablen Amplituden deuten darüber hinaus darauf hin, dass die verwendete Hypothese zur Schädigungsakkumulation zu einer konservativen Bemessung führt. Bezüglich des Unterschieds der Ermüdungsfestigkeit bei unbeschichteten und feuerverzinkten Garnituren weisen die Versuche an M36 und M64 Schrauben uneinheitliche Ergebnisse auf, was eine mögliche Besserstellung schwarzer Schrauben in Frage stellt.

Das für die Anwendung auf große HV-Schrauben weiterentwickelte analytische Bewertungsverfahren der Ermüdungsfestigkeit liefert Ergebnisse in guter Näherung mit Versuchen unterschiedlicher Durchmesser und Lastverhältnisse. Ein vorgeschlagenes Ingenieurmodell ermöglicht dabei ebenfalls die Ermüdungsberechnung feuerverzinkter Schrauben.

---

## Executive Summary

High-strength 'System HV' bolting assemblies with large bolt diameters of M36 and bigger are frequently used in ring-flange connections in steel support structures for on- and offshore wind turbines. At the bottom parts of the supporting steel towers the magnitude of the acting loads usually requires the application of very large bolt diameters M64 or M72. The bolts are subjected to high cyclic loads with considerable numbers of load cycles and variable amplitudes. Thus, for reduction of fatigue loads, preloading of bolts with high forces is mandatory. Reliable protection against corrosion is commonly achieved by hot-dip galvanizing. It is known that the zinc coating has an impact on the fatigue strength of structural steel components. Moreover, the high mean stress level affects the bolts' fatigue behaviour and thus needs to be appropriately considered in experimental as well as analytical fatigue analyses.

Fatigue testing of HV-bolts with large diameters under a representative mean stress level imposes challenges to the required testing equipment. Hence, S-N curves in applicable design standards, in particular EN 1993-1-9, are mostly validated on tests with smaller bolts and the influence of an increased diameter is yet to be verified. Moreover, the quantitative effect of hot-dip galvanizing on the fatigue strength of large-size HV-bolts is still under investigation.

Analytical fatigue assessment procedures provide valuable potentials to supplement expensive experimental test series and to discretely investigate specific impact factors with relevance to the fatigue strength. However, to this end suitable assessment methodologies need to be adapted and validated for the application to HV-bolts with large diameters as well as for an appropriate consideration of the effect of hot-dip galvanizing.

This dissertation presents comprehensive research work on the experimental and analytical fatigue assessment of large-size HV-bolts. The performed fatigue tests extend the range of the experimental validation of normative regulations to a bolt diameter of M64, representative for the upper end of bolt sizes applied in today's modern wind turbine support structures. Thereby, the safe applicability of the relevant fatigue class FAT 50 of the Eurocode 3 is confirmed. The comparison of performed tests on hot-dip galvanized bolts of diameters M36 and M64, as well as further analytical analyses, indicate a minor impact of the bolt size in the considered large diameter range. The corresponding reduction function of the Eurocode 3 thus tends to overestimate the diameter related effect. Moreover, the results of tests with variable amplitude loading suggest a rather conservative hypothesis of damage accumulation, considered in the Eurocode. Regarding the discrepancy of fatigue strength between uncoated and hot-dip galvanized HV-bolts ambiguous results are obtained for bolt sizes M36 and M64. Thus, the results put into question a superior fatigue classification of uncoated, black large-size HV-bolts, as for instance suggested in the VDI Guideline 2230.

The systematically elaborated analytical fatigue assessment methodology, specifically refined for the application to large size HV-bolts, yields calculations in good agreement with experimental results for different bolt sizes and loading conditions. Thereby, an introduced engineering model also enables the calculation of the fatigue life for hot-dip galvanized bolts.

---

**Keywords**

HV-bolt sets, fatigue, strain-life concept, wind turbines, hot-dip galvanizing

**Schlagwörter**

HV-Schraubengarnituren, Ermüdung, Kerbdehnungskonzept, Windenergieanlagen, Feuerverzinkung

**Acknowledgements**

Large parts of the investigations presented in this dissertation were performed within the framework of the research project “Experimental and analytical assessment of the fatigue strength of bolts with large dimensions under consideration of boundary layer effects”. The IGF project 486 ZN / P925 from the Research Association for Steel Application (FOSTA) was supported by the Federal Ministry of Economic Affairs and Energy through the German Federation of Industrial Research Associations (AiF) as part of the programme for promoting industrial cooperative research (IGF) on the basis of a decision by the German Bundestag. The before mentioned institutions as well as the project partners at the Chair and Institute for Materials Science, Technische Universität Darmstadt and the industrial project partners are kindly acknowledged.

## Contents

<b>1</b>	<b>INTRODUCTION .....</b>	<b>1</b>
1.1	Motivation and objective .....	1
1.2	Scientific approach .....	3
<b>2</b>	<b>STATE OF THE ART.....</b>	<b>5</b>
2.1	Fatigue of large-size bolting assemblies .....	5
2.1.1	High-strength bolts in ring-flange connections.....	5
2.1.2	Fatigue damage characteristics.....	6
2.1.3	Fatigue curves.....	9
2.1.4	Influencing factors on bolt fatigue .....	12
2.1.5	Experimental background for large-size HV-bolts.....	19
2.1.6	Normative situation .....	20
2.2	Fatigue assessment with local concepts .....	23
2.2.1	Local fatigue assessment approaches .....	23
2.2.2	Material characteristics.....	25
2.2.3	Computing of local stresses and strains .....	29
2.2.4	Mean stresses and damage parameters .....	31
2.2.5	Size- and surface effects.....	34
2.2.6	Sequence effects and loading conditions .....	37
2.2.7	Application of local concepts to threaded fasteners .....	38
2.3	Findings.....	41
<b>3</b>	<b>EXPERIMENTAL FATIGUE INVESTIGATIONS .....</b>	<b>43</b>
3.1	Scope .....	43
3.2	Test specimens and general boundary conditions .....	43
3.3	Test on M36 HV-bolt sets with constant amplitude loading .....	45
3.3.1	Test execution.....	45
3.3.2	Test results and statistical evaluation .....	48
3.3.3	Assessment of the boundary layer effect.....	61
3.4	Test on M64 HV-bolt sets with constant amplitude loading .....	64
3.4.1	Test execution.....	64
3.4.2	Test results and statistical evaluation .....	66
3.4.3	Assessment of the boundary layer effect and comparisons to M36 bolts.....	67
3.5	Test on M36 HV-bolt sets with variable amplitude loading .....	71
3.5.1	Test execution and loading sequence .....	71
3.5.2	Test results .....	74
3.6	Assessment of normative regulations .....	76
3.6.1	Validation of normative S-N curves .....	76
3.6.2	Assessment of diameter reduction functions .....	78
3.6.3	Assessment of damage accumulation hypotheses .....	82
3.7	Findings.....	86



---

<b>4</b>	<b>ANALYTICAL FATIGUE INVESTIGATIONS .....</b>	<b>89</b>
4.1	Evaluation methodology.....	89
4.2	Base materials description .....	91
4.2.1	Monotonic loading .....	92
4.2.2	Cyclic loading without mean strain ( $\epsilon_m = 0$ ).....	94
4.2.3	Cyclic loading with high mean strain ( $\epsilon_m > 0$ ).....	100
4.2.4	Conclusions for application of material data in analytical fatigue calculations .....	101
4.3	Assessment of local loading conditions.....	102
4.3.1	Description of numerical models .....	102
4.3.2	Evaluation of numerical results.....	105
4.3.3	Approximation of the local stress-strain response under cyclic loading .....	110
4.3.4	Conclusions for application of numerical results in analytical fatigue calculations .....	113
4.4	Fatigue damage assessment.....	114
4.4.1	Technical crack initiation .....	114
4.4.2	Approximation of endurance limit .....	122
4.4.3	Macroscopic crack propagation.....	127
4.4.4	Consideration of the boundary-layer effect.....	133
4.5	Extended sensitivity studies .....	139
4.5.1	Impact of the bolt geometry .....	139
4.5.2	Impact of the bolt material .....	145
4.5.3	Impact of loading conditions .....	150
4.6	Findings.....	156
<b>5</b>	<b>SUMMARY AND FUTURE RESEARCH .....</b>	<b>161</b>
5.1	Summary .....	161
5.2	Recommendations and future research .....	164
<b>6</b>	<b>REFERENCES .....</b>	<b>167</b>
6.1	Standards and technical guidelines.....	167
6.2	Books, articles and handbooks .....	169
6.3	Product information and data sources.....	178
<b>7</b>	<b>LISTS .....</b>	<b>181</b>
7.1	List of Figures .....	181
7.2	List of Tables .....	188
<b>8</b>	<b>APPENDIX .....</b>	<b>189</b>

## Symbols and Abbreviations

### Capital Latin symbols

A	[-], [%]	Ultimate strain (i.e., strain at rupture in monotonic material test)
A <sub>g</sub>	[-], [%]	Uniform strain (i.e., strain at R <sub>m</sub> in monotonic material test)
A <sub>ref</sub>	[mm <sup>2</sup> ]	Reference surface area of material specimen
A <sub>σ</sub>	[mm <sup>2</sup> ]	Critically loaded surface area inside the bolt thread
A <sub>sp</sub>	[mm <sup>2</sup> ]	Tensile stress area of the bolt thread
A <sub>0</sub>	[mm <sup>2</sup> ]	Nominal shaft cross section area
C	[-]	Material constant in <i>Paris'</i> law
C	[-]	Damage accumulation adjustment parameter
D	[-]	Calculated fatigue damage with <i>Miner's</i> rule
E	[N/mm <sup>2</sup> ]	<i>Young's</i> modulus of elasticity
F	[kN]	Force
F <sub>a</sub>	[kN]	Force amplitude
F <sub>b</sub>	[kN]	Acting bolt force
F <sub>p,c</sub> *	[kN]	Reduced nominal preload level acc. to DIN EN 1993-1-8/NA
F <sub>v</sub>	[kN]	Nominal target preload
H	[-]	Cumulative frequency
K	[-]	Stress intensity at the crack tip
K'	[N/mm <sup>2</sup> ]	Cyclic strain hardening coefficient
K <sub>f</sub>	[-]	Fatigue notch factor
K <sub>t</sub>	[-]	Notch stress concentration factor
N	[-]	Load cycles
N <sub>c</sub>	[-]	Endurable load cycles until crack initiation
N <sub>D</sub>	[-]	Load cycles at endurance limit (knee point)
N <sub>i</sub>	[-]	Endurable load cycles for a particular load level or test run
P <sub>J</sub>	[N/mm <sup>2</sup> ]	Damage parameter acc. to <i>Vormwald</i>
P <sub>M</sub>	[N/mm <sup>2</sup> ]	Damage parameter acc. to <i>Narberhaus</i>
P <sub>SWT</sub>	[N/mm <sup>2</sup> ]	Damage parameter acc. to <i>Smith, Watson and Topper</i>
P <sub>s</sub>	[%]	Survival probability
R	[mm]	Bolt thread radius
R	[-]	Stress or strain ratio (also R <sub>S</sub> , R <sub>σ</sub> , R <sub>ε</sub> )
R <sub>m</sub>	[N/mm <sup>2</sup> ]	Tensile strength at monotonic loading (nominal or experimental)

$R_{p,0.2}$	[N/mm <sup>2</sup> ]	0.2 % plastic strain limit at monotonic loading (nominal or experimental)
$S$	[N/mm <sup>2</sup> ]	Nominal stress
$S_a$	[N/mm <sup>2</sup> ]	Nominal stress amplitude
$S_{a,c}$	[N/mm <sup>2</sup> ]	Characteristic nominal stress amplitude acc. to DIN EN 1993-1-9
$S_{a,D}$	[N/mm <sup>2</sup> ]	Nominal cyclic stress at endurance limit (range or amplitude)
$S_m$	[N/mm <sup>2</sup> ]	Nominal mean stress
$S_{max}$	[N/mm <sup>2</sup> ]	Maximum nominal stress
$Z$	[kN]	Flange segment force

### Small Latin symbols

$a$	[mm]	Crack depth
$a_e$	[mm]	Final crack depth before rupture
$a_i$	[mm]	Initial crack depth
$b$	[-]	Fatigue strength exponent
$c$	[-]	Fatigue ductility exponent
$c$	[mm]	Crack width
$d$	[mm]	Nominal bolt shaft diameter
$d_3$	[mm]	Bolt core diameter
$f$	[-]	Strain enhancement factor
$h_3$	[mm]	Bolt thread depth
$j$	[-]	Index of a distinct IST test run
$k$	[-]	Index of distinct strain amplitude in a load sequence of an IST
$k$	[-]	Slope of S-N curve above the endurance limit
$k^*$	[-]	Slope of S-N curve below the constant amplitude endurance limit
$k_s$	[-]	Diameter reduction factor acc. to DIN EN 1993-1-9
$k_w$	[-]	<i>Weibull</i> exponent
$m$	[-]	Material constant in <i>Paris'</i> law
$m$	[-]	Number of endured blocks in an IST
$n'$	[-]	Cyclic strain hardening exponent
$n_i$	[-]	Number of load cycles with a particular load level
$n_s$	[-]	Notch sensitivity factor
$n_p$	[-]	Macroscopic notch sensitivity
$n_w$	[-]	Statistical notch sensitivity factor (weakest link model)
$n_{\gamma^*}$	[-]	Stress-mechanical notch sensitivity factor

$p$	[mm]	Pitch of the bolt thread (elevation per turn)
$p$	[-]	Number of load cycles per half block in an IST
$r$	[mm]	Radius

### Greek symbols

$\chi^*$	[1/mm]	Related stress gradient
$\Delta\sigma_{,relax}$	[N/mm <sup>2</sup> ]	Stress level decrease due to cyclic relaxation
$\Delta S$	[N/mm <sup>2</sup> ]	Cyclic nominal stress range $\Delta S = 2 S_a$ (also $\Delta\sigma$ , $\Delta\epsilon$ )
$\epsilon$	[-], [%]	Local strain
$\epsilon^*$	[-], [%]	Local strain adjusted by engineering model
$\epsilon_1$	[-], [%]	1 <sup>st</sup> principle local strain
$\epsilon_a$	[-], [%]	Local strain amplitude
$\epsilon_{a,e}$	[-], [%]	Elastic part of local strain amplitude
$\epsilon_{a,p}$	[-], [%]	Plastic part of local strain amplitude
$\epsilon_{a,D}$	[-], [%]	Strain endurance limit
$\epsilon_{op} / \epsilon_{cl}$	[-], [%]	Crack opening / closing strain
$\Delta\epsilon_{p,eff}$	[-], [%]	Damage effective plastic strain range
$\epsilon'_f$	[-]	Fatigue ductility coefficient
$\sigma$	[N/mm <sup>2</sup> ]	Local stress
$\sigma_1$	[N/mm <sup>2</sup> ]	1 <sup>st</sup> principle local stress
$\sigma_a$	[N/mm <sup>2</sup> ]	Local stress amplitude
$\sigma_{a,D}$	[N/mm <sup>2</sup> ]	Local stress amplitude at endurance limit
$\sigma_{op} / \sigma_{cl}$	[N/mm <sup>2</sup> ]	Crack opening / closing stress
$\Delta\sigma_{eff}$	[N/mm <sup>2</sup> ]	Damage effective stress range
$\sigma'_f$	[N/mm <sup>2</sup> ]	Fatigue strength coefficient
$\sigma_m / \epsilon_m$	[N/mm <sup>2</sup> ] / [-]	Mean stress / strain of local hysteresis
$\sigma_o / \epsilon_o$	[N/mm <sup>2</sup> ] / [-]	Maximum stress / strain of local hysteresis
$\sigma_u / \epsilon_u$	[N/mm <sup>2</sup> ] / [-]	Minimum stress / strain of local hysteresis
$\sigma_r / \epsilon_r$	[N/mm <sup>2</sup> ] / [-]	Local residual stress / strain
$\mu$	[-]	Friction coefficient
$\xi$	[mm]	Eligible geometric coordinate

**Abbreviations**

APDL	ANSYS parametric design language
B	Uncoated, black
BC	Boundary conditions
CA	Constant amplitudes
FAT	Fatigue detail category acc. to DIN EN 1993-1-9
FEM	Finite Element Method
HCF	High cycle fatigue
HT	High temperature
HV	'System HV' bolt assembly acc. to DIN EN 14399-4 or DAST-Guideline 021
IST	Incremental-Step-Test
L1...L5	Load levels in variable amplitude loading tests
LMAC	Liquid metal assisted cracking
MOT	Electromotive testing actuation
NT	Normal temperature
RBHT	Rolled before heat treatment
RRO	Raised run-out
TEL	Transition region to the endurance limit
UML	Uniform Material Law

# 1 Introduction

## 1.1 Motivation and objective

Bolted ring-flange connections are widely used in steel support structures for wind turbines, for the conjunction between tower segments or the connection of towers to offshore substructures (see Figure 1-1, left). The connections are commonly equipped with high-strength bolting assemblies, so-called HV-bolt sets, with large diameters M36 and bigger (see Figure 1-1, right). Especially at lower tower levels, the magnitude of the acting loads usually requires the application of very large bolt diameters M64 or M72, not only at strong-wind offshore turbines but also at modern towers with large hub-heights developed for onshore locations. Frequently, for a single ring-flange 100 or more circumferentially arranged HV-bolt sets are required. With multiple connections in every tower, an appropriate ring-flange design thus has a pivotal impact on the overall tower reliability and costs.



**Figure 1-1: Ring-flange connection in wind turbine support structure (left) and HV-bolt sets with large diameters (right)**

Throughout their aspired service life of at least 20 years or more, support structures for wind turbines are subjected to high cyclic loads with variable amplitudes, reaching up to  $10^9$  load cycles. As a consequence of the strong notch effect of the thread, HV-bolts are decidedly susceptible to fatigue damage. Hence, for reduction of fatigue loads, preloading of bolts is mandatory to ensure the structural integrity. Still, an accurate fatigue assessment of the bolts is an essential part of the design process.

Due to the high required loads, experimental fatigue investigations on large-size HV-bolts are a demanding and time consuming task, especially when performed at representative mean load level. Moreover, in constructional engineering the application of large-size HV-bolts, especially in the upper end of the diameter range, mostly focusses on the emerging wind energy sector. Therefore, even though applicable design regulations do not exclude their application to bolts with large diameters, thus far the experimental validation of relevant fatigue properties is mostly limited to smaller dimensions.

For a reliable protection against corrosion, HV-bolts are commonly hot-dip galvanized. Research by *Ungermann et al.* (2014) has conclusively verified that the thermally applied zinc coating leads to a

considerable reduction of the fatigue strength at welded structural components. The causative damage mechanism was traced back to shrinkage cracks within the zinc boundary layer. Further investigations by *Simonsen* (2015) have confirmed a similar effect at small-scale specimens with bolt-like notch geometry. However, prior to the research presented in this dissertation, the actual quantitative impact of hot-dip galvanizing to the fatigue behaviour of HV-bolt sets with large diameters has not yet been conclusively investigated. Moreover, contrary to the service loading conditions of wind turbines, all thus far performed systematic investigations on the impact of hot-dip galvanizing on the fatigue strength of structural steel components have focussed on testing conditions with constant amplitudes.

In regard to practical applications, by far the most relevant normative regulation for the fatigue verification of HV-bolts in support structures for wind turbines is the DIN EN 1993-1-9 (2010), or simply Eurocode 3 (which entitles the entire EN 1993 series). Additionally, the VDI Guideline 2230 (2015) provides a relevant design background, its applicability is however mostly limited to mechanical components. Whereas the latter guideline generally acknowledges a quantitative difference of the fatigue strength between uncoated and hot-dip galvanized bolts, the Eurocode 3 follows a uniform fatigue classification. Both regulations consider different reduction functions of the fatigue strength that are dependent to the diameter. However, in the large diameter range these functions are not experimentally substantiated.

Fundamental for the initial validation of the normative background for the design of common-sized HV-bolts in wind turbines, *Marten* (2009) has established comprehensive fatigue test results for hot-dip galvanized HV-bolts with a diameter of M48. However, due to limitations of the applied testing facility, the tests had to be performed under a reduced mean load level, compared to the nominal preload. This presumably has led to an overestimation of endurable load cycles at higher load levels. The potential impact of further increased bolt diameters was not verified. Moreover, no comparative tests have been performed on uncoated specimens to specifically quantify the effect of the zinc boundary layer.

To supplement costly experimental test series for the evaluation of fatigue-relevant impact factors, analytical fatigue assessment procedures may have valuable potential. In his research works, *Marten* (2009) has acknowledged the general applicability of the strain-life approach to large-size HV-bolts for the calculation of crack initiation load cycles. However, also due to the limited experimental background, a fully appropriate and validated evaluation procedure could not be established. *Schneider* (2011) has introduced a further elaborated comprehensive assessment approach, specifically intended for the evaluation of threaded fasteners under high mean stress conditions. Thereby, the methodical fatigue evaluation encompassed both technical crack initiation and macro-crack propagation phases. Still, validation has only been provided for HV-bolts with relatively small dimensions, unrepresentative for the commonly applied bolt-sizes in support structures for wind turbine. Moreover, the analytical procedure only encompassed boundary layer conditions without hot-dip galvanizing.

Given the outlined initial situation, the necessity for further research to establish an adequate knowledge base on the fatigue characteristics and assessment principles of large-size HV-bolts becomes obvious. To address this requirement, the joint research project “Experimental and analytical assessment of the fatigue strength of bolts with large dimensions under consideration of boundary layer effects” (Oechsner *et al.*, 2015) was initiated within the programme for promoting industrial cooperative research (IGF) via funding of the German Federal Ministry of Economic Affairs and Energy. Large parts of the experimental and analytical investigations presented in this dissertation were performed within the framework of this project.

The performed research specifically aims for the validation of the normative design background as well as the identification of potential for its improvement. Thereby, the adequate consideration of representative boundary conditions concerning loading and production of the bolts is a prerequisite for the investigations. A meaningful extension of the available experimental background forms a vital part to the objectives. Furthermore, the research intends to accurately refine and validate suitable analytical fatigue assessment measures, which then can provide further insights to the subject of large-size bolt fatigue.

## **1.2 Scientific approach**

To accomplish the previously described research objectives, the dissertation in hands is constituted by three major scientific steps.

In Chapter 2, a thorough evaluation of the given initial state of the art concerning the subject under investigation is performed. Orientated on the methodical approach of the ensuing self-performed investigations, the literature review is subdivided into two superior sections. In the first part, the essential knowledge background on fatigue characteristics of large-size bolting assemblies is collected. This includes the general characteristics of the fatigue process and its methodical description as well as the collation of the fundamentals regarding fatigue-relevant impact factors, established at both small scale and, as far as available, larger-scale bolt assemblies. The second part focusses on the methodical background for an analytical fatigue assessment of threaded fasteners in general and large-size HV-bolts in particular. At the end, fundamental requirements for the own investigations are derived.

The core of the performed investigations, established by a comprehensive experimental program, is presented in Chapter 3. It comprises detailed evaluations from three fatigue test series on large-size HV-bolt sets. The performed tests extend the previous experimental background for HV-bolts into the very large diameter range. By performing tests with variant bolt sizes, the potential impact of an increased diameter on the fatigue strength is evaluated. Thereby, different bolt surface configurations with and without hot-dip galvanizing are considered, thus enabling the quantification of the boundary layer effect. Moreover, the tests include the comparison of fatigue characteristics at testing conditions with constant and variable amplitude loading. Based on the obtained results, normative



design regulations are evaluated. Thereby, also the regulations' respectively considered fatigue reduction functions in dependence of the diameter as well as their incorporated damage accumulation approaches are contemplated in particular.

The experimental results also serve as an essential validation background for the analytical fatigue investigations, presented in Chapter 4. The applied methodology is based on the strain-life concept and supplemented by the fracture mechanics approach. The different fundamental steps of the analytical procedure are systematically evaluated for their specific application to large-size HV-bolts. In the first instance, this includes the essential provision of relevant monotonic and cyclic material data from the experimentally investigated HV-bolts' base materials. Based on this, the appropriate numerical approximation of the local cyclic stress-strain relation inside the paired thread with elastic-plastic material behaviour is addressed. The investigation of the actual fatigue damage assessment then encompasses aspects of an appropriate mean stress consideration, calculations in variant fatigue life regimes and the introduction of an engineering model for consideration of the effect of hot-dip galvanizing. Finally, the developed refined assessment procedure is used to evaluate specific potential fatigue-relevant impact factors, such as different size-effects, load conditions or the material.

The dissertation concludes with a final summary of the performed research, derived findings and recommendations as well as suggestions for future research.

## 2 State of the Art

### 2.1 Fatigue of large-size bolting assemblies

#### 2.1.1 High-strength bolts in ring-flange connections

Ring-flange connections in wind turbines are equipped with large numbers of circumferentially arranged high-strength bolt assemblies. Commonly “System HV” bolt sets are utilized, consisting of geometrically aligned bolts, nuts and washers. With specifically adjusted characteristics for the requirements of preloading, HV-bolt sets are regulated in DIN EN 14399-4 (2015) and for diameters larger than M36 up to M72 in the German DASt - Guideline 021 (2013). Protection against corrosion is usually maintained by zinc based protection systems such as hot-dip galvanizing.

Preloading is essential for the structural integrity of the bolts. Due to practicality reasons, especially for large bolt diameters, preloading is commonly accomplished with the torque method. Thereby the nut is tightened with a hydraulic wrench until a defined torque moment is reached. In order to securely avoid large plastic deformations during torque-obtained tensioning, the nominal target preload  $F_V$ , given in DASt – Guideline 021 for large HV-bolt sets, corresponds to a “reduced” nominal preload level  $F_{p,C}^*$ , calculated according to DIN EN 1993-1-8/NA (2010):

$$F_V = 0.7 \cdot R_{p,0.2} \cdot A_{sp} \quad \text{Eq. 2-1}$$

where:

$F_V$	nominal target preload
$R_{p,0.2}$	nominal 0.2%-plastic strain limit (yield stress)
$A_{sp}$	tensile stress area of the bolt thread

Since preloading with the torque method is particularly sensitive to potentially scattering friction coefficients in the paired contact surface between bolt and nut, recent developments focus on measurement assisted tightening tools and procedures, which enable a more precise attainment of the nominal preload. Allowing for these developments, in the recent standard for certification of support structures for wind turbine DNVGL-ST-0126 (2016) (contrary to e.g. GL Guideline, 2012) a controlled nominal preload is permitted, which corresponds to the minimum preload level  $F_{p,C}$ , established in DIN EN 1090-2 (2011). Thereby the 0.2%-plastic strain limit  $R_{p,0.2}$  in Eq. 2-1 is substituted by the nominal tensile strength  $R_m$ . Nevertheless, the current situation of standardisation regarding appropriate preload levels and procedures remains ambiguous, especially for large bolt diameters. Thus, project specifically developed preload measurement and maintenance procedures are the norm. A thorough discussion of allowable preload levels and procedures for the general application of threaded fasteners in civil engineering in the context of German and European standardisation is given by *Stranghöner et al.* (2016).

For simplification purposes, dimensioning of bolts in flange connections is classically performed under assessment of the isolated, maximal loaded segment of the flange (Figure 2-1, left). Modern finite element approaches also consider the interacting load-bearing contributions of the bolts along

the circumference. Nevertheless, the approach remains to perform a design for the most critically loaded bolt inside the flange and adapt it to the entire connection. Even though the eccentricity between tower wall and bolt axis leads to a certain amount of bending, the main contribution to the loading conditions of bolts inside ring-flanges derives from axial loads (e.g., see *Seidel, 2001*; *Schaumann et al., 2018*). Preloading and eccentric geometry cause a non-linear load transfer behaviour between tensile force  $Z$  in the tower shell segment and resulting bolt force  $F_b$  (Figure 2-1, right). The slope of the corresponding transfer function, which is decisive for the magnitude of the bolt's fatigue loads (i.e., load ranges  $\Delta F_b$ ), is crucially affected by the preload. Moreover, flange imperfections (here exemplary introduced by a tower sided flange gapping angle  $\phi_{imp}$ ) have a severe impact on the transfer behaviour (e.g., see *Schaumann et al., 2018*; *Feldmann et al., 2011*; *Jakubowski, 2003*).

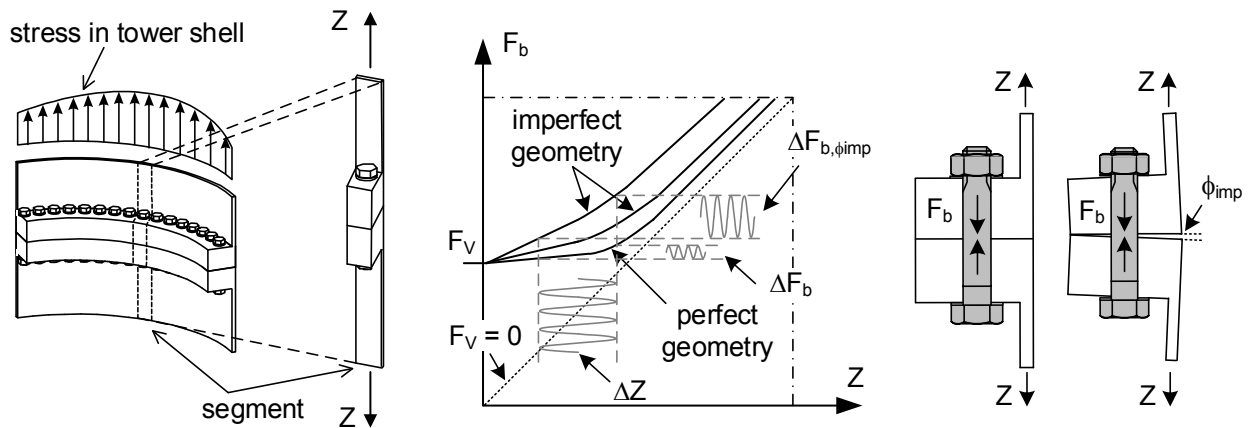


**Figure 2-1: Segment approach for the design of ring-flange connections acc. to *Seidel (2001)* (left) and schematic depiction of load transfer behaviour considering preload and flange imperfections acc. to *Schaumann et al. (2018)* (mid and right)**

### 2.1.2 Fatigue damage characteristics

Under cyclic loading metallic components are prone to failure at load levels considerably below their static strength level; the reason is the complex physical damage mechanism, known as fatigue. A pronounced notch effect (i.e., a local stress concentration at a geometrical notch) significantly reduces the fatigue strength of a structural component. Consequently, due to the strong notch effect of the thread, bolt assemblies are distinctly susceptible to fatigue damage.

Commonly, the stress flow of a bolt-to-nut connection causes a decisive peak stress concentration inside the first fully loaded pitch of the thread (Figure 2-2, left). The notch stress concentration  $K_t$  is generally defined as the relation of maximum local stress  $\sigma_{max}$  and nominal stress  $S$  under linear elastic conditions (for a clear distinction, within this entire thesis local stresses are denoted with the Greek letter  $\sigma$ , whereas nominal stresses are indicated by a Latin capital  $S$ ). At various occasions within this thesis, the  $K_t$  parameter is also used to express the development of the linear elastic stress concentration over an eligible geometric coordinate  $\xi$ :

$$K_t = \frac{\sigma_{max}}{S} \quad \text{or} \quad K_t = K_t(\xi) = \frac{\sigma(\xi)}{S} \quad \text{Eq. 2-2}$$

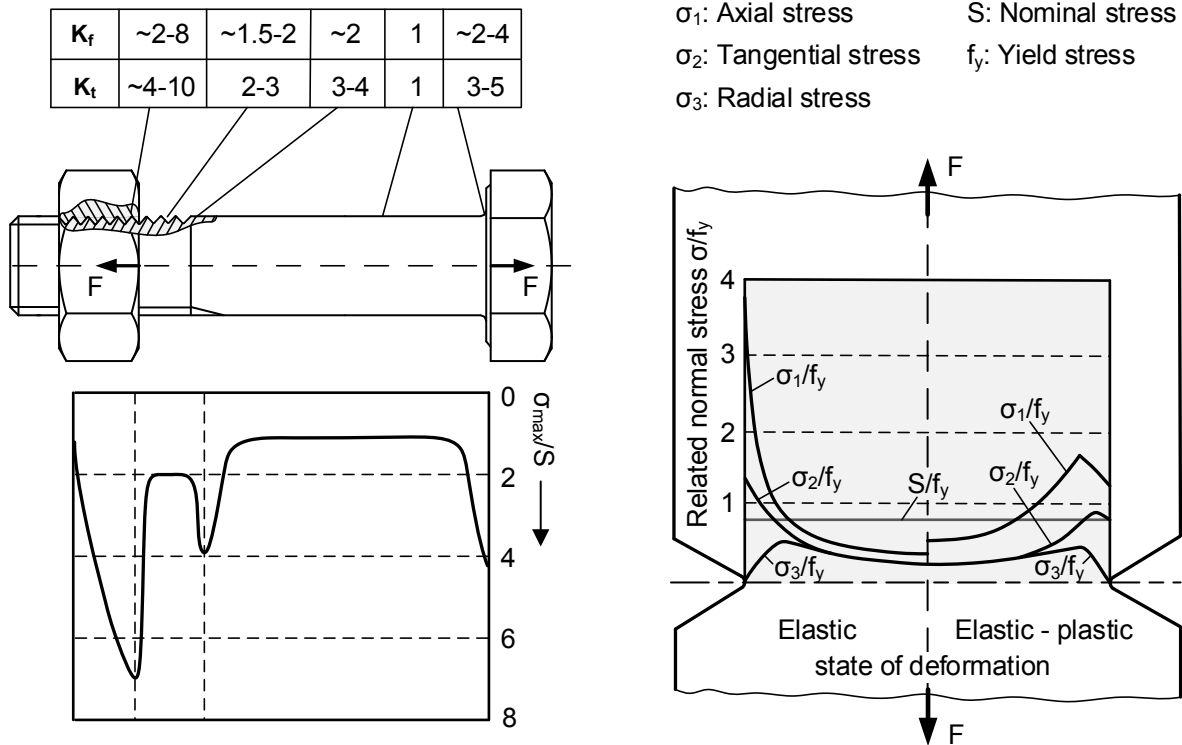


**Figure 2-2: Schematic stress distribution and usual range of  $K_t$  and  $K_f$  for a bolt-to-nut connection (left) and three-axial stress state in the cross-section of a notched specimen (right) acc. to *Wiegand et al. (2007)***

Contrary to the unnotched shaft, under axial loading a three-axial stress state of axial, tangential and radial stresses develops inside the thread, which is inconstant throughout the cross-section (Figure 2-2, right). Thus, due to its lower strength utilisation, the surrounding material provides a support effect on the critically loaded notch root. Moreover, the ductility of bolt materials allows a certain stress redistribution under local plasticity. As a consequence, the fatigue strength of notched components is typically higher as expectable from the solely geometry dependent notch stress concentration  $K_t$ . This circumstance is considered by the fatigue notch factor  $K_f$ , which is defined as the quotient of constant amplitude fatigue limit (i.e., endurance limit, see section 2.1.3) of an unnotched specimen  $\sigma_{a,D(K_t=1)}$  (for unnotched specimens:  $\sigma = S$ ) and the nominal stress endurance limit of the notched component  $S_{a,D(K_t>1)}$ , with otherwise identical properties. As quotient of  $K_t$  and  $K_f$ , the so-called ‘stress-mechanical’ or geometric support effect is also expressed by the number  $n_\sigma$ :

$$K_f = \frac{\sigma_{a,D(K_t=1)}}{S_{a,D(K_t>1)}} = \frac{K_t}{n_\sigma}, \text{ with } n_\sigma \geq 1 \tag{Eq. 2-3}$$

As it inherently describes the actual fatigue strength of a component, the magnitude of the fatigue notch factor is affected for instance by loading conditions, mean stress, geometric properties and material. The depicted range of typical fatigue notch factors for bolt-to-nut connections in Figure 2-2 emphasises the high importance of accurate fatigue assessment of bolts. Unlike in the depicted free notch in Figure 2-2 (right), the maximum stress concentration in the first loaded pitch of a paired

thread is not situated directly at the notch root but about  $30^\circ$  relocated towards the loaded thread flank (Wiegand *et al.*, 2007). Usually, at this location a fatigue crack is initiated.

The process of fatigue crack formation and ultimately resulting failure is constituted by a sequence of metallurgical phases, which is schematically depicted in Figure 2-3. Most generally, as sufficient for most engineering purposes, it is subdivided into the phases of initiation and succeeding propagation of a macroscopic 'technical crack'. Lacking a precise physical definition, it is accepted that the initiation of a technical crack is indicated by the occurrence of a crack size, which is detectable by 'common technical means' (Gudehus & Zenner, 1999; Radaj *et al.*, 2006). Collating estimations stated by the latter as well as by Radaj & Vormwald (2007), this corresponds to a crack with an approximate surface length of ~1-2 mm and depth of ~0.5 mm.

On microscopic scale, the fatigue process under cyclic loading is initiated by dislocation movements at areas of local stress concentration, which cause slip bands perpendicular to the maximum alternating shear stresses in an order of magnitude smaller than the material's grain size. The number of occurring slip bands, which essentially form as ex- or intrusions at the surface of the material (in certain cases an internal surface), increases with the magnitude of the alternating load (Socie & Marquis, 2000). At the slip bands, micro cracks nucleate which eventually, when they reach a crack length approximately equivalent to the grain size, start propagating due to local slip mechanisms at the crack tip (Radaj & Vormwald, 2007; Radaj *et al.*, 2006). Under coalescence with other micro cracks, a stable phase of micro crack propagation is followed by the stable macro crack propagation. Finally, instable crack propagation and static overload leads to the rupture of the remaining cross-section.

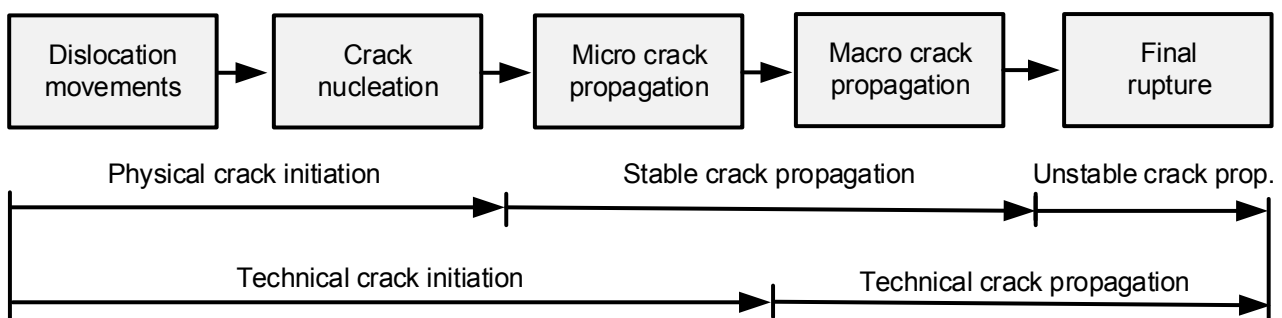


**Figure 2-3: Phases of the metallurgical fatigue process acc. to Radaj *et al.* (2006)**

The proportions of crack initiation and crack propagation phase to the overall fatigue life highly depend on case individual attributes such as cyclic load magnitude, mean stress, surface and geometric notch conditions as well as microscopic or macroscopic point of view (Radaj & Vormwald, 2007). Kremer (2005) found in his experimental studies on HV-bolt sets (see also section 2.2.7) that in the region of the endurance limit the total number of endurable load cycles is dominated with over 90 % by load cycles until technical crack initiation. However, at higher load levels macroscopic crack propagation covers a substantial part of the overall load cycles until rupture.

Vormwald (1989) emphasizes that on micro-structural scale, crack propagation occurs significantly before the formation of a macroscopic technical crack. Moreover, Radaj & Vormwald (2007) refer to

experiments from *Neumann et al.* on unnotched specimens with macroscopically homogeneous material and without mean stress. These investigations have proven that only about the initial 10 % of the fatigue life until technical crack initiation are formed by the actual physical crack nucleation. Afterwards the fatigue process is characterised by micro crack propagation.

### 2.1.3 Fatigue curves

#### Constant amplitude loading

Most popularly, the load level dependent fatigue strength of structural details and components is described by S-N curves (also known as *Wöhler* curves). Based on experiments under harmonic constant amplitude loading, endurable load cycles until failure ( $N$ ) are usually plotted against nominal stress amplitudes ( $S_a$ ) or stress ranges ( $\Delta S$ ) in double-logarithmic scale (see Figure 2-4). Commonly, the failure criterion is the complete rupture of the specimen or in some cases the initiation of a defined technical crack. The underlying experiments are performed with either constant mean stress ( $S_m$ ) or constant load ratio ( $R$ ) (Figure 2-4, right). Characteristic for preloaded bolted connections are swelling tensional loads with load ratios  $R > 0$ .

In dependence of the endurable load cycles, the path of an S-N curve can be subdivided into different sections (*Gudehus & Zenner, 1999; Haibach, 2006; Radaj & Vormwald, 2007*). The low cycle fatigue range (LCF) up to about  $N \approx 10^4$ - $10^5$ , with load levels close to the component's strength limit, is characterised by considerable plastic deformations. In the succeeding high cycle fatigue range (HCF) global deformations are linear elastic and the path of the S-N curve reaches a linear progression. Commonly, in the literature the denotation 'high cycle fatigue' is used to describe a fatigue range up to  $10^7$  load cycles, followed by the 'very high cycle fatigue' range (VHCF) (e.g., *Pyttel et al., 2011; Wang et al., 2012*). Thus, for the sake of a clear distinction of the relevant parts of the S-N curve, in the course of this thesis the denotation 'upper' high cycle fatigue regime is applied to the fatigue range where the path of the S-N curve can be approximated linearly with the slope exponent  $k$ , when expressed in double logarithmic scale.

The upper HCF blends over into the succeeding transition region to the endurance limit (TEL), which is indicated by a pronounced widening of the statistic scatter of ruptures at identical load levels and a continuous change of the S-N curve's slope. Finally, the course of the S-N curve again reaches a linear progression, which indicates the endurance or constant amplitude fatigue limit ( $S_{a,D}$ ). The common 'knee point', where the straight lines from upper HCF regime and endurance limit coincide, is an engineering approximation with no physical substantiation; however, it forms an important characteristic parameter for a practicable definition of experimentally determined S-N curves. For ferrous structural components the knee point usually is in an order of magnitude of  $N_D \approx 10^6$ - $10^7$  (*Radaj & Vormwald, 2007*).

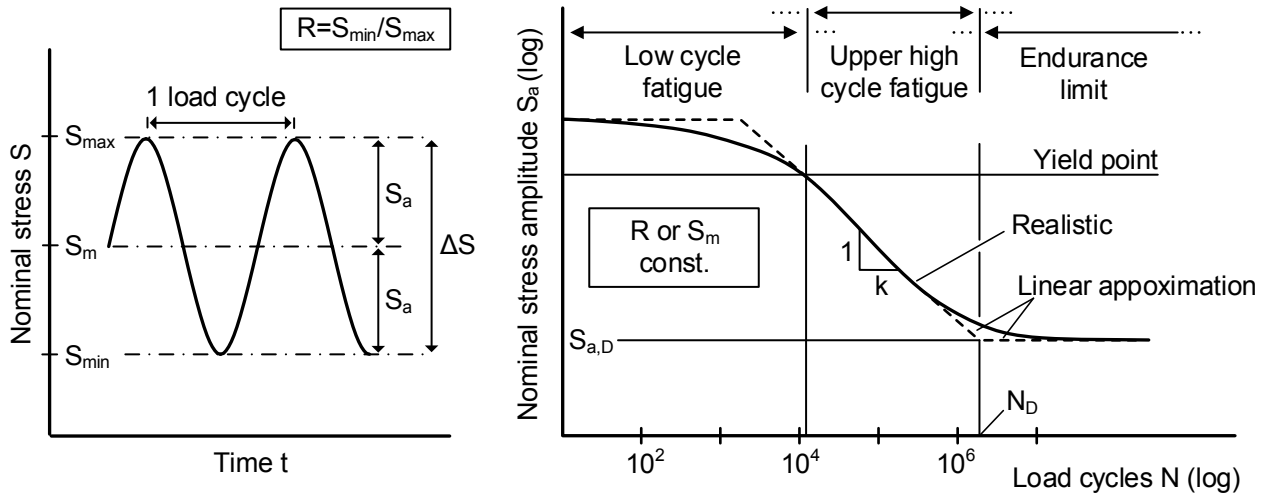


**Figure 2-4: Characteristic values of a harmonic, constant amplitude loading (left) and schematic progression of an S-N curve (right; adapted from Gudehus & Zenner, 1999 and Radaj & Vormwald, 2007)**

The progression of the S-N curve after the knee point is controversially discussed in the scientific community and certainly depends on material composition as well as environmental boundary conditions, like for example corrosive impacts or high temperatures (e.g., *Sonsino, 2005; Marines et al., 2003*). According to *Radaj & Vormwald (2007)*, under laboratory conditions, a transition to a virtually horizontal progress of the S-N curve at a low load level is typical for strongly notched steel components. As such, it is traditionally acknowledged (e.g., *Kloos & Thomala, 1979; Wiegand et al., 2007*) and also incorporated in normative regulations (e.g., VDI Guideline 2230, 2015) that for threaded fasteners constant amplitude loads below the endurance limit do not cause fatigue damage.

Results from fatigue tests on HV-bolt sets with high load cycle numbers do not show late failures with  $N > 10^7$  (*Weber, 2010*). However, experiments which reach into the VHCF range are very cost and time consuming and for bolt assemblies no experimental results exist with load cycles  $N > 5 \cdot 10^7$ . Nevertheless, experimental investigations from *Steppeleer (2014)* on butt weld specimens indicate a horizontal progression of the S-N curve in the range of very high load cycle numbers up to  $N = 5 \cdot 10^8$ . As bolt assemblies show a stronger notch effect than the welds, a comparable behaviour could be presumed; however, in order to draw clear conclusion a more detailed evaluation would be needed. *Radaj et al. (2006)* propose the distinction between a 'technical endurance limit' and a 'true endurance limit' in order to imply that, albeit small, a certain decline of the S-N curve may be included. In that sense, within the course of this thesis the denotation 'endurance limit' always refers to a technical endurance limit.

Generally, the results of fatigue experiments are subjected to a pronounced scatter. Consequently, an appropriate statistical planning and evaluation is indispensable for the experimental determination of fatigue curves.

## Service loading

Contrary to most experimental fatigue investigations, the actual service loading conditions of bolts in wind turbines are characterised by strongly inconstant amplitudes and sequences of stochastic nature (wind and wave loading). By use of appropriate counting algorithms (e.g., *Clormann & Seeger, 1986*), the inherent load cycles of a loading sequences can be transformed into a collective of load amplitudes and corresponding sums of their occurring cycles (Figure 2-5, left). Thereby the information about the specific succession of cyclic loads is lost.

Most widely applied in structural engineering applications is the analytical estimation of an occurring fatigue damage under variable service loads by *Miner's-rule* (Eq. 2-4) (*Miner, 1945*). Thereby it is assumed that the overall damage  $D$  is linearly formed by the sum of partial damage, defined as quotient of occurring load cycles  $n_i$  of a particular stress amplitude  $S_{a,i}$  and the number of endurable load cycle  $N_i$  from the constant amplitude reference S-N curve (hypothesis of linear damage accumulation).

$$D = \sum_{i=1}^{i=n} D_i = \sum_{i=1}^{i=n} \frac{n_i}{N_i} \quad \text{Eq. 2-4}$$

In a load sequence with variable amplitudes, the damage caused at higher stress levels in form of micro-cracks, which are capable of propagation, may lead to a successive reduction of the initial endurance limit. Therefore, also stress amplitudes below the initial endurance limit may contribute to the progression of damage (*Radaj & Vormwald, 2007; Haibach, 2006*). Thus, in its original form, with a horizontal path of the S-N curve after the endurance limit, the application of the *Miner* hypothesis can cause a significant overestimation of fatigue life. On the contrary, the 'elementary' form of *Miner's* rule describes the hypothesis of a virtually non-existent endurance limit and an S-N curve with constant progression over the entire range of stress amplitudes. While accurate for specific conditions such as for structural steel under corrosive impact, it usually leads to a rather conservative fatigue life calculation (*Haibach, 2006*). In order to provide a more accurate approximation of the actual fatigue damage development, modified versions of the *Miner* hypothesis have been developed. The most popular modification was established by *Haibach (1970)*, where a fictitious progression of the reference S-N curve after the endurance limit is introduced with a slope exponent  $k^* = 2k-1$ ; it is also included in the European standard for fatigue design of steel structures DIN EN 1993-1-9 (2010). The three described variants of the *Miner* hypothesis are illustrated in Figure 2-5, right. Other modifications have been proposed for example by *Hüeck et al. (1988)* and *Zenner & Liu (1992)*.

All approaches, mentioned above, neglect the possible impact of sequence effects (e.g., see *Radaj & Vormwald, 2007*). A damage calculation considering a damage dependent and load cycle wise successive reduction of the endurance limit, denoted as the 'consequent' form of *Miner's*-rule, is described in *Haibach (2006)*. Additional to its non-linear characteristic, the consequent interpretation directly allows for the circumstance that also under variable amplitude loading no fatigue damage needs to be expected if the maximum stress amplitude of the load collective is smaller than the constant amplitude endurance limit.



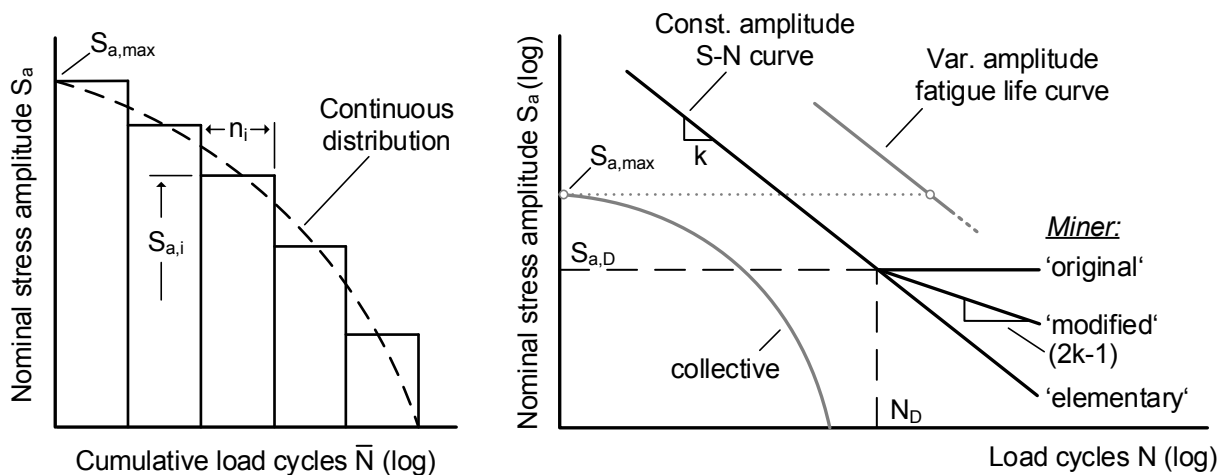


**Figure 2-5: Schematic depiction of a load collective in discrete and continuous form (left) and fatigue-life curve and variants of the *Miner* hypothesis (original, elementary and modified form proposed by *Haibach*, 1970) (right)**

For fatigue tests with variable amplitudes, the spectrum of applied loads is commonly approximated by a generic stochastically distributed load collective (e.g., a normal distributed *Gauss* collective). The collective can be scaled relatively to the maximum load level and the actually applied succession of loads may be arbitrarily rearranged from the declining order of the collective. When fatigue tests are performed with load sequences, derived from collectives with different maximum load levels but identical relative distribution of stresses, the variable amplitude 'fatigue-life curve' (also *Gaßner* curve) can be derived. Thereby the endurable load cycles are plotted against the maximum stress amplitude of the investigated load collective (Figure 2-5, right). Such experiments allow the evaluation of analytical damage accumulation hypotheses. First comprehensive experimental investigations of damage accumulation for HV-bolts under variable loading were published by *Weber* (2010). A profound evaluation of damage hypotheses on the example of welded connections has been performed by *Al Shamaa* (2015).

#### 2.1.4 Influencing factors on bolt fatigue

Influences on the fatigue strength of bolting assemblies, as for metallic components in general, are multifarious. Within the following sections, specific characteristics with particular significance to large-size HV-bolt sets in wind turbines and the objectives of this thesis are discussed.

##### Material and production

According to *Wiegand et al.* (2007) suitable materials for structural bolt fasteners are characterised by high strengths while maintaining sufficient toughness and ductility. These enable preloading with high forces, which is essential to reduce the acting fatigue loads, and simultaneously allows a plastic redistribution of stresses inside the thread. For high-strength bolts of nominal strength class 8.8 or 10.9 (HV-bolt sets) the achievement of these attributes usually requires the application of low-alloy carbon steels, with common additional alloying elements being for instance chromium (Cr), nickel (Ni), molybdenum (Mo) or boron (B). The appropriate chemical alloys are regulated in DIN EN

10263-4 (2018) and DIN EN 10083-3 (2007). The detailed requirements for the mechanical properties of the specified strength classes for bolt materials and bolts are defined in DIN EN ISO 898-1 (2013).

Generally, a high material strength has a positive impact on the fatigue resistance of metals. However, the effect diminishes with an increased notch effect (e.g., *Schütz*, 1974). Accordingly, the fatigue strength of HV-bolts can be considered as mostly unaffected by the material's strength class. Nevertheless, cyclic material characteristics (see section 2.2.2), which may vary with the specific material composition, are important to consider in a detailed fatigue assessment with local concepts. Moreover, good toughness attributes are crucial to prevent premature cracking (*Wiegand et al.*, 2007). Experiments on HV-bolts under static loading by *Stranghöner et al.* (2018), considering two representative high-strength material alloys and diameters up to M64, verified that no brittle fractures need to be expected also at very low temperatures.

Typically, in industrial production the thread forming of HV-bolts from the raw material workpiece is performed in a non-cutting rolling process. Whether the heat treatment for realisation of the required mechanical properties is performed before or after forming of the thread has a significant impact on the bolts fatigue strength (e.g., *Thomala*, 1978; *Kremer*, 2005). Compressive residual stresses introduced by the inhomogeneous deformations during rolling are acknowledged to cause a favourable influence. Since the residual stresses diminish during the thermal tempering process, bolts which are rolled before heat treatment do not benefit from this effect. Measurements by *Marten* (2009) on HV-bolts M48 after different production stages have shown that significant longitudinal residual stresses, present after rolling in the vicinity of the notch root surface, are plastically relieved during a succeeding thermal treatment. A subsequently performed normal temperature hot-dip galvanizing did not show further effects in the measurements. Thus, he concludes that bolts which are rolled before heat treatment may essentially be considered as free of longitudinal residual stresses.

Due to plasticization, the beneficial effect of residual stresses to the endurance limit decreases with an increasing preload level (*Wiegand et al.*, 2007). Furthermore, *Kremer* (2005) has found a shallower progression in the upper HCF of S-N curves of residual stress affected bolts. Still, also under high preloads and fatigue load levels, bolts which are rolled after heat treatment usually provide a superior fatigue strength than bolts rolled before heat treatment. Nevertheless, to enable an economic manufacturing process, HV-bolts with large diameters are commonly rolled before heat treatment.

## **Loading conditions**

### *Preload*

Under dynamic loading, the preload causes a systematically established tensile mean stress level. Contrary to residual stress affected bolts, rolled after heat treatment, the fatigue strength of bolts which are rolled before heat treatment shows a less severe mean stress dependency. According to results from *Schneider* (1992), at mean stress levels within a range of approximately ~25% to ~60% of the bolt material's measured plastic strain limit  $R_{p,0.2}$  ( $0.25 \cdot R_{p,0.2} \leq S_m \leq 0.60 \cdot R_{p,0.2}$ ) the endurance

limit is mostly unaffected by the mean stress. At higher mean stress levels, he found a reduction of the endurance limit, reaching up to 30% for a mean stress of  $0.9 \cdot R_{p,0.2}$ . This tendency was also confirmed by *Weber* (2010).

Generally, the moderate mean stress dependency of the endurance limit of bolts, rolled before heat treatment, results from the early local plastic deformations at the notch root. Due to the high stress concentration at the first load-bearing turn of the thread, these deformations occur already at relatively low preloads (*Kloos & Thomala*, 1979). A further increasing preload level does not lead to substantial changes of the local mean stress. However, at higher preloads (i.e., nominal mean stress levels) the area of plastic deformation can be considered to expand from the notch root in lateral direction. *Dünkel* (1999) suspects this as reason for the aforementioned reduction of the endurance limit at high preloads observed by *Schneider*.

At very low preload levels *Thomala* (1978) expects a negative effect on the endurance limit of bolts, rolled before heat treatment, which is caused by an insufficient stress redistribution inside the paired thread. With respect to the upper HCF, *Marten* (2009) came to the conclusion that the low nominal mean stress ( $0.15 \cdot R_{p,0.2,nom}$ ) in his experimental investigations has led to a beneficial effect on the endurable load cycles, especially at higher fatigue load levels. He explains this with the increasing contribution of macroscopic crack propagation to the overall load cycles and a resulting sensitivity to the maximum stress of the cyclic loading. The observation by *Marten* is also confirmed in experiments from *Dünkel* (1999) as well as *Schneider* (2011). Here, compliantly, bolt fatigue tests with a constant low stress ratio  $R = 0.1$  resulted in higher endurable load cycles in the upper HCF, compared to tests with constant mean stress  $S_m = 0.7 \cdot R_{p,0.2}$ . Only a minor effect on the endurance limit was observed, with slightly lower values for the test series with  $R = 0.1$ . Moreover, indicating the influence of low mean stress level and inadequate stress distribution, fatigue cracks were found outside the first load-bearing turn of the thread.

In addition to the axial bolt force, preloading by torque causes torsion inside the bolt thread. Directly after removing the tightening tool, the torsional stresses are partly relieved. In experiments from *Schneider* (1992) on bolts, rolled before heat treatment, a preload obtained by torque instead of axial loading by the testing machine had no significant impact on the bolts endurance limit, except from a widening of statistic scatter. Likewise, in experiments by *Alt et al.* (2007) only a minor improvement of the endurance limit was observed when preloading was obtained by torque. Contradictory results were reported by *Kuperus* (1974) for the upper HCF, where the bolts showed a reduction of fatigue strength when preloaded by torque. However, from the documentation it is not entirely clear whether the bolts were rolled before or after heat treatment.

### Bending

The geometric eccentricity of L-shaped ring-flanges leads to a certain overlay of the dominating axial stresses by bending. Thus, the actual loading conditions of large-size bolts in wind turbines differ from the common experimental set-up with pure axial nominal loads.

It is acknowledged that under identical nominal stress levels, a bending affected stress state causes a higher fatigue strength than pure axial loading, provided the bolts are previously axially preloaded (*Agatonović, 1973; Kampf, 1997; Seidel, 2001; Alt, 2005*). Accordingly, fatigue tests on preloaded high-strength bolts M48 (*Schaumann & Marten, 2008; Schaumann & Marten, 2009*) have confirmed a superior fatigue performance under cyclic bending than cyclic axial loading. Reasons for the improved fatigue strength under bending are a stronger stress-mechanical support effect and a favourable stress distribution within the paired thread. Moreover, in strain gauge measurements from *Alt (2005)* the measured bending moment varied along the longitudinal bolt axis, which he ascribed to an inconstant stiffness distribution.

As a consequence, bending may lead to a change of location of the maximum stress concentration and thus the location of fatigue crack initiation. However, while in the bending dominated investigations by *Alt* ruptures occurred regularly in the transition from thread to shaft, *Kampf* reported ruptures only in the first load-bearing turn of the thread. *Schaumann & Marten* found a strong manufacturer dependency for the location of crack initiation, with most failures occurring in the first load-bearing turn of the thread and under the bolt head, while only individual cases showed failures at the shaft transition. The described inconsistencies elucidate that under bending and locally plastic conditions the magnitude of stress concentrations is distributed more evenly along the bolt than under axial loading (*Kaiser et al., 1995; Schneider, 1992*). Generally, a higher sensitivity to boundary conditions and a substantial scatter of results is characteristic for fatigue tests under bending.

Unplanned bending stresses, caused for instance by imperfect head and nut bearing surfaces, may deteriorate the fatigue performance as they cause higher stress levels than anticipated by the outer loading (e.g., see *Kaiser et al., 1995*). An internal bending impact introduced by the non-symmetric initial pairing between bolt and nut decreases with progressing plasticization and thus may be considered as negligible under relevant preload levels (*Seybold, 2005*).

### Frequency

In the fundamental literature, the impact of the testing frequency on the fatigue strength of steel is considered to be small within a range of 1 – 1000 Hz, if corrosion, higher temperatures and load levels close to the material's yield strength are avoided (*Radaj & Vormwald, 2007; Haibach, 2006*). The applicable standard for fatigue testing of threaded fasteners DIN 969 (1997) defines a maximum testing frequency of 250 Hz, whereby temperature of the specimens should be limited to a maximum of 50°C. Accordingly, results from *Alt et al. (2007)* have shown an invariable endurance limit of steel bolts within a range of testing frequencies between approximately 100 – 500 Hz. Based on numerically calculated deformations inside the thread, the authors concluded that also at load levels in the upper HCF no frequency impact needs to be expected. Nevertheless, based on results which he

does not specifically present or discuss, *Dünkel* (1999) reported of a reduction of bearable load cycles in the upper HCF range when reducing the testing frequency by a decade from 13 Hz to 1.3 Hz. A slight reduction of the fatigue strength at low test frequency and higher load levels is also present in test results from *Berger et al.* (2008) for a comparison between 20 Hz and 2 Hz; however the tests provide very limited statistical proof.

It could be assumed that rather low frequencies and resultant low strain rates in combination with local plastic strains may lead to a certain aggravation of the fatigue strength of bolts at high load levels. Considering common natural frequencies of wind turbine structures, load frequencies around and lower than 1 Hz are of particular practical relevance. However, for an economical and time efficient obtainment of statistically relevant results, especially in the transition region to the endurance limit, testing with such frequencies is not feasible. Especially for low frequencies, the impact on the fatigue strength of bolts is not conclusively investigated.

### **Geometry- and size effects**

As discussed in section 2.1.2, the notch geometry is a decisive factor for the fatigue strength of HV-bolt assemblies. Generally, the geometry as well as tolerances of the ISO metric threads of HV-bolts are standardized within the standard series DIN 13, ISO 68-1 and ISO 965, respectively. According to *Wiegand et al.* (2007) within the range of regulated tolerances regarding angle and overlap of the V-shaped flanks of the paired thread, no significant impact on the stress concentration and thus on the fatigue performance need to be expected. Only for flank overlaps notably below the defined tolerances the notch stress concentration increases (*Kaiser et al.*, 1995; *Seybold*, 2005; *Marten*, 2009). However, the specific normatively defined geometric properties of nuts for HV-bolts (DIN EN 14399-4, 2015; DASt - Guideline 021, 2013) in terms of thread engagement length and wrench width lead to an increased maximum stress concentration compared to regular ISO fasteners and a reduction of fatigue strength of about 10 % (*Weber*, 2010).

The ratio of nominal diameter and pitch of the thread  $d/p$  increases at larger bolt diameters (e.g., M24:  $d/p = 8$ ; M72  $d/p = 12$ ). *Seybold* (2005) found in numerical studies on bolt size M24 with varying thread pitches that under identical nominal stresses an increasing  $d/p$ -ratio (i.e., decreasing thread pitch) leads to an increasing stress concentration and thus reduced analytically calculated endurance limit. Thereby, he qualitatively confirmed experimental fatigue analyses from *Thomala* (1978) on identical thread geometries. Even though a finer thread (i.e., higher  $d/p$ -ratio) causes a sharper notch geometry, it may also lead to a more homogenous stress distribution and a certain stress relief of the first load-bearing turn. Thus, the effect of an increased  $d/p$ -ratio on the fatigue strength depends on the bolt material characteristics and is more pronounced for higher-strength materials (*Wiegand & Strigens*, 1970).

Based on test results for bolt sizes between M6 and M24, *Thomala* (1978) found an approximately hyperbolic correlation between bolt diameter and experimentally determined endurance limit. He partly ascribed this to the increasing notch sharpness caused by the changing  $d/p$ -ratio. Accordingly, a reduction of fatigue strength with increasing diameter is especially pronounced for smaller bolt diameters. Based on an empirically derived approximation formula, which also found entrance into

normative regulation (VDI Guideline 2230, 2015), he concluded that the diameter effect should mostly be resolved until bolt diameter M40. However, he also emphasized that possibilities for further extrapolation are limited because of the pronounced changes of the  $d/p$ -ratio in the diameter range  $> M40$ .

Additionally to the  $d/p$ -ratio, the diameter dependency of the fatigue strength of bolts is affected by a variety of interacting size effects, which according to *Kloos* (1976) can be subdivided into stress-mechanical, statistical, technological and surface-technological size effect.

The stress-mechanical size effect considers the support effect of the material, surrounding the notch root. The stress gradient in lateral direction throughout the bolt decreases with increasing bolt diameter. This leads to a larger area of strongly loaded material in the vicinity of the notch root and hence a reduced support effect for larger bolts (see also Chapter 2.2.5).

The statistical size effect is substantiated on the assumption that damage relevant defects at the most critically loaded zone at the notch are statistically more likely to occur with increasing size of a structural component. Consequently, the probability of micro crack initiation is higher for large diameters. However, according to studies from *Böhm & Heckel* (1982) on a representative high-strength material, the impact of the statistical size effect decreases with increasing diameter of a specimen. Moreover, the effect is just slightly pronounced for strongly notched components.

Furthermore, production and surface treatment procedures, which can influence the fatigue strength, may vary in dependence of the bolt diameter. Fatigue-relevant diameter dependencies caused by the manufacturing process, such as mechanical forming or heat treatment, are described by the technological size effect. The surface-technological size effect considers dependencies between specific boundary layer conditions (e.g., residual stresses), component thickness and fatigue strength. Both effects are strongly dependent to the individual production process. The general impact of different surface conditions to the fatigue strength of bolts is further discussed in the subsequent section.

Due to the changes of the  $d/p$ -ratio, threads of bolts with different diameters are not geometrically similar. Moreover, the geometry dependent variations of fatigue characteristics are affected by a variety of interacting parameters. Thus, an isolated experimental investigation of size effects for bolts is hardly achievable and fatigue tests on customary bolt assemblies mostly allow a general assessment of the changing fatigue performance with increasing diameter.

### **Surface conditions and corrosion protection**

The surface conditions may severely affect the fatigue performance of bolts. For HV-bolts, changes of the surface conditions especially result from the applied corrosion protection.

Popular as a very reliable and long lasting corrosion protection system is hot-dip galvanizing, where in an elaborate production process (e.g., see *Maaß & Peißker*, 2008) a durable alloy surface layer is established by immersing the steel or iron component into a hot bath of molten zinc. The process can be performed as normal temperature (NT;  $\sim 440\text{-}470^\circ\text{C}$ ) or high temperature (HT;  $\sim 530\text{-}620^\circ\text{C}$ )

hot-dip galvanizing. The application for bolts is standardized according to DSV-GAV (2009), DAST - Guideline 022 (2009) and DIN EN ISO 1461 (2009).

Comprehensive experimental investigations by *Ungermann et al.* (2014) and *Simonsen* (2015) have conclusively proven the considerable impact of NT hot-dip galvanizing on the fatigue strength of structural steel. Based on the investigations, mainly on welded or flat structural details relevant for steel bridges but also on specimens with bolt-alike notch geometry, *Simonsen* (2015) recommends a reduction of the endurance limit of 20 % compared to uncoated black components. For coating thicknesses  $> 100 \mu\text{m}$  a further deterioration of the fatigue strength needs to be considered. Especially the test results on bolt-alike notched specimens also clearly show a reduction of bearable load cycles in the upper HCF. The results confirm findings for hot-dip galvanized HV-bolt assemblies by *Weber* (2010) and *Berger et al.* (2008) as well as further earlier investigations (see *Wiegand et al.*, 2007). Nevertheless, one test series by *Weber* as well as experiments from *Lacher* (1986) showed a slightly lower reduction of the endurance limit of about 12 %.

Microscopic analyses of metallographic sections from aborted fatigue tests on flat steel specimens with constant stress ratio  $R = 0.05$  (*Ungermann et al.*, 2014; *Ungermann et al.*, 2015) as well as bolt-alike notched specimens with constant mean stress  $S_m = 0.7 \cdot R_{p,0.2}$  (*Oechsner et al.*, 2015; *Simonsen*, 2015) could compliantly document the underlying failure mechanism caused by hot-dip galvanizing (see Figure 2-6). Thereby, shrinkage cracks, present in the initial state prior to loading in the brittle  $\zeta$ - and  $\delta_1$ -phases of the iron-zinc alloy surface layer, reached up to the ferocious base material. Under cyclic loading, the fatigue cracks in the base materials were initiated at the location of the shrinkage cracks. It could be precluded that already in the initial state pre-damage was caused to the base material (e.g., due to liquid metal assisted cracking, LMAC). Thus, the authors elaborated the model assumption that a microscopic notch effect at the tips of the shrinkage cracks leads to stress peaks at the base material, which cause the premature fatigue crack initiation (i.e., an “extension” of the shrinkage cracks into the base material).

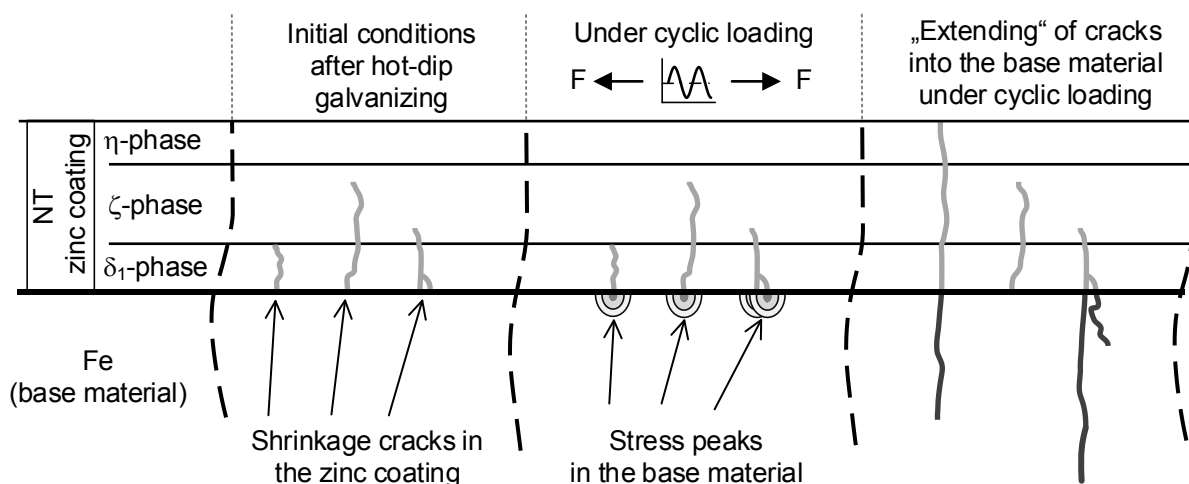


**Figure 2-6: Schematic depiction of fatigue crack initiation of hot-dip galvanized structural components acc. to *Ungermann et al.* (2015)**

The investigations performed by *Simonsen* suggest that the described effect leads to a comparable reduction of fatigue strength also for HT hot-dip galvanized components. Correspondingly, fatigue tests from *Valtinat* (1994) have shown an equal fatigue performance of NT and HT hot-dip galvanized HV-bolts of diameter M30. Thereby, bolts were initially preloaded by torque, approaching the plastic range at  $\sim 0.9 \cdot R_{p,0.2}$  (the following fatigue tests were performed under  $S_m = \sim 0.7 \cdot R_{p,0.2}$ ). The initial high preloading did not lead to a severe deterioration of fatigue strength, as it could have been expected to occur by a potential pre-damage of the base material. This is in accordance with the findings of *Simonsen*, which show that the zinc coating does not affect the initial state of the base material, provided hot-dip galvanizing is applied properly in accordance with the given normative protocols. Nevertheless, according to current German national guideline DSV-GAV (2009), HT hot-dip galvanizing is only allowed for high-strength bolts up to diameters  $\leq M24$  because of risk of LMAC.

Concerning alternative corrosion protection systems, *Kremer* (2005) found a notable reduction of fatigue strength in the transition region to the endurance limit and upper HCF also for electro-chemically galvanized bolts. Likewise, in test results from *Weber* (2010) bolts treated with zinc flake coating showed a lower fatigue strength than black uncoated bolts. For both protection systems a fatigue strength reducing tendency was also confirmed by *Simonsen* (2015) on bolt-alike specimens. He showed that after loading cracks are present in the surface coating of electrogalvanized specimens. How and whether these cracks cause a reduction of fatigue strength is not yet investigated. For zinc flake coated specimens no indications for an underlying damage mechanism could be found and the cause of the reduction remains unclear. Nevertheless, it needs to be emphasized that under corrosive impact, hot-dip galvanized or otherwise protected components provide a vastly superior fatigue resistance than unprotected steel.

Additional to the corrosion protection system itself, lubrication of the thread may have an effect on the fatigue performance of bolts, for example due to altered friction properties. *Thomala* (1978), *Dünkel* (1999), *Kremer* (2005) and *Weber* (2010) compliantly found an improved fatigue strength of bolts with liquid lubricated threads compared to degreased bolts. However, *Seybold* (2005) and *Marten* (2009) report only of a moderate influence of an increasing friction coefficient  $\mu$  to the analytically calculated loading conditions in paired threads of bolt assemblies. The specific effect imposed by lubrication to the fatigue strength of bolts is not yet conclusively quantified.

### 2.1.5 Experimental background for large-size HV-bolts

The majority of the aforementioned studies in the previous chapter were realized on smaller bolts, mostly limited to diameters  $\leq M24$ . Publically available fatigue test results with representative characteristics for HV-bolts with larger diameters are very limited to this date. This can be attributed to the high test facility requirements and corresponding costs. Fatigue investigations on tension rod systems which reach into high diameter ranges (e.g., *Unglaub et al.*, 2015) provided limited comparability to customary HV-bolt sets and vice versa because of different elementary characteristics concerning materials and production. In order to avoid the uncertainties deriving from these parameters and to enable clear interpretation, it is focused on the subsequently described studies on large-size HV-bolts. In all investigations, the HV-bolts were rolled before heat treatment.



The previously cited investigations from *Valtinat* (1994) were performed on relatively large-size HV-bolts M30. Due to the implemented testing program, the drawn conclusions mainly concern the equivalence of fatigue performance in direct comparison between NT and HT hot-dip galvanized bolts and the course of the S-N curves in the upper HCF. A statistical determination of the endurance limit was not performed. Under a similar mean stress level  $S_m = 0.7 \cdot R_{p,0.2}$ , a complete S-N curve on NT hot-dip galvanized M36 HV-bolts sets was statistically determined within the test series by *Berger et al.* (2008), which apart from this was mainly focussed on smaller diameters.

With the aim of establishing a more reliable design basis for HV-bolt sets with larger diameters, an extensive test series on HV-bolt sets M48 was performed at the Institute for Steel Construction, Leibniz Universität Hannover (*Marten, 2009, Schaumann & Marten, 2008*). In order to achieve a high degree of general validity, NT hot-dip galvanized bolt sets from three different manufacturers (and consequently materials and manufacturing batches) were treated as one single set of samples within the statistical evaluation of the S-N curve. Due to the capacity of the applied resonance testing machine (testing frequency approx. 60 Hz), the mean stress level for the axial load fatigue tests had to be reduced to  $S_m \approx 0.15 \cdot R_{p,0.2}$ . As discussed in section 2.1.4, it needs to be presumed that this has led to a certain overestimation of endurable load cycles, especially at higher load levels. Moreover, the low mean stress level and testing with specimens from differing manufacturing batches and production chains has led to relatively large scatter of results. Nevertheless, the test series established a decisive validation background of normative regulations required for the practical application of large-size bolts (see following section 2.1.6). However, the results emphasized the importance for further fatigue tests on large-size HV-bolt sets to be performed under a representative mean stress level.

Additionally to the main objective of axially loaded fatigue tests, the experiments by *Schaumann & Marten* (2008) also included fatigue tests under bending loading on the same set of samples from different bolt manufacturers. The results have been discussed in section 2.1.4. Regardless of identical nominal production conditions (NT hot-dip galvanized, rolled before heat treatment) for both loading conditions the results have revealed a notably manufacturer dependent fatigue performance.

### 2.1.6 Normative situation

Applicable design S-N curves for axially loaded bolts are given in Eurocode 3 (EC 3, DIN EN 1993-1-9, 2010), as decisive standard for civil engineering applications in Europe, as well as in the internationally renowned VDI Guideline 2230 (2015), which has been developed for application of heavy duty bolted joints in mechanical engineering.

For fatigue strength calculation VDI 2230 distinctly differentiates between the production sequence (i.e., rolled before or after heat treatment) and considers explicit reduction factors considering the HV-nut geometry (10%) and a hot-dip galvanized surface layer (20%). In contrast, EC 3 does not provide any possibilities for differentiation regarding geometry, production or boundary layer and the defined fatigue class can be interpreted as a lower bound for the possible configuration of axially loaded bolt assemblies.

Even though the regulations lack corresponding experimental background data, they allow application also to larger bolt diameters. However, both consider a reduction of fatigue strength with increasing bolt diameter  $d$ . The calculation of the reference values for the fatigue strength at  $N = 2 \cdot 10^6$  load cycles for the decisive Eurocode 3 fatigue class FAT 50 is given in Eq. 2-5, and according to VDI 2230 for hot-dip galvanized HV-bolt sets, rolled before heat treatment, in Eq. 2-6. In order to provide better comparability, different to the standard, the fatigue strength according to Eurocode 3 is stated in stress amplitudes instead of stress ranges ( $S_a = \Delta S/2$ ).

Eurocode 3 (FAT 50,  $k_s$  for  $d > 30$  mm):

$$S_{a,c}(N = 2 \cdot 10^6) = \frac{\Delta S_c}{2} \cdot k_s = \frac{50}{2} \cdot \left(\frac{30}{d}\right)^{0.25} \tag{Eq. 2-5}$$

VDI 2230 (rolled before heat treatment (RBHT), HV, hot-dip galvanized):

$$S_{a,D}(N = 2 \cdot 10^6) = 0.7 \cdot 0.85 \cdot \left(\frac{150}{d} + 45\right) \tag{Eq. 2-6}$$

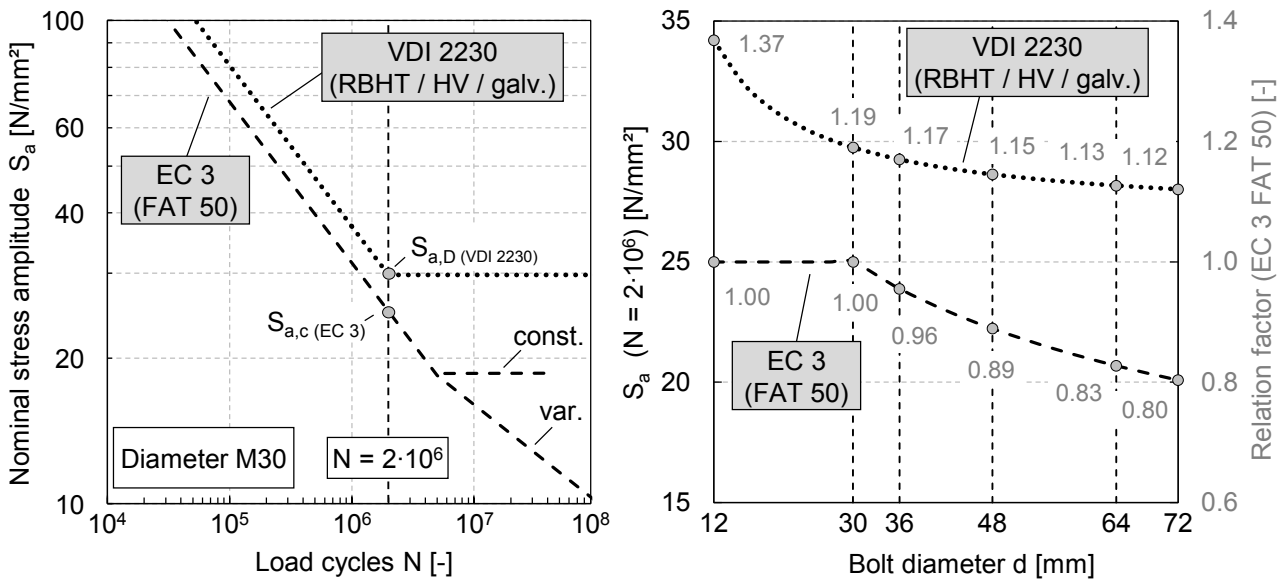


**Figure 2-7: Normative S-N curves from EC 3 and VDI 2230 (left) and reference value of fatigue curves at  $N = 2 \cdot 10^6$  load cycles as a function of bolt diameter (right)**

The juxtaposition of the S-N curves of both regulations and their reference values according to Eqs. 2-5 and 2-6 in Figure 2-7 highlight that over the entire diameter range the fatigue strength is regulated considerably more conservative in EC 3 than in VDI 2230. Where exceeding the range of experimental validation (see section 2.1.4), the course of the diameter dependent function of the endurance limit in VDI 2230 is supported by numerical estimations (see *Schaumann & Marten, 2009*). Eurocode 3, besides not accounting for an improved fatigue strength of smaller bolts, also estimates a more strongly pronounced diameter dependent reduction for bolts  $> M30$ . For both diameter dependent reduction functions no experimental verification for large-size HV-bolts exists.

It needs to be noted that the reference values of fatigue strength at  $N = 2 \cdot 10^6$  load cycles of both regulations are related to different characteristic values of the S-N curves and are based on different statistical evaluation procedures (see Chapter 3.6.2). Moreover, in VDI 2230 the value  $S_{a,D}$  denotes the knee point to the endurance limit with succeeding horizontal progression of the S-N curve. In EC 3 a transition to the endurance limit is not assumed until  $N = 5 \cdot 10^6$  load cycles.

Analogously to VDI 2230, EC 3 allows the consideration of a following horizontal S-N curve progression for constant amplitude loading or load collectives which maximum values do not exceed the respective endurance limit. However, as dominating case in structural engineering, the S-N curves in EC 3 are mainly developed for service load verification with variable amplitudes and application of *Miner's* linear damage accumulation, see section 2.1.3. For this case, after the knee point at  $N = 5 \cdot 10^6$  the progression of the S-N curve is defined in accordance with *Haibach's* modification of *Miner's*-rule (see Section 2.1.3). A threshold value of the fatigue strength with following horizontal progression also under variable amplitude loading is designated at  $N = 10^8$  load cycles. The S-N curves from VDI 2230 were originally not intended for a service load verification with load levels both above and under the endurance limit. To enable service load verification, a recommendation for a *Miner's* rule modification, which can be applied to the S-N curves from VDI 2230, is given by *Weber* (2010).

Specific adaptations for fatigue verification of bolts in support structures for wind turbines are made in relevant guidelines such as DIN 18088-3 (2019), DNVGL-ST-0126 (2016) and DIBt (2012). Therein it is defined that, due to the lack of experimental knowledge, a consideration of the threshold value of the fatigue strength, defined in EC 3, is not permissible. Moreover, DNVGL-ST-0126 (2016) allows a fatigue classification of bolts, rolled before heat treatment without hot-dip galvanizing into a higher EC 3 fatigue category FAT 71 and a modified fatigue class FAT 71\* for bolts rolled after heat treatment. Since bending affected stress states show an improved fatigue life compared to axial loading (see section 2.1.4) the present contribution of bending, arising from the eccentric geometry of the ring-flange, can be regarded uncritical when using the design fatigue curves, representative for pure axial loading. However, this only applies if the bending stresses are actually considered in the structural load analysis of the bolts. If the bending stresses are neglected, the above mentioned fatigue classifications do not apply. Instead, for all bolts a reduced fatigue class FAT 36\* is to be used, in order to compensate for potentially underestimated bolt stresses. Generally, all mentioned fatigue classes need to consider the respective diameter reduction factor  $k_s$  as included in Eq. 2-5.

## 2.2 Fatigue assessment with local concepts

### 2.2.1 Local fatigue assessment approaches

Alternatively to the nominal stress concept, used as basis for fatigue design according to the previously described normative regulations, approaches based on the local loading conditions and deformations at the notch root have been developed. These enable fatigue assessment without the requirement of experimentally determined S-N curves for the entire structural detail. Thereby, different influencing factors may be considered separately, which otherwise are collectively included in the constructional member's design S-N curve. Thus, to a certain degree local concepts provide the possibility for an isolated investigation of different aspects to the overall fatigue performance without the necessity of demanding experimental test series with changing attributes. However, since the models are based on the distinct characteristics of the base material, their application requires knowledge about specific material parameters. Moreover, local concepts are affected by accuracy and quality of the necessary model representations of the actual physical behaviour. Different approaches exist for the estimation of endurable load cycles until initial cracking and of fatigue life between crack initiation and rupture. In the sequel, the local concepts, which are most relevant for the fatigue assessment of threaded fasteners, are introduced. For detailed descriptions it can be referred to fundamental literature such as *Radaj & Vormwald (2007)*, *Haibach (2006)*, *Bannantine et al. (1990)*.

#### Strain-life approach

The local strain-life approach follows the assumption that material behaviour and damage mechanisms at the notch root of a structural component are equivalent to a smooth unnotched specimen under uniaxial loading, see Figure 2-8, left. Since the fatigue driving plastic strains caused by the notch effect are confined in a local area at the notch root, the plastic zone is usually surrounded by solely elastically deformed material. Due to the constraint of its elastic surrounding the plastic region is considered to follow a cyclic hysteresis with steady elastic-plastic strains instead of steady stresses, even though the nominal loading is stress-controlled. Hence, strain-controlled laboratory tests on unnotched specimens are used to determine the required material characteristics.

An emulated local stress-strain response at the notch root based on the obtained material behaviour (Figure 2-8, right) and the material's strain-life curve, providing the relation between strain amplitude and endurable load cycles, enable the fatigue life prediction. Since the strain-life curve is usually determined for stress and strain relation  $R = -1$ , mean stress dependencies need to be considered by appropriate damage parameters, see section 2.2.4. The failure of a smooth specimen without elastic constrains is approximately equivalent to the formation of an initial technical crack at a notch root of the structural component, see *Radaj & Vormwald (2007)*. Therefore, the strain-life concept provides load cycle numbers only until technical crack initiation. The succeeding crack propagation life needs to be assessed separately.

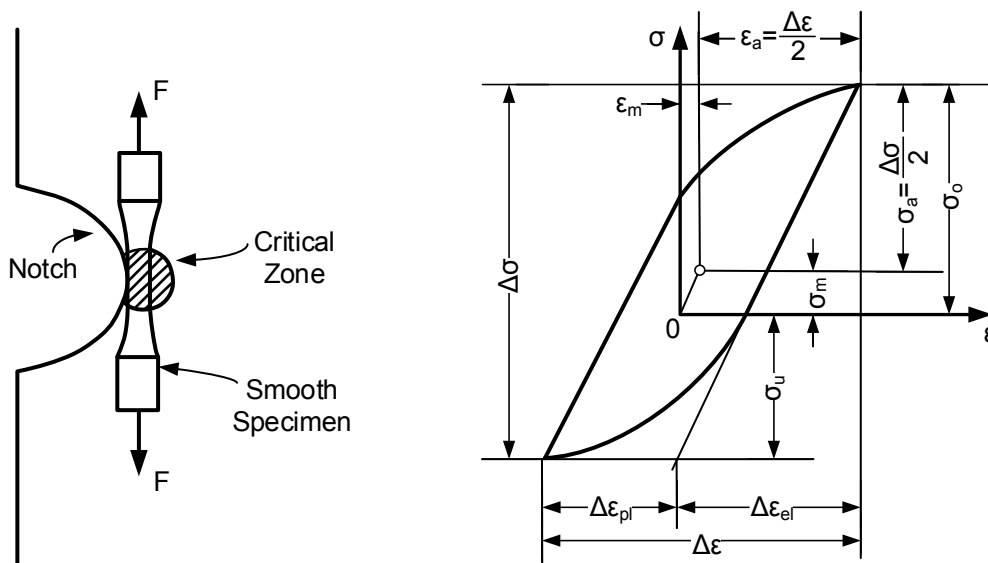


**Figure 2-8: Equivalence of critical material volume at notch root and unnotched specimen acc. to Bannantine et al. (1990) (left) and denotations at hysteresis of local stresses and strains acc. to Hainbach (2006) (right)**

### Fracture mechanics approach

The application of linear elastic or elastic-plastic fracture mechanics assumes the presence of an already existing crack or crack alike defect. Linear elastic fracture mechanics may be applied if plastic deformation at the crack tip are small compared to the size of the crack and cracked component, which is common for materials with brittle failure behaviour. However, even for materials which exhibit a certain amount of ductility, the elementary assumption for application of linear elastic fracture mechanics remains valid, see Bannantine et al. (1990).

Most commonly in engineering structures the decisive loading mode is a tensile surface displacement perpendicular to the crack surface. Commonly applied as driving load characteristic is the cyclic range of the stress intensity factor at the tip of the crack  $\Delta K$  (henceforth denoted as cyclic stress intensity). It is calculated proportional to the nominal loading and in dependence of crack length and geometric properties with respective model formulations.

Fatigue crack growth curves, describing the resistance against propagation of cracks, can generally be subdivided into three phases, see Figure 2-9. Thereby, propagation only occurs if a threshold cyclic stress intensity  $\Delta K_{th}$  is exceeded. The succeeding stable crack propagation is commonly described by empirical Paris' law (established by Paris, 1962 and Paris & Erdogan, 1963), which follows a linear path in double logarithmic scale (Eq. 2-7). Therein, the crack growth rate  $da/dN$  is calculated as function of the cyclic stress intensity  $\Delta K$  with the material, stress ratio and environment dependent parameters  $C$  and  $m$ .

$$\frac{da}{dN} = C \cdot (\Delta K)^m \quad \text{with} \quad \Delta K_{th} < \Delta K < \Delta K_c \quad \text{Eq. 2-7}$$

The critical cyclic stress intensity  $\Delta K_c$  indicates the transition to the final phase of unstable crack growth, shortly followed by rupture. Using *Paris' law*, fatigue life can be calculated by integration within the limits of the considered initial and final crack depth. Depending on the applicable model for determination of  $\Delta K$ , the correlation of the cyclic stress intensity to changing geometric crack properties often makes a numerical integration necessary.

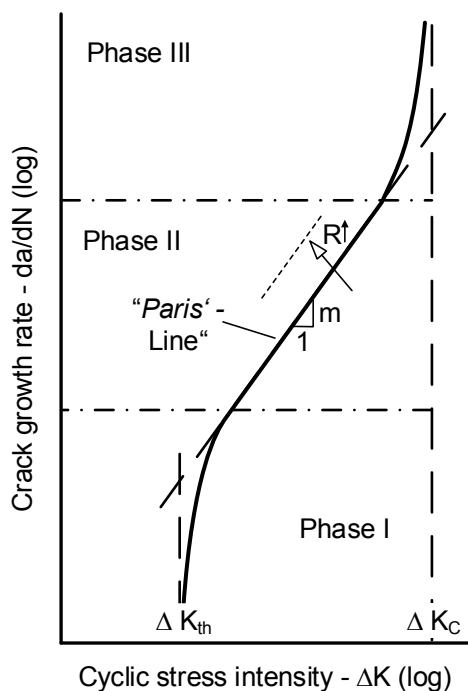


**Figure 2-9: Schematic depiction of fatigue crack growth rate curve (adapted from Haibach, 2006)**

The application of *Paris' law* and linear elastic stress intensity is only appropriate when assessing cracks of macroscopic scale with crack depths  $a \geq 0.1$  mm, see *Radaj & Vormwald (2007)*. This is due to short-crack formation and propagation being affected by microscopic material phenomena, which are not accurately covered in the conventional empirical approach, described above. Moreover, the general assumption of locally restricted plastic zones compared to the crack size is not valid for microscale cracks, which more likely are embedded into the plastic zone. Microscopic small-crack propagation is more suitably described by use of J-integral formulations (e.g., *Vormwald, 1989*; see section 2.2.4).

### 2.2.2 Material characteristics

#### Cyclic stress-strain and strain-life behaviour

For application of the strain-life concept, practical representations of base material properties regarding the relations between cyclic stresses and strains as well as strain amplitude and fatigue life are required. In Eq. 2-8 the strain - fatigue life ( $\epsilon_a-N$ ) relation, known in the literature as the relation according to *Manson, Coffin* and *Morrow*, is given as function of the four material constants: fatigue strength coefficient  $\sigma'_f$ , fatigue strength exponent  $b$ , fatigue ductility coefficient  $\epsilon'_f$  and fatigue ductility exponent  $c$ .

$$\epsilon_a = \epsilon_{a,e} + \epsilon_{a,p} = \frac{\sigma'_f}{E} (2N)^b + \epsilon'_f (2N)^c \tag{Eq. 2-8}$$

Originated over time from a number of different studies, it is formed by the summation of elastic and plastic strain contributions to the fatigue damage. A historical derivation can be found for example in *Christ* (1991). In double logarithmic scale the elastic and plastic terms of the equation form linear lines, whereby the curve of total strain asymptotically approximates the plastic line at high and the elastic line at lower amplitudes, see Figure 2-10, left.

Under strain-controlled cyclic loading, the majority of metals tend to either cyclic softening or hardening behaviour, where the cyclic stress-strain relation deviates from its initial monotonic path. Usually saturation occurs during the early loading phase well before half of the load cycles to failure, see *Haibach* (2006). For the remainder of the endurable load cycles until initial cracking the material behaviour can then commonly be characterised as approximately stabilized and under constant loading the cyclic stress-strain hysteresis forms a closed loop. The conjunction of the peak values of stabilized cyclic hysteresis with different strain amplitudes leads to the material's cyclic stress-strain curve (Figure 2-10, right). It is described by the three parameter approach according to *Ramberg & Osgood* (1943), where the relation between strain amplitude  $\epsilon_a$  and stress amplitude  $\sigma_a$  is given in dependence of *Young's modulus* (*Hooke's law*) and a supplemented plastic power law with the strain hardening coefficient  $K'$  and exponent  $n'$  (Eq. 2-9). Commonly thermally treated high-strength and alloyed materials, as applied for HV-bolts, exhibit a cyclic strain softening behaviour, see *Christ* (1991), *Bargel & Schulze* (2012).

$$\epsilon_a = \epsilon_{a,e} + \epsilon_{a,p} = \frac{\sigma_a}{E} + \left( \frac{\sigma_a}{K'} \right)^{1/n'} \tag{Eq. 2-9}$$

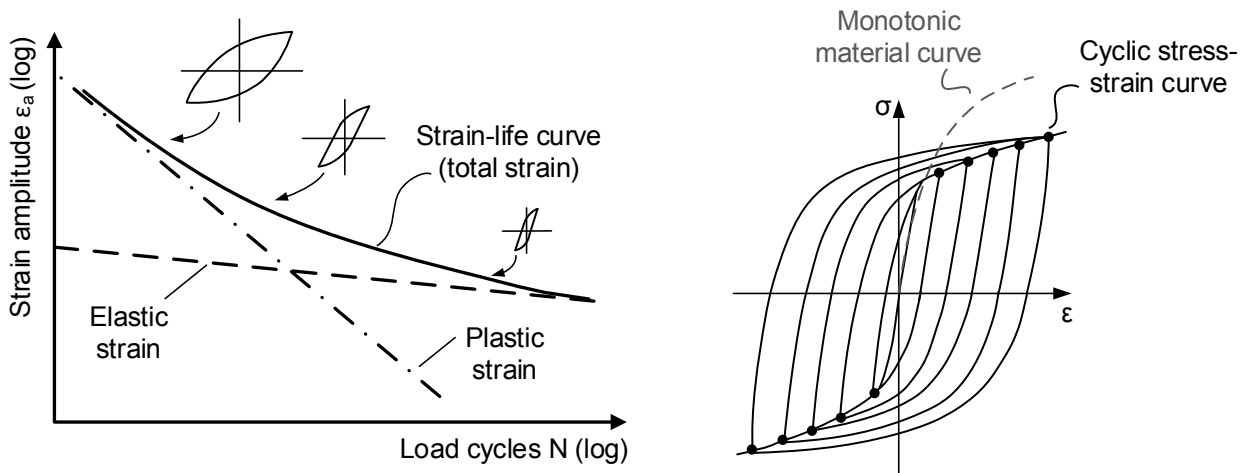


**Figure 2-10: Schematic depiction of strain-life curve with elastic and plastic parts in dependence of hysteresis shape (left) and cyclic stress-strain curve as conjunction of peak values of stabilized cyclic hysteresis loops for material with cyclic softening behaviour (right) (adapted from *Bannantine et al.*, 1990)**

In order to achieve compatibility between the *Ramberg-Osgood* equation (Eq. 2-9) and the strain-life curve according to *Manson, Coffin and Morrow* (Eq. 2-8), in terms of necessarily identical proportions between elastic and plastic contributions to the total strain amplitude, the following conditions need to be satisfied:

$$K' = \frac{\sigma'_f}{(\varepsilon'_f)^{n'}} \quad \text{Eq. 2-10}$$

$$n' = \frac{b}{c} \quad \text{Eq. 2-11}$$

As illustrated in Figure 2-10, after a given point of load reversal, due to the *Bauschinger* effect, the path of the cyclic hysteresis does not follow the original cyclic stress-strain curve. Known as the *Masing* model (*Masing, 1926*), it is established that from its origin a de- or increasing hysteresis branch can adequately be approximated in the form of the stabilized cyclic-stress strain curve with doubled stresses and strains. Accordingly adapting the *Ramberg-Osgood* equation (e.g., see *Bannantine et al., 1990*), from a point of load reversal a hysteresis branch with strain range  $\Delta\varepsilon$  and stress range  $\Delta\sigma$  can be described with Eq. 2-12:

$$\Delta\varepsilon = \frac{\Delta\sigma}{E} + 2 \left( \frac{\Delta\sigma}{2K'} \right)^{\frac{1}{n'}} \quad \text{Eq. 2-12}$$

### Transient effects

As described, the cyclic stress-strain curve considers the hardening or softening characteristic of a material in their stabilized form. Thus, the transition period between initial loading and saturation is usually neglected in analytical calculations and stabilized conditions are assumed throughout the entire fatigue life. While cyclic softening, as characteristic for high-strength bolt materials, is considered to occur independently of the mean strain level, preloading and consequently tensile mean stresses and strains significantly different from zero cause additional material transitions. Under strain-controlled cyclic loading this is exhibited by a successive reduction of the mean stress level of the hysteresis (see *Christ, 1991*). The magnitude of the effect, denoted as cyclic relaxation, is dependent on material as well as mean strain level and magnitude of the strain amplitude. Since it typically represents stabilized material conditions with stress and strain ratio  $R = -1$ , the cyclic stress-strain curve does not cover cyclic relaxation. Thus, for its consideration the effect needs to be investigated separately. The two different transient effects, which are most relevant for the assessment of high-strength bolts, are illustrated in Figure 2-11.



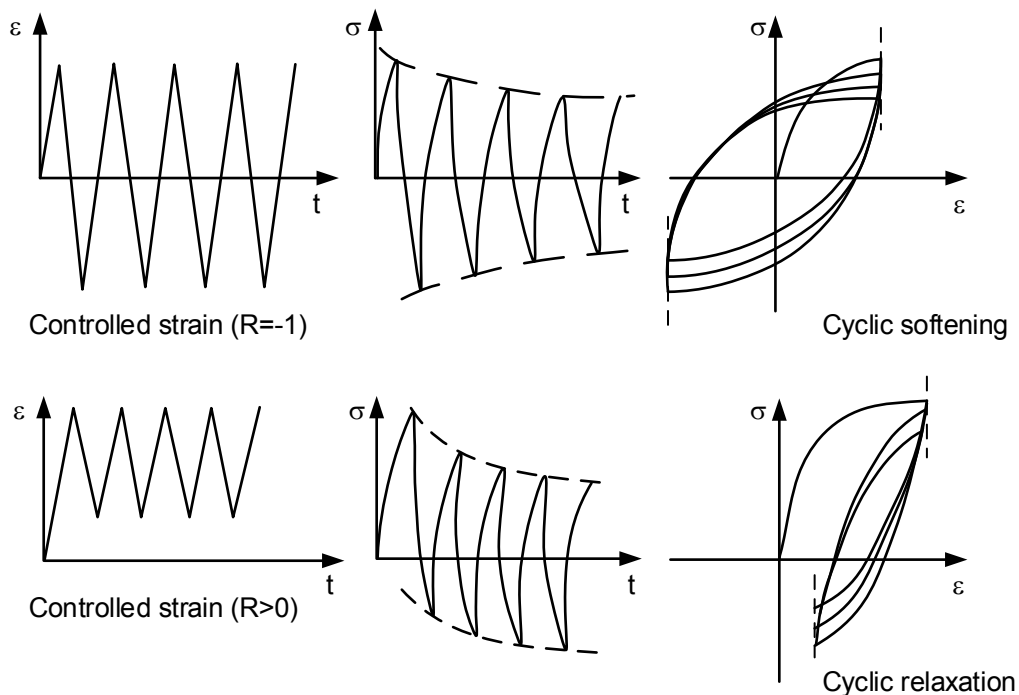


**Figure 2-11: Transient material effects under strain controlled loading acc. to Christ (1991)**

### Determination of cyclic material data

For determination of required material parameters uniaxial, strain-controlled cyclic material tests on unnotched specimens are necessary. Commonly, these are performed without mean strain ( $R_{\epsilon} = -1$ ). Most accurately, cyclic material parameters are determined within a comprehensive series of constant amplitude tests until crack initiation in order to experimentally determine the strain-life curve of the material. The information about the cyclic stress-strain relation results inherently as a by-product of such tests. To limit testing efforts the conduction of strain-controlled tests is usually restricted to moderate load cycle numbers in the upper high-cycle fatigue regime. At load levels close to the endurance limit the relation between local stresses and strains becomes largely linear. Hence, for determination of the endurance limit stress-controlled tests may be performed which enable higher testing frequencies and facilitate conduction. Nevertheless, a precise determination of the strain-life curve requires high experimental efforts, which in many cases may exceed available or reasonable expenditures.

As an alternative *Vormwald & Seeger* (1988) have proposed a simplified approach, where all required material parameters may be derived with only two test specimens. The tests are performed as strain-controlled Incremental-Step-Tests (IST), first developed by *Landgraf et al.* (1969) for the accelerated determination of the cyclic stress-strain curve. Thereby, cyclic loading is established as a sequence of blocks with continuously increasing and declining amplitudes. It has been shown by *Vormwald & Seeger* that sequence effects have a minor influence for the given load history of IST. Thus, based on the analytical descriptions of material characteristics according to Eq. 2-8 to Eq. 2-12 and under the premise of linear damage accumulation, the evaluation of load cycles until crack initiation enables the additional characterization of the strain-life curve. In the high cycle fatigue range,

the method is proven to provide a close approximation of strain-life curves of low alloy steels, derived from constant-amplitude test. Accuracy decreases with lower strain amplitudes. An endurance limit cannot be determined. Best results are achieved when using two IST with maximum strains differing by a factor of 2 or higher, whereby influence of natural scatter to the results is limited. In order to ensure compliant stress-strain relations, both strain levels should include a notable plastic proportion. When estimating the cyclic ductility exponent  $c$  (which represents the slope of the plastic part of the strain-life curve) according to *Morrow* (1965) or *Manson* (1965) an approximation of the strain-life curve can also be derived based on one single IST.

An analytical estimation of cyclic material parameters in dependence of its monotonic properties is proposed with the Uniform Material Law (UML), which was developed by *Bäumel & Seeger* (1990) based on collective cyclic material data. However, *Marten* (2009) emphasises the limited accuracy when using the UML for the fatigue estimation with the strain-life concept under loading conditions with high mean stresses.

For quantification of cyclic relaxation, *Schneider* (2011) suggests the conduction of additional strain-controlled material tests under a constant high mean strain  $\epsilon_m \gg 0$  with varying strain amplitudes. Alternatively, *Oechsner et al.* (2014) propose the analytical estimation of mean stress relaxation according to *Landgraf & Chernenkoff* (1988).

### 2.2.3 Computing of local stresses and strains

In traditional applications of local fatigue assessment concepts the local loading conditions at the notch root are approximated based on analytical approaches, most popular according to *Neuber* (1961) or in a modified version *Neuber* (1985). For application on bolted connections and threaded fasteners in general, these approaches are commonly supported by linear elastic finite element calculations which are used to compute the required notch stress concentration factor (e.g., *Marten*, 2009). Modern finite element software implementations and enhanced computational hardware capabilities enable and facilitate the direct numerical calculation of local stresses and strains by use of non-linear material implementations, making the application of classic analytical approaches virtually superseded. Nevertheless, for application to preloaded threaded fasteners *Oechsner et al.* (2014) still acknowledge analytical approaches as valid, yet slightly non-conservative approximations in order to simplify the calculation procedure and improve practicability.

For computation of local loading conditions inside the paired thread of bolt assemblies by use of finite element models, *Seybold* (2005) (bolt size M24), *Marten* (2009) (bolt size M48) and *Schneider* (*Schneider*, 2011; *Schneider et al.*, 2010) (bolt size M10) investigated the necessity of considering the actual continuous pitch of the thread, including an accurate representation of the thread run-out, within 3D model implementations. Considering linear elastic material conditions, all three concluded that no over critical effect of the circumferential thread variation is imposed to the maximum stress concentration and that for the sake of reduced modelling efforts the application of rotationally symmetric 2D models is acceptable. *Schneider* confirms this conclusion also for calculations with elastic-plastic material behaviour. Nevertheless, the results from *Marten* have shown a slightly higher elastic

notch stress concentration of about 10% for the full 3D model implementation. In his studies, this has led to a reduced analytically calculated fatigue strength in a comparable order of magnitude.

Based on his extensive sensitivity studies, *Seybold* (2005) provides reference regarding impact of mesh density inside the thread of bolt and nut to the result accuracy, thereby confirming findings from comparable investigations performed by *Hobbs et al.* (2003). Moreover, *Seybold* systematically discusses influences of sub-modelling techniques and circumferential element density for the 3D modelling approach and validates analytical calculations on electronic strain gauge measurements along the circumferential path of the thread of a geometrically similar magnified M6 bolt. Under elastic local loading conditions, the studies show good agreement between numerical and measurement results, especially concerning the stress maximum in the first load-bearing turn of the thread.

*Marten* (2009) further investigated the influence of different boundary conditions, considered in the aforementioned studies. Thereby, neglecting the washers and applying bearing conditions directly at the bottom surface of the nut led to considerably higher linear elastic stress concentrations, compared to a model with washers included and rough contact inside the parting lines. The additional inclusion of the complete flange package and additional contact surfaces between washers and flange plates only cause a marginal effect on the stress concentration. *Marten* explains the enhancement of the stress concentration factor with the restraint of the nut in radial direction caused by the direct bearing. The results confirm similar findings from *Feldmann* (1981) and *Alt* (2005), whereby experiments by *Alt* have shown that the stress concentration in the first load-bearing turn of the thread is directly affected by an increased stiffness of the nut bearing surface.

This puts the validity of the experimental validation given by *Seybold* (2005) into question, where constraints in the numerical model were directly applied to the nut, as these are bearing conditions which may not be supposed for the considered experimental investigation (see also *Marten*, 2009). Moreover, due to given uncertainties caused for example by strain gauge calibration, precision of gauge placement as well as imperfections, the expectable accuracy of such measurements, targeting for local stress concentrations, is generally limited. Nevertheless, the application of the finite element method for approximation of local stresses and strains inside the paired thread can be regarded as a strongly qualified tool in the analytical fatigue assessment of bolts.

As decisive loading characteristic once a macroscopic technical crack is established, the crack tip stress intensity  $K$  is commonly described by Eq. 2-13 in dependence of nominal stress  $S$ , crack depth  $a$  and a dimensionless geometry function  $Y(a)$ .

$$K = S \cdot \sqrt{\pi a} \cdot Y(a) \quad \text{Eq. 2-13}$$

Since until today no explicit geometry models exist for threaded bolt to nut connections, cylinder models with surface cracks (e.g., according to FKM-Guideline, 2006) are applied as alternative approximation. Recent investigations also consider the direct numerical simulation of crack propagation at threaded fasteners (see *Oechsner et al.*, 2014; *Eder et al.*, 2018).

## 2.2.4 Mean stresses and damage parameters

Since the underlying material parameters for application of the strain-life concept are typically derived for a stress ratio  $R = -1$ , so-called damage parameters are available to allow for loading conditions with mean stresses different from zero. Due to the regularly given high tensile mean load level, this becomes of special importance for HV-bolts. Damage parameters are used to adjust the calculation of bearable load cycles from the basis of the original strain-life curve. Their function may be interpreted as the ability to transfer loading conditions with arbitrary mean stress to fatigue damage equivalent loading conditions with mean stress  $\sigma_m = 0$ . The characterization of local loading condition with cyclic stress-strain curve and *Masing* behaviour, as input criterion for the damage calculation, remains unaffected. A discussion of the broad field of developed damage parameters can be found for example in *Haibach (2006)* or *Vormwald & Seeger (2015)*. In the sequel, three damage parameters are introduced, which are assessed in this dissertation in regard to their suitability for the application to preloaded large-size HV-bolts. Subsequently, an overview is given for consideration of tensile mean stresses in linear elastic fracture mechanics.

### Damage parameter $P_{SWT}$

Most commonly applied (see *Haibach, 2006, Vormwald & Seeger, 2015*) is the damage parameter  $P_{SWT}$  (Eq. 2-14) proposed by *Smith, Watson and Topper (Smith et al., 1970)*. It is distinguished by its relatively straightforward application. Based on the local hysteresis (for definition of denotations see Figure 2-8) damage relevance is contributed to the product of upper stress  $\sigma_o$  and strain amplitude  $\varepsilon_a$ .

$$P_{SWT} = \sqrt{(\sigma_a + \sigma_m) \cdot \varepsilon_a \cdot E} = \sqrt{\sigma_o \cdot \varepsilon_a \cdot E} \quad \text{Eq. 2-14}$$

The damage relevant contribution can be interpreted as density of the strain energy of the upper part of the hysteresis, see *Radaj & Vormwald (2007)*. Making allowance to the fact that the damage parameter must be valid for all possible mean stresses, including  $\sigma_m = 0$ , the mean stress independent damage parameter (P) - life curve (i.e., the relation between damage parameter value and endurable load cycles N) can be analytically expressed by inclusion of Eq. 2-8 as:

$$P_{SWT}(N) = \sqrt{\sigma_f'^2 \cdot (2N)^{2b} + \varepsilon_f' \cdot \sigma_f' \cdot E \cdot (2N)^{b+c}} \quad \text{Eq. 2-15}$$

It is recognized that especially for higher strength materials the  $P_{SWT}$  parameter underestimates the influence of tensional mean stresses, see *Haibach (2006)*. Consequently, in its original form its suitability for the assessment of preloaded HV-bolts is questionable. However, due to its broad practical importance and given documented experiences it is expedient to maintain the parameter in the assessment concept for comparison.

### Damage parameter $P_M$

Taking into account experimental results and derived theoretical model representations, showing that mean stress dependent damage contributions exist which are underestimated by the  $P_{SWT}$  parameter, *Narberhaus* (1999) proposed an empirically justified extension. In the resulting damage parameter  $P_M$  (Eq. 2-16) a supplemental addend, aiming to directly consider the mean stress driven damage contribution, is added to the original  $P_{SWT}$  formulation together with nominal stress ratio  $R$  and notch concentration factor  $K_t$  dependent weighting functions  $Y_a$  and  $Y_m$ :

$$P_M = \sqrt{(\sigma_a + \sigma_m) \cdot \varepsilon_a \cdot E} \cdot Y_a + \sqrt{\frac{\sigma_m^2}{R_m} \cdot \varepsilon_a \cdot E} \cdot Y_m \quad \text{Eq. 2-16}$$

$$Y_a = -\exp\left(\frac{R - \sqrt{K_t}}{1 + (R - \sqrt{K_t})^2}\right) + 1.55 \quad \text{Eq. 2-17}$$

$$Y_m = -\exp\left(\frac{R - \sqrt{K_t}}{1 + (R - \sqrt{K_t})^2}\right) - 0.55 \quad \text{Eq. 2-18}$$

The P - life curve can be formed analogously to the  $P_{SWT}$  - life curve, whereby the omission of mean stresses leads to dropping out of the second addend.

### Damage parameter $P_J$

*Vormwald* (1989) has developed a damage parameter, which is substantiated by a fracture mechanical consideration of microscopic short crack opening and closure. Using a formulation by *Dowling* (1987) for a semicircular surface crack model under uniaxial loading to describe an effective (i.e., damage relevant) cyclic J-integral, he derives the following damage parameter description:

$$P_J = 1.24 \cdot \frac{\Delta\sigma_{\text{eff}}^2}{E} + \frac{1.02}{\sqrt{n'}} \cdot \Delta\sigma_{\text{eff}} \cdot \Delta\varepsilon_{p,\text{eff}} \quad \text{Eq. 2-19}$$

The relevant definitions of the cyclic hysteresis for calculation of the  $P_J$ -parameter are illustrated in Figure 2-12. The stress levels at crack opening  $\sigma_{op}$  and closing  $\sigma_{cl}$  are determined, using an approximation formula from *Newman* (1984) for  $\sigma_{op}$ , under the assumption that the corresponding strains for crack opening and closing  $\varepsilon_{op}$  and  $\varepsilon_{cl}$  are identical. The remaining required parameters for description of the damage relevant part of the hysteresis can then be derived in an iterative process, applying the established descriptions of local material behaviour (i.e., the cyclic stress-strain characterizations according to *Ramberg-Osgood* and *Masing*, see section 2.2.2).

In contrast to the previously described two damage parameters, the  $P_J$ - life curve cannot distinctly be expressed by an analytical equation. However, alternatively to its direct extraction from strain-controlled material tests, it can be determined stepwise, in dependence of endurable load cycles,

from the material's strain-life curve, see *Haibach* (2006). An analytical expression is then enabled by a regression formulation.

According to a literature review by *Haibach* (2006), the  $P_J$  parameter commonly leads to a lower calculated fatigue life and thus better compliance with experimental results than  $P_{SWT}$ . Moreover, with respect to the current state of knowledge it is the superior parameter in terms of mechanical correct incorporation of load sequence dependent damage behaviour, which was also a primary aim for the damage parameter development (see section 2.2.5).

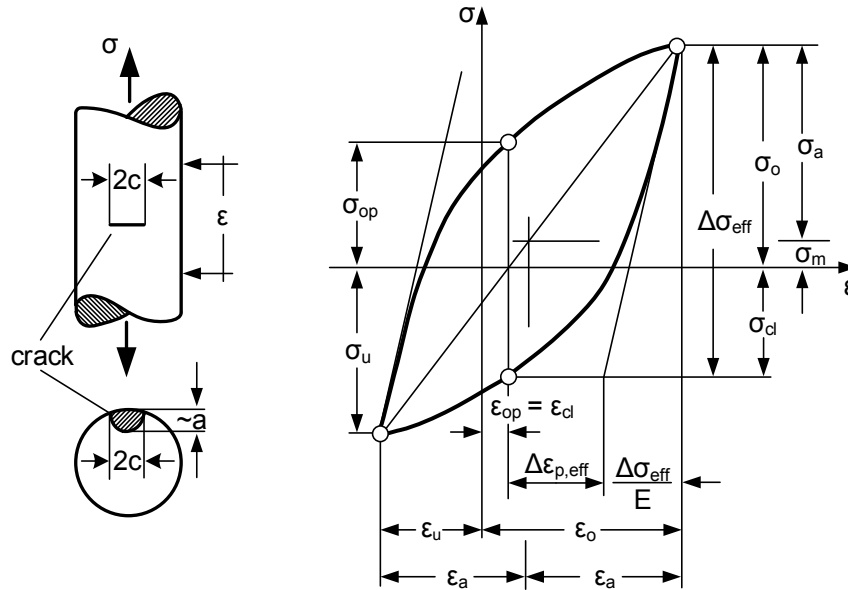


Figure 2-12: Definitions for the damage parameter  $P_J$  acc. to *Haibach* (2006)

### Mean stresses in macroscopic fracture mechanics

Generally, mean stress dependency in linear elastic fracture mechanics is incorporated to the description by *Paris'* law (Eq. 2-7) within the empirical material constants  $C$  and  $m$ , which are affected by the stress ratio. The majority of material data is available for pure tensional swelling loads with stress ratios  $R \approx 0$  (e.g., FKM-Guideline, 2006). For increasing stress ratios a transition of the crack growth curve to the left (see Figure 2-9) has to be expected, see *Radaj & Vormwald* (2007). Thereby, the crack propagation rate  $da/dN$  increases and reductions of threshold- and critical cyclic stress intensity  $\Delta K_{th}$  and  $\Delta K_c$  occur.

The formulation by *Forman et al.* (1967), extended by *Erdogan & Ratwani* (1970), includes the stress ratio in an adaption of *Paris'* law, which enables the application of stress ratio independent material constants. Furthermore, it aims for describing the non-linear transitions of the crack growth function when approximating threshold and critical stress intensity.

$$\frac{da}{dN} = \frac{C \cdot (\Delta K - \Delta K_{th})^m}{(1-R) \cdot K_c - \Delta K} \tag{Eq. 2-20}$$

However, the material constants  $C'$  and  $m'$  are not identical to their corresponding values in Eq. 2-7, and significantly less data is available in the literature. Consequently, a practical applicability is limited. According to *Radaj & Vormwald* (2007), Eq. 2-20 can be transferred to the original *Paris'* law formulation, enhanced by the influence of  $R$ , under the condition of  $\Delta K_{th} \ll \Delta K \ll (1 - R) \cdot K_c$  (with  $(1 - R) \cdot K_c$  considering the stress ratio dependent reduction of the critical cyclic stress intensity):

$$\frac{da}{dN} = \frac{C \cdot (\Delta K)^m}{1 - R} \quad \text{Eq. 2-21}$$

### 2.2.5 Size- and surface effects

Popularly in fatigue assessment with the strain-life concept, the stress-mechanical size effect can be incorporated by multiplying the P-life curve with the stress gradient dependent notch sensitivity factor  $n_{\chi^*}$ , calculated with the empirical formulation according to *Siebel & Stieler* (1955) and FKM-Guideline (2012):

$$n_{\chi^*} = 1 + \sqrt[4]{\chi^* \cdot \text{mm}} \cdot 10^{-\left(a_G + \frac{R_m}{b_G \cdot N / \text{mm}^2}\right)} \quad \text{for } 1 \text{ mm}^{-1} < \chi^* < 100 \text{ mm}^{-1} \quad \text{Eq. 2-22}$$

$$\chi^* = \frac{1}{\sigma_{\max}} \cdot \left( \frac{d\sigma}{dx} \right)_{\max} \quad \text{Eq. 2-23}$$

The related stress gradient  $\chi^*$  can be calculated according to Eq. 2-23 by use of linear elastic finite element calculations. For approximation of a fictitious shear band depth, as introduced in the original theory by *Siebel & Stieler*, the material dependent constants in Eq. 2-22 are given in the FKM-Guideline (2012) as  $a_G = 0.5$  and  $b_G = 2700$  for structural steel. Since the stress gradient and thus the support effect decreases with increasing diameter (see Figure 2-13, left), considering identical material parameters, lower fatigue strengths are obtained for larger than for smaller bolt sizes.

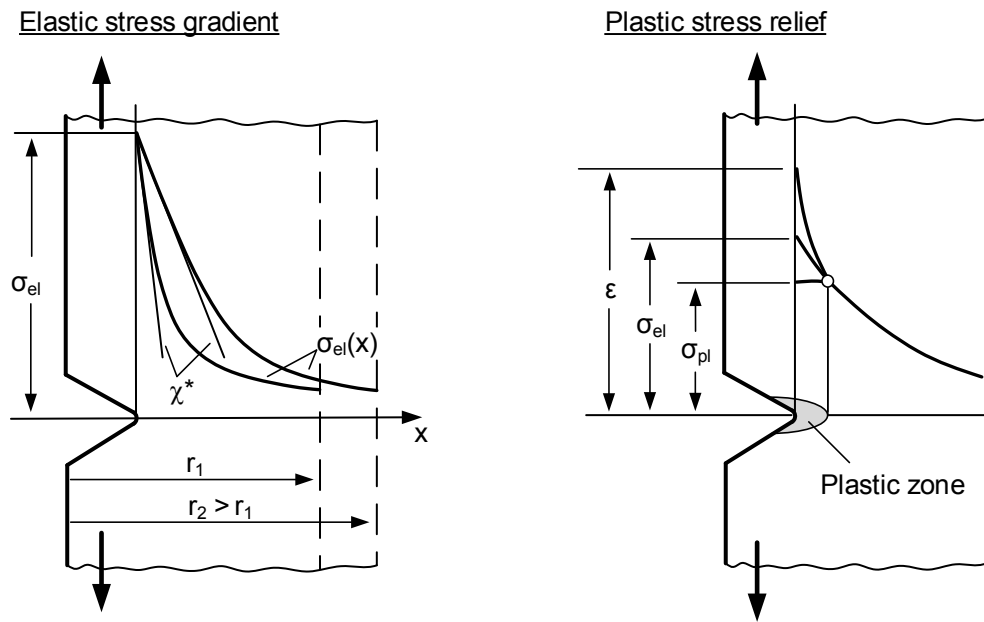


**Figure 2-13: Schematic depiction of elastic stress gradient for calculation of the stress-mechanical support effect (left) and macroscopic support effect by plastic stress relief (right) acc. to Vormwald & Seeger (2015)**

Additional to the effect of the stress gradient, the empirically substantiated approach by *Siebel & Stieler* simultaneously includes the beneficial effect of the stress behaviour at the notch root under local plasticity, which causes a limitation of stresses under increasing strains (denoted by *Neuber* (1985) as macroscopic support effect; see Figure 2-13, right). This behaviour is inherently incorporated by the application of the strain-life concept. Hence, *Vormwald & Seeger* (2015) emphasize that, to avoid double consideration, the amount of the macroscopic support effect needs to be eliminated from the stress-mechanical notch sensitivity factor  $n_{\chi^*}$ . If at the base material's endurance limit a certain plastic strain amplitude  $\epsilon_{a,D,p}$  is tolerable, this can be expressed by a macroscopic notch sensitivity factor  $n_p$  according to Eq. 2-24, in relation to the corresponding elastic strain amplitude  $\epsilon_{a,D,e}$ . Consequently, the magnitude of the described effect is solely material related and independent from the bolt diameter.

$$n_p = \sqrt{1 + \frac{\epsilon_{a,D,p}}{\epsilon_{a,D,e}}} \tag{Eq. 2-24}$$

As an alternative to the approach by *Siebel & Stieler*, the FKM-Guideline (2012) also provides a fracture-mechanic based approximation of the stress-mechanical size effect, which is declared to provide a better approximation for very high and very low stress gradients.

An additional statistical size effect can be incorporated by use of a notch sensitivity factor  $n_w$ , which considers the increased probability of damage inducing defects, dependent on the size of the highly loaded volume or surface area at the notch root, see *Vormwald et al.* (1994), *Vormwald & Seeger* (2015). The statistical distribution of the defect probability may be calculated with the weakest-link model according to *Weibull* (1949). By reference to the volume or surface area of the unnotched



specimen, contrary to the stress-mechanical size effect, the statistical notch sensitivity factor  $n_w$  may become smaller than 1. The final notch sensitivity factor (also denotes as support number)  $n_s$ , which is used for multiplication of the P-life curve, is then calculated according to Eq. 2-25.

$$n_s = n_w \cdot (n_{\chi^*} / n_p) \quad \text{Eq. 2-25}$$

In the short crack growth model the statistical size effects can also be incorporated by accordingly adapting the considered initial micro crack size, see *Hertel & Vormwald (2014)*.

*Seeger & Heuler (1984)* introduced a model for consideration of manufacturing related residual stress states or variations of material strength, which occur predominantly in a thin boundary layer adjacent to the material surface. The so-called “thin surface layer model”, illustrated in Figure 2-14, is based on the assumption that the deformation behaviour of the notched component is dominated by the base material. Consequently, the relation between external loading  $\Delta L$  and deformations at the notch root  $\Delta \epsilon$  can be determined without consideration of the boundary layer. Due to compatibility reasons, the boundary layer is subjected to identical deformations (Figure 2-14, mid). However, it may show a different local stress-strain behaviour (Figure 2-14, right). Moreover, possibly existing initial residual stresses  $\sigma_r$  are accounted for by shifting the load-strain and consequently local stress-strain relation of the surface layer by the amount of the corresponding residual strain  $\epsilon_r$ .

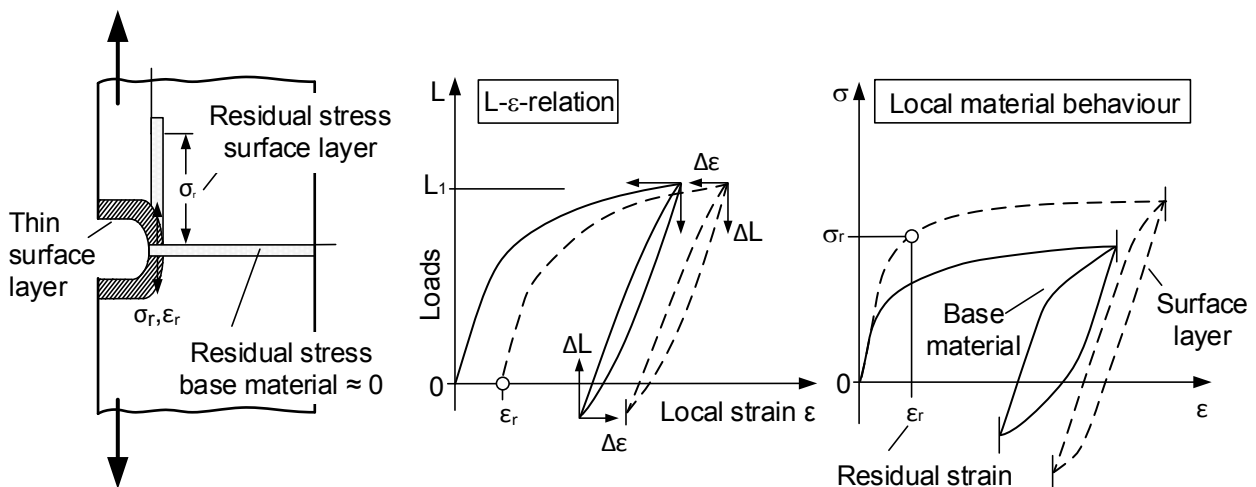


**Figure 2-14: “Thin surface layer model” acc. to Seeger & Heuler (1984)**

Surface roughness effects, which influence the fatigue strength of a component, may be incorporated based on cyclic material data from specimens with the respective surface characteristics (e.g., by use of a correction factor) or within the small crack growth model by adding a measured roughness depth to the initial micro crack size, see *Vormwald & Seeger (2015)*.

### 2.2.6 Sequence effects and loading conditions

The majority of investigations on bolted connections under cyclic loading, both experimental and analytical, focus on the rather academic loading condition with constant amplitudes. Nevertheless, the strain-life concept generally provides the possibility to incorporate loading conditions with variable amplitudes in a thorough physical approximation. Based on the cyclic-stress-strain curve with *Masing*-behaviour the local stress-strain relation for a given load sequence can be emulated using the micro-structural substantiated “material memory model” (e.g., see *Haibach*, 2006 or *Radaj & Vormwald*, 2007). Thereby effects of material memory are introduced, which consider the effect of the previous load history to the local stress-strain relation.

For the calculation of fatigue life, every closed hysteresis loop can be assessed based on the chosen damage parameter  $P$  and fatigue damage accumulation with *Miner's* rule. Thereby, additionally to the consideration of load sequence dependent mean stresses and strains (and other relevant hysteresis parameter) resulting from the memory model, further load sequence effects on the fatigue resistance (i.e., transition of endurance limit, see chapter 2.1.3) may be incorporated. The  $P_J$  parameter formulation developed by *Vormwald* (1989) enables the direct inclusion of the crack size dependent reduction of the endurance limit as function of the advancing damage sum, achieved by load cycle wise integration of the crack propagation function. As described by *Haibach* (2006), alternatively the damage dependent fatigue resistance can also be considered by analytical expression of the  $P_J$  - life curve (see section 2.2.4) and damage accumulation with the consequent form of *Miner's* rule (see section 2.1.3).

Linear damage accumulation, or an equivalent increment wise calculation with the crack propagation formula using momentary values for  $\Delta K$  and  $R$ , is generally also applicable for the calculation of macroscopic crack propagation. The analytical quantification of interacting delays and acceleration effects resulting from stochastic load sequences are still subject of current research. An overview of calculation models to calculated crack propagation under consideration of sequence effects is given in *Haibach* (2006).

All so far described model representations are derived under the assumption of a uniaxial loading situation. Under multiaxial local loading conditions with constant principle stress direction (proportional loading), uniaxiality may be emulated by the established effective stress criteria (or their strain-based equivalents) derived for monotonic loading, as the “distortion energy hypothesis” (*von Mises*) or the “maximum normal stress hypothesis”, see *Radaj & Vormwald* (2007) and *Socie & Marquis* (2000). Under non-proportional loading conditions, different effective stress criteria as well as damage assessment methods are required. A comprehensive calculation procedure of fatigue life until technical crack initiation under consideration of non-proportional multiaxial stress states and arbitrary load histories has been developed by *Hertel* (2016) on the basis of the short crack growth formulation by *Vormwald* (1989). Calculation approaches for macro crack propagation with interacting loading modes due to multiaxia loading are introduced in *Socie & Marquis* (2000).

### 2.2.7 Application of local concepts to threaded fasteners

Regarding general applications in structural engineering, the strain-life approach still has a mainly scientific character. In contrast, linear elastic fracture mechanics are widely commercialized with a variety of industrial software solutions, for example for solving geometrically complex models for determination of the cyclic stress intensity. Moreover, the linear elastic fracture mechanics approach is also incorporated in structural and mechanical engineering standards and guidelines such as BS 7608 (2014) and FKM-Guideline (2006) for selected fatigue assessment applications. However, usually also the fracture mechanics approach cannot entirely substitute the nominal stress concept in design standards for secure fatigue life assessment, see *Radaj et al.* (2006). Both, strain-life and fracture mechanics approach are characterised by sensitivities and uncertainties with respect to their input parameters and introduced assumptions. Thus, a thorough validation for the respective application is required.

The literature contains a number of studies dealing with numerically supported analytical assessment approaches for selected fatigue properties of bolts and threaded fasteners. Early works focused on the effects of thread geometry and bolt diameter on the endurance limit, based on linear elastic notch stress concentration  $K_t$  and fatigue notch factor  $K_f$  (e.g., *Otaki*, 1979; *Koenigsmann & Vogt*, 1981; *Dragoni*, 1997). The effect of nut positioning was investigated by *Feldmann* (1981), showing an increasing fatigue notch factor if less than two turns towards the run-out of the bolt thread remain unloaded.

Bi-linear kinematic FEM based approximations of the local cyclic stress-strain response were used by *Alt* (2005) to evaluate influencing factors on the endurance limit such as nut height and positioning, as well as bearing and loading conditions. A comparable approach was included in the studies from *Bercea* (2001) on an integrated digital calculation system, assessing parameters like material and dimensions of bolt and nut. In both studies, positive validation based on experimental data from the literature was given with respect to general tendencies but not quantitative results.

In distinction to these primary qualitative investigations, within his extensive studies on modelling of the local loading situation inside the thread (see section 2.2.3), *Seybold* (2005) was first to introduce a more specific attempt to compute the endurance limit of bolts. Based on the notch-strain approach he used elastic-plastic stress-strain relations from FEM simulations to compute limit values of the damage parameter  $P_{SWT}$  according to *Smith et al.* (1970). The critical damage parameter value, corresponding to the endurance limit, was determined by use of fatigue test results for a high-strength bolt material provided by *Thomala* (1978). The stress-mechanical support effect at the notch was considered by multiplication with the notch sensitivity factor  $n_{\sigma}$  according to *Siebel & Stieler* (1955) and FKM-Guideline (2012). Through comparison of his calculation results to various test results from the literature for bolts up to a diameter M24, *Seybold* concluded that typical impact factors to the fatigue strength, such as preload, thread geometry and diameter are generally adequately displayed by the calculation approach. The limited accuracy to the actual endurance limit was ascribed to the rather roughly approximated material properties.

*Marten* (2009) investigated the application of the strain-life approach for fatigue assessment of large-size high-strength bolts, thereby providing the first and thus far unique comprehensive study considering the relevant range of bolt diameters in today's modern wind turbine structures. Based on notch stress concentration factors  $K_t$ , determined within linear elastic finite element calculations, the local stress-strain relation was primarily calculated by *Marten* by use of the analytical approximation according to *Neuber* (1985). Even though full damage parameter-life curves were determined, studies focused on the transition region to the endurance limit, which is dominated by fatigue life until crack initiation. The calculation of crack propagation load cycles and hence the assessment of the upper high-cycle fatigue range was omitted. The analytical calculations were validated on experimental results for hot-dip galvanized HV-bolts M48. Since the preload level of the experiments was limited to about 15%  $R_{p0,2}$  and the effect of the zinc coating remained unconsidered in the analytical calculations, test results from *Lacher* (1986) on black, uncoated high-strength bolts M20 were additionally used for comparison. For high tensile mean stresses the deployment of the damage parameter  $P_M$  according to *Narberhaus* (1999) instead of *Smith et al.* ( $P_{SWT}$ ) led to a reduced fatigue strength in the relevant region of load cycle  $N \approx 10^6$ . However, with both damage parameters the experimental results were overestimated. The inclusion of the stress-mechanical support effect by use of the notch sensitivity factor  $n_{\gamma^*}$  caused a further exceedance of the experimental fatigue strength. *Marten* assumed that the discrepancy between analytical and experimental results was caused by utilization of imprecise cyclic material data. Moreover, as a result of the analyses the application of the Uniform Material Law according to *Bäumel & Seeger* (1990) was deemed unsuitable for determination of the endurance limit at loading conditions with high mean stress. He thus emphasized the relevance of availability of cyclic material data for the actual investigated bolt material. Nevertheless, he concluded that the strain-life approach is generally appropriate for estimation of the endurance limit of highly pre-stressed large-size bolts.

In his analytical studies, *Kremer* (2005) focused on assessment of the crack propagation phase, starting from an initial crack depth  $a_i = 0.1$  mm. He compared calculations using *Paris' law* (Eq. 2-7) to experimentally determined macro crack propagation load cycle, obtained by use of electrical resistance measurements. The experimental validation basis mainly comprised fatigue tests on high-strength bolts M8 with varying configurations regarding strength class, boundary layer and manufacturing procedure. Furthermore, one test series for bolt diameter M16 was included. Dealing with the absence of a distinct model for determination of the cyclic stress intensity  $\Delta K$  for bolted connections, he found a tensional loaded round bar model according to FKM-Guideline (2006) as an adequate approximation. The model provided the best general validity for application within the considered range of parameter variation and analytical results in good and mostly conservative agreement with the experimental data. However, according to *Pyttel et al.* (2008) by alternative application of a hollow cylinder model a better approximation of stress intensity factors at the crack tip can be achieved, when compared to calculations with a rotational symmetric finite element model of a high-strength M12 bolt.

A comprehensive approach for fatigue calculation of threaded fasteners, targeting a broad applicability, was established by *Schneider* (2011). After validation of their transferability to the notch root,

the required material parameters were determined on specimens extracted directly out of the core of the investigated fasteners. These were applied in non-linear finite element calculations in order to compute the local stress strain hysteresis. Contrary to common application of the strain-life concept, where initial loading is usually approximated by use of the cyclic stress strain-curve, *Schneider* suggested the application of the actual monotonic material path. This enabled to a superior description of the actual local loading condition under high static mean stresses. In order to consider cyclic relaxation effects, he used results of material tests under high mean strain and accordingly adjusted the mean stress level of the analytically determined local hysteresis. Considering the stress-mechanical notch sensitivity factor  $n_{\chi^*}$ , load cycles until crack initiation were calculated in comparison between the damage parameters  $P_{\text{SWT}}$  and  $P_J$  by *Vormwald* (1989). Thereby, the latter was identified as more accurate for the aspired application. Finally, full load cycles until rupture were calculated by addition of crack propagation load cycles, computed with *Paris'* law. Following the suggestion of *Pyttel et al.* (2008), a hollow cylinder stress intensity model was applied. The resulting crack propagation load cycles were in good agreement with the experimental results from *Kremer* (2005). Among other threaded fasteners, *Schneider* validated the calculation procedure on fatigue tests with uncoated HV-bolt sets M10 and M16. Generally, he found a good compliance of experimental and analytical results for high mean-stress states, when calculated with the  $P_J$  damage parameter. However, for low mean stress levels ( $R = 0.1$ ) the analytical results considerably overestimated the experimental fatigue strengths.

The calculation procedure from *Schneider* (2011) provides basis for newer studies such as *Panic et al.* (2014), who focused on the direct incorporation of transient effects by advanced material implementations in non-linear finite element calculations. Moreover, within the framework of the same research project, *Olveda et al.* (2014) investigated the approximation of the crack tip stress intensity for the actual geometric properties of bolt-nut connections by application of the Extended Finite Element Method (XFEM). For both studies validation was performed on experimental results for high-strength bolts M16 and other threaded connection types (see *Oechsner et al.*, 2014). *Schaumann & Eichstädt* (2015) and *Schaumann & Eichstädt* (2016) presented first investigations on application of the calculation procedure according to *Schneider* for preloaded bolts with large diameters with the  $P_{\text{SWT}}$  damage parameter, and validated results on experiments on uncoated M36 HV-bolt sets.

Fatigue life calculations based on a numerically assisted assessment of fatigue crack growth with an extended *Paris's* law formulation are presented by *Eder et al.* (2018). Thereby steel samples with bolt alike notch geometry and uncoated as well as hot-dip galvanized boundary layer were analysed. The effect of galvanizing was included as a function of the coating thickness, whereby the strain energy, stored within the coating, contributes to the analytical linear elastic crack tip stress intensity. The calculation results were validated on experiments on notched specimens of diameter M20 in the upper high cycle fatigue range. Within the frame work of investigations on brittle fracture, fracture mechanical calculations of HV-bots M36 with and without pre-damage by artificially introduced initial cracks are presented by *Stranghöner et al.* (2018). Thereby the crack tip stress intensity was calculated within a complex numerically assists calculation algorithm. For the calculation of macroscopic

crack propagation with *Paris'* law, self-determined crack propagation constants of the actual bolt materials were used. The calculations showed good agreement with experimental results; however, accuracy needs to be regarded as strongly dependent on the assumed initial crack depth. For the calculation of bolts without pre-damage, no crack initiation phase was considered.

### 2.3 Findings

The priorly given presentation of the current state of the art revealed a number of uncertainties regarding fatigue performance and assessment of large-size, high strength bolting assemblies and constitute necessity for further research.

Generally, the number of experimental studies on HV-bolt sets with large dimensions is very limited, and, thus far, normative fatigue curves and corresponding design procedures are not validated for the range of bolt diameters, commonly applied in support structures for wind turbines. Available fatigue results on HV-bolts of size M48, which is the largest investigated bolt diameter priorly to the studies presented in this thesis, were supposedly affected by a low mean stress level. The performed review emphasizes the importance of an accurate mean stress level consideration in future experimental investigations on large-size bolts. This, however, vastly complicates the technical test execution because of the required high mean loads and the limitations of suitable testing facilities.

Even though fatigue tests under representative mean load level exist up to large bolt diameter M36, the effect of zinc-based corrosion protection, and - with particular practical importance - hot-dip galvanizing, has not yet conclusively been quantified for bolts with large dimensions. Furthermore, for smaller bolts partially varying results regarding the amount of corresponding fatigue strength reduction are present in the literature. Moreover, the damage behaviour of HV-bolts under variable amplitude loading has not been investigated for bolt diameters larger than M12.

Due to the demanding technical requirements for the execution of representative fatigue tests, local analytical approaches gain particular importance for the assessment of the fatigue performance of large-size HV-bolts. A comprehensive fatigue assessment method for calculation of complete constant amplitude S-N curves, including both technical crack initiation and propagation phases has been developed and validated for smaller bolt diameters. For large-size bolts up to diameter M48, thus far only the general applicability of the strain-life approach for assessment of load cycles in the transition region to the endurance limit, dominated by the technical crack initiation phase, has been proven. However, accuracy of results is limitedly satisfactory. Among others, this can be traced back to the applied damage parameters and the limited available basis of material data. Moreover, no experimental validation could be provided for representative high mean stresses and no crack propagation load cycles were calculated. The effect of the boundary layer, imposed by hot-dip galvanizing, was not considered in investigations on analytical fatigue calculation, regardless of the bolt diameter.

From the analysed situation of current knowledge, the following aims and requirements for the scientific work described in the framework of this dissertation are derived:

- Experimental investigations on large-size HV-bolt sets are required, which extend the current experimental background and provide further validation of normative design fatigue curves with regard to large bolt diameters. These experiments need to be performed under a representative high mean stress level.
- The impact on the fatigue performance of hot-dip galvanizing, the most widely used corrosion protection system in practical application, needs to be accurately verified for large bolt diameters.
- To ensure and verify transferability of conclusions derived from, mostly academically, constant amplitude loading to actual service loading conditions of large-size HV-bolts, variable amplitude tests are a valuable supplement in an appropriate experimental testing program.
- To improve the potential utilization of analytical fatigue assessment procedures, existing methodologies need to be further investigated and adapted for the application to large-size HV-bolts. This includes the appropriate consideration of specific size-effects, provision of material data, appropriate damage parameters and measures for determination of local loading conditions.
- Engineering approaches are required which enable the consideration of the potential boundary layer effect of hot-dip galvanizing within an analytical fatigue assessment methodology.

In the following chapters, a widely augmented knowledge basis will be elaborated from the combination of both experimental and analytical investigations. Thereby, an initially established extended experimental background will provide a valuable validation basis for succeeding analytical calculations. Based on these, possibilities and limitations of the analytical calculation procedure will be revealed and utilized. The overall results will yield the opportunity for systematic evaluation of fatigue characteristics and current design procedures for HV-bolts with large diameters.

## 3 Experimental Fatigue Investigations

### 3.1 Scope

To cope with the pre-existing gap regarding experimentally verified fatigue characteristics of large-size HV-bolts, a comprehensive testing program was implemented. It predominantly aimed for an extension of the available test basis to the upper bolt diameter range applied in today's modern wind turbine structures as well as a thorough evaluation of the boundary layer effect imposed by hot-dip galvanizing. Thereby, it was prerequisite to appropriately consider a representative high mean stress level. All tests on HV-bolt sets were performed within the framework of the research project "Experimental and analytical assessment of the fatigue strength of bolts with large dimensions under consideration of boundary layer effects" (Oechsner *et al.*, 2015). The experimental implementation, statistical evaluation and results are described in the course of this chapter.

The performed testing program largely focussed on 'classical' constant amplitude fatigue tests (i.e., *Wöhler* tests) under axial loading. Firstly, a fundamental test series was performed on HV-bolts of diameter M36 with an ample number of specimens (Chapter 3.3). It laid the background for the further series. Afterwards, given the demanding test execution requirements, tests on HV-bolts with very large diameter M64 were performed with a notably reduced number of specimens (Chapter 3.4). These tests enabled the validation of the previously obtained results in order to investigate the effect of the increased diameter.

Additionally to the tests with constant amplitude loading, the research project also comprised a further test series using variable amplitude loading sequences, to verify the bolt's fatigue performance at more operation-alike loading conditions. These tests, performed solely on HV-bolts of diameter M36, are presented in Chapter 3.5.

### 3.2 Test specimens and general boundary conditions

The fatigue tests were performed on customary 'System HV' bolting assemblies (including aligned bolt nut and two washers) of strength class 10.9 with geometrical properties according to DIN EN 14399-4 (2015) (bolt size M36) and DAST - Guideline 021 (2013) (bolt size M64). All tested bolts were rolled before heat treatment. Thus, it can be supposed that residual compressive stresses resulting from the non-cutting shaping process were mostly dissipated during the subsequent tempering. Within the test series of the two respectively investigated bolt sizes, all bolts were produced with identical material and from a single manufacturing batch. However, batch and bolt manufacturer as well as base material varied between the bolts M36 (material 32CrB4) and M64 (material 30CrNiMo8).

To analyse and quantify the impact of hot-dip galvanizing to the bolt's fatigue strength, a comparative testing program was implemented, using equivalent numbers of uncoated black (B) as well as normal-temperature (NT, approx. 450 °C) and high-temperature (HT, approx. 550 °C) hot-dip galvanized bolts. However, given the likelihood of premature liquid metal assisted cracking (LMAC) at high galvanizing temperatures, which accumulates with increasing bolt diameter, it was refrained



from testing HT-galvanized M64 HV-bolts. It is noted that likewise for bolt diameter M36 allowance for HT-galvanizing is not consistently granted in national regulations. For instance, German guideline DSV-GAV (2009) limits the application to bolt sizes  $\leq$  M24. Nonetheless, HT-galvanized M36 bolts were included to the test program for academic purposes.

The investigated HV-bolt configurations are depicted in Figure 3-1.

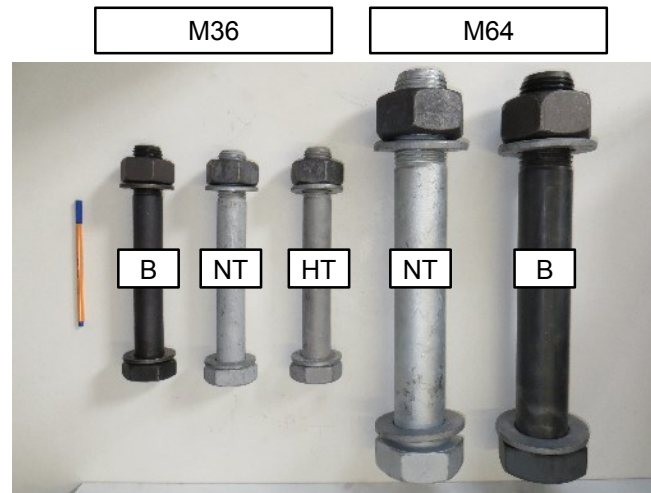


**Figure 3-1: Investigated HV-bolt sets with different boundary layers (B: uncoated black; NT: normal temperature hot-dip galvanized; HT: high temperature hot-dip galvanized)**

The performed fatigue test complied with the general requirements given in DIN 969 (1997) for the test set-up and execution of fatigue tests on threaded fasteners under axial loads. All tests were performed under sinusoidally applied cyclic swelling loads (in case of variable amplitude tests with blocks of changing load level) and with constant tensile mean stress, corresponding to the nominal preload level for HV-bolts in wind turbines (Eq. 3-1). Maintaining an unchanged mean stress led to variant stress ratios  $R$  throughout the test series, dependent on the respective load level.

$$S_m = 0.7 \cdot R_{p,0.2,nom} = 630 \text{ N/mm}^2 \quad \text{Eq. 3-1}$$

As the mean stress was applied directly by the testing machine, the specimens remained free from torsion. The methodically introduced loading conditions were purely axial (i.e., without any nominal contribution of bending). Generally, the application of axial spherical plain bearings may further exclude possibly existing bending impacts caused by imperfections within the test set-up. However, efforts for construction of an axial bearing, suitable for the high test loads for M64 bolts, were deemed unpractical. Thus, it was refrained from using axial bearings in all test series to maintain comparable testing conditions. Failure of the bolts was defined as complete rupture, which location was characteristically expected in the first load-bearing turn of the thread. Variant load magnitude or load sequence characteristics of the three test series imposed fundamentally varying requirements to the testing machinery. As a consequence, the series were executed at different test facilities, which also resulted in a variation of testing frequencies. The basic characteristics of the test series are summarised in Table 3-1. Specific information is given in the respective chapters.

**Table 3-1: Basic characteristics of performed fatigue test series on HV-bolts**

HV-bolt sets	Manu- facturer	Boundary layer configurations	Material	Mean load	Test frequency	Total No. of specimens
Constant amplitude axial loading (sinusoidal):						
M36x270 10.9	Man. A	B, NT, HT	32CrB4	515 kN	~ 50 Hz	105
M64x450 10.9	Man. B	B, NT	30CrNiMo8	1680 kN	~ 2-4 Hz	18
Variable amplitude axial loading (sinusoidal blocks):						
M36x270 10.9	Man. A	B, NT, HT	32CrB4	515 kN	~ 5-35 Hz	31

### 3.3 Test on M36 HV-bolt sets with constant amplitude loading

#### 3.3.1 Test execution

The constant amplitude tests on HV-bolt sets of size M36 were performed in an electromotive high frequency pulsator with 1 MN maximum tensile loading capacity (1MN MOT) located in the Test Centre for Support Structures of the Leibniz Universität Hannover. The test set-up is illustrated in Figure 3-2. Stiffness of the test rig and applied load levels led to a resonance frequency of approximately 50 Hz. These enabled application of  $1 \cdot 10^6$  load cycles in approximately 5.5 hours.

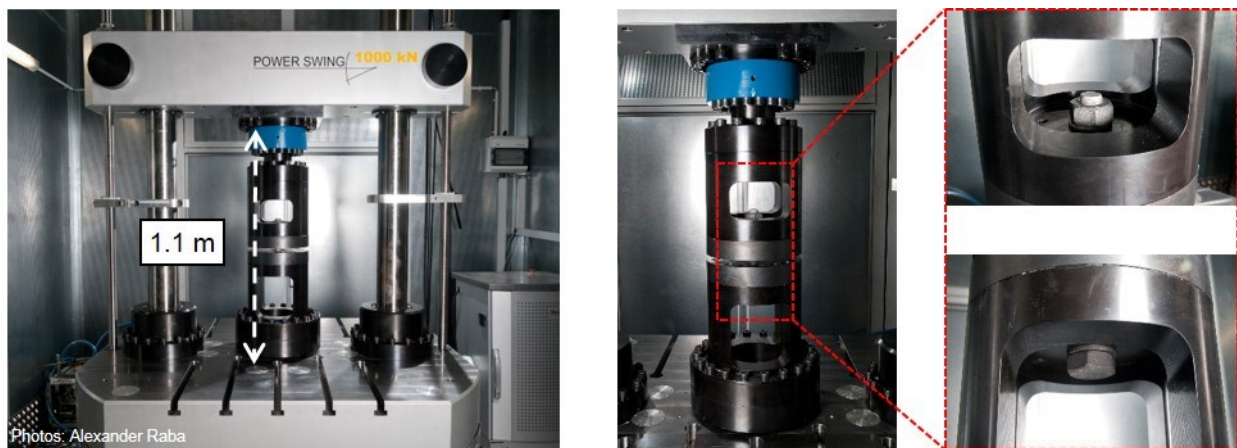


**Figure 3-2: Test set-up for M36 HV-bolt tests under constant amplitude loading in electromotive resonance testing machine**

For all three considered boundary layer conditions (B, NT, HT) complete S-N curves were determined, which encompass both the upper high cycle fatigue range (upper HCF) as well as the transition region to the endurance limit (TEL). Thereby, each boundary layer configuration was treated as a separate sample of specimens.

In a first experimental step the bolt's endurance limit was statistically estimated using the 'staircase method', developed by *Dixon & Mood* (1948). Thereby, while maintaining an equidistant load step size, the fatigue load level is successively decreased in the following experiment, in case a failure of the bolt (i.e., rupture) occurs. Likewise, in cases where bolts remain free from failure the load level is increased by an equivalent load step. Consequently, the applied load level is defined by the result of the prior experiment. In the present investigation the limit load cycle number was defined to  $N = 5 \cdot 10^6$  (denoted as run-outs). After reaching the run-out limit, bolts are assumed to remain free from failure, even at (theoretically infinite) further cyclic loading of the same amplitude. The individually applied load increments and starting load levels were chosen under consideration of corresponding recommendations given by *Dünkel* (1999) as well as *Mauch* (1999).

The above described procedure provides the advantage that commonly applied load levels quickly centre around the mean of the endurance limit (survival probability  $P_s, 50\%$ ). It hence can be estimated reasonably accurate with a relatively low number of specimens, compared to other testing procedures. Assuming a *Gaussian* normal distribution, the method also enables estimation of upper and lower bound of the scatter band around the mean (e.g.,  $P_s, 10\%$  and  $P_s, 90\%$ ). However, to reliably ascertain the required standard deviation of the sample, a larger number of specimens is necessary. The applied calculation formulae for statistical evaluation of the endurance limit with the staircase method, as given in DIN 969 (1997), are included in Appendix A.1.

Test execution and evaluation for the upper HCF was implemented separately with the so-called "horizon method", whereby several tests are performed at distinct load levels (i.e., horizons). Since the pathway of the S-N curve in the upper HCF can be assumed linear when plotted in double logarithmic scale, usually testing at two horizons is sufficient for determination of location and slope of the S-N curve. Thereby, a sufficient margin to the TEL as well as the plasticity affected low cycle fatigue range (at which both assuming linearity becomes invalid) needs to be ascertained. Therefore, it was followed the recommendation given by DIN 969 (1997) of testing at load horizons at about  $1.6 \cdot S_{d,50}$  and  $2.4 \cdot S_{d,50}$ , with  $S_{d,50}$  being the priorly determined endurance limit with 50% survival probability.

Statistical evaluation for estimation of mean value as well as scatter band of endurable load cycles  $N$  may either be performed graphically in a normal probability plot, as so described in DIN 969 (1997), or analytically with the below equations Eq. 3-2 to 3-5. Thereby, commonly, a log-normal distribution can be supposed (i.e., the logarithms of load cycles until failure can be approximated with a normal distribution). In the present investigation, for all samples applicability of a log-normal distribution was verified with the *Anderson-Darling* test (*D'Agostino*, 1986).

Logarithm of sample mean value:

$$\log N_{50\%} = \frac{1}{n} \sum_{i=1}^n \log N_i \quad \text{Eq. 3-2}$$

Sample standard deviation:

$$s = \sqrt{\frac{1}{n-1} \sum_{i=1}^n (\log N_i - \log N_{50\%})^2} \quad \text{Eq. 3-3}$$

Logarithms of load cycles with survival probability  $P_{s,10\%}$  and  $P_{s,50\%}$ :

$$\log N_{90\%} = \log N_{50\%} - 1.28 \cdot s \quad \text{Eq. 3-4}$$

$$\log N_{90\%} = \log N_{50\%} + 1.28 \cdot s \quad \text{Eq. 3-5}$$

The evaluation is performed separately for each load horizon. Afterwards, the S-N curve with different survival probabilities can be constructed by connecting the results of the two tested load levels linearly in the double logarithmic representation, which also allows extrapolation above and below. The fictitious knee point results from the intercept of the upper HCF regression line and the horizontal of the endurance limit (see also Chapter 2.1.3).

The primary aim of the here presented test program at M36 HV-bolts with constant amplitudes was the accurate assessment of the effect of hot-dip galvanizing at representative mean stress level. Therefore, the test execution focussed on a statistically secured estimation of the median S-N curves ( $P_{s,50\%}$ ) of all three boundary layer configurations, rather than their full statistical ascertainment. Thus, by correspondingly choosing the required specimen numbers, economical efforts could be reasonably limited. In accordance with recommendations given in DIN 969 (1997) as well as *Mauch* (1999) for each boundary layer the sample size included at least 15 statistically relevant specimens in the TEL and at least 5 specimens at each load horizon in the upper HCF. This sample size can be considered appropriate for the given evaluation aim. However, for a secured estimation of the samples' standard deviation higher specimen numbers of about 25-30 in the TEL and 8-10 at each upper HCF load horizon are required. Thus, it needs to be considered that the statistically determined scatter bands and corresponding percentiles S-N curves (i.e.,  $P_{s,10\%}$  and  $P_{s,90\%}$ ) stated in the result presentation in the following chapter are subject to a certain statistical insecurity. Given the limited number of specimens per sample, it was also refrained from application of an improved version of the original stair case method, for example introduced by *Hück* (1983). The latter is proven to provide a superior statistical approximation but likewise requires a sufficiently larger sample size. Nonetheless, the evaluation of the statistical scatter remains important to verify the general quality and significance of the obtained results.

Additional to the regularly tested specimens, for each boundary layer a certain number of unbroken specimens from the series in the TEL was tested until rupture as "raised run-outs" (RRO) at load horizons in the upper HCF. These tests aimed for a spot-check evaluation of potential impacts of the previous loading history with lower amplitude to the fatigue strength in the upper HCF.

In total, more than 100 test runs were performed within the framework of the constant amplitude tests on M36 HV-bolt, which took about 3 month of testing. A summary of the test program is given in Table 3-2.

**Table 3-2: Summary of test program for constant amplitude tests on M36 HV-bolt sets**

	Boundary layer	Transition region to the endurance limit (TEL)	Upper high cycle fatigue range	
			HCF 1 $S_{a,HCF1} \approx 1.6 \cdot S_{a,d50}$	HCF 2 $S_{a,HCF2} \approx 2.4 \cdot S_{a,d50}$
Mean stress $S_m \approx 0.7 \cdot R_{p,0.2}$		630 N/mm <sup>2</sup>	630 N/mm <sup>2</sup>	630 N/mm <sup>2</sup>
Amplitude $S_a$	B	40-59 N/mm <sup>2</sup>	67 N/mm <sup>2</sup>	103 N/mm <sup>2</sup>
	NT	27-44 N/mm <sup>2</sup>	54 N/mm <sup>2</sup>	81 N/mm <sup>2</sup>
	HT	32-39 N/mm <sup>2</sup>	54 N/mm <sup>2</sup>	81 N/mm <sup>2</sup>
No. of specimens	B	23	5 (+2 RRO)	5 (+2 RRO)
	NT	19	5 (+2 RRO)	5 (+2 RRO)
	HT	18	5 (+2 RRO)	5 (+2 RRO)
Loading conditions	purely axial, constant amplitude loading, $R \approx 0.7 - 0.9$			
Test end criteria	5 · 10 <sup>6</sup> load cycles (= run-out) / rupture			
Testing frequency	approx. 50 Hz			

### 3.3.2 Test results and statistical evaluation

In the sequel, result evaluation and transpired particularities of the constant amplitude tests on M36 HV-bolt sets are described in detail, separately for each boundary layer configuration and fatigue regime. The complete tabulated test results are included in Appendix A.2. It is noted that during the initial test series in the TEL on uncoated black M36 HV-bolt sets the testing machine was programmed to abort testing automatically after the limit load cycle number of  $N = 5 \cdot 10^6$  was reached. To optimally utilize machine capacity and avoid standstill, in the following series all tests without failure were ended manually. Hence, a certain number of tests with NT- and HT-galvanized bolts were run with substantially larger load cycle numbers than  $5 \cdot 10^6$ .

#### Uncoated black bolts

##### Transition region to the endurance limit (TEL)

Figure 3-3 shows the evaluation scheme of the staircase method with results in terms of decisive test events (i.e., rupture or run-out) for the complete test series in the TEL for uncoated, black M36 HV-bolts. The initial experimental approximation of the endurance limit was performed “from above”, at tendentially higher load levels, which were more likely to produce ruptures than run-outs. As the first three tested load levels were not reached again within the remainder of the test series, they were to be disregarded in the statistical evaluation. As the initially chosen load increment was found large compared to the actually occurring scatter of results, it was bisected within the course of the

series. Thereby, number of considered load levels could be increased, which improved the statistical value of the results. Consequently, the chronological sequence of experiments (test number) does not coincide with the contiguous sequence, necessary for result evaluation (specimen number). The statistical relevant sequence of test results of the full series comprised 21 specimens at 5 load levels.

$F_a$ [kN]	$S_a$ [N/mm <sup>2</sup> ]	X = Rupture O = Run-out																								X	O		
48.0	58.8	x																										1	0
45.0	55.1		x																									1	0
42.0	51.4			x																								1	0
39.0	47.8				X																							2	0
37.5	45.9					X																						3	1
36.0	44.1						X																					4	2
34.5	42.2							X																				3	3
33.0	40.4																											0	3
Specimen No.		1	2	3	4	5	6	7	8	9	10	11	12	13	14	15	16	17	18	19	20	21	22	23	24	Σ	12	9	
Test No.		1	2	3	4	13	5	14	6	15	7	16	9	17	8	18	11	19	20	21	12	22	23	24	10				
Test series: BLACK																													

**Figure 3-3: Evaluation scheme of results in the TEL with the staircase method for black M36 HV-bolts**

The majority of the ruptures in the TEL occurred within a range of approximately  $1.5 \cdot 10^6$  and  $3.1 \cdot 10^6$  load cycles (see Figure 3-5). With a sufficient margin to the limit load cycle number, this generally confirms an appropriately chosen test end criterion for run-outs. Except for one, all ruptures were initiated in the first load-bearing turn of the thread. However, in the later stages of the series ruptures occurred after load cycles only slightly less than the limit load cycle number. During inquiry of possible causes, it was found that a certain number of fasteners at the top of the specimen adaption (Figure 3-2) had lost required pre-tension. As no axial spherical plain bearings were used, it is possible that a slightly unlevelled specimen adaption has led to a distortion of the load application and thus an altered stress distribution inside the bolt thread. A found fatigue crack initiation at one of the affected bolts in the second instead of the first load-bearing turn of the thread corroborates this hypothesis. The final test of the series (test no. 24), which was performed after re-tightening of all fasteners at the specimen adaption, with approximately  $2.0 \cdot 10^6$  load cycles failed within the regularly expected range of load cycles until failure. During the following experiments in the upper HCF as well as the test series at NT- and HT-galvanized bolts the fasteners were regularly checked but no further loosening occurred. In Figure 3-3, as well as in the corresponding result data table in Appendix A.2, the experiments, where an impact of a distorted load application needs to be expected, are coloured grey.

To assess the potential impact of the found irregularities to the validity of results, an alternative evaluation with reduced sample size was performed. Thereby the following assumptions were taken for granted:

1. The irregularities were caused by a temporary distortion of the axial load application induced by loosened fasteners of the specimen adaption which could be resolved after re-tightening.



Figure 3-5 and Table 3-3 include the results of both variants for statistical evaluation with full and reduced sample size. The comparison demonstrates that the determined statistical mean value of the endurance limit varies only marginally between the two variants. It may thus be considered mostly unaffected by the irregularities noticed during the test series. A notable effect is imposed to the test series' standard deviation and resulting percentile values ( $P_s,10\%$ ,  $P_s,90\%$ ). This substantiates that indeed a divergence of testing conditions compared to the early (i.e., regular) stages of the test series was present in the omitted experiments. However, as elaborated previously, secured determination of the samples' scatter band was not aim of the presented test program and both considered sample sizes are not sufficient to obtain a conclusive prediction.

Since the specific cause for the found irregularities remains subject to assumptions, in the further course of the experimental evaluation the results obtained with the full sample size are utilized. It needs to be considered that the thereby included scatter of results was presumably affected by a temporally distortion in the testing conditions. The statistical mean value of the endurance limit was securely estimated.

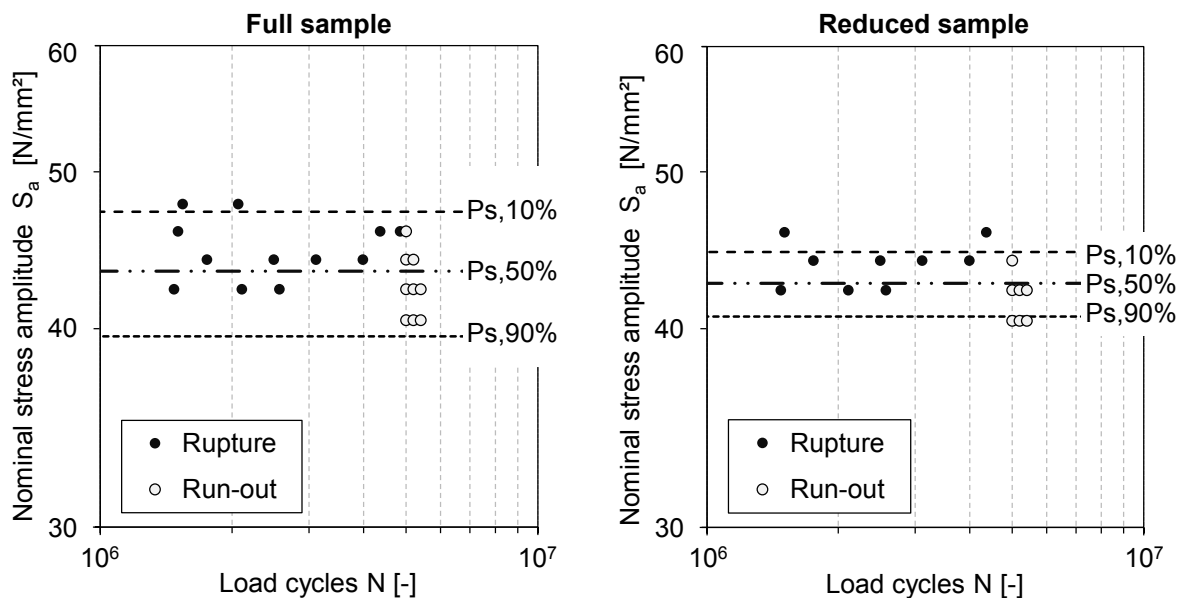


Figure 3-5: Statistic scatter band and test results in the TEL for black M36 HV-bolts with full sample (left) and reduced sample (right)

Table 3-3: Results of the statistic evaluation in the TEL for black M36 HV-bolts

		Full sample	Reduced sample
Mean ( $P_s,50\%$ )	[kN]	35.42	34.82
	[N/mm <sup>2</sup> ]	43.36	42.64
Standard deviation	[%]	7.0	3.6
	[N/mm <sup>2</sup> ]	3.0	1.5
Survival probability $P_s,10\%$	[N/mm <sup>2</sup> ]	47.24	44.61
Survival probability $P_s,90\%$	[N/mm <sup>2</sup> ]	39.49	40.66





**Table 3-4: Results of statistical evaluation in the upper HCF for black M36 HV-bolts**

HCF/ RRO	Ampl. $F_a$ [kN]	Ampl. $S_a$ [N/mm <sup>2</sup> ]	No. of tests [-]	Load cycles until failure			
				w/o RRO		with RRO	
				Mean (Ps,50%)	Standard- deviation	Mean (Ps,50%)	Standard- deviation
<b>Load horizon HCF 1; <math>F_{a,HCF1} \approx 1,6 \cdot F_{a,d,50}</math></b>							
HCF	56.0	68.6	5	310 178	21 374 (6.9 %)	329 214	65 264 (19.8%)
RRO			2				
<b>Load horizon HCF 2; <math>F_{a,HCF1} \approx 2,4 \cdot F_{a,d,50}</math></b>							
HCF	84.0	102.9	5	102 762	17 197 (16.7 %)	105 264	14 789 (14.1%)
RRO			2				
<b>Load horizon HCF 3 = HCF 2 (galv.) (only RRO)</b>							
RRO	66.0	80.8	2				

Percentile S-N curves

The complete percentile S-N curves for black M36 HV-bolt sets, synthesised from the tests in TEL and upper HCF, are illustrated in Figure 3-7 with and without consideration of RRO. The corresponding characteristic values are given in Table 3-5. Including RRO, the statistical S-N curve pattern exhibits a more homogenous progression with characteristically approximating percentile S-N curve with increasing load level. Furthermore, the scatter band of the enhanced sample superiorly covers the statistically unconsidered experiments from the initial approach to the TEL. The converse appearance of the evaluation without RRO is due to the relatively low sample size. In the further course of this thesis result representations refer to the enhanced sample.

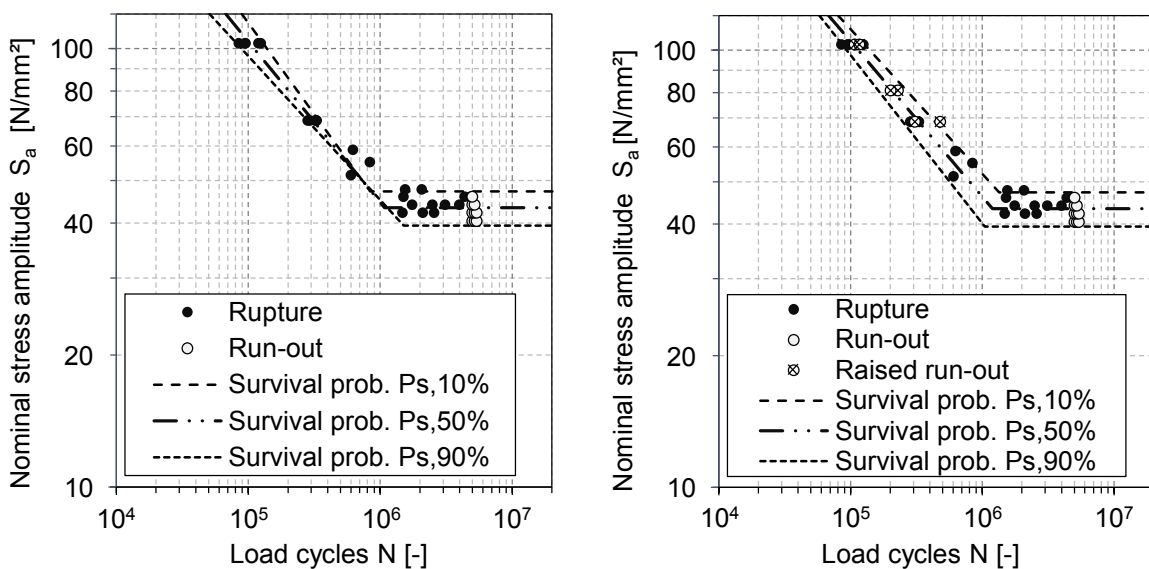


**Figure 3-7: Percentile S-N curves for black M36 HV-bolts; left: without RRO; right: with RRO**

**Table 3-5: Characteristic values of percentile S-N curves for black M36 HV-bolts**

	Percentile S-N curves without raised run-outs in the upper HCF			Percentile S-N curves with raised run-outs in the upper HCF		
	10%	50%	90%	10%	50%	90%
Survival probability $P_s$	10%	50%	90%	10%	50%	90%
Endurance limit $S_{a,d}$ [N/mm <sup>2</sup> ]	47.24	43.36	39.49	47.24	43.36	39.49
Knee point $N_D$ [-]	837 812	1 080 818	1 510 620	1 344 334	1 194 114	1 044 916
Upper HCF slope $k$ [-]	2.40	2.72	3.05	3.02	2.81	2.60

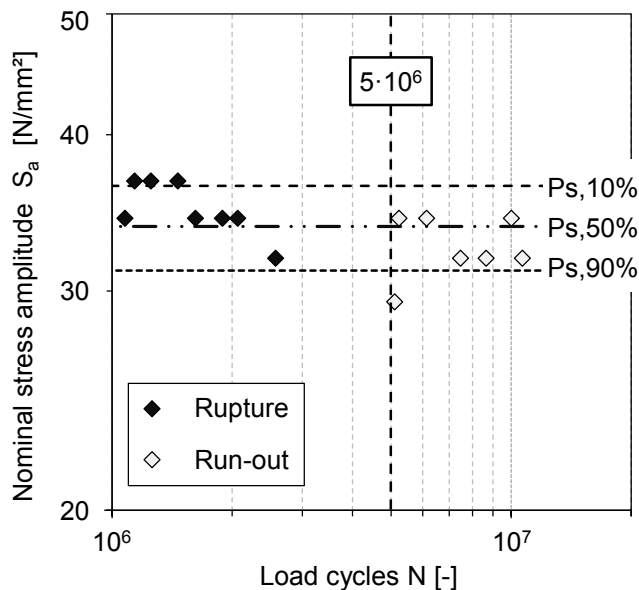
### Normal temperature hot-dip galvanized bolts

#### Transition region to the endurance limit (TEL)

Figure 3-8 shows the evaluation scheme of the staircase method for the fatigue tests on NT-galvanized M36 HV-bolts in the TEL. All ruptures occurred regularly in the first load-bearing turn of the thread and the load cycles until rupture showed a sufficient margin to the limit load cycle number  $N = 5 \cdot 10^6$  (see Figure 3-9). With three initial test runs on load levels which were not reached again in the remainder of the series, the statistical relevant test sequence contained 16 specimens at 4 load levels. Since no adaption of the initially chosen load increment was necessary, the contiguous sequence was performed in chronological order (though, partly alternating with specimens from the series on HT-galvanized bolts). The results of the statistical evaluation are given in Figure 3-9, right.

$F_a$ [kN]	$S_a$ [N/mm <sup>2</sup> ]	X = Rupture    O = Run-out																		X	O				
36.0	44.1	x																					1	0	
34.0	41.6		x																					1	0
32.0	39.2			x																				1	0
30.0	36.7				X					X	X	X												4	0
28.0	34.3				X	X	O	O	O	X											X			4	3
26.0	31.8					O	O														X	O		1	3
24.0	29.4																					O		0	1
Specimen / Test No.		1	2	3	4	5	6	7	8	9	10	11	12	13	14	15	16	17	18	19			$\Sigma$	9	7
																							Test series: NT-galvanized		

**Figure 3-8: Evaluation scheme of results in the TEL with the staircase method for NT-galvanized M36-HV bolts**



Mean (Ps,50%)	[kN]	27.57
	[N/mm²]	33.76
Standard deviation	[%]	6.1
	[N/mm²]	2.1
Survival probability Ps,10%	[N/mm²]	36.40
Survival probability Ps,90%	[N/mm²]	31.12

Figure 3-9: Scatter band and results of the statistic evaluation in the TEL for NT-galvanized M36 HV-bolts

Upper high cycle fatigue range (upper HCF)

The test results of the NT-galvanized M36 HV-bolts in the upper HCF are shown in Figure 3-10. Again, all ruptures occurred in the first load-bearing turn of the thread. The 4 RRO from the TEL are located closely within the scatter band of the regular sample. As can be seen from the results of the statistical evaluation, given in Table 3-6, both mean value and standard deviation are altered only slightly, using the extended sample. Overall, the results in the upper HCF yield a very narrow scatter.

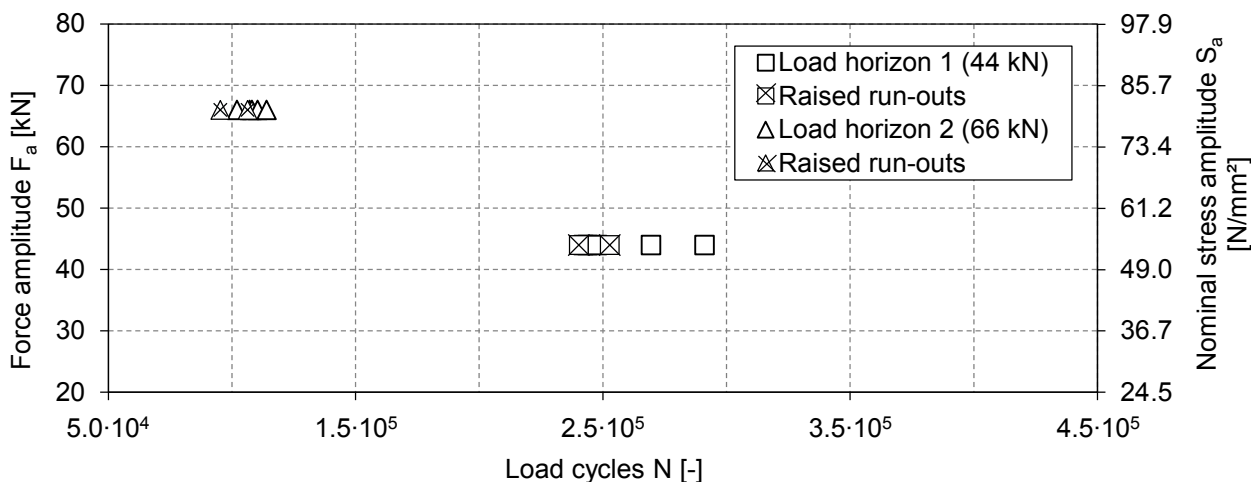


Figure 3-10: Test results in the upper HCF for NT-galvanized M36 HV-bolt

**Table 3-6: Results of statistical evaluation in the upper HCF for NT-galvanized M36 HV-bolts**

HCF/ RRO	Ampl. $F_a$ [kN]	Ampl. $S_a$ [N/mm <sup>2</sup> ]	No. of tests [-]	Load cycles until failure			
				w/o RRO		w/o RRO	
				Mean (Ps,50%)	Mean (Ps,50%)	Mean (Ps,50%)	Mean (Ps,50%)
<b>Load horizon HCF 1; <math>F_{a,HCF1} \approx 1,6 \cdot F_{a,d,50}</math></b>							
HCF	44.0	53.9	5	258 144	21 134 (8.2 %)	254 731	18 627 (7.3%)
RRO			2				
<b>Load horizon HCF 2; <math>F_{a,HCF1} \approx 2,4 \cdot F_{a,d,50}</math></b>							
HCF	66.0	80.8	5	108 238	4 412 (4.1 %)	106 010	6 040 (5.7%)
RRO			2				

### Percentile S-N curves

The complete percentile S-N curves for NT hot-dip galvanized M36 HV-bolts with and without consideration of raised run-outs in the upper HCF are shown in Figure 3-11 together with the corresponding characteristic values. Due to the marginal deviation between results with and without consideration of RRO in the upper HCF, only the variant with the enhanced sample size is shown and considered in the further course of this thesis.

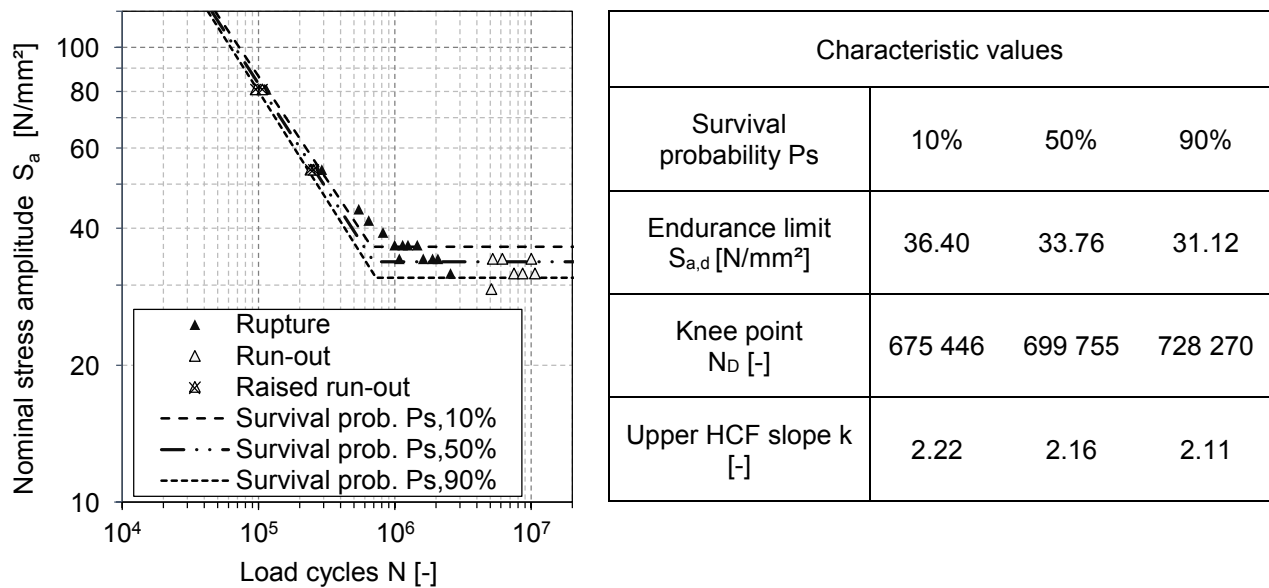


**Figure 3-11: Percentile S-N curves and characteristic values for NT-galvanized M36 HV-bolts (with consideration of RRO)**

## High temperature hot-dip galvanized bolts

### Transition region to the endurance limit (TEL)

During the tests on HT-galvanized M36 HV-bolts in the TEL, apart from characteristic failure locations in the first load-bearing turn of the thread, a number of ruptures also occurred under the bolt head as well as at the unnotched bolt shaft (see Figure 3-12). To investigate the potential influence of a distorted load application (as supposed to have occurred temporarily at the test series on black M36-bolts) or production related impact, alternately, specimens were tested from the test series on NT-galvanized bolts at comparable load levels. However, at all NT-galvanized specimens ruptures occurred in the first load-bearing turn of the thread (henceforth denoted as regular failure location). It can thus be assumed that the irregular failure locations can directly be attributed to the HT-galvanized boundary layer configuration. As can be observed in Figure 3-15, the ruptures outside the thread, with one exception, occurred only after the originally defined limit load cycle number  $N = 5 \cdot 10^6$ . Moreover, a further specimen with regular rupture location failed after reaching the run-out limit.

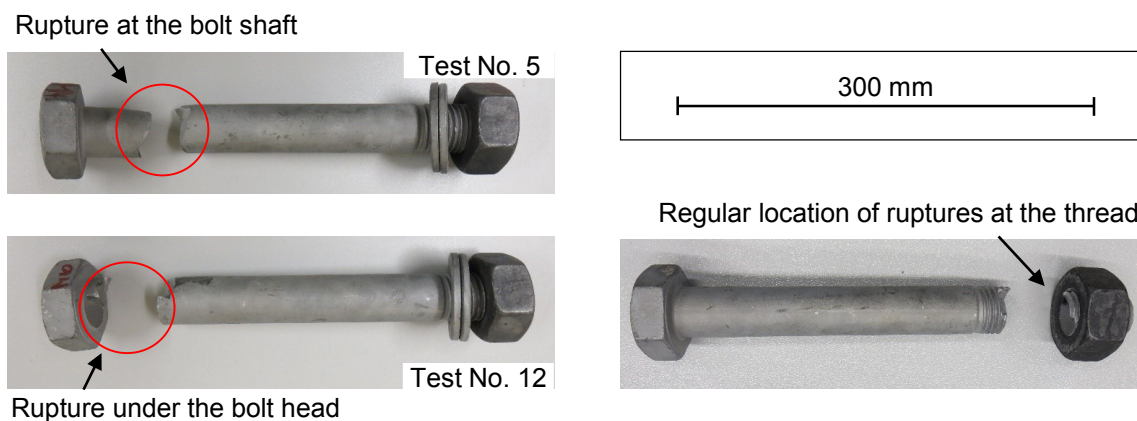


**Figure 3-12: High temperature hot-dip galvanized M36 HV-bolt sets with irregular failure locations at the shaft and under the bolt head**

The observed irregularities regarding failure location and high failure load cycles imposed uncertainties to the statistical evaluation. The variations of the failure location, especially to the unnotched shaft, suggest that at the affected specimens different damage mechanisms have been present compared to the HT-galvanized bolts, as well as black and NT-galvanized bolts, with regular failures (the potential causes are further discussed in Chapter 3.3.3). In general, the validity of a collective statistical evaluation of specimens with ambiguous failure mechanisms certainly is questionable. For a conclusive evaluation it can be regarded preferable to investigate specimens separately, which distinctly belong to different statistical populations (e.g., as done in the framework of this investigation for the specimens with different boundary layer production process). However, in the present case an unequivocal differentiation between different initial conditions of specimens, causative for different damage mechanisms, is not possible. Moreover, the occurrence of varying failure locations did not show a distinguishable systematic and it cannot be precluded that also failures inside the paired thread might have been affected by a varying damage mechanism. Therefore, it was considered

legitimate to interpret the general failure of the specimen, independent from failure locations and decisive damage mechanism, as pivotal event for the evaluation of the bolts' survival probability. The specimens with varying locations of failure are thereby evaluated within a single sample.

Nonetheless, the obtained high load cycle number until failure, partly considerable exceeding  $5 \cdot 10^6$ , still imposes the questions whether the originally defined limit load cycle number was chosen too low for the HT-galvanized bolts. Therefore, it was assessed within an additional evaluation whether an increased limit load cycle number affects the statistical results. To this end, given the obtained test results, a maximal shift of the limit load cycle number up to  $9 \cdot 10^6$  was possible.

The regular staircase evaluation scheme with a limit load cycle number of  $N_{lim} = 5 \cdot 10^6$  is shown in Figure 3-13. It included 15 statistically relevant specimens at 4 load levels. Therein, ruptures which occurred after reaching the defined load cycle limit were classified as run-outs. Figure 3-14 shows the alternative evaluation scheme with increased limit load cycle number  $N_{lim} = 9 \cdot 10^6$ . In this staircase sequence, the specimens where rupture occurred between  $5 \cdot 10^6$  and  $9 \cdot 10^6$  load cycles were classified as ruptures instead of run-outs. The resulting sequence comprised 15 statistically relevant specimens at 3 load levels. Since the staircase method requires the formation of a contiguous sequence, at both variants a certain number of performed experiments needed to be excluded from the evaluation. These are appended at the end of the evaluation schemes for informative purposes. In the illustrations, test runs with irregular failure location are coloured dark grey. The test run with regular location of rupture but very high load cycle number is coloured light grey. The allocation of test runs and failure characteristics can also be found in a concise representation in Appendix A.2.

$F_a$ [kN]	$S_a$ [N/mm <sup>2</sup> ]	X = Rupture O = Run-out															X	O							
32.0	39.2	X							X												2	0	■		
30.0	36.7		X			X		○		X		X		X								5	1		
28.0	34.3			X		○		○					○	○		○						1	5	■	
26.0	31.8				○															○	○	0	1	■	
Specimen No.		1	2	3	4	5	6	7	8	9	10	11	12	13	14	15	16	17	18			Σ	8	7	
Test No.		1	2	4	5	3	10	7	12	13	14	15	16	17	18	9	6	8	11						
Test series: HT-galvanized																									

Figure 3-13: Regular evaluation scheme of results in the TEL with the staircase method for HT-galvanized M36-HV bolts and limit load cycle number  $N_{lim} = 5 \cdot 10^6$

$F_a$ [kN]	$S_a$ [N/mm <sup>2</sup> ]	X = Rupture O = Run-out															X	O							
32.0	39.2															X	X					0	0	■	
30.0	36.7	X			X				X		X		X									5	0		
28.0	34.3		X		○		X		○				○		X							3	4	■	
26.0	31.8			○				○								X						1	2	■	
Specimen No.		1	2	3	4	5	6	7	8	9	10	11	12	13	14	15	16	17	18			Σ	9	6	
Test No.		2	3	6	9	10	4	8	11	12	15	14	17	16	7	5	1	13	18						
Test series: HT-galvanized																									

Figure 3-14: Alternative evaluation scheme of results in the TEL with the staircase method for HT-galvanized M36-HV bolts and limit load cycle number  $N_{lim} = 9 \cdot 10^6$

The comparison of results obtained with the two evaluation variants, shown in Table 3-7, demonstrates that the adjustment of the limit load cycle number barely affects neither the resultant statistical mean value nor the standard deviation of the endurance limit. To obtain a contiguous staircase sequence with at least 15 specimens it was presupposed in the evaluation with increased limit load cycle number, that a test run which was ended manually without rupture after approximately  $7.5 \cdot 10^6$  load cycles would likewise have reached the adjusted run-out limit. Rejecting this test run from the evaluation reduced the evaluable staircase series to 12 specimens. Likewise, with this series the results of the statistical evaluation only vary marginally. The performed test series is thus considered to have produced statistically meaningful results, despite the occurrence of ruptures after the defined limit load cycle number. In the sequel, the results from the statistical evaluation with regular limit load cycle number  $N_{lim} = 5 \cdot 10^6$  are considered decisive.

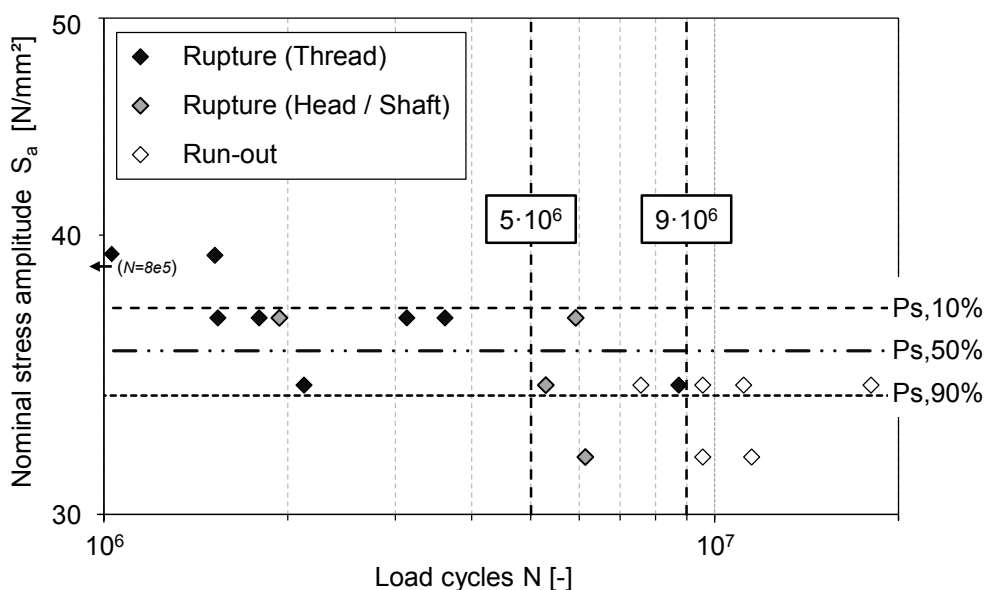


Figure 3-15: Statistic scatter band and test results in the TEL for HT-galvanized M36 HV-bolts (limit load cycle number  $N_{lim} = 5 \cdot 10^6$ )

Table 3-7: Results of statistic evaluation in the TEL for HT-galvanized M36 HV-bolts considering different limit load cycle number  $N_{lim}$

		$N_{lim} = 5 \cdot 10^6$	$N_{lim} = 9 \cdot 10^6$	
			15 spec.	12 spec.
Mean (Ps,50%)	[kN]	29.00	28.33	28.20
	[N/mm <sup>2</sup> ]	35.51	34.69	34.53
Standard deviation	[%]	4.0	2.9	3.1
	[N/mm <sup>2</sup> ]	1.4	1.0	1.1
Survival probability Ps,10%	[N/mm <sup>2</sup> ]	37.35	35.97	35.90
Survival probability Ps,90%	[N/mm <sup>2</sup> ]	33.67	33.41	33.16



### Upper high cycle fatigue range (upper HCF)

The results of HT-galvanized M36 HV-bolts in the upper HCF are shown in Figure 3-16. Thereby, all ruptures were located regularly in the first load-bearing turn of the thread. The results from the four raised run-outs from the TEL are located within the scatter of results of the regular sample. The results of the statistical evaluation with the horizon method with and without consideration of raised run-outs are given in Table 3-8. Only marginal variations of the evaluation results arise from the enhancement of the sample size.

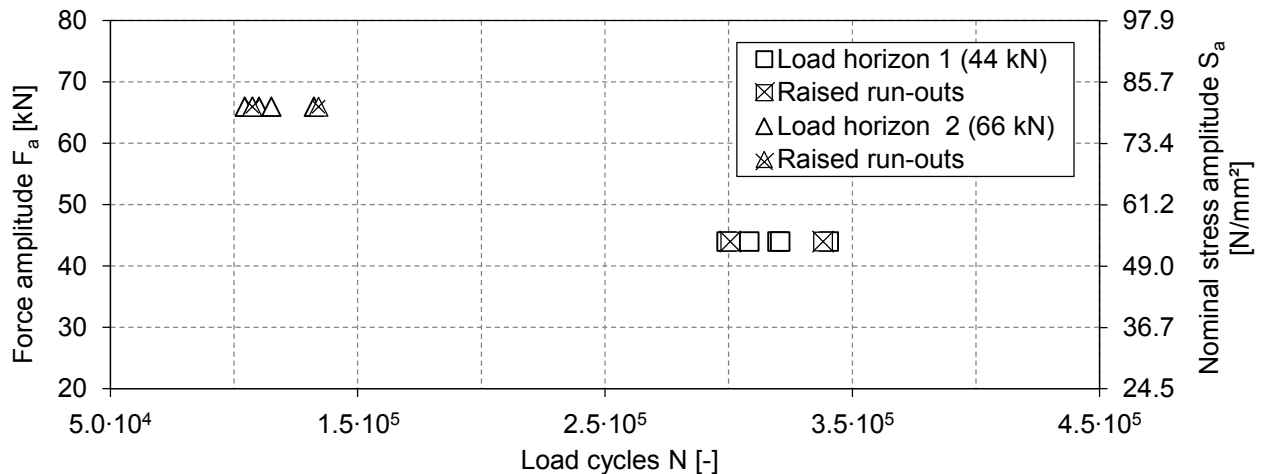


**Figure 3-16: Test results in the upper HCF for HT-galvanized M36 HV-bolt**

**Table 3-8: Results of statistical evaluation in the upper HCF for HT-galvanized M36 HV-bolts**

HCF/ RRO	Ampl. $F_a$ [kN]	Ampl. $S_a$ [N/mm <sup>2</sup> ]	No. of tests [-]	Load cycles until failure			
				w/o RRO		with RRO	
				Mean (Ps,50%)	Standard- deviation	Mean (Ps,50%)	Standard- deviation
<b>Load horizon HCF 1; <math>F_{a,HCF1} \approx 1,6 \cdot F_{a,d,50}</math></b>							
HCF	44.0	53.9	5	317 409	15 538 (4.9 %)	317 830	16 697 (5.3%)
RRO			2				
<b>Load horizon HCF 2; <math>F_{a,HCF1} \approx 2,4 \cdot F_{a,d,50}</math></b>							
HCF	66.0	80.8	5	113 420	11 058 (9.8 %)	115 272	12 373 (10.7%)
RRO			2				

### Percentile S-N curves

Figure 3-17 depicts the percentile S-N curves and characteristic values for the HT-galvanized M36-bolts, resultant from statistical evaluations in the TEL with regular limit load cycle number  $N_{lim} = 5 \cdot 10^6$  and upper HCF with specimen sample enhanced by RRO. Since the obtained standard deviation of results in the upper HCF was smaller at the lower than at the upper tested load horizon, the percentile S-N curves show an uncharacteristically divergent pattern at increasing loads. This can be led back

to the relatively low number of considered specimens. It needs to be assumed that the actual scatter, especially at the lower load horizon, is underestimated by the results. The test series' main objective of determining the progression of the mean S-N curve remains unaffected.

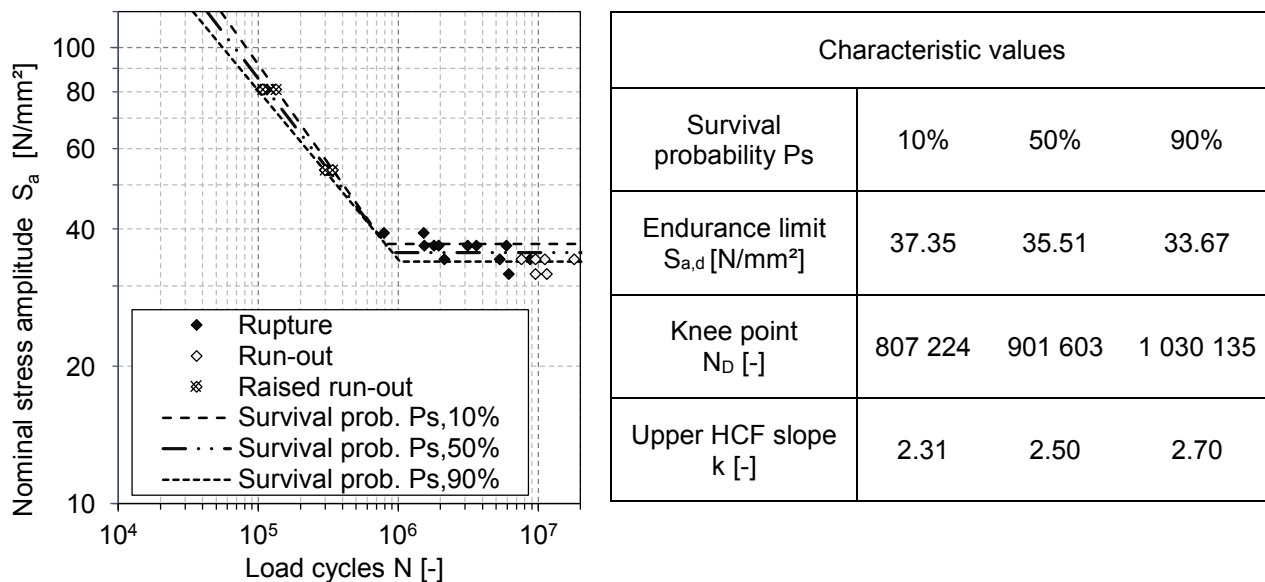


**Figure 3-17: Percentile S-N curves and characteristic values for HT-galvanized M36 HV-bolts (with consideration of RRO)**

### 3.3.3 Assessment of the boundary layer effect

The comparison of the complete test results of the three performed test series on M36 HV-bolts with different boundary layer configurations “black” (B), “normal temperature hot-dip galvanized” (NT) and “high temperature hot-dip galvanized” (HT) is shown in Figure 3-18. The results reveal a considerable reduction of the fatigue strength induced by hot-dip galvanizing. Considering the depicted mean S-N curves (Ps,50%), as given in Table 3-5 as well as Figure 3-11 and Figure 3-17, a reduction of the endurance limit of about 20 % compared to the uncoated specimens is given for both NT- and HT- galvanized bolts. Moreover, a clear reduction of endurable load cycles is also present in the upper HCF.

As such, the experiments confirm the findings from *Ungermann et al. (2014)* regarding the quantitative effect of hot dip-galvanizing, experimentally derived for welded construction details as well as notched specimens with bolt-alike notch geometry published by *Oechsner et al. (2015)* and *Simonsen (2015)* (see Chapter 2.1.4). In the previously mentioned studies the fatigue crack initiation process at galvanized specimens could be documented by microscopic analyses of systematically aborted test runs. The given characteristics of the here analysed bolt-to-nut connections, where the fatigue critical location is sited in the area of the overlaid thread, impede an equivalent documentation. However, since they were performed within the framework of the same research project, the experimental investigations on notched specimens by *Oechsner et al. (2015)* were intentionally designed in terms of material characteristics and notch geometry, to provide high transferability of failure characteristics to the here presented test series. Considering the qualitative and quantitative

similarity of the results, it can thus safely be presumed that a similar failure mechanism, induced by shrinkage cracks in the brittle phases of the zinc coating, is responsible for the found reduction of fatigue strength.

Additionally to the sole difference of the boundary layer, the paired thread of uncoated, black and hot-dip galvanized HV-bolt sets is also subject to a certain geometrical variation, which is induced by differing tolerance zones between bolt and nut. To provide clearance for the additional zinc coating the here tested hot-dip galvanized bolts were executed with tolerance zone 6g/AZ, contrasting the black bolts with tolerance zone 6g/6H (bolt/nut according to ISO 965). According to *Wiegand et al. (2007)* a larger tolerance zone may be assumed to rather impose a favourable than a negative effect on the fatigue strength, because of a higher resilience of the thread and a more homogenous load distribution. Within the framework of the here described test series, additional exemplary test runs were performed at distinct load levels, where black bolts (6g) were paired with nuts originally designated for galvanized bolts (6AZ). The results, which are published in *Oechsner et al. (2015)*, did not indicate any impact of the changed tolerance. This is in general accordance with the state of knowledge from the literature, which testifies a negligibly influence of thread geometry tolerances in the normative regulated range (see Chapter 2.1.4). Consequently, the variation of the tolerance zones does not need to be presumed to have affected the obtained results.

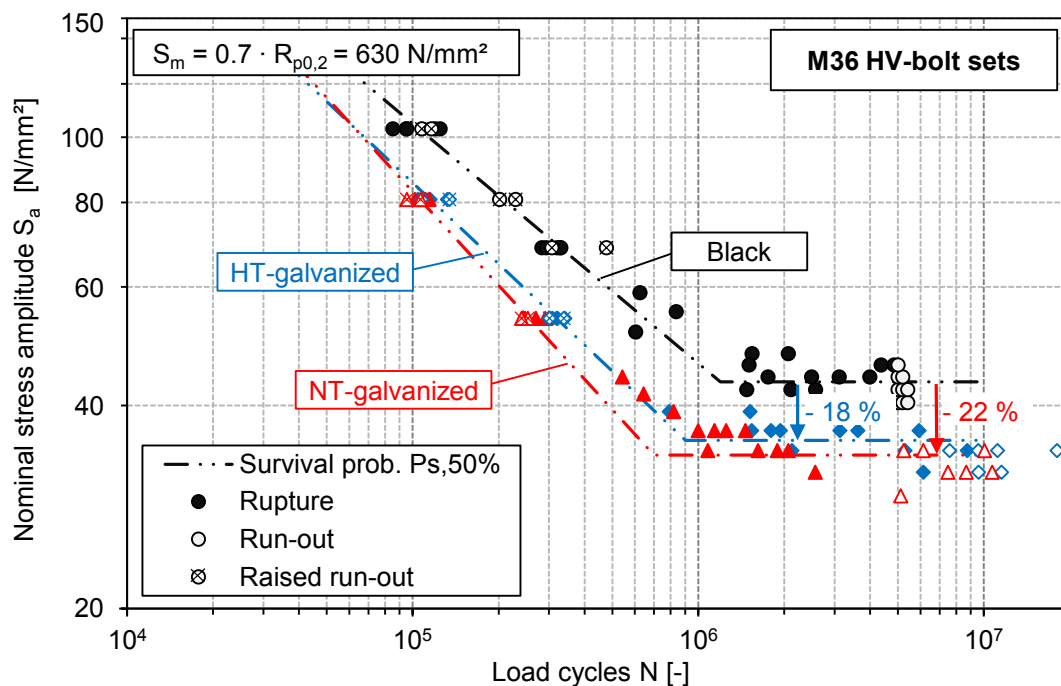


**Figure 3-18: Comparison of test results of M36 HV-bolts with different boundary layers**

Comparing the test results of the boundary layer affected test series with different galvanizing temperature, the statistical evaluation of the HT-galvanized bolts suggests a slightly superior fatigue performance to their NT-galvanized counterparts. A similar tendency could be observed in test results on bolts of size M16 by *Berger et al. (2008)*. However, in both cases the strongly overlapping scatter bands of the test series on NT- and HT-galvanized bolts do not allow the conclusion that a

statistically significant variation is to be supposed. Instead, a rather comparable effect of the galvanizing boundary layer to the bolts fatigue strength can be assumed. As such, the results also confirm test results from *Valtinat* (1994) on bolts of size M30 and are in general accordance with the recommendation given in VDI Guideline 2230 (2015) to reduce the endurance limit of both NT- and HT-galvanized bolts equally by 20 % (a detailed verification of the normative regulations is carried out in Chapter 3.6).

Even though the results of the statistical evaluation do not imply a significant variation of the fatigue strength, the found peculiarities in the failure behaviour of the HT-galvanized specimens are to be taken into consideration. As described in the previous section, the occurrence of ruptures at irregular locations can be directly related to the HT-galvanized production state. The fact that irregular ruptures did not only occur under the bolt head but also in the unnotched shaft indicated that a surface layer related damage mechanism was present, which enabled a fatigue crack initiation incoherent to the maximum stress concentration. Thereby, the variant damage mechanism only was decisive at load levels in the TEL, where a regular fatigue crack initiation inside the thread was less likely to occur. At higher loads in the upper HCF, the potential fatigue crack initiation was dominated by the strong notch effect inside the thread resulting in solely regular ruptures in the first load-bearing turn. Fracture surface analyses at the affected specimens with irregular ruptures, described in *Oechsner et al.* (2015), revealed that at the locations of fatigue crack initiation zinc had intruded into the bolts' base material. As stated by the authors of the Chair and Institute for Materials Science, Technische Universität Darmstadt, who performed the metallographical analysis, the observed presence of zinc in the base material hints to an intrusion into production related surface defects or to liquid metal assisted cracking (LMAC). However, a final ascertainment could not be made.

Nonetheless, the results highlight that the application of high temperature hot-dip galvanizing to HV bolts of size M36 implies uncertainties in the fatigue damage behaviour, which may potentially undermine a systematic fatigue assessment and design. To securely verify the practical applicability of HT-galvanizing up to bolt diameter M36 further specifically designated studies are necessary.

### 3.4 Test on M64 HV-bolt sets with constant amplitude loading

#### 3.4.1 Test execution

Aiming for an extension of the achieved experimental test basis on M36 HV-bolts, subsequently the test series on very large diameter M64 HV-bolt sets was performed. Based on the results of both series, for the first time the influence to the fatigue strength of an increased diameter, reaching into the top end of applied bolt sizes in modern wind turbine structures, could be investigated for uncoated black (B) as well as normal temperature hot-dip galvanized bolts (NT).

To realise the requisite testing conditions at representative mean load level (1680 kN), the tests on the M64 HV-bolt sets were performed in a high-strength servo-hydraulic testing machine (10 MN), belonging to the test facilities of the Institute for Building Materials Science of the Leibniz Universität Hannover. An appropriate test specimen adaption was specifically designed and manufactured for the test series. The test set-up is depicted in Figure 3-19.

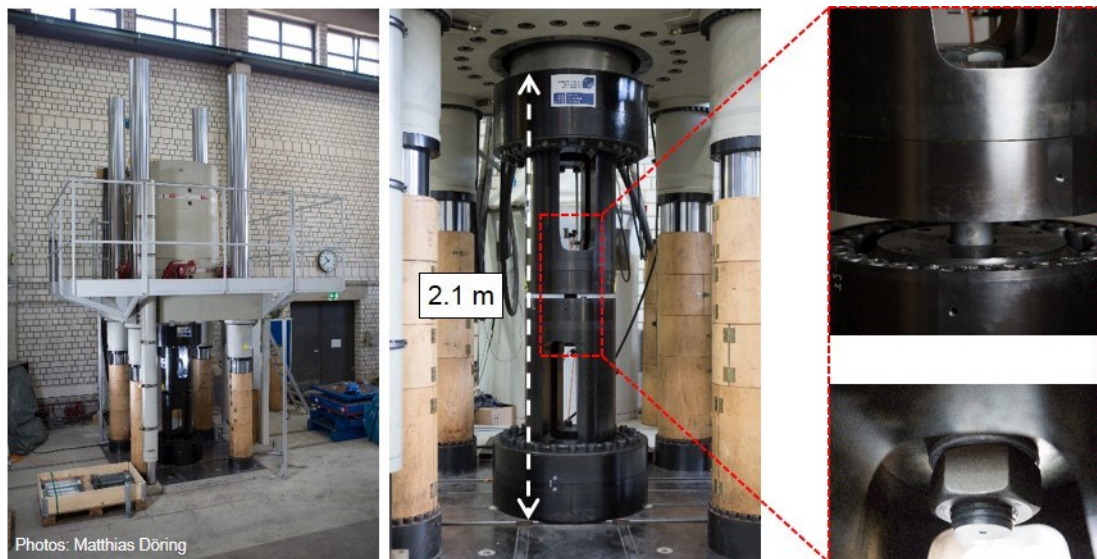


**Figure 3-19: Test set-up for M64 HV-bolt tests under constant amplitude loading in servo-hydraulic testing machine**

With 2-4 Hz, the achievable testing frequency was considerably lower than in the previously described test series on M36 bolts (~50 Hz). Given the much longer testing durations ( $1 \cdot 10^5$  load cycles in about 9 hours) and higher testing costs, the objective was to validate the obtained test results on M36 bolts with a reduced number of specimens. Thereby, tests were primarily performed in the upper HCF.

Due to the limited number of available test specimens and lack of previous information about the endurance limit, testing and evaluation had to be performed differently to the horizon method, used in the test series on the M36 bolts. Thereby, the individual test runs were performed at diverse load levels instead of designated load horizons. Denoted as “*Perlenschnurverfahren*” (engl.: string of pearls), the procedure, for example described in *Mauch* (1999), is based on the presupposition that

the S-N curve in the upper HCF, when plotted in double logarithmic scale, follows a linear progression. Thus, test results enable the determination of location and slope  $k$  of the resultant mean S-N curve with 50 % survival probability by a corresponding linear regression analyses.

Towards to the horizon method, the procedure provides the advantage that usually a smaller test quantity is required for an appropriate estimation of the mean survival probability. However, for a further evaluation of the statistical scatter band it is presupposed that the slopes of the percentile S-N curves ( $P_s,10\%$ ,  $P_s,50\%$ ,  $P_s,90\%$ ) are identical. Thus, with the previously determined slope, all results located in the upper HCF can be transferred to a mutual, freely eligible reference load horizon. The obtained modified test results enable a statistical evaluation, analogues to the horizon methods with equations Eq. 3-2 to 3-5. In this way, locations of parallel shifted percentile S-N curves can be determined. The usually apparent load level dependent variation of the scatter band remains unconsidered in the evaluation. However, this simplification was considered acceptable for the given evaluation purpose.

To maximise the validity of the obtained results it was crucial that the performed tests cover an ample load cycle range in the upper HCF without, however, reaching to far above or below into low cycle fatigue range or TEL. For the performed evaluation, it was presumed that a linear progression of the S-N curves could safely be assumed within a range of  $1 \cdot 10^4$  and  $5 \cdot 10^5$  load cycles. Without the knowledge of a previously determined endurance limit, the initially applied load levels were chosen based on the results of the M36 bolts. In the ongoing of the test series the applied loads were then successively adapted for an appropriate coverage of the fatigue range within the defined boundaries.

Additionally to the tests in the upper HCF, for each considered boundary layer state (B, NT) two further test runs were performed, which reached into the TEL. Within the given limitations of available specimens and economically reasonable testing durations, these tests aimed for a spot test wise evaluation of the tendential location of the endurance limit. To this end, the obtained results in the upper HCF as well as the determined endurance limits of the M36 bolts served as reference benchmark. A summary of the testing program on M64 HV-bolts is given in Table 3-9.

**Table 3-9: Summary of testing program for constant amplitude tests on M64 HV-bolt sets**

Boundary layer	Black	NT-galvanized
Mean stress $S_m \approx 0.7 \cdot R_{p,0.2}$	630 N/mm <sup>2</sup>	630 N/mm <sup>2</sup>
<b>Upper HCF</b> Amplitude $S_a$ Number of specimens	47-131 N/mm <sup>2</sup> 7	47-112 N/mm <sup>2</sup> 7
<b>TEL*</b> Amplitude $S_a$ Number of specimens	34-39 N/mm <sup>2</sup> 2	32-37 N/mm <sup>2</sup> 2
Loading conditions Test end criteria Testing frequency	purely axial, constant amplitude loading, $R \approx 0.65 - 0.9$ rupture 2-4 Hz	

\*Test in the TEL without statistical evaluation

### 3.4.2 Test results and statistical evaluation

Figure 3-20 and Figure 3-21 show the obtained test results of the M64 HV-bolt sets separately for the two investigated boundary layer configurations. The tabulated results can be found in Appendix A.3. All ruptures occurred regularly in the first load-bearing turn of the thread.

For both boundary layer configurations, the performed test program resulted in 7 statistically relevant test runs, with load cycle numbers reaching throughout the full upper HCF and reasonable margin to the defined lower and upper bounds. To quantify the scatter band the results were transferred to a mutual reference load level of  $\bar{S}_a = 50$  N/mm<sup>2</sup> (green horizontal line). In the result illustrations the modified test points (M64-B/NT\*) are shown with grey colouring.

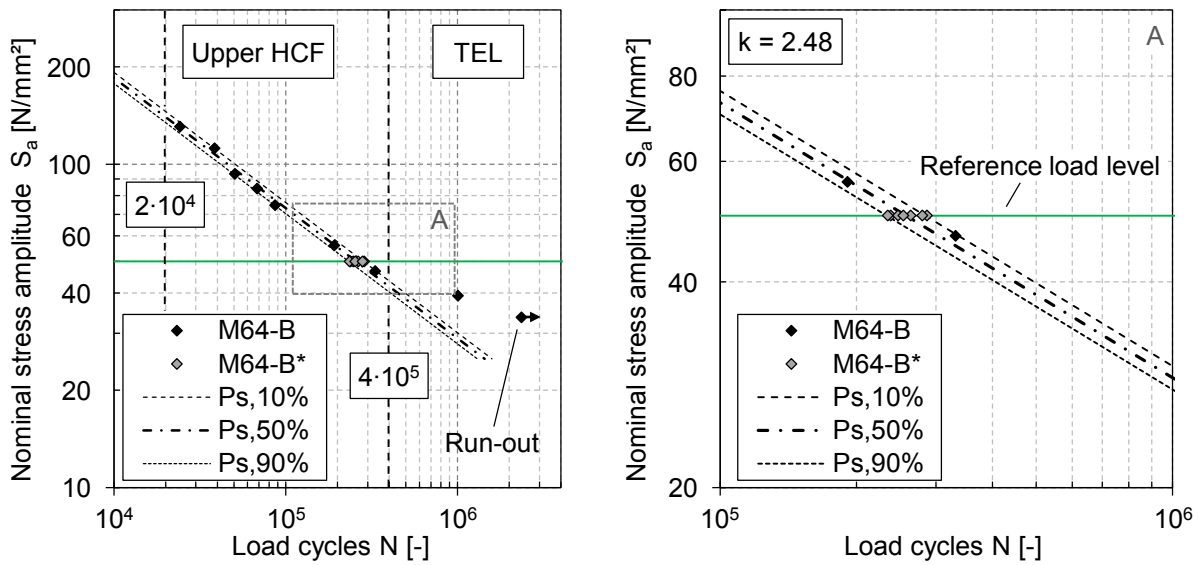


Figure 3-20: Test results and percentile S-N curves for black M64 HV-bolts (left: full results; right: excerpt (A) of the reference load horizon with modified test point M64-B\*)

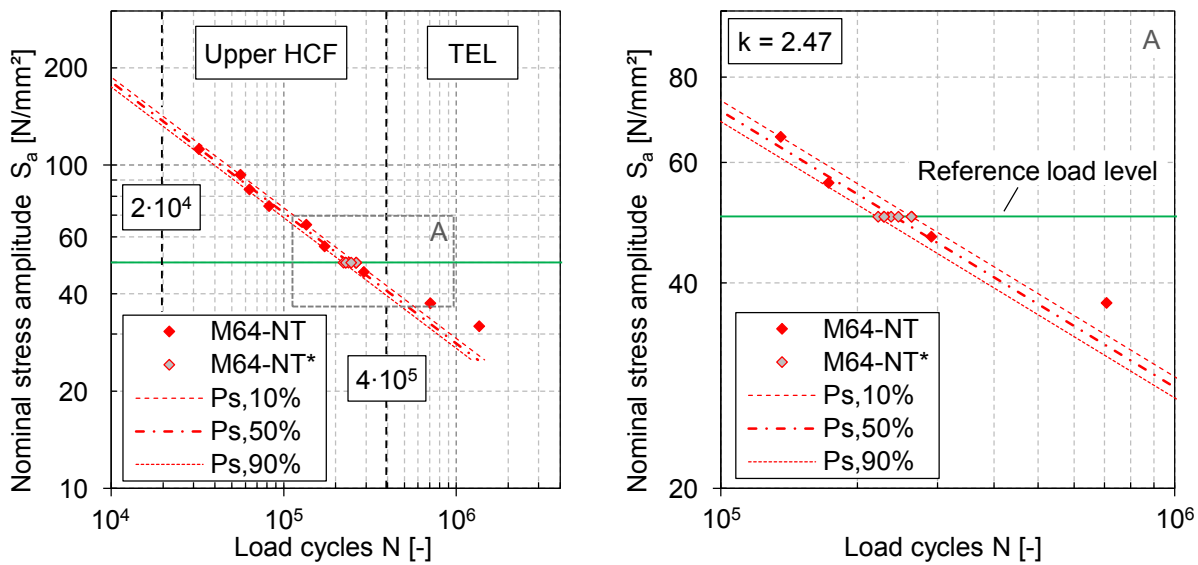


Figure 3-21: Test results and percentile S-N curves for NT-galvanized M64 HV-bolts (left: full results; right: excerpt (A) of the reference load horizon with modified test point M64-NT\*)

The results of the statistical evaluation, given in Table 3-10, are stated on the basis of the selected reference load level. Together with the determined slopes, the S-N curves in the upper HCF can be fully described. As becomes apparent from the graphical illustrations, at both series the results in the upper HCF line up closely to the determined median S-N curve. This is also reflected by the moderate standard deviations. The low result scatter demonstrates a high overall quality of obtained results, appropriate bolt production and test set-up conditions.

As can be seen, at four test runs (two for each boundary layer configuration) load cycles until rupture intendedly exceeded the defined limit for the upper HCF. These are not considered in the statistical evaluation. One test run was aborted manually as “run-out” after exceeding  $2 \cdot 10^6$  load cycles. The remainder failed within a range of  $7 \cdot 10^5$  and  $1.3 \cdot 10^6$  load cycles. With results notably deviating to the scatter band from the statistical evaluation, the tests are to be allocated to the TEL. They are further assessed qualitatively in comparison to the test results on the M36 bolts in the subsequent section.

**Table 3-10: Results of statistic evaluation of M64 fatigue tests in high cycle fatigue range for reference load level  $\bar{S}_a = 50 \text{ N/mm}^2$**

	Black	NT-galvanized
Reference load horizon	50 N/mm <sup>2</sup>	50 N/mm <sup>2</sup>
Load cycles until rupture with survival prob. Ps,10%	283700	262819
survival prob. Ps,50%	257160	240801
survival prob. Ps,90%	233103	220628
Standard deviation	7.76 %	6.92 %
Upper HCF slope k	2.48	2.47

### 3.4.3 Assessment of the boundary layer effect and comparisons to M36 bolts

#### Result comparison

The direct comparison between test results on black and NT-galvanized M64 HV-bolts is shown in Figure 3-22. It becomes obvious that, contrary to the results on the M36 bolts (see Figure 3-18), in the upper HCF no statistically measurable deviation between the two boundary layer configurations can be detected. With strongly overlapping scatter bands, the results of both series are effectively on an identical level.

In the comparison of test results on M64 and M36 HV-bolts in Figure 3-23, left it can be observed that the fatigue strength of the black M64 bolts (here for better differentiation coloured green) is measurably reduced compared to their counterparts with diameter M36 (coloured black). In point of fact, consistently throughout the upper HCF the endured load cycles until rupture are more than 50 % less than the statistic mean (survival probability Ps,50%), determined for the black M36 bolts.



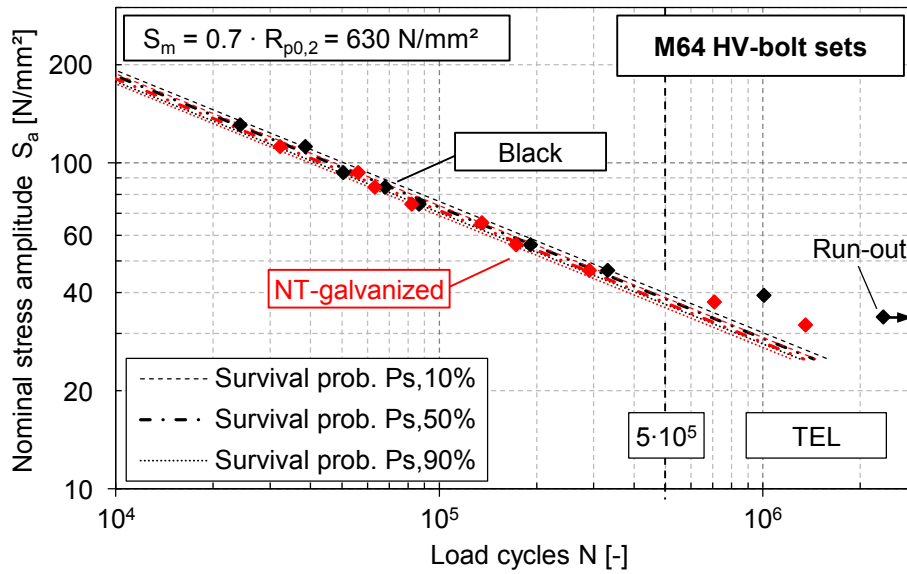


**Figure 3-22: Comparison of test results of M64 HV-bolts with different boundary layers**

Considering the comparison of the NT-galvanized HV-bolts in Figure 3-23, right, likewise a reduction of fatigue strength in the upper HCF of M64 (coloured violet) compared to M36 bolts (coloured red) is visible. However, the difference of bearable load cycles is considerably less than present at the bolts without galvanizing and it tendentially reduces with decreasing load level. Consequently, the close conformity of obtained results of M64 bolts with different boundary layer is to be ascribed to a deterioration of fatigue strength at black bolts, compared to their M36 diameter equivalents, rather than to a less severe impact of the zinc coating at the galvanized bolts.

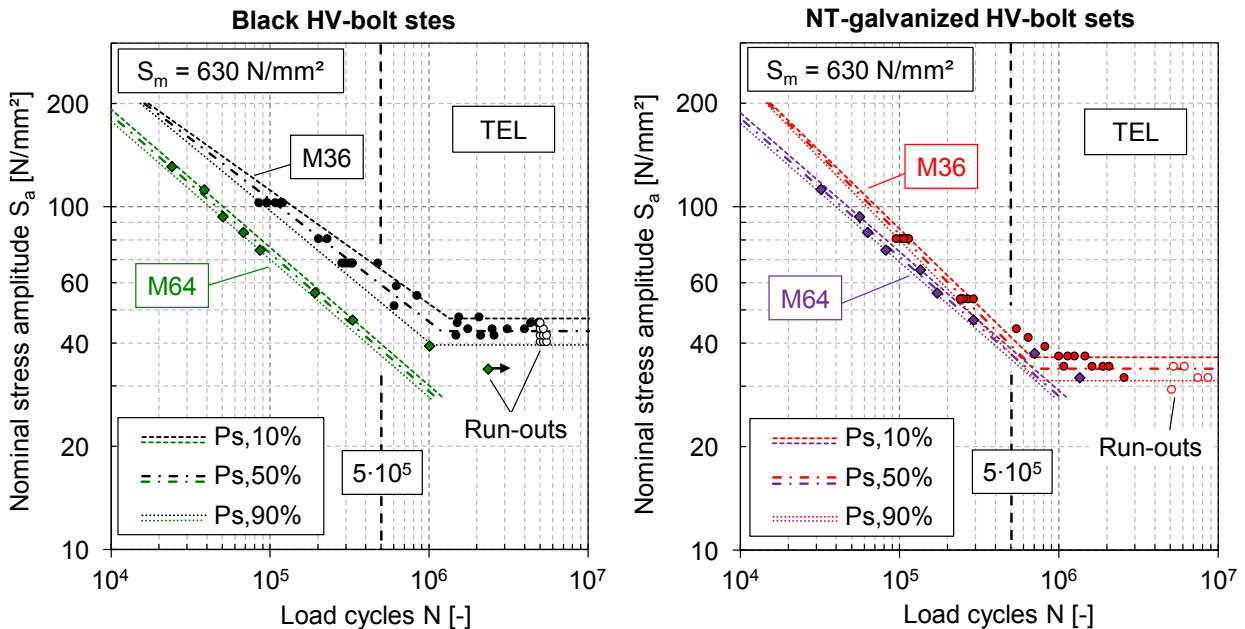


**Figure 3-23: Comparison of test results of M64 and M36 HV-bolt sets with uncoated, black (left) and NT hot-dip galvanized (right) boundary layer configuration**

For each boundary layer condition, test runs were performed at load levels, located within the determined scatter bands of the M36 bolts' endurance limit. With reference to the latter and the statistical evaluation for M64 bolts in the upper HCF, there are cogent indications that for the black M64 bolts also a notable reduction of the endurance limit, compared to the M36 bolts, needs to be assumed. At a load level, slightly lower than the black M36 bolts' 10 % survival probability ( $P_s, 10\%$ ), the tested M64 bolt (lowest result point in Figure 3-23, left before the defined transition line to the TEL at  $N = 5 \cdot 10^5$ ) reached a significantly lower load cycle number than the respective M36 bolts. The test run is located within the narrow scatter band of the remaining upper HCF test results. Only at further reduction of the cyclic load, the two test results exhibit a notable deviation from the upper HCF scatter. Still, at a load level slightly below the 90 % survival probability mark ( $P_s, 90\%$ ) of the black M36 bolts' endurance limit, where all tested M36 bolts reached the defined run-out limit of  $5 \cdot 10^6$  load cycles, the M64 bolt's endured fatigue life is distinguishable lower.

Considering the NT-galvanized M64 bolts, already at the test run in the upper region of the TEL ( $P_s, 10\%$ ) determined for the M36 bolts (first result point in Figure 3-23, right after the defined transition line to the TEL at  $N = 5 \cdot 10^5$ ), a deviation from the M64 bolts upper HCF scatter band is recognizable. This suggests that TEL of NT-galvanized M36 and M64 as well as black M64 bolts are within a comparable order of magnitude. However, endured load cycles in the TEL indicate a slightly inferior fatigue strength of NT-galvanized M64 bolts compared to the other two mentioned configurations. However, since fatigue tests in the TEL are subject to pronounced scatter, for a secured evaluation a considerably higher number of time and cost-consuming tests would be necessary. The interpretations regarding the M64 bolts endurance limit are thus given only as a general estimate.

### Discussion

Taken together, despite a significant difference in the order of magnitude, the result comparison of the performed constant amplitude fatigue tests revealed a reduction of fatigue strength for both black and NT hot dip-galvanized HV-bolts at an increased diameter. Thereby, it needs to be considered that, additionally to the larger bolt size, other factors varied between the performed test series on M36 and M64 bolts, such as the bolt manufacturer, base material and production batch as well as test facility and frequency. Considering potential scatter of bolt fatigue tests on specimens from different manufactures, as present for instance in test results from *Marten* (2009) on M48 HV-bolts performed with otherwise identical boundary conditions, the here obtained reduction of fatigue strength between NT-galvanized M36 and M64 bolts does not appear overly critical. It is still within a reasonable order of magnitude of general scattering test results. Moreover, also a certain impact of the significantly lower testing frequency, which had to be reduced by more than a factor of 10 in the M64 compared to the M36 experiments, cannot entirely be precluded. Within the review of the corresponding state of knowledge in Chapter 2.1.4, it was elaborated that there is, albeit not conclusively confirmed, certain evidence that suggests that a low testing frequency, as applied in the M64 tests, has a tendentially fatigue life reducing effect, especially at higher load levels. This behaviour is generally reflected by the obtained test results, where the scatter bands of NT-galvanized M64

and M36 bolts approximate with decreasing load level. Still, the actual presence of a testing frequency related effect on the test results can neither be affirmed nor ruled out by either, the performed test program or priorly existing investigations.

The investigation of the impact of loading frequency to the fatigue damage by numerical means is to be ascribed to fundamental research work and not feasible within the framework of this dissertation. Still, to obtain further insights into the potential impact factors to the fatigue strength of large-size bolts, specific geometry and material related aspects will be further investigated in the analytical studies of the thesis at hands.

Concerning the reason for the detected prominent reduction of fatigue strength of the tested black M64 HV-bolt sets, it may mostly be hypothesised. It is plausible to assume that for the uncoated black bolts a manufacturing related unfavourable impact was present, which was not of decisive nature at bolts with hot-dip galvanized surface layer. Due to the lack of corrosion protection, uncoated black bolts commonly show a certain amount of surface oxidation, also in a minorly corrosive environment. However, in the metallurgical investigation by *Oechsner et al. (2015)*, performed on the here analysed specimens, an equivalent surface oxidation of both black M36 and M64 bolts was detected up to a depth of about 10  $\mu\text{m}$ . Thus, differences in surface oxidation are disqualified as possible explanation. Nonetheless, the surface conditions between the two bolt diameters may have been altered because of the specifically applied lubrication by the two different bolt manufacturers. Indeed, in the handling during the experimental series (which were performed apart by a timescale of approx. 1 year) a somewhat more modestly applied amount of lubrication came to notice at the M64 than M36 bolts. This may have affected the friction properties in the paired thread. For instance, in test results by *Kremer (2005)* the complete removal of lubrication from uncoated black bolts of small diameter M8 has led to a significant reduction of fatigue strength. This highlights that lubrication may in general have a meaningful effect on the fatigue strength. However, the mentioned investigations are only limitedly comparable to the here presented test series, where the exact difference of lubrication properties remains unknown. Moreover, a variety of potential fatigue-relevant impact factors, such as diameter, manufacturer and testing conditions, are superimposed. For a conclusive evaluation of the found reduction of fatigue strength at uncoated, black M64 HV-bolts further experimental investigations are required. A potential impact of the friction properties inside the paired thread of the M64 bolts is further discussed in the sensitivity studies within the analytical fatigue investigations (see Chapter 4.5.2).

### 3.5 Test on M36 HV-bolt sets with variable amplitude loading

In addition to the two major test series on M36 and M64 HV-bolt sets with constant amplitude loading, the research project *Oechsner et al. (2015)* included a further verification of the boundary layer effect at M36 HV-bolts at variable amplitudes, as closer to operating loading conditions. The tested specimens were taken from the same production batch as for the constant amplitude tests. Contrary to the two previously described test series in Chapters 3.3 and 3.4, implementation of the variable amplitude tests was not directly supervised by the author of this dissertation. However, planning of test program and loading sequences was performed in close collaboration between the author and the primarily responsible research partner Chair and Institute for Materials Science, Technische Universität Darmstadt. Test boundary conditions and general results are presented in the sequel. The test results are then further used in Chapter 3.6.3 for the evaluation of damage accumulation hypotheses.

#### 3.5.1 Test execution and loading sequence

The variable amplitude tests were performed in a servo-hydraulic pulsator with 630 kN maximum tensile capacity, located in the test facilities of the Chair and Institute for Materials Science, Technische Universität Darmstadt. This enabled the required accurate control of the mixed loading sequences with in size varying amplitudes between 4 kN and 90 kN, while maintaining a representative mean load level of 515 kN. The test frequencies were specifically adapted to the respective amplitudes and ranged between 35 Hz and 5 Hz. Similar to the constant amplitude tests on M36 HV-bolts, specimens with three boundary layer configurations uncoated black (B), normal temperature (NT) and high temperature (HT) hot-dip galvanized were tested.

The systematic axial loading was applied as sinusoidal tensile swelling loads in varying blocks of steady amplitudes. As appropriate basis for the applied loading sequence a normal distributed *Gauss* collective was chosen. It can be regarded as a customary generic collective for service-loading tests. The applied load distribution thus reflects the condition of a purely stochastic, stationary (i.e., invariant in time) process. Even though theoretical, a normal distributed loading sequence ensures good comparability and general validity of the results. Moreover, it also implies representative characteristics for loading conditions of wind turbines, which are likewise affected by dominantly stochastic processes (e.g., wind and wave loading). The derivation of the actual experimentally applied load collective is illustrated in Figure 3-24. The following described procedure has been implemented based on recommendations given in *Haibach (2006)*.

In accordance with common conventions for the implementation of service-loading tests, the total cumulative frequency (i.e., extent) of the underlying *Gauss* collective was defined to  $H = 10^6$ . For the test implementation, the continuous collective needed to be transformed to a discrete, block shaped representation. Assuming validity of linear damage accumulation, extent and stress level of the blocks were calculated damage equivalent to the respectively approximated parts of the continuous collective ( $D_{\text{continuous}} = D_{\text{discrete}}$ ). Thereby, a theoretical constant S-N curve slope  $k = 4$  was assumed. In total, the chosen discrete collective comprised 20 different loading blocks, which was considered

an appropriate compromise between the general aim of using preferably small block sizes and a reasonable test implementation.

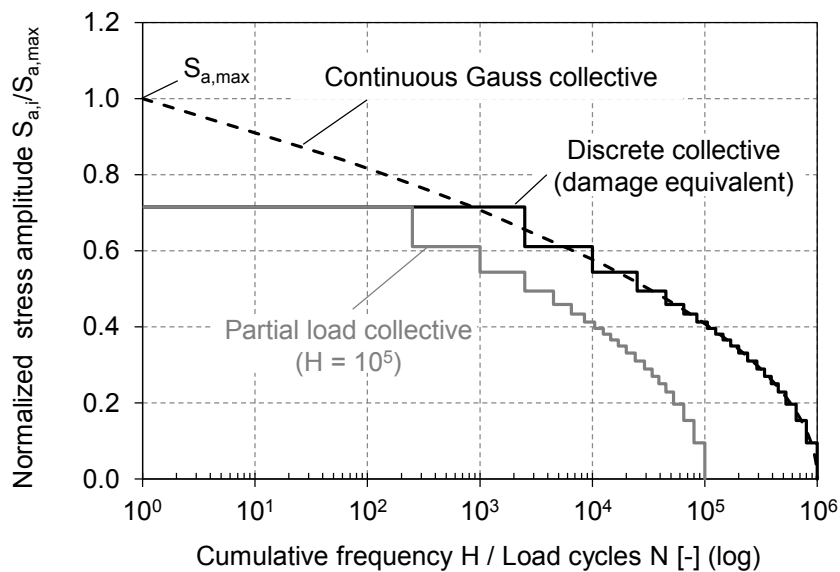


**Figure 3-24: Derivation of an experimental load collective from the continuous *Gauss* collective in normalized representation ( $S_{a,i} / S_{a,max}$ )**

For a sufficient alternation between higher and lower stress levels, and thus a superior approximation of realistic loading conditions, it was crucial that the defined loading sequence was multiply repeated. *Sonsino* (2008) recommends in this context to define a loading sequence that is run through at least 5 to 10 times before rupture of the specimen. Therefore, for the test execution the discretely approximated load collective was reduced from its original extent to a partial load collective with a cumulative frequency (i.e., load cycles) of  $H = 10^5$  (shown in Figure 3-24 in grey colouring). Correspondingly, after 10 iterations of the partial load collective the extent of the original load collective is reached. For a practicable test execution the minimum extent of the applied loading blocks  $n_i$  was limited to at least 250 load cycles. Thus, due to the damage equivalent conversion, the discrete load distributions exhibit a lower maximum load level than the underlying continuous collective (in the latter the maximum occurring load level  $S_{a,max}$  corresponds to one occurrence every  $10^6$  load cycles).

Finally, to further improve the mixing of considered load amplitudes, the decreasing order of the 20 blocks of the partial load collective was rearranged. Thereby, starting from a medium sized load level, two local maxima were approached in a stepwise in- and decreasing manner, see Figure 3-25. The stress amplitudes of the ultimately applied loading sequences were derived by multiplication of the normalized stress amplitudes  $S_{a,i}$  with the maximum value of the respectively aspired load level. Thereby, according to common conventions, the maximum stress level  $S_{a,max}$  of the underlying, continuous *Gauss* collective is determinative. These load levels are used for classification of the variable amplitude test results.

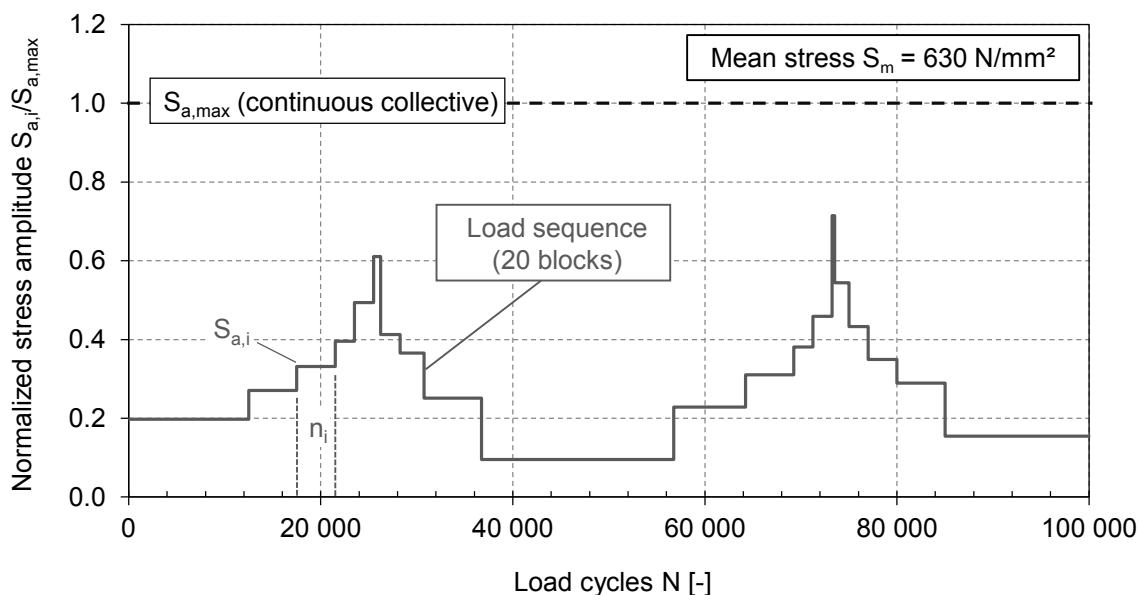


**Figure 3-25: Load sequence of variable amplitude tests in normalized representation derived from partial load collective**

Table 3-11 summarises the implemented test program at variable amplitude loads with the previously introduced standardized loading sequences. Based on the results of the constant amplitude loading tests, the applied test load levels (L1 to L5) were chosen, aiming for at least 5 iterations of the test sequence (i.e.,  $5 \cdot 10^5$  load cycles). With the thereof derived alternation of stress amplitudes of varying magnitude it may be presupposed that a potential impact of sequence effects can be effectively precluded. As the applied test procedure was chosen with reference to the variable amplitude loading tests by *Weber* (2010) on smaller bolts of diameter M12, a good comparability to this fundamental test series is ensured.

**Table 3-11: Summary of testing program for variable amplitude tests on M36 HV-bolt sets, performed at the Chair and Institute for Material Science, Technische Universität Darmstadt**

Boundary layer	Black	NT-galvanized	HT-galvanized
Mean stress $S_m \approx 0.7 \cdot R_{p,0.2}$	630 N/mm <sup>2</sup>	630 N/mm <sup>2</sup>	630 N/mm <sup>2</sup>
Number of specimens:			
Load levels $S_{a,max}$	L1: 153.0 N/mm <sup>2</sup>	3	3
	L2: 122.4 N/mm <sup>2</sup>	3	3
	L3: 98.0 N/mm <sup>2</sup>	2	3
	L4: 73.5 N/mm <sup>2</sup>	-	2
	L5: 49.0 N/mm <sup>2</sup>	-	1
Loading conditions	purely axial, variable amplitude loading, $R \approx 0.70 - 0.98$		
Test end criteria	rupture		
Testing frequency	var. 5-35 Hz		

### 3.5.2 Test results

Figure 3-26 shows the collective test results of the variable amplitude loading tests on M36 HV-bolts with all three boundary layer configurations. To visualize the correlation between the underlying load distribution and the test data, the repetitively applied partial load collectives in both continuous and actually tested discrete form are depicted for the uppermost tested load level (L1) and the two lowest load levels (L4 and L5). The inclusion of the collectives at the two intermediate load levels (L2 and L3) was omitted for improved lucidity. Additionally, for classification of test results and load distributions the S-N curves (survival probability  $P_s, 50\%$ ), derived from the constant amplitude tests presented in Chapter 3.3, are shown.

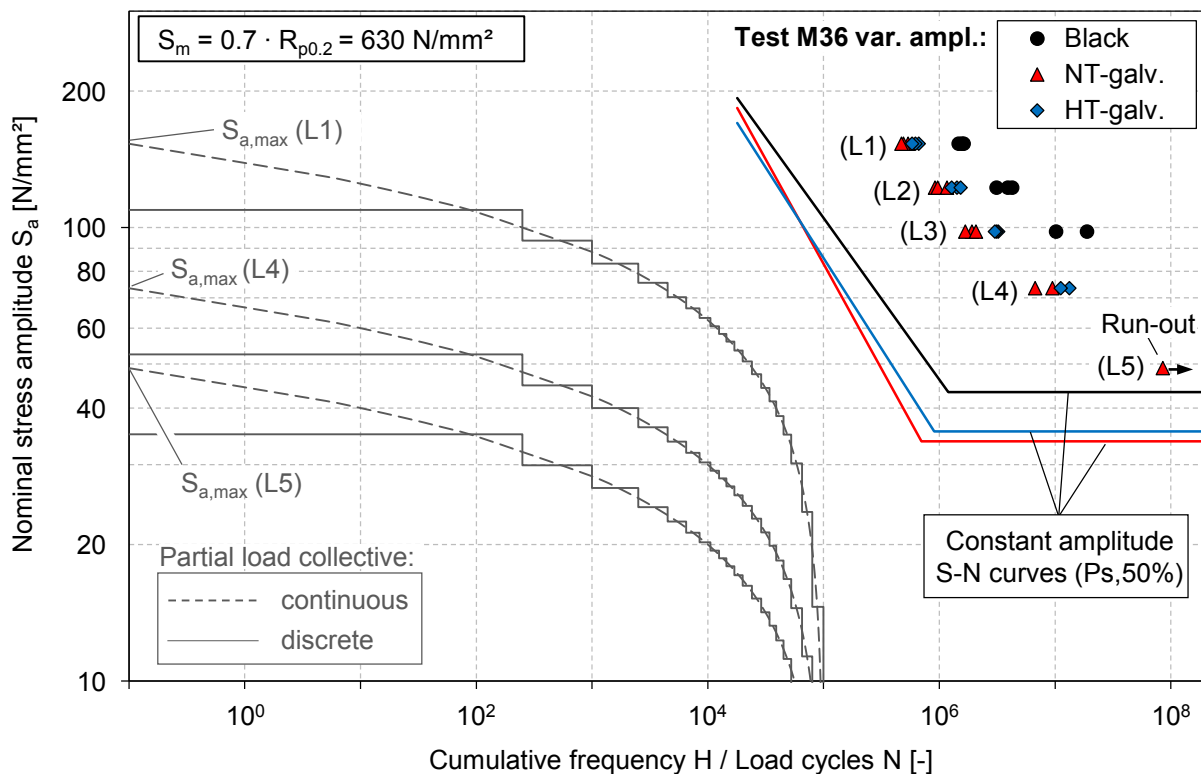


**Figure 3-26: Classification and comparison of fatigue test results at variable amplitude loading of M36 HV-bolt sets with different boundary layer configurations**

The results of the variable amplitude loading tests reflect well the found tendencies between the different boundary layer configurations obtained from the constant amplitude tests. Accordingly, a clear reduction of fatigue life at identical load levels is present between uncoated black and both variants of hot-dip galvanized bolts. Moreover, in compliance with the determined S-N curves, the HT-galvanized bolts show a slightly better fatigue performance than the NT-galvanized bolts. For all three boundary layers, all ruptures occurred regularly in the first load-bearing turn of the thread. This is consistent with the findings from the constant amplitude tests, where irregular ruptures at HT-galvanized bolts were observed only at low load levels in the transition region to the endurance limit. As can be seen in the above figure, also at the lowest load level (L4) considered for HT-galvanized

bolts, the upper test amplitudes of the load collective are well within the upper high cycle fatigue range (HCF) of the galvanized bolts. In fact, the maximum tested amplitude of the discrete load distribution for load level L4 is equivalent to the test horizon HCF 1 in the constant amplitude tests. These upper amplitudes constitute a significant damage contribution. It is thus plausible, that the deviating damage mechanism, presumed causative for the found irregular ruptures of HT-galvanized bolts (see Chapter 3.3.3), was not of decisive nature in the variable amplitude tests.

With exemplary purpose, a single test was performed at the lowest load level L5. Here, due to the theoretical damage equivalent conversion, the actual tested maximum amplitude of the partial load collective (and load sequence, respectively) is already located close to the determined endurance limit. The test was aborted manually without rupture after reaching an experimentally considered load cycle number of almost  $N = 10^8$ . The spot test is thus in accordance with the general assumption that a variable amplitude load collective, which maximum level approaches or lies below the constant amplitude endurance limit, is not fatigue critical. With reference to the experimentally superiorly validated load levels (L1 to L4), the potential damage contribution of amplitudes below the endurance limit is further investigated within the framework of the evaluation of damage accumulation hypotheses, applied in service load verification procedures (see Chapter 3.6.3).

Based on performed damage calculations, using the respective constant amplitude S-N curves (see Chapter 3.6.3 as well as Appendix A.4), it can be approved that the magnitude of fatigue strength deviations of bolts with different boundary layers is in good agreement between the constant and variable amplitude tests. Hence, the obtained results confirm that the damage effect induced by hot-dip galvanizing, thus far acknowledged for constant amplitude loading, equivalently effects the fatigue life of HV-bolts at service loading conditions with variable amplitudes.

It is noted that during implementation of the presented variable amplitude loading tests, at certain test runs a reduced loading sequence was used. Thereby, the four lowest loading blocks were omitted during testing while their corresponding load cycles were still accounted for in the result evaluation (i.e. load cycles until failure). This acknowledged procedure for the time reduction of service-loading tests (e.g., see *Haibach, 2006*) is based on the assumption that the lowest load levels of the collective do not constitute a meaningful contribution to the overall damage. In the here presented test series omission was only used at loading blocks with amplitudes of a maximum of about half of the respective constant amplitude endurance limit. Moreover, except from the single test at load level L5, test runs subjected to omission were confirmed by at least one further test with full loading sequence. Appendix A.4 contains a close-up result illustration of the variable amplitude loading tests, where the test runs with reduced loading sequence are marked. As the affected test runs classify well with the remaining test series, in the context of the here presented evaluations they are treated as equivalent test results. For further details in this regard it is referred to *Oechsner et al. (2015)*.



### 3.6 Assessment of normative regulations

#### 3.6.1 Validation of normative S-N curves

The validation of normative S-N curves given in the two most relevant regulations for the fatigue verification of HV-bolts, Eurocode DIN EN 1993-1-9 (2010) (henceforth denoted as EC 3) and VDI Guideline 2230 (2015), is performed graphically for black bolts in Figure 3-27 and hot-dip galvanized bolts (NT and HT) in Figure 3-28. For a comprehensive classification, additionally to the test results obtained within the framework of this dissertation, also results from the pivotal test series by *Marten* (2009) on NT hot-dip galvanized HV-bolt sets of large diameter M48 are considered. It is noted that the latter had to be performed at a reduced mean stress level, compared to the nominal preload of HV-bolts (approx. 20%  $F_{p,c}^*$ , see Chapter 2.1.5). In the juxtaposition to the experimental results, the normative S-N curves are depicted with consideration of the respectively designated diameter dependent reduction of the fatigue strength (see Chapter 2.1.6). In contrast to the original representation in the EC 3, all S-N curves are plotted here in terms of stress amplitudes  $S_a$  instead of stress ranges  $\Delta S$  ( $\Delta S = 2S_a$ ).

It becomes apparent that, despite the considerable reduction of fatigue strength at the tested black M64 bolts, the permissible EC 3 fatigue class FAT 50 provides a secure design basis for all considered size- and boundary layer configurations. With one exception, all test runs lie above the normative S-N curve defined in EC 3 for diameter M36. The single outlier, present in the test series on M48 bolts, can be explained statistically by the large number of considered specimens (see also *Marten*, 2009). Consequently, the collective test results indicate that the considered diameter dependent reduction of the fatigue class leads to a certain underestimation of the fatigue strength of large-size HV-bolts in the upper HCF. A further assessment of the considered size-reduction function is therefore performed in the subsequent Section 3.6.2. Considering the test results of M36 and M48 bolts in the transition region to the endurance limit (TEL), the characteristic S-N curve progression of the EC 3, with a kink to the endurance limit only at  $5 \cdot 10^6$  load cycles, provides a rather conservative design assumption at lower load levels. In this context it is noted that for harmonic cyclic loading, as present in all here considered fatigue tests, the EC 3 in fact allows the consideration of an actual endurance limit with horizontal progression of the S-N curve after  $N = 5 \cdot 10^6$  (see also Chapter 2.1.6). However, for reasons of comprehensibility the common representation of the standard's S-N curve progression was chosen here. The above stated observation remains unaffected. The normatively defined procedure for assessment of fatigue damage accumulation at service loading is evaluated in Section 3.6.3 based on the performed tests with variable amplitude loading.

A superior classification of uncoated black HV-bolts into EC 3 fatigue class FAT 71, as suggested in DNVGL-ST-0126 (2016) or the older GL Guideline (2012), is confirmed only by the test results with diameter M36. Given the notable shortfall of the M64 test results to the FAT 71 fatigue curve, this classification is to be scrutinized for large-size bolts. For a secured application of a higher fatigue class for black than for galvanized bolts it is crucial to carefully consider the required boundary and production conditions, which are required to ensure the requisite fatigue strength of the bolts. To this end, further investigations are advisable.

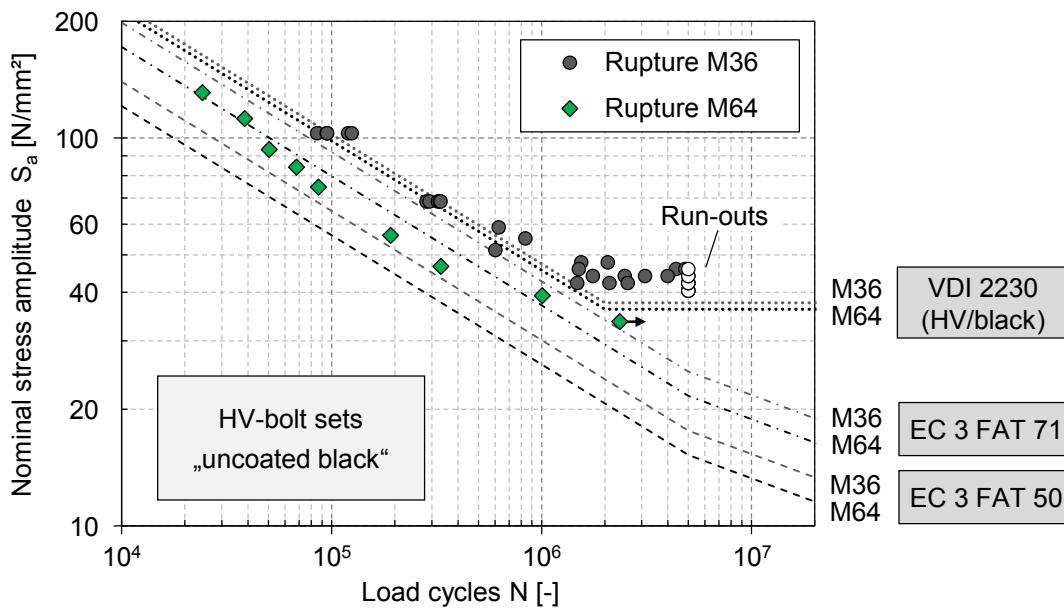


**Figure 3-27: Comparison of experimental results on uncoated black M36 and M64 HV-bolt sets with normative S-N curves from EC 3 and VDI 2230**

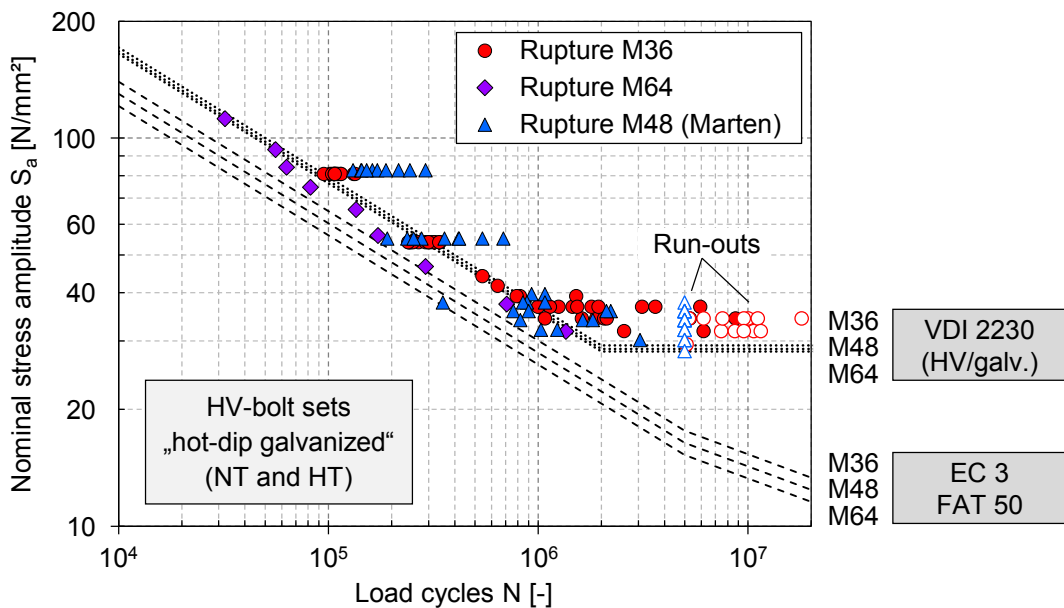


**Figure 3-28: Comparison of experimental results for hot-dip galvanized M36, M48 and M64 HV-bolt sets with normative S-N curves from EC 3 and VDI 2230**

The S-N curves from VDI 2230 with consideration of the additional reductions for System HV nut geometries and, if applicable, galvanized boundary layer, provide a safe approximation of the endurance limit for all bolt configurations tested in the TEL (i.e., M36 B / NT / HT and M48 NT). However, in the upper HCF the fatigue strength is overestimated. Throughout the spectrum of considered bolt configurations, numerous failures of test specimens occurred at load cycles below the corresponding fatigue curves from the guideline. As visible in Figure 3-28, for hot-dip galvanized bolts this tendency is increasingly pronounced at larger bolt diameters and especially at the tested M64 bolts.

Solely at the upper tested load horizon of the M48 bolts all test runs lie above the design S-N curve from the guideline. However, the comparison to the further test results emphasizes the probably present beneficial impact of the reduced mean stress level to obtained fatigue life at this high load level. It can be concluded that the experimentally found reduction of fatigue strength at the NT-galvanized M64 HV-bolts in the upper HCF is not covered by the guideline. It is noted that besides the increased diameter also the low testing frequency needs to be kept in mind as potential unfavourable impact factor. Still, among all here considered results, in terms of frequency and mean load level, the test series on M64 bolts provides the closest approximation of the loading conditions in practical application of HV-bolt sets. A superior coverage of the test results could be achieved by shifting the kink of the S-N curve from  $2 \cdot 10^6$  to  $1 \cdot 10^6$  load cycles, at an unvaried endurance limit.

Regarding the superior classification of black compared to hot-dip galvanized bolts, considered in the guideline, the same restrictions apply as noted in the context of the evaluation of the EC 3 fatigue curves.

### 3.6.2 Assessment of diameter reduction functions

As the juxtaposition of test results for hot-dip galvanized large-size HV-bolt sets and normative S-N curves of the EC 3 has revealed, in consequence of the diameter dependent reduction of the applicable fatigue class FAT 50, endurable load cycles are underestimated. Thus, for a closer evaluation of the size-reduction function included in the standard, the available test results were evaluated, using the statistical assessment methodology which is applied for a consistent and comparable classification of structural details into the fatigue class catalogue of the Eurocode 3 (consulted in *Sedlacek et al.*, 2003, 2007). Thereby, a linear regression analysis of the logarithmized load cycles until rupture is performed with a fixed predefined slope  $k = 3$ . In the evaluation, test runs with load cycle numbers between  $1 \cdot 10^4$  and  $5 \cdot 10^6$  are considered. Consequently, the fixed slope regression mutually encompasses both upper HCF and TEL. Based on the mean regression line with survival probability  $P_s,50\%$ , a *Student's-t* distribution can be used, also at low sample sizes, to statistically predict the parallelly progressing S-N curve with survival probability  $P_s,95\%$ . From the latter, the characteristic reference fatigue strength is extracted at  $N = 2 \cdot 10^6$  load cycles. This represents the benchmark for the fatigue strength classification.

Figure 3-29 illustrates the obtained results with the above described evaluation method for the test series on NT hot-dip galvanized HV-bolt sets M36, M48 (taken from *Marten*, 2009) and M64. To enable a direct comparison to the fatigue detail classification from EC 3, contrary to the customary applied form of result presentation in this dissertation, fatigue levels are expressed in nominal stress ranges instead of amplitudes. Besides the underlying test results and fixed slope regression lines with 50 % and 95 % survival probability, the experimentally determined reference fatigue strengths at  $2 \cdot 10^6$  load cycles are depicted in the figure as red coloured dots. The corresponding characteristic fatigue strength from the Eurocode  $\Delta S_c$ , calculated for fatigue class FAT 50 with the respective diameter dependent reduction (see Eq. 2-5), are indicated by the yellow dots. Furthermore, the normative fatigue curves without size reduction are shown by the blue lines, as additional reference.

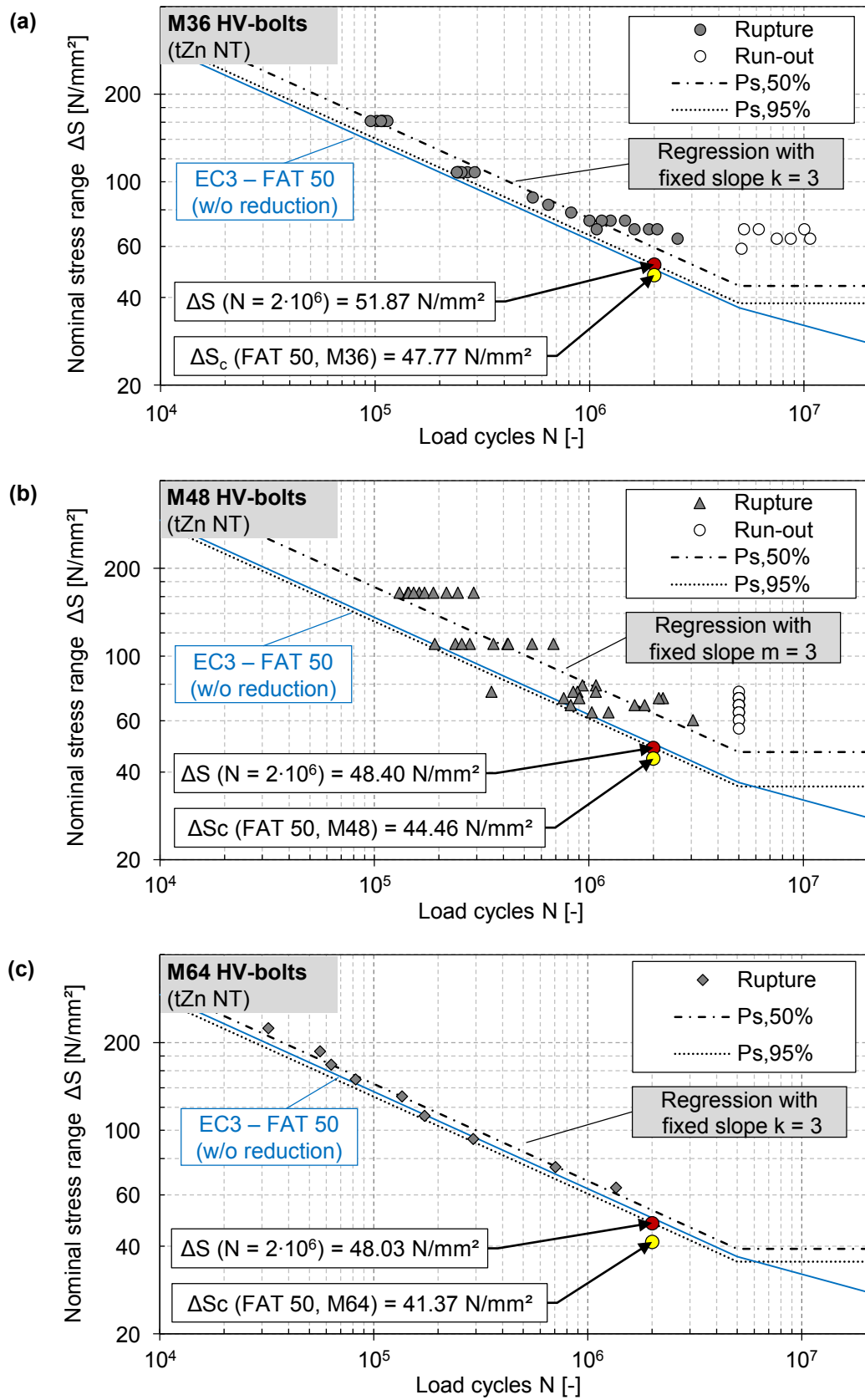
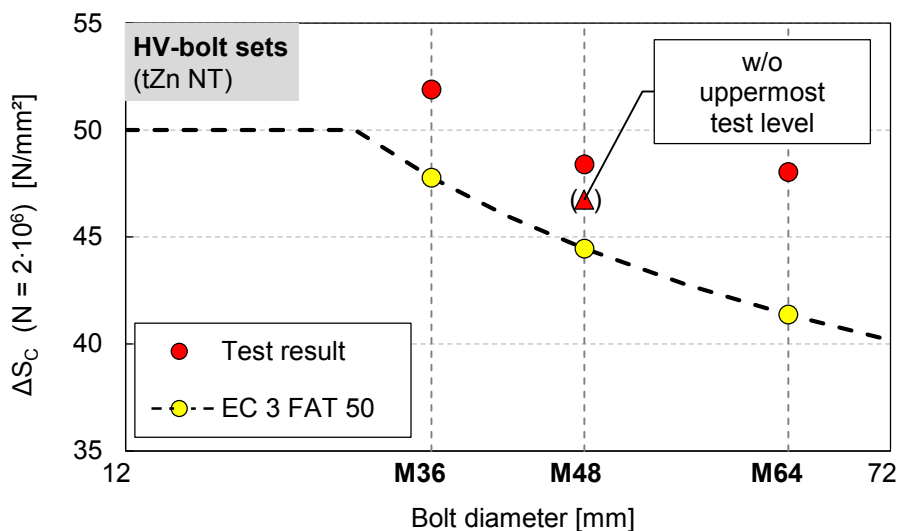


Figure 3-29: Evaluation of test results by linear regression of logarithmic load cycle numbers with fixed slope of S-N curve for NT hot-dip galvanized HV-bolt sets of diameter M36 (a), M48 (b) and M64 (c)

Even though only few test runs fall below the normative S-N curve for fatigue class FAT 50 without diameter consideration, the experimental reference fatigue strength values for both M48 and M64 bolts are smaller than the original fatigue class reference of  $\Delta S_c = 50 \text{ N/mm}^2$ . Hence, the statistical evaluation highlights that a diameter related reduction of the considered fatigue strength is generally appropriate for bolt sizes larger than M36. Nevertheless, the results indicate that the actual diameter related effect is smaller than estimated by the Eurocode.

To highlight this circumstance, the experimentally determined and normative values for the diameter dependent characteristic fatigue values at  $N = 2 \cdot 10^6$  are directly compared in Figure 3-30. Therein, additionally to the results illustrated in Figure 3-29, an alternative evaluation for the M48 HV-bolts is included, where the test runs with presumably overestimated fatigue strength at the uppermost tested load level were neglected (red triangular marker). Even with this conservative evaluation approach, a secure margin to the normative reference fatigue strength is maintained. Compared to the test results on the M48 bolts, no decisive further reduction of the reference fatigue strength is indicated for the M64 bolts. Thus, the discrepancy to the normative size-reduction function increases.

Certainly, between the comparison of the three test series, the tests performed by *Marten* (2009) on M48 HV-bolts are characterised by a notably larger result scatter (see Figure 3-29). This is due to the larger number of specimens and the fact that bolts from multiple manufacturers were included. As a consequence, the discrepancy between resultant mean S-N curve and outer bound of the scatter band with  $P_{s,95\%}$  is significantly larger than at the other two test series. The tests on M36 and M64 HV-bolts lack this level of statistical security. Nevertheless, also the evaluation of the M64 bolts is affected by a certain level of conservatism because only few experiments reached into the TEL. Due to the increasing fatigue life in this load level range, such tests have a beneficial effect in the applied evaluation procedure.



**Figure 3-30: Evaluation of the diameter dependent fatigue strength reduction considered in EC 3 based on experimental results by reference to the characteristic fatigue strength  $\Delta S_c$  (nominal stress range)**

In short, it can be confirmed that the diameter related fatigue classification of large-size HV-bolts in the EC 3 provides a conservative design approximation. Even though not yet experimentally investigated, the evaluation strongly indicates that this also applies for a further increased diameter M72. Moreover, the here obtained results on M64 HV-bolts suggests that an adaption of the normative size-reduction function may be justified for bolt sizes larger M48. However, to this end an extended validation by use of additional fatigue investigations in this diameter range would be desirable. Potential diameter related impact factors of large-size bolts are also further evaluated within the analytical fatigue investigations in Chapter 4.

In VDI Guideline 2230 (2015) a potential size effect on the fatigue strength is considered within the diameter dependent calculation of the endurance limit  $S_{a,D}$  (see Eq. 2-6). In terms of its statistical interpretation, the latter may directly be related to the endurance limit determined in constant amplitude experiments, such as performed in the framework of this dissertation on M36 bolts with the staircase method (see Chapter 3.3). Consequently, the reference value of the fatigue curves from VDI 2230 needs to be distinctly differentiated from the statistical evaluation of the characteristic fatigue strength  $\Delta S_c$ , used in EC 3.

Figure 3-31 shows the comparison of the normatively estimated, diameter dependent endurance limit and available experimental results for hot-dip galvanized HV-bolt sets. Additionally to the test performed within the frame work of the thesis at hands, relevant previous studies by *Berger et al.* (2008) and *Marten* (2009) are considered (see Chapter 2.1.5). The design values of the fatigue strength in VDI 2230 are stated with an estimated (theoretical) survival probability  $P_s,99\%$ . However, for the here aspired assessment it is preferable to consult the median reference values with  $P_s,50\%$ . In this way, statistical uncertainties, which arise from determination of the outer bound of the scatter band and varying sample sizes, can be limited. In accordance with the conventions of the VDI Guideline, fatigue loading here again is expressed in terms of nominal stress amplitudes  $S_a$  instead of ranges  $\Delta S$ .

The reduction of the endurance limit with increasing diameter, displayed by the available experimental results up to diameter M48, is generally reflected well by the calculation formula used in the guideline. By addition of the here established experimental results for diameter M36 to the previously existing test basis the verification of the normatively considered behaviour is improved. Moreover, the comparable order of magnitude of the results on M36 and M48 bolts confirms the mitigation of the diameter impact at larger bolt sizes. The observed tendency of a presumably slightly reduced endurance limit of here tested NT hot-dip galvanized M64 compared to M36 bolts qualitatively matches the assumed progression of the diameter function in the guideline. However, as mentioned before, no verified prediction can be made about the actual magnitude of the endurance limit of the M64 bolts because of the low number of available test results. A verification of a secure approximation of the endurance limit by VDI 2230 for bolt sizes larger than M48 is yet to be performed. Moreover, despite the verifiably adequate estimation of the endurance limit for the experimentally proven diameter range, it is anew noted that the fatigue life of galvanized HV-bolts in the upper HCF is, to a

certain degree, overestimated by the VDI 2230 fatigue curves, especially for diameter M64 (see Section 3.6.1).

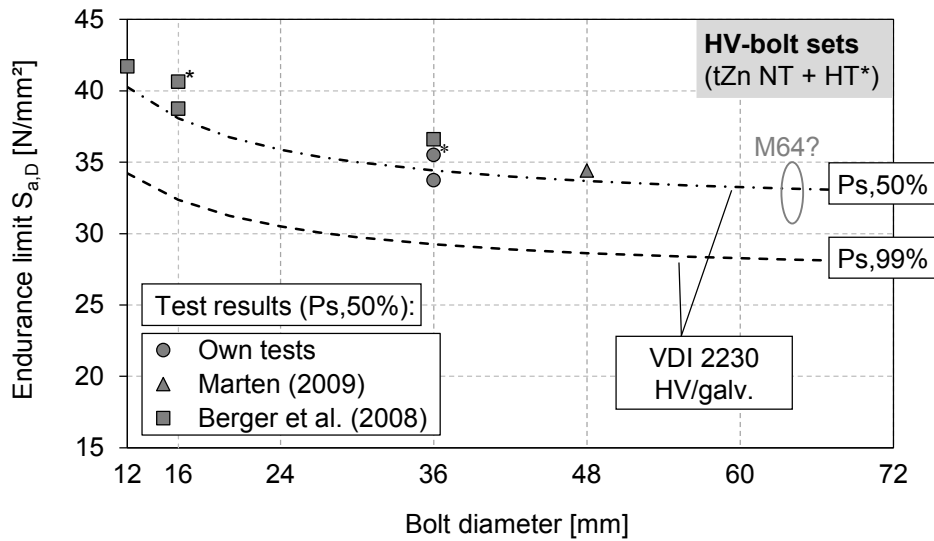


**Figure 3-31: Evaluation of the diameter dependent fatigue strength reduction considered in VDI 2230 based on experimental results by reference to the endurance limit  $S_{a,D}$  (nominal stress amplitude)**

### 3.6.3 Assessment of damage accumulation hypotheses

For the actual fatigue assessment of bolts – and other structural components – at service loading, design procedures require the application of appropriate damage accumulation hypotheses. In practical application, this usually implies an adaption of *Miner's*-rule (Eq. 2-4) for consideration of potential damage of load cycles below the constant amplitude endurance limit. The damage calculation is thereby based on the original constant amplitude S-N curve. The most common adaptations of the *Miner* hypothesis were introduced in Chapter 2.1.3.

Deriving from different technical origins, the two technical regulations DIN EN 1993-1-9 (2010) (EC 3) and VDI Guideline 2230 (2015) pursue variant approaches for the assessment of variable amplitude service loading. With the main focus on application in structural engineering, the EC 3 inherently implies the damage accumulation with the modification of the *Miner* hypothesis by *Hai-bach* (1970), on the basis of the regulation's standardized S-N curves. On the contrary, the application of VDI 2230 for mechanical engineering purposes is not primarily intended for a comparable verification of service loads at multiple load levels, as aimed for in the EC 3. The references for the fatigue resistance of bolts are given for a fatigue safe design with maximum load levels of either constant or variable amplitude collectives below the endurance limit or for dominantly constant amplitude loading in the upper HCF. However, *Weber* (2010) proposed an extended service load assessment procedure with the VDI 2230 fatigue curves, based on a *Miner's* rule modification by *Hück et al.* (1988). A reference to this proposal is included in the guideline since the revision of 2014.

In the sequel, the variable amplitude loading tests on M36 HV-bolts described in Chapter 3.5 are used to evaluate different variants of *Miner's*-rule given in the literature and considered in the design regulations. Despite the limited number of performed tests and scope of evaluation compared to extended studies on fatigue damage progression at service loading as performed by *Weber* (2010) or – for welded connections - by *Al Shamaa* (2015), the tests enable a valuable fundamental assessment of suitability of the most relevant damage accumulation hypotheses for the application to large-size HV-bolts. The implementation of the subsequently shown damage calculations was assisted by the work of *Kielbus & Abe* (2016) for their seminar paper.

In a first step, damage accumulations are evaluated based on the S-N curves (survival probability  $P_s, 50\%$ ) from the original fatigue test results of M36 HV-bolts with constant amplitude loading. The thereby considered variants of the *Miner* hypothesis are the “original” and “elementary” form as well as the modification by *Haibach* (1970) (see Figure 2-5). Moreover, calculations with the *Miner* adaptation proposed by *Hüeck et al.* (1988) are included. Based on the underlying constant amplitude S-N curve, defined by endurance limit  $S_{a,D}$ , load cycle number at the knee point  $N_D$  and slope  $k$  in the upper HCF, theoretically endurable load cycles  $N_i$  for a specific stress amplitude  $S_{a,i}$  can be calculated with the below formulas Eqs. 3-6 to 3-11.

$$N_i = N_D \cdot \left( \frac{S_{a,i}}{S_{a,D}} \right)^{-k} \quad \text{for } S_a \geq S_{a,D} \quad \text{Eq. 3-6}$$

$$N_i = N_D \cdot \left( \frac{S_{a,i}}{S_{a,D}} \right)^{-k^*} \quad \text{for } S_a < S_{a,D} \quad \text{Eq. 3-7}$$

where:

$$k^* \rightarrow \infty \quad \text{Miner original} \quad \text{Eq. 3-8}$$

$$k^* = k \quad \text{Miner elementary} \quad \text{Eq. 3-9}$$

$$k^* = 2k - 1 \quad \text{Miner / Haibach (1970)} \quad \text{Eq. 3-10}$$

$$k^* = k \left( 1 + \frac{C}{\frac{S_{a,\max}}{S_{a,D}} - 1} \right) \quad \text{Miner / Hüeck et al. (1988)} \quad \text{Eq. 3-11}$$

Contrary to the other damage accumulation hypothesis, the modification by *Hüeck et al.* considers a variant slope of the S-N curve below the constant amplitude endurance limit, which is adapted based on the magnitude of the maximum stress level  $S_{a,\max}$  of the respectively considered load collective. Thereby, a higher slope and thus lower damage contribution of fatigue load levels below the endurance limit is considered with decreasing  $S_{a,\max}$ . Moreover, the slope can be specifically adapted by the parameter  $C$  to account for characteristics of the analysed structural component (e.g., geometry



or material) and loading conditions (e.g., mean stress level, shape of the present load collective). For preloaded bolts *Weber* (2010) recommends values  $C \approx 0.3 - 1.0$ .

Figure 3-32 shows the comparison of the test results at variable amplitude loading of NT-galvanized M36 HV-bolts to fatigue damage calculations of the corresponding loading sequence, performed with the different damage accumulation hypotheses. Moreover, the experimental S-N curve at constant amplitude loading, used as basis for the damage calculation, is shown as reference. In all depicted analytical calculations failure is assumed at a damage sum of  $D = 1.0$ . At the uppermost load level (L1), where the loading sequence is strongly dominated by amplitudes above the constant amplitude endurance limit, all *Miner* variations approximate closely the experimental results. This validates the general suitability of the underlying hypothesis of linear damage summation (Eq. 2-4). At decreasing load levels, the best approximation of the experimental results is provided by the original form of the *Miner* hypothesis (i.e., neglecting any potential damage contribution below the constant amplitude endurance limit). Still, the visible shortfall of the experimental results at load levels L3 and L4 to the *Miner*-original fatigue-life curve indicate that an adaption of the hypothesis is required.

While notably deviating from the theoretical lower bound with the elementary *Miner* adaption, the popular *Miner* modification by *Haibach* still shows a rather conservative tendency. The two depicted calculations with the *Miner* modification by *Hück et al.* highlight the potential of improving the calculation results by adapting the introduced C-parameter. Confirming the suggestion by *Weber* (2010), a calculation with  $C = 1$  can be regarded suitable for the investigated HV-bolts. Thereby, also the single test-run classified as run-out, which reached into the very high load cycle range close to  $N = 10^8$ , is conservatively covered. A further improved approximation of the test results could be achieved when using notably higher C-values. However, this would require a meaningful validation by experimental results in the very high cycle range, which is neither given here nor by *Weber* (2010).

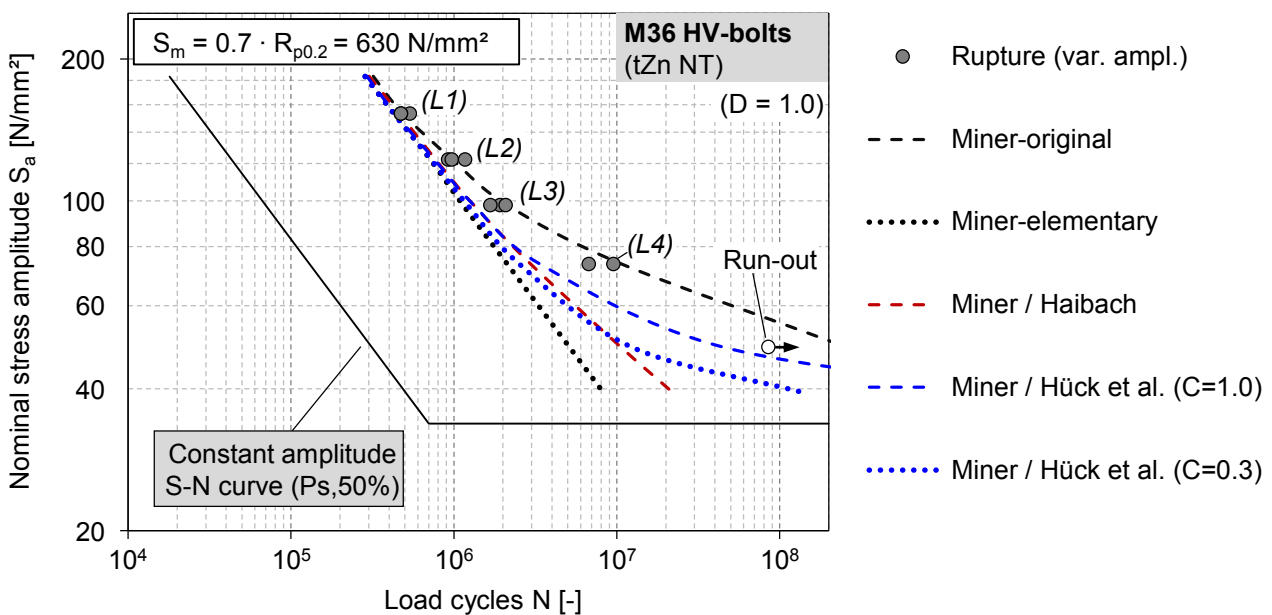


**Figure 3-32: Comparison of test results of NT-galvanized M36 HV-bolts at variable amplitudes to damage calculations with different adaptations of *Miner's* rule based on the experimental S-N curve**

Analogous evaluations, as shown in Figure 3-32 for NT-galvanized M36 HV-bolts, were also performed for the other two bolt configurations with HT-galvanized and uncoated, black boundary layer. Since the results exhibit equivalent tendencies as described above, they are not shown here but included in Appendix A.4. It is noted, however, that the experimental results of these two test series exhibit an even stronger affinity to the calculation with the original *Miner* hypothesis.

Finally, the variable amplitude test results are compared to corresponding calculations with the service load assessment approaches and underlying S-N curves from EC 3 and VDI 2230 in Figure 3-33. To fully utilize the available test background, experimental results for both NT- and HT-galvanized M36 HV-bolts are shown. For the proposed application of the *Miner* modification by *Hück et al.* (1988) to the VDI 2230 design S-N curves, *Weber* (2010) recommends a conservative consideration of parameter  $C = 0.3$  as well as a reduced failure indicating damage sum  $D = 0.9$ . He also implied that in the service load verification the knee point  $N_D$  of the original VDI 2230 S-N curves would need to be adapted from  $2 \cdot 10^6$  to  $1 \cdot 10^6$  load cycles. It is noted that *Weber* had intended the analytical procedure for an approximative design, which would afterwards be supplemented by a detailed experimental based dimensioning. He therefore proposed the application of the adapted VDI guideline's S-N curve based on the endurance limit given in the guideline for 50% survival probability. An experimental based design is, however, unpractical for very high load cycle collectives, characteristic for large-size HV-bolts in wind turbine structures. Thus, the here presented calculations consider the guideline's actual design fatigue strength (i.e., factor 0.85 included in Eq. 2-6). In the underlying S-N curves of both regulations, VDI 2230 and EC 3, the respectively considered diameter reductions are included. No "cut-off" limit was used.

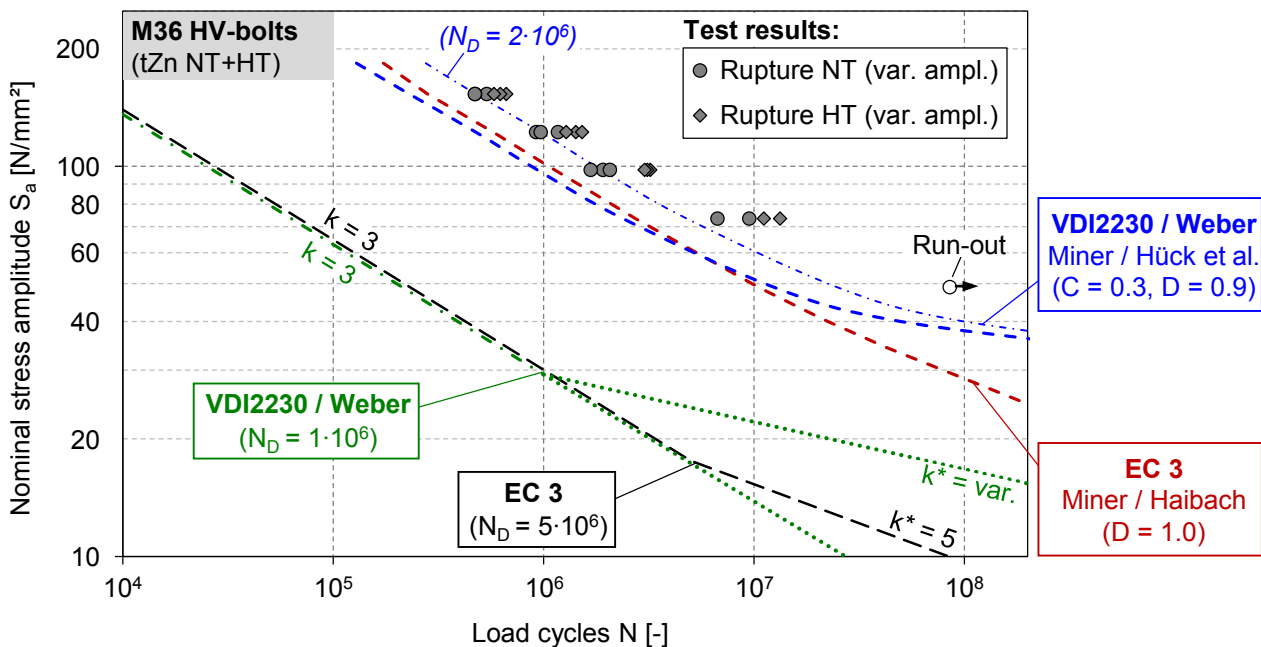


Figure 3-33: Comparison of test results of hot-dip galvanized M36 HV-bolts (NT and HT) at variable amplitudes to damage calculations with normative design S-N curves

The comparison to the test results verifies a conservative tendency to both considered design approaches. When using the adapted design S-N curve of VDI 2230 with  $N_D = 1 \cdot 10^6$ , at the experimentally proven load horizons the consideration of a failure indicating damage sum  $D = 0.9$  leads to an even lower fatigue life estimation than obtained with the EC 3 approach. It can therefore be regarded acceptable to increase the decisive damage sum to  $D = 1.0$ . In the moderate load cycle range, both design approaches then lead to equivalent results. It is, however, emphasized that the proposed adaption of the knee point ( $N_D$ ) is strongly advisable, when using the VDI 2230 S-N curve for design purposes. As highlighted by an additionally performed damage calculation with  $N_D = 2 \cdot 10^6$ , shown in Figure 3-33 by the thinner dashed blue line, similar to the validation of the constant amplitude S-N curves (Chapter 3.6.1), endurable load cycles are overestimated when using the guideline's original recommendation.

Even though no decisive validation by experimental results is given, the evaluations in both Figure 3-32 and Figure 3-33 strongly indicate that at low load levels the design approach of the EC 3, implying the *Miner* modification by *Haibach*, includes a high degree of conservatism. It seems plausible to assume that, especially at load collectives dominated by amplitude below the endurance limit, the standard's design procedure leads to a significant underestimation of endurable load cycles. A less conservative fatigue life estimation in the very high load cycle range is obtained with the adapted design approach according to VDI2230 and *Weber*.

### 3.7 Findings

In the previous chapter, comprehensive experimental fatigue investigations on large-size HV-bolt sets were presented. Tests were performed on bolts of diameter M36 as well as very large diameter M64. Additional to conventional fatigue tests with constant amplitude loading, the fatigue characteristics on bolt diameter M36 were also validated in tests with variable loading sequences, which superiorly reflect the actual service loading conditions experienced by large-size HV-bolts. For all tests it was prerequisite to ensure a representative high mean stress level, which corresponded to the nominal preload of the HV-bolts. To investigate the impact of the boundary layer, specimens with uncoated black surface as well as hot-dip galvanizing, established with different process temperatures, were included in the series.

From the performed experimental investigations, the subsequently summarised findings could be derived:

#### Impact of hot-dip galvanizing

It was verified that hot-dip galvanizing of large-size HV-bolts achieved with both normal ( $\sim 450$  °C) and high ( $\sim 550$  °C) process temperature causes a substantial decrease of the endurance limit (approx. 20 % to uncoated surface conditions) as well as the fatigue strength in the upper high cycle fatigue range. The found impact was of equivalent magnitude and characteristic at both constant amplitude as well as service condition emulating variable amplitude loading. Given the compliance with studies from the literature on hot-dip galvanized structural steel components, most probably, the effect is caused by pre-existing shrinkage cracks in the zinc boundary layer, which reach up to

the base material surface. It can be assumed that at the tip of the shrinkage cracks premature fatigue cracks are initiated, hypothetically due to microscopic stress concentrations.

### **Fatigue strength of HV-bolts with uncoated, black boundary layer**

For HV-bolts with diameter M64 and uncoated, black surface layer a severe reduction of the fatigue strength was found compared to the equivalents with diameter M36. Surface oxidation was excluded as possible reason. However, contrary to the hot-dip galvanized bolts, different lubrication characteristics inside the paired thread might have had a potential negative impact. For a conclusive evaluation, further investigations are necessary.

### **Impact of the bolt diameter**

A certain reduction of the experimentally determined fatigue strength of M64 compared to M36 HV-bolts was also found for specimens with normal temperature hot-dip galvanizing. However, the impact was significantly less severe than found at the uncoated specimens and the divergence reduced with decreasing load level. This hints to a potential overlaid impact of the testing frequency, which had to be reduced by a factor of about 10 compared between constant amplitude test on M36 and M64 bolts. Moreover, between the two test series other varying boundary conditions existed, such as the base material as well as the production batch and manufacturer. Taking this into account, the found deviations are within a reasonable order of magnitude of general statistical scatter and no critical impact of the increased bolt diameter is indicated. Still, the obtained experimental results mostly validate the fatigue characteristics in the upper high cycle fatigue range and further verification concerning the endurance limit would be desirable.

### **Applicability of high temperature hot-dip galvanizing**

The performed tests with both constant and variable amplitudes consistently indicate a slight improvement of the fatigue performance of M36 HV-bolts at an increased galvanizing temperature. However, with overlapping scatter bands statistical significance is limited. Moreover, irregular ruptures outside the paired thread at high temperature galvanized HV-bolts, which correlate to found zinc intrusions into the base material, suggest an impact of an unplanned failure mechanism. The irregularities were decisive only at low fatigue load levels, close to the endurance limit. Since in practical application of HV-bolts fatigue loading commonly reaches the very high cycle fatigue range, this is of specific relevance. The observed particularities indicate that at this loading conditions unexpected failures might occur. Thus, without further investigation of the found effect, practical application of high-temperature hot-dip galvanizing to bolts with diameter M36 needs to be regarded critical. For larger diameters high temperature galvanizing is to be omitted because of potential liquid metal assisted cracking.

### **Design assumptions of DIN EN 1993-1-9 (Eurocode 3)**

It was experimentally verified that the applicable detail category FAT 50 from Eurocode 3 provides a secure design basis for black and normal temperature hot-dip galvanized HV-bolts with diameters up to M64. However, a superior fatigue classification within the boundaries of the standardized S-N curves of the Eurocode 3 is not justified by the results. Moreover, given the observed reduction of

fatigue strength at M64 HV-bolts, the application of a higher fatigue class FAT 71 for uncoated, black bolts is questionable. Further investigations are required to ascertain the specific boundary conditions, which can ensure an improved fatigue performance, as found for black M36 HV-bolts.

The appropriate statistical evaluation of test results from bolts with diameter M48 and M64 confirms that the considered reduction of the applicable fatigue class FAT 50 for diameters larger than M30 is generally appropriate. However, the thus far available test results on large-size HV-bolts indicate that the diameter related reduction function used in Eurocode 3 overestimates the actually given effect of the bolt diameter. Moreover, the combination of the standardized progression of the normative S-N curves and the applied damage accumulation hypothesis can be considered to provide a high degree of conservatism in the service-life verification of HV-bolts, especially with load collectives dominated by smaller amplitudes.

### **Design assumptions of VDI 2230**

For the application of the design S-N curves defined in VDI 2230 for hot-dip galvanized large-size HV-bolts, it is advisable to shift the knee point from  $2 \cdot 10^6$  to  $1 \cdot 10^6$  load cycles, while maintaining the specified endurance limit. Otherwise, endurable load cycles in the upper high cycle fatigue range are overestimated. At this condition, the proposed amendment by *Weber* (2010) for a service load verification based on the VDI 2230 S-N curves could be confirmed also for large-size HV-bolts. Thereby, when using the guideline's specified design instead of mean values for the fatigue strength, the considered failure decisive damage sum may be increased from  $D = 0.9$  to 1.0.

For a superior classification of the fatigue strength of black compared to galvanized large-size HV-bolts, the same restrictions apply as mentioned above for Eurocode 3.

## 4 Analytical Fatigue Investigations

### 4.1 Evaluation methodology

Analytical fatigue evaluations have the potential to meaningfully complement expensive and time-consuming testing programs on large-size HV-bolts. Thus, an appropriate assessment method and its potentials are further investigated in this next major scientific segment of this dissertation. Figure 4-1 shows the schematic depiction of the applied evaluation methodology. The approach is fundamentally based on the strain-life concept, introduced in Chapter 2.2, and the specific adaptations recommended by *Schneider* (2011) for the application to threaded fasteners. Indicated in the figure by the grey coloured boxes, the procedure can be effectively subdivided into three consecutive stages. In the course of the subsequently performed investigations, these stages are each systematically covered in a separate chapter. The aim of each chapter, which successively synthesizes with each other, is to establish a fundamental understanding of impact factors and characteristics as well as to refine the assessment steps for applying of the analytical evaluation method to large-size HV-bolts.

Chapter 4.2 covers performed experimental material analyses on the base materials of experimentally investigated HV-bolts. On the one hand, this includes the determination of the materials' stress-strain behaviours at cyclic and monotonic loading. On the other hand, crucially, knowledge about the strain-fatigue life behaviour needs to be established. To this end, two different evaluation procedures with varying experimental effort are used and compared.

The established material data serve as input for the evaluation of the local stress and strain development inside the paired thread. Chapter 4.3 presents detailed numerical studies on the assessment of the local loading conditions at linear elastic and elastic-plastic material behaviour. Thereby, modelling approaches with and without inclusion of the continuous pitch of the thread are considered and the effects of model upscaling to larger diameters is assessed. Lastly, the constitution of the stress-strain response at cyclic loading under high mean stress is discussed and boundary conditions for the further evaluation are defined.

Based on the determined local stress-strain response, derived from a given outer load-time sequence (here focussed on constant amplitude loading) and the materials' strain-life behaviours, the actual fatigue damage assessment is enabled. The corresponding investigations are described in Chapter 4.4. In a first step, thorough evaluations focus on the qualified mean stress consideration with the aid of the damage parameters introduced in Chapter 2.2.4. Furthermore, the impact of methodological variations derived from the previous two assessment stages are quantified in terms of the actually calculated fatigue life. Secondly, to amend the thus far enabled calculation of crack initiation load cycles with the strain-life approach, the fracture mechanics approach is used to analytically estimate the full load cycles until rupture. Moreover, an engineering approach is introduced which enables the incorporation of the boundary layer effect, induced by hot-dip galvanizing.

In the previously described analytical fatigue calculations, validation is principally gained by comparison to the results from the M36 HV-bolts' fatigue tests, which provide the broadest experimental

background. Ultimately, in Chapter 4.5 extended sensitivity studies are presented, where the developed and refined analytical assessment method is applied for specific investigations of potential fatigue impact factors, such as the size effect or base material characteristics. Thereby, validation of the analytical approach is also extended to the available experimental results on large-size M64 as well as M48 HV-bolts.

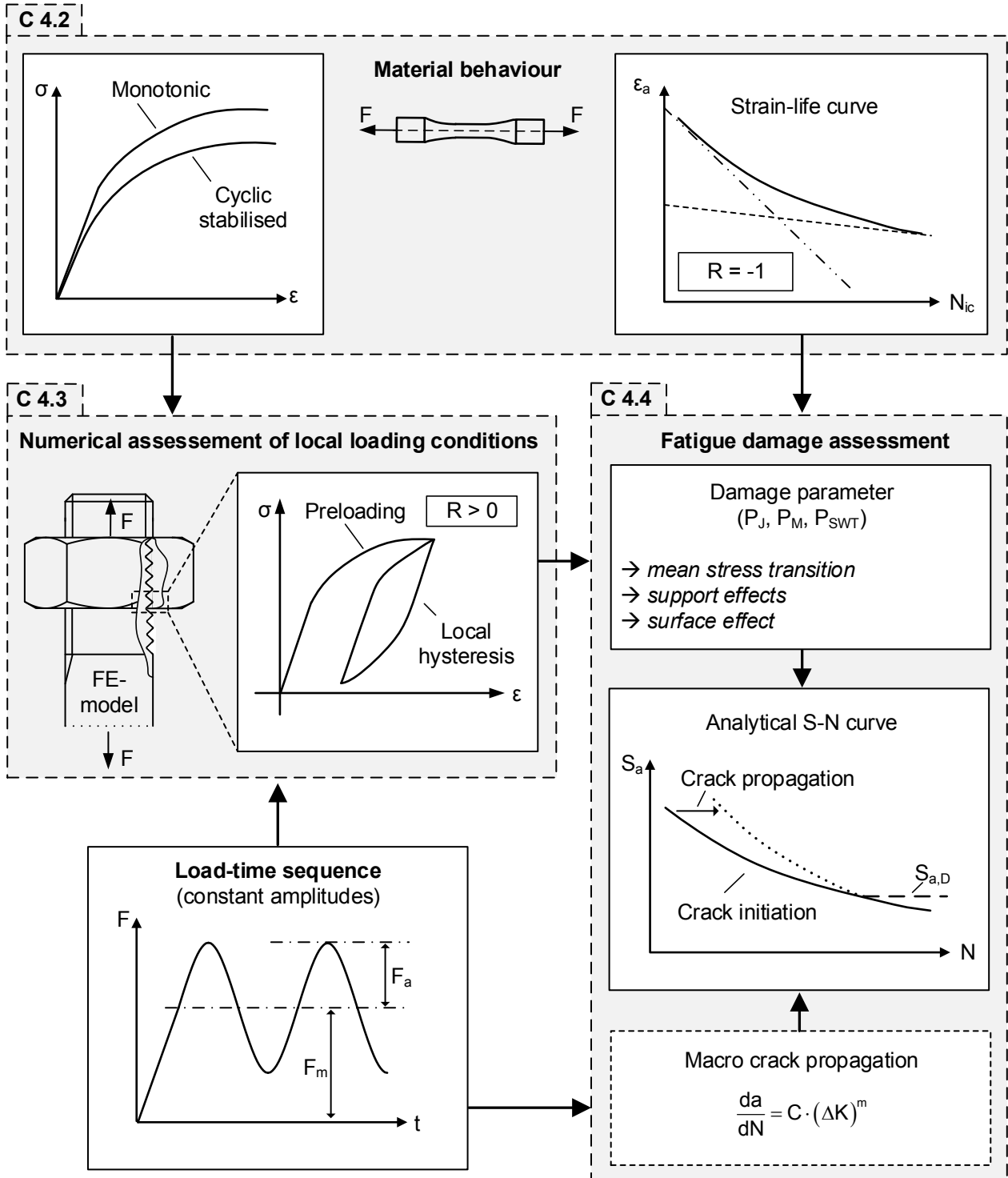


Figure 4-1: Schematic illustration of the applied analytical fatigue assessment methodology

## 4.2 Base materials description

The previously described analytical fatigue assessment methodology, based on the strain-life concept, requires knowledge about the characteristics of the bolts base material under monotonic and cyclic loading. While monotonic material characteristics are relatively easy to obtain from tensile tests, the determination of strain-dependent cyclic material parameters requires much higher testing efforts. Cyclic material data collections such as *Boller & Seeger (1987)* or the valuable online material database *Boller et al. (2008)* provide comprehensive material data also for a number of relevant high-strength bolt materials. However, it is questionable whether or under which conditions the documented cyclic material parameters provide a suitable analysis basis or whether distinct material tests for the actual bolt material are necessary. This question is further investigated within the sensitivity studies in Chapter 4.5. The subsequently described results of base material surveys for the experimentally investigated HV-bolts serve as analysis background.

Within the research project “Experimental and analytical assessment of the fatigue strength of bolts with large dimensions under consideration of boundary layer effects” (*Oechsner et al., 2015*), a characterisation of base material and boundary layer was performed for the M36 bolts, analysed in the experimental investigations presented in Chapters 3.3 and 3.5. Within the base material characterisation, executed by the Chair and Institute for Materials Science, Technische Universität Darmstadt, cyclic material characteristics were determined in strain-controlled constant amplitude tests without mean strain. Moreover, strain-controlled tests under high mean strain were implemented to quantify the material’s cyclic relaxation behaviour. Additionally, monotonic material properties were determined in force controlled tensile tests for the M36 bolts’ base material as well as the base material of the bolts M64, examined in Chapter 3.4.

Supplementing the available material data basis from the research project, additional material tests were performed to provide cyclic material data also for the investigated M64 bolts. Moreover, to enable further verification of the analytical fatigue assessment approach, material parameters were also determined for bolts of size M48, which were used for the fatigue tests by *Marten (2009)* (see Chapter 2.1.5). The required HV-bolts were made available from the remainders of the test series at the Institute for Steel Construction, Leibniz Universität Hannover. Due to the limited number of available specimens and in order to confine testing efforts, the required cyclic material parameters were determined by use of strain-controlled Incremental-Step-Tests (IST) and not constant amplitude tests (see Chapter 2.2.2). The inclusion of the M36 bolt material to the test program enables classification and direct comparison between results of the two testing procedures. The test series further comprised additional monotonic tensile tests for all materials. Practical implementation of the tests was commissioned to the Institute of Materials Science, Leibniz Universität Hannover. Scientific planning and evaluation was performed by the author.

For all material tests the required test specimens were extracted directly out of the core of bolts, belonging to the corresponding manufacturing batch of the respective test series. To avoid influences of the surface conditions the specimens were mechanically polished. It has been verified by *Oechsner et al. (2015)* that, independently of the boundary layer state, the *Vickers* hardness of the



investigated M36 and M64 bolts is homogenous throughout the bolt diameter, confirming a high material manufacturing grade. Equivalent results are reported by *Schneider* (2011) for analogously investigated threaded fasteners. The investigations by *Schneider* also confirmed a good compliance between measured micro hardness along the bolt diameter and along the root of the thread. Moreover, *Charpy V*-notch tests by *Stranghöner et al.* (2018) on high-strength bolt materials did not show significant differences of results between specimens extracted from the bolts core and notch root surface area. It can thus be regarded as legitimate to utilize material characteristics determined on specimens from the bolts core for approximation of the material behaviour in the notched thread. Since all investigated bolts were rolled before heat treatment, they may be considered as free from residual stresses from the manufacturing process.

The performed base material tests for the experimentally investigated HV-bolts are summarized in Table 4-1. In order to determine the required set of cyclic material parameters by IST, technically only two specimens per bolt material are required. However, to provide a broader evaluation background a slightly higher number of tests were performed. The quantity of actually performed IST was mainly defined by the number of available bolts and extractable specimens.

**Table 4-1: Examined high-strength bolt materials and number of considered specimens for monotonic and cyclic material tests**

HV-bolts	Material	Tensile tests <sup>1/2</sup>	Strain-controlled cyclic tests		
			Constant amplitudes <sup>1</sup>		Incremental-Step-Tests <sup>2</sup>
			( $\epsilon_m = 0$ )	( $\epsilon_m > 0$ )	( $\epsilon_m = 0$ )
M36x270 10.9	(B)	4 / 0	8	4	3
	(NT)	0 / 4			4
	(HT)	0 / 8			5
M64x450 10.9	(B)	2 / 8	-	-	7
	(NT)	2 / 0			0
M48x275 10.9	(NT)	0 / 4			4

<sup>1</sup> performed by the Chair and Institute for Materials Science, Technische Universität Darmstadt (*Oechsner et al.*, 2015)

<sup>2</sup> performed by the Institute for Steel Construction and the Institute of Materials Science, Leibniz Universität Hannover

#### 4.2.1 Monotonic loading

Monotonic material properties were determined in tensile tests referring to DIN EN ISO 6892-1 (2017 and 2009). Figure 4-2, left shows the comparison of the obtained material strength values for all investigated material configurations under distinction of the boundary layer state of the bolts from which specimens were extracted. Additional to the depicted mean values represented by the main bars, the error bars show the maximum and minimum values from the underlying data. The number in brackets indicates the number of considered specimens.

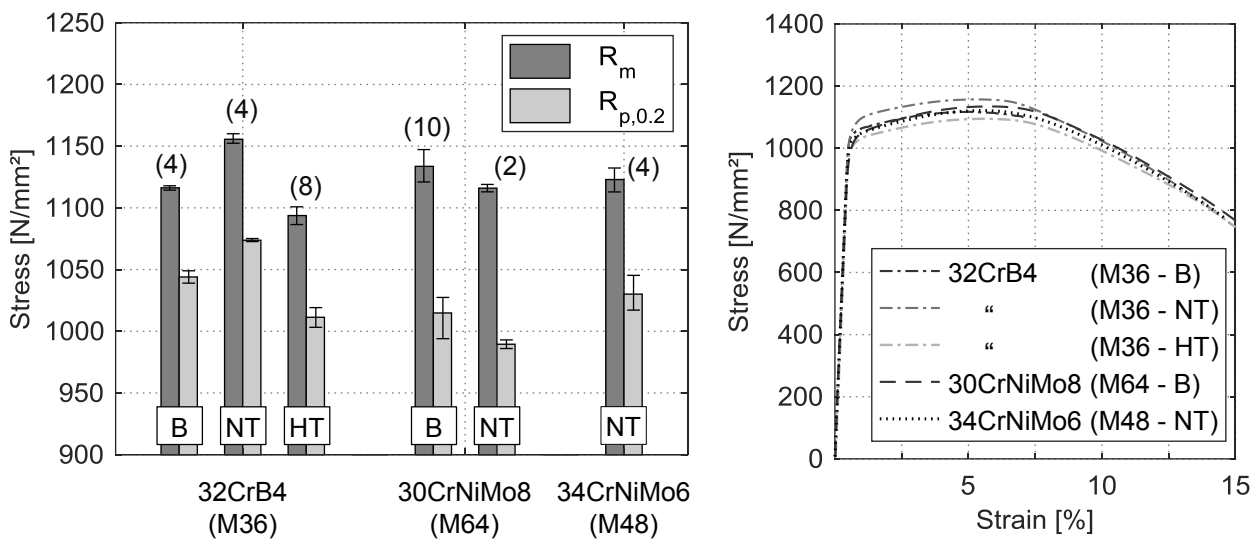


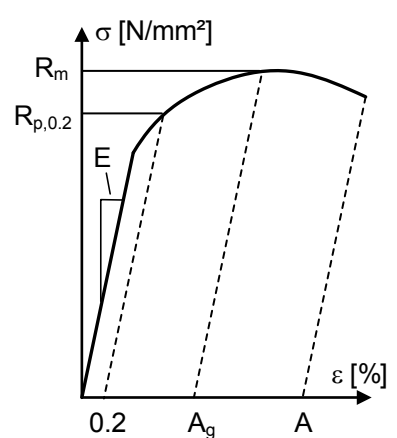
**Figure 4-2: Means and scatter of materials strength values (left) and selected representative monotonic stress-strain relations (right) of investigated bolt materials**

All materials fulfil the requirements of strength class 10.9 regarding tensile strength ( $R_m \geq 1040 \text{ N/mm}^2$ ) and 0.2%-plastic strain limit ( $R_{p,0.2} \geq 940 \text{ N/mm}^2$ ) from DIN EN ISO 898-1 (2013). For the M36 bolt material 32CrB4, the material specimens extracted from HT-galvanized bolts show a reduced material strength compared to specimens from bolts with the other two boundary layer configurations. This tendency was also observed by *Oechsner et al.* (2015) in tensile tests on whole M36 bolts from the same manufacturing batch as investigated here, as well as in tensile tests on notched and un-notched small specimens ( $d_0 = 6 \text{ mm}$ ) of the same material composition. A possible cause is the modification of the materials microstructure at the high galvanizing temperature of approximately  $550^\circ\text{C}$ , which is above the applied tempering temperature of approximately  $500^\circ\text{C}$ .

An improvement of material strength for specimens extracted from NT-galvanized compared to black bolts, as observed here for the M36 bolt material 32CrB4, was not present in the aforementioned results from *Oechsner et al.*. Moreover, for the M64 bolt material 30CrNiMo6 the measured material strength at specimens extracted from the NT-galvanized bolts was slightly lower than at their equivalents from uncoated, black bolts. Presumably, the detected differences between black and NT-galvanized base conditions can mostly be ascribed to generally existing scatter and the low number of considered specimens. Throughout the test series, a notable scatter of material strength values was also observed for specimens extracted from different bolts with the same boundary layer configuration.

Figure 4-2, right shows full monotonic stress-strain relations from tensile tests, which are representative for the means of the respective material conditions. All materials show a notable amount of ductility and plastic strains at the tensile strengths level  $A_g$  of around 5 %. For the specimens from NT-galvanized M64 bolts, which are not represented in the figure, no full stress-strain results were available to the author. The mean values of the obtained monotonic material parameters are summarized in Table 4-2. The individual test results can be found in Appendix B.1.

**Table 4-2: Summary of monotonic material parameters from tensile tests (mean values)**

	Parameter / Material	$R_{p,0.2}$ [N/mm <sup>2</sup> ]	$R_m$ [N/mm <sup>2</sup> ]	$E$ [N/mm <sup>2</sup> ]	$A_g$ [%]	$A$ [%]
	32CrB4 (M36)	B	1044	1116	214290	4.4
NT		1074	1156	207456	4.8	14.7
HT		1011	1094	216173	5.1	15.3
30CrNiMo8 (M64)	B	1015	1134	203675	5.4	15.9
	NT	990	1116	203600	5.3	n. d.
34CrNiMo6 (M48)	NT	1030	1123	207261	5.1	15.6

#### 4.2.2 Cyclic loading without mean strain ( $\epsilon_m = 0$ )

##### Material curves from strain-controlled constant amplitude tests

Figure 4-3 shows the test results from the constant amplitude tests on the M36 bolt material 32CrB4, given in *Oechsner et al. (2015)*, together with the resulting strain-life curve according to the description by *Manson, Coffin and Morrow (Eq. 2-8)* and the cyclic stress-strain curve by use of the *Ramberg-Osgood equation (Eq. 2-9)*. The comparison of the cyclic stress-strain curve to the additionally depicted monotonic material behaviour highlights the cyclic softening characteristic of the material.

Since stress amplitudes decreased especially throughout the initial phase of the strain-controlled tests, following common conventions (e.g., see *Radaj & Vormwald, 2007, el Dsoki et al., 2008*), the stabilized stress amplitudes were adopted from the test runs at half of the load cycles until initial cracking ( $1/2 \cdot N_c$ ). An exemplary test result depiction, which illustrates the transient stress behaviour during the constant strain amplitude tests, is given in Appendix B.2.

In the literature, different regression approaches with varying degrees of complexity are proposed for determination of the relevant cyclic material parameters. *Wächter (2016)* has shown that methods with higher complexity, for example a 3-dimensional regression according to *el Dsoki et al. (2008)*, do not lead to superior results regarding the assessment of the median strain-life and cyclic stress-strain curves. Since the relatively low number of available test specimens does not provide a valid basis for determination of full statistical scatter of the cyclic material curves, the estimation of the outer domains of the probability distribution was not aim of this analysis. Hence, a linear regression of the logarithms of elastic and plastic parts of the strain-life curve based on the least squares method was used, whereby the squares of the distances were minimized in direction of the load cycle number. With this standard procedure for evaluation of linearized stress- or strain-life, described for example in *ASTM E739 (2010)* or *Wächter (2016)*, the parameters for the analytical strain-life curve representation were determined. The parameters for the *Ramberg-Osgood equation* were then derived by use of the compatibility conditions (Eq. 2-10 and Eq. 2-11). The resulting cyclic material parameters are given in Table 4-3.

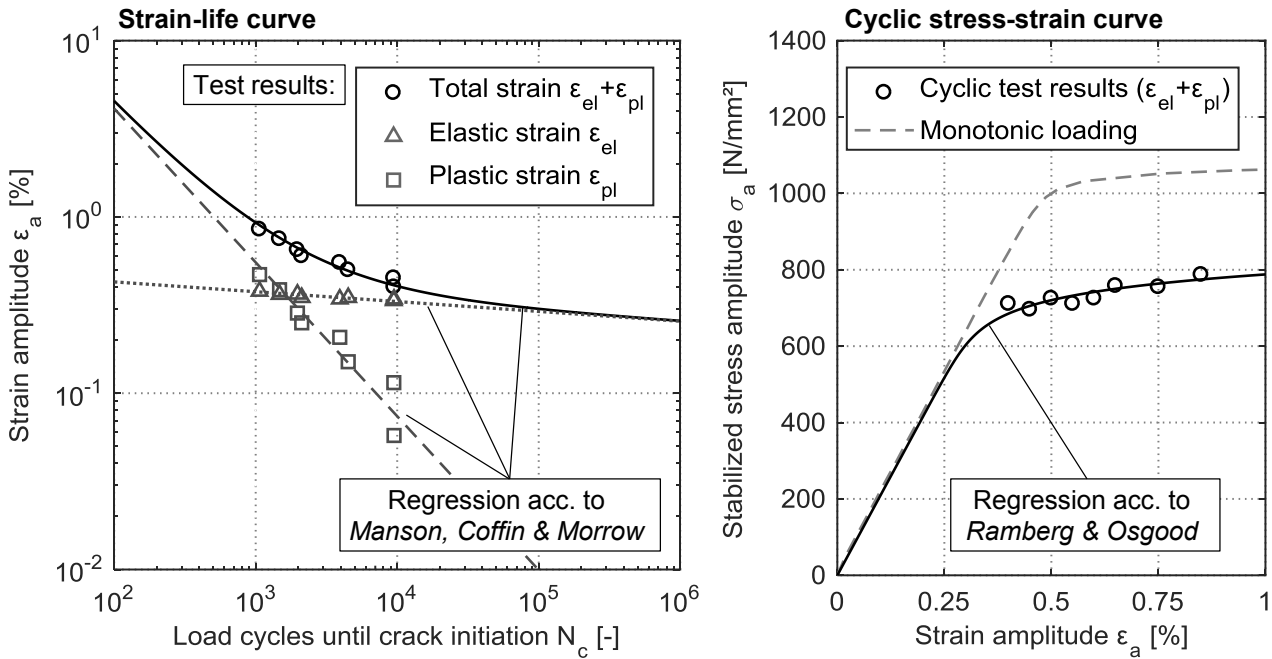


**Figure 4-3: Cyclic material curves of M36 bolt material 32CrB4 derived from strain-controlled tests with constant amplitudes by Oechsner et al. (2015); left: strain-life curve; right: cyclic stress-strain curve**

Material curves from strain controlled Incremental-Step-Tests

For each examined material Incremental-Step-Tests (IST) were performed at two different strain levels with maximum strain amplitudes differing by a factor of ~2. The load series, depicted in Figure 4-4, were defined as repetitive blocks with stepwise de- and increasing peak strains with a constant strain increment after every half-cycle. As such, each block consisted of two point-symmetrical half blocks with a number of  $p = 20$  load cycles with linearly changing strain amplitudes.

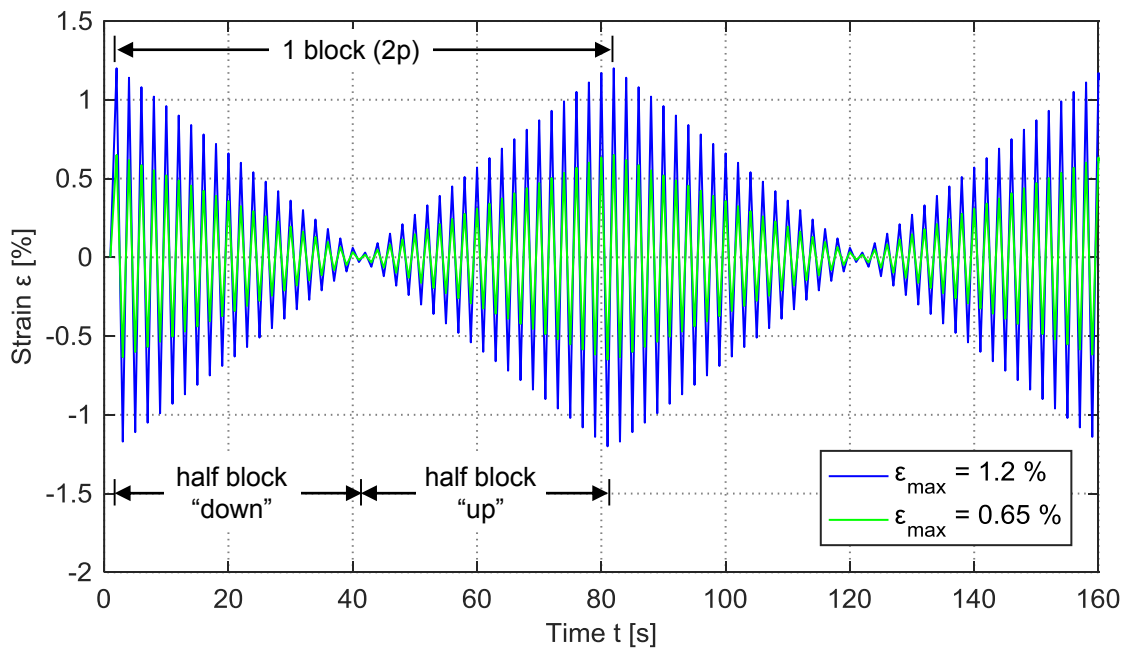


**Figure 4-4: Load sequences of Incremental-Step-Tests**

Figure 4-5 exemplary shows the stress-strain paths of two loading blocks of an IST with strain level  $\varepsilon_{\max} = 1.2\%$  for the M36 bolt material 32CrB4. The visible cyclic softening process, indicated by the decline of peak stresses during the first loading block (Figure 4-5, left), stabilized after run-trough of the initial blocks. The loading sequence was continued until the initiation of a technical fatigue crack was indicated by renewed destabilization of the cyclic stress-strain behaviour (see Appendix B.2). The parameters of the cyclic stress-strain relation according to Eq. 2-9 were determined by a 'best-fit' regression analysis of the peak values of a stabilized loading block; in analogy to the constant amplitude strain-controlled tests, this was performed at a block at half of the load cycles until crack initiation ( $1/2 N_c$ ) (Figure 4-5, right).

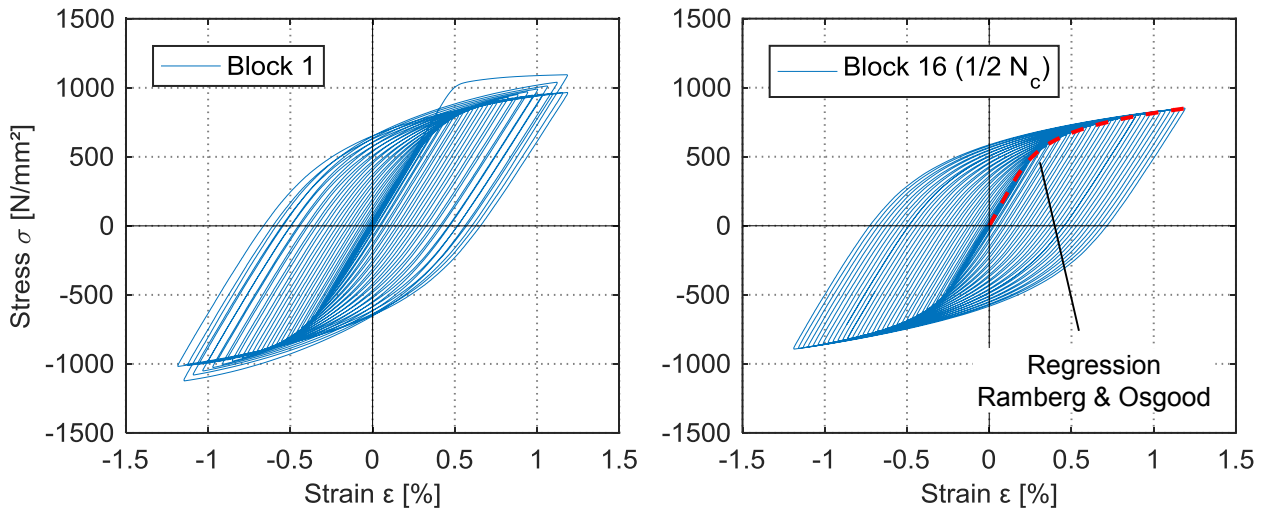


**Figure 4-5: Stress-strain path of the first loading block (left) and a stabilized loading block at  $1/2 N_c$  (right) from IST for M36 bolt material 32CrB4 (specimen extracted from black bolt) with  $\varepsilon_{\max} = 1.2\%$**

Applying a rain-flow cycle count (e.g., *Clormann & Seeger, 1986*), one full block generates a number of  $2p = 40$  closed hysteresis loops. Following the procedure proposed by *Vormwald & Seeger (1988)*, the strain-life curve approximations were determined based on the calculated damage of the plastic parts of the strain amplitudes. Subsequently the calculation procedure is described.

The plastic strain- as well as the corresponding stress amplitudes of the applied load series can be computed from the determined *Ramberg-Osgood* relation (Eq. 2-9). According to the strain-life curve description by *Manson, Coffin and Morrow (Eq. 2-8)*, the number of endurable load cycles until damage (i.e., initial cracking)  $N_{c,k}$  for a single plastic strain amplitude of the load sequence  $\varepsilon_{a,p,k}$  can then be calculated with Eq. 4-1:

$$N_{c,k} = \frac{1}{2} \left( \frac{\varepsilon_{a,p,k}}{\varepsilon'_f} \right)^{\frac{1}{c}} \quad \text{Eq. 4-1}$$

For an IST with the running number  $j$  the known number of load cycles until crack initiation  $N_{c,j}$  can equivalently be expressed by the number of loading blocks passed through  $m_j$ . Assuming validity of *Miner's-rule* and linear damage accumulation, each block causes equal damage  $D_{\text{block},j}$  and the failure condition for an IST can be stated as:

$$m_j \cdot D_{\text{block},j} = m_j \cdot \sum_{k=1}^{2p_j} \frac{1}{N_{c,k,j}} = 1 = m_j \cdot 2 (\epsilon'_f)^c \sum_{k=1}^{2p_j} (\epsilon_{a,p,k,j})^{-\frac{1}{c}} \quad \text{Eq. 4-2}$$

With two unknown material constants, the division of the equations Eq. 4-2 for the two IST with different maximum strain amplitude ( $j = 1$  and  $j = 2$ ) but equivalent cyclic stress-strain relations provides a system of equations, where the cyclic ductility exponent  $c$  can be determined iteratively:

$$\frac{m_2}{m_1} = \frac{\sum_{i=1}^{2p_1} (\epsilon_{a,p,i,1})^{-\frac{1}{c}}}{\sum_{i=1}^{2p_2} (\epsilon_{a,p,i,2})^{-\frac{1}{c}}} \quad \text{Eq. 4-3}$$

With parameter  $c$  known, solving Equation 4-2 followed by the conditions of compatibility Eq. 2-10 and 2-11 enables the determination of the remaining material constants.

Figure 4-6 shows the fatigue results of the performed IST at the two different strain levels as input for the calculation procedure, described above. It becomes clear that with the present limited number of tests and considerably overlapping scatter of results no distinct differentiation between the 32CrB4 material specimens from bolts with different boundary layer conditions (B, NT, HT) is enabled by the results. In the comparison between the different analysed materials certain observations are possible. For all IST on both investigated load levels higher endurable load cycle numbers were obtained for the M48 bolt material 34CrNiMo6 than the M64 bolt material 30CrNiMo8. Thereby, consistently the fatigue results of the former material lie in the upper and of the latter material in the mid to lower range of the scatter of results for M36 bolt material 32CrB4. In the following section, the resultant cyclic material curves are compared and discussed.

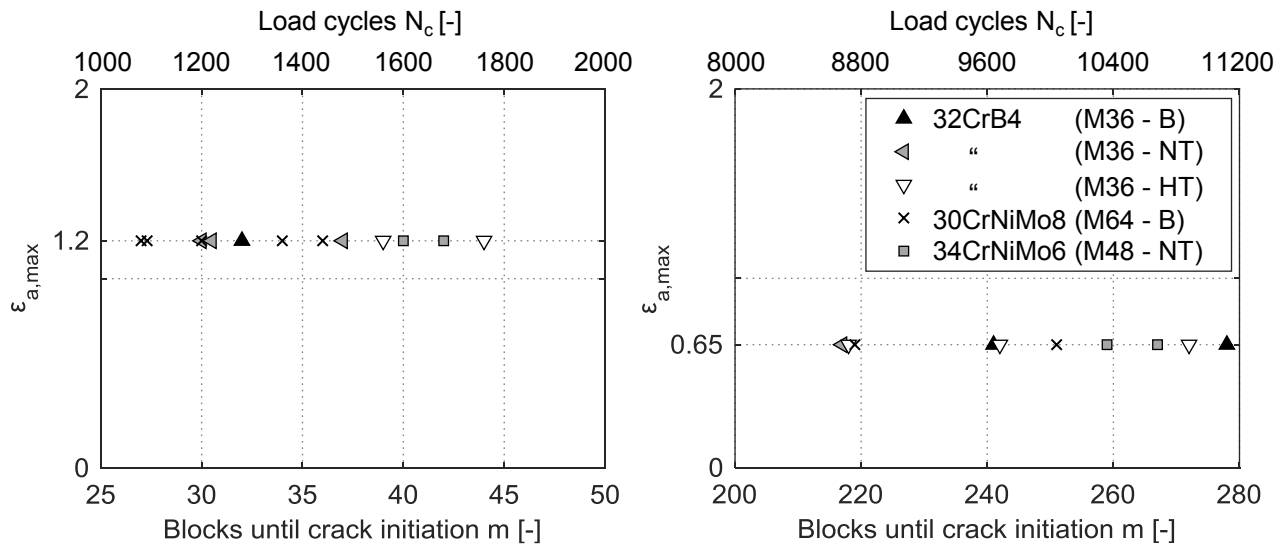


**Figure 4-6: Fatigue results of IST at different strain levels in terms of endurable blocks until crack initiation and corresponding load cycles as input for determination of strain-life curve**

Comparison of cyclic material curves

The comparison of the cyclic material curves for all investigated bolt materials determined with different experimental procedures is presented in Figure 4-7. The corresponding material parameters are given in Table 4-3.

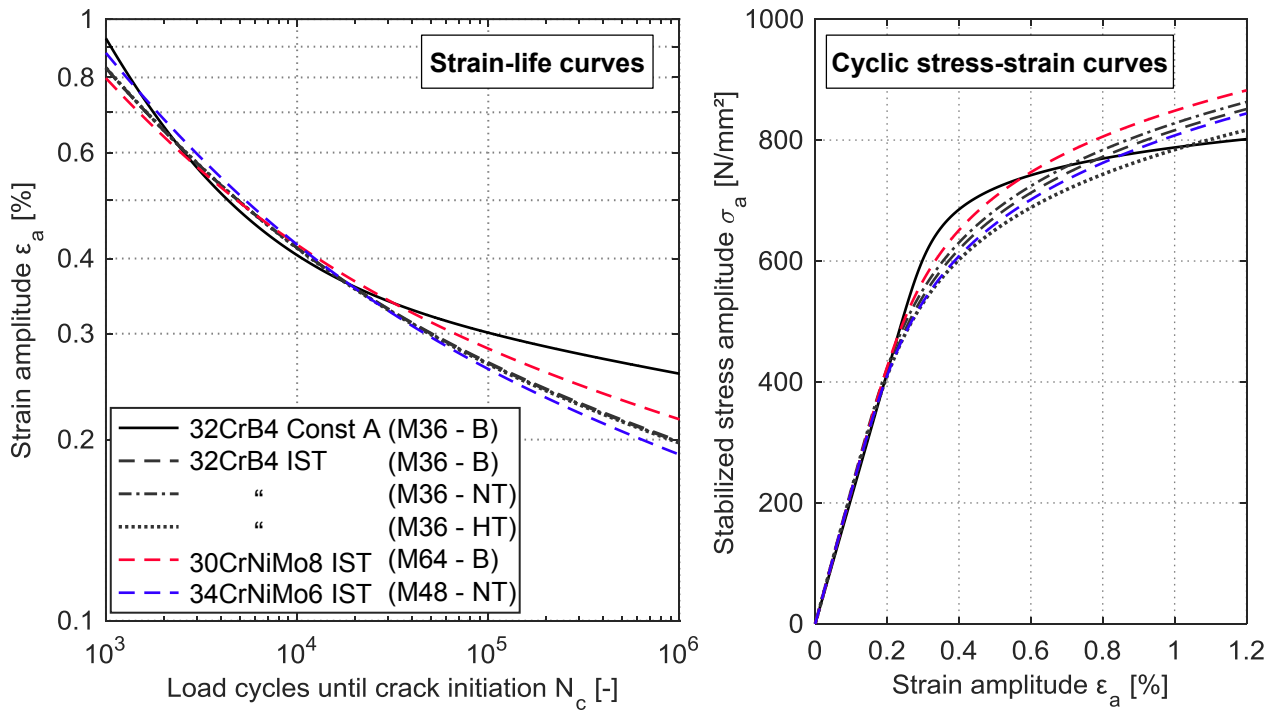


**Figure 4-7: Comparison of cyclic material curves**

**Table 4-3: Cyclic material parameters from strain controlled tests without mean strain ( $\epsilon_m = 0$ )**

Parameter / Material	E (cycl.) [N/mm <sup>2</sup> ]	$\sigma'_f$ [N/mm <sup>2</sup> ]	$\epsilon'_f$ [-]	b [-]	c [-]	K' [N/mm <sup>2</sup> ]	n' [-]	
<b>Constant Amplitude Tests:</b>								
32CrB4 (M36 - B)	207638	1195	4.194	-0.056	-0.873	1090	0.064	
<b>Incremental-Step-Tests (IST):</b>								
32CrB4 (M36)	B	216470	1578	0.359	-0.093	-0.571	1864	0.163
	NT	222823	1587	0.349	-0.092	-0.565	1882	0.162
	HT	216840	1475	0.334	-0.089	-0.557	1758	0.160
30CrNiMo8 (M64 - B)	218526	1516	0.308	-0.083	-0.562	1804	0.148	
34CrNiMo6 (M48 - NT)	218942	1668	0.418	-0.010	-0.577	1940	0.173	

The given cyclic stress-strain curves from IST are determined as means from the tests with higher strain level  $\varepsilon_{\max} = 1.2\%$ . For all investigated material configurations the individual stress-strain relations from different specimens showed a high compliance. Thus, the here depicted means can be considered as representative. Caused by the deviating test procedure a diverging material response is present, especially at higher strain amplitudes  $\varepsilon_a > \sim 0.3\%$ . This known phenomenon can be explained with a deviating microstructural slipping behaviour under constant and variable amplitudes (see *Wagener, 2007*).

For material 32CrB4, similar to monotonic conditions, the stress-strain relation of specimens from HT-galvanized bolts lies below its equivalents from black and NT-galvanized bolts. However, considering the lower initial monotonic stress level, the amount of peak stress decline, caused by cyclic softening, is in a comparable order of magnitude as for the other two configurations. No additional impact from the introduced temperature during galvanizing can be detected. The proximity of the cyclic stress-strain curves for black and NT-galvanized base conditions of the 32CrB4 material confirms the earlier stated assumption that the higher monotonic strength values detected for NT-galvanized conditions can mainly be ascribed to scatter and a low number of considered specimens. Still, a slightly higher stress level is also visible from the cyclic test results. For the further two investigated bolt materials, specimens for IST were only extracted from bolts with one boundary layer configuration.

Since no clear production state related tendency (B, NT, HT) could be derived from the fatigue results, the IST based strain - life curves for material 32CrB4 were calculated with the means of the loading blocks until crack initiation throughout all tested specimens. Thereby the boundary layer state of the bolts from which specimens were extracted is disregarded. Still, the depicted strain-life curves are calculated with the distinct cyclic stress-strain relations, determined for the three production conditions. However, these had no significant effect on the resultant strain - fatigue life relations.

In the region of moderate load cycle numbers, the IST based strain-life curve from the M36 bolt material 32CrB4 provides a good approximation of the corresponding fatigue curve from constant amplitude tests. In the region of lower strain amplitudes and load cycle numbers  $N_c > \sim 5 \cdot 10^4$  an advancing lower deviation occurs. This tendency is generally acknowledged by the developer of the applied evaluation procedure (see Chapter 2.2.2). However, also the strain-life curve from the constant amplitude tests lacks experimental representation at high load cycle numbers (see Figure 4-3).

Between the three investigated bolt materials certain deviations of progress of their strain-life curves arise from the fatigue results (see Figure 4-6). Nevertheless, since the original purpose of the IST based evaluation procedure was to provide a general approximation of strain-life curves, using a low number of specimens, the results most of all emphasize that the investigated bolt materials exhibit fairly comparable cyclic characteristics.



### 4.2.3 Cyclic loading with high mean strain ( $\epsilon_m > 0$ )

Figure 4-8 shows the stress-strain histories from two strain-controlled material tests on M36 bolt material 32CrB4 under high mean strain performed by *Oechsner et al.* (2015). The depicted results were provided to the author by the Chair and Institute for Materials Science, Technische Universität Darmstadt. Additionally, the cyclic-stress strain curve derived from constant amplitude tests without mean strain is plotted for comparison in the red dashed lines. The results show a successive cyclic relaxation of the upper and respectively the mean stress level of the cyclic hysteresis, which increases with the strain amplitude. The test results of all performed material tests under high mean strain, given in *Oechsner et al.* (2015), are presented in Figure 4-9.

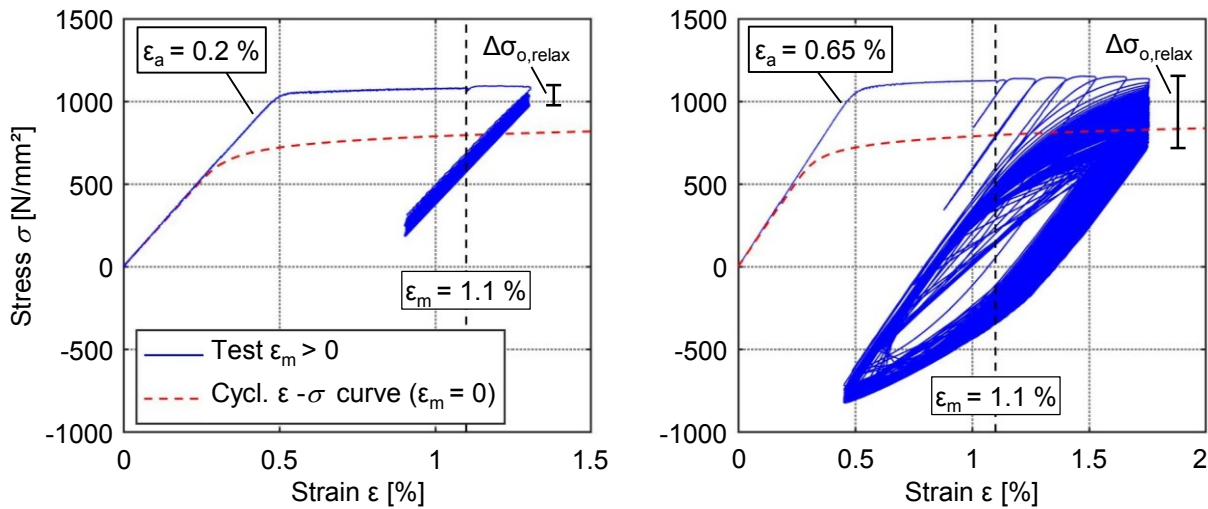


**Figure 4-8: Stress-strain histories from tests on M36 bolt material 32CrB4 with high mean strain  $\epsilon_m = 1.1\%$  performed by *Oechsner et al.* (2015)**

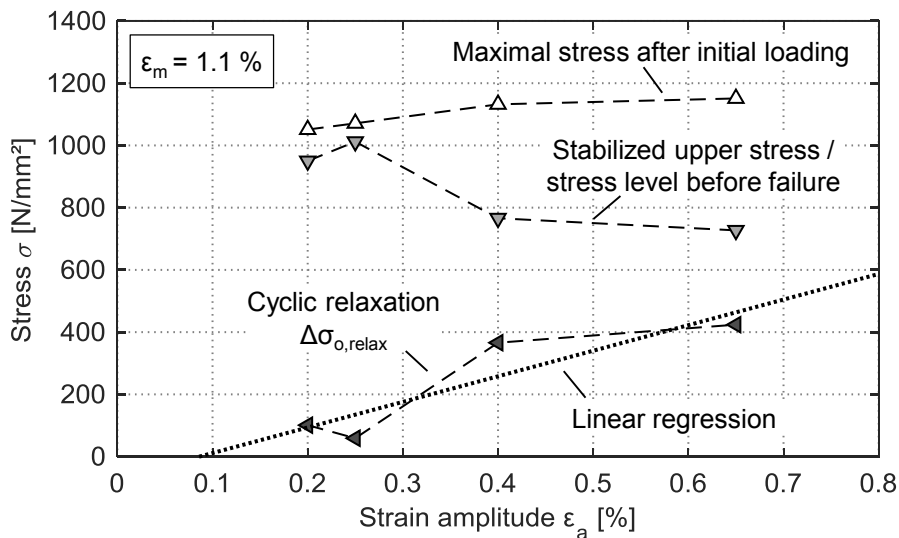


**Figure 4-9: Results of strain-controlled tests under high mean strain  $\epsilon_m = 1.1\%$  for M36 bolt material 32CrB4 according to *Oechsner et al.* (2015)**

Since not in all tests the stress level reached a plateau during cyclic loading, the ‘stabilized’ upper stress was determined by the stress level before detection of initial cracking. The amount of cyclic relaxation  $\Delta\sigma_{o,relax}$  is calculated as difference to the maximum stress level after initial loading. Considering the expectable scatter of results and the limited number of the effortful tests, only a general approximation of the relation between strain amplitude and cyclic relaxation can be determined from the results. For consideration within the analytical fatigue calculation, a linear regression function is used. Thereby, it is assumed that for strain amplitudes below  $\sim 0.1\%$  no decline of the cyclic stress level occurs.

#### **4.2.4 Conclusions for application of material data in analytical fatigue calculations**

For the further application of the determined base material properties in analytical fatigue calculations the following conclusions apply:

- Differences in the cyclic material curves mainly arise from the two methods investigated for their determination (i.e., constant amplitude tests and IST). The three bolt materials investigated by IST show a rather comparable cyclic behaviour.
- The original purpose of the IST based investigation method is to provide a general approximation of the strain-life curve, based on a low number of test specimens. Hence, the procedure is not suitable to profoundly detect influences of the previous production state (B, NT, HT) of the bolts from which specimens were extracted. For a detailed study, comprehensive series with constant amplitude tests would be required. Based on the available data, no significant effect of the production condition is detectable, although a possible influence cannot entirely be precluded, either. The highest validity of the IST based strain-life curves can be presumed when neglecting a possible impact of the production condition to the endurable load cycles and using the resulting means throughout all performed IST of the respective material.
- No endurance limit was determined, and strain-life curves from both procedures lack experimental background for higher load cycle numbers. Therefore, results from analytical calculations at lower stress and strain levels must be considered with care.
- Strain controlled tests under high mean strain were only performed for one material, and with a limited number of specimens. Therefore, the results need to be regarded as a rather general approximation of the occurring order of magnitude of cyclic relaxation.

### 4.3 Assessment of local loading conditions

#### 4.3.1 Description of numerical models

The local stresses and strains inside the bolt thread are determined with finite element (FE) models of HV-bolt sets, using the software package ANSYS 17.2 (APDL). The geometric properties are set according to the relevant normative standards, particularly DIN EN 14399-4 (2015), DAST - Guideline 021 (2013) and the DIN 13 series. In order to avoid restraint of radial nut widening (see Chapter 2.2.3), models consist of all relevant parts of the clamping package, including washers and flanges. Model constrains (boundary conditions – BC) were defined at the horizontal parting surfaces between the circular clamping bodies. As such, the models provided a strong geometric approximation of the experimental test set-up for bolt tests under axial loads (see Chapter 3). Accordingly, loading is applied as stress directly to the bolt shaft.

An elaborate basis of the used models was developed by *Marten* in his studies on large-size HV-bolts performed at the Institute for Steel Construction (see *Marten*, 2009). For the here presented investigations the models were specifically refined for the calculation with non-linear material properties and especially adjusted in terms of modern element technologies, required contact definitions and mesh densities. Large parts of the subsequently described numerical studies only became possible because of the powerful computational hardware capacities provided by the Leibniz Universität Hannover (Leibniz Universität IT Services - LUIS).

#### Modelling approach

As discussed in Chapter 2.2.3, 2D axisymmetric plane element models can be considered to provide an acceptable degree of accuracy for the determination of local loading conditions inside the thread under nominal axial loads, while effectively confining the required numerical and modelling effort. However, linear elastic comparative calculations from *Marten* (2009) indicate that the consideration of the actual continuous pitch of the thread within a 3D volume element model may lead to a certain aggravation of the stress concentration and thus reduction of analytically calculated fatigue resistance. He assumes that increased notch stresses are caused by the asymmetry of the initial interlock between bolt and nut thread whereby the area of maximum stresses concentrates at one side of the thread rather than uniformly over the entire first pitch. Therefore, in the present study it shall be investigated whether a 'full' 3D modelling approach significantly affects the accuracy of the investigated analytical fatigue calculation methodology.

Additionally, for the assessment of bending affected nominal stress states, as they are common for bolts in ring-flanges, 3D model implementations are required to establish the non-axisymmetric loading pattern. This can either be achieved also with a full 3D model implementation with continuous pitch of the thread or simplified with a 3D axisymmetric rotational volume element extension of an initial 2D model. A modelling approach with "General Axisymmetric Elements" (see ANSYS Inc., 2016) could not be found appropriate for the given task of highly non-linear and contact dependent analyses because no clear result convergence for the contact definition could be achieved.

Moreover, with the required circumferential node density no advantage of numerical effort was obtained compared to an axisymmetric volume element model.

As a consequence, the following three modelling approaches have been used within the framework of this investigation:

- 2D axisymmetric model
- 3D axisymmetric model (extension from 2D model)
- Full 3D model with continuous pitch of the thread (global and sub model)

Figure 4-10 shows the fundamental 2D axisymmetric plane element model and its rotational 3D volume element extension of a M36 HV-bolt set. To optimally take advantage of the simplified modelling approach and to maintain direct comparability, the mesh pattern of both axisymmetric models was kept identical. However, to confine numerical effort, in the 3D model the bottom part of the clamping package is omitted, as it is not of relevance for the determination of local loading conditions inside the thread. Furthermore, symmetry is still used by confining the modelled parts of the clamping package to 180° in circumferential direction.

The two models used for the assessment of local loading conditions under consideration of the continuous pitch of the thread are depicted in Figure 4-11. In a first calculation step, deformations are determined in a global model with a coarser mesh density. Thereby, as for the axisymmetric 3D model, only the top part of the clamping package is represented. However, due to the non-symmetrical thread, full 360° need to be considered (the opened clamping package in the graphic is for visualisation purposes only). For determination of the local stresses and strains at the notch root deformations from the global model are applied to a sub model of the first two pitches of the loaded bolt thread (i.e., with contact to the nut), which provides a highly refined mesh density compared to the global model. All subsequently depicted results from the full 3D model refer to the sub model.

#### Numerical characteristics

With the primary aim of performing non-linear calculations, structural solid elements with linear shape functions were used (2D: 4 nodes, 3D: 8 nodes). The element types were maintained also for performed complementary calculations with linear elastic material behaviour. All models were analysed and adjusted in convergence studies in terms of element density inside the thread and around the circumference. Thereby, corresponding recommendations given in the literature (e.g., Seybold, 2005) were considered. Still, for the full 3D sub model certain limitations had to be accepted, which are discussed within the evaluation of numerical results.

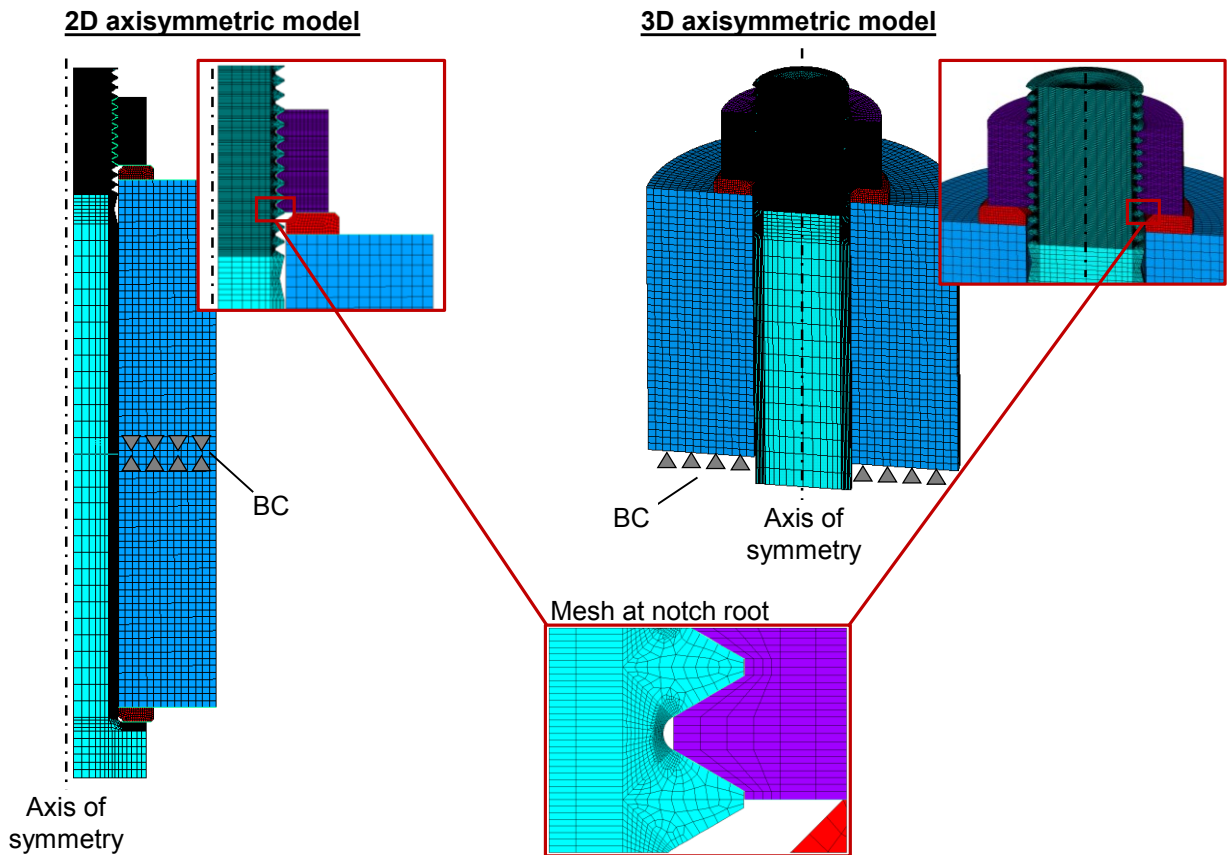


Figure 4-10: Axisymmetric finite element models of a M36 HV-bolt set (left: 2D plane element model, right: 3D rotational volume element extension)

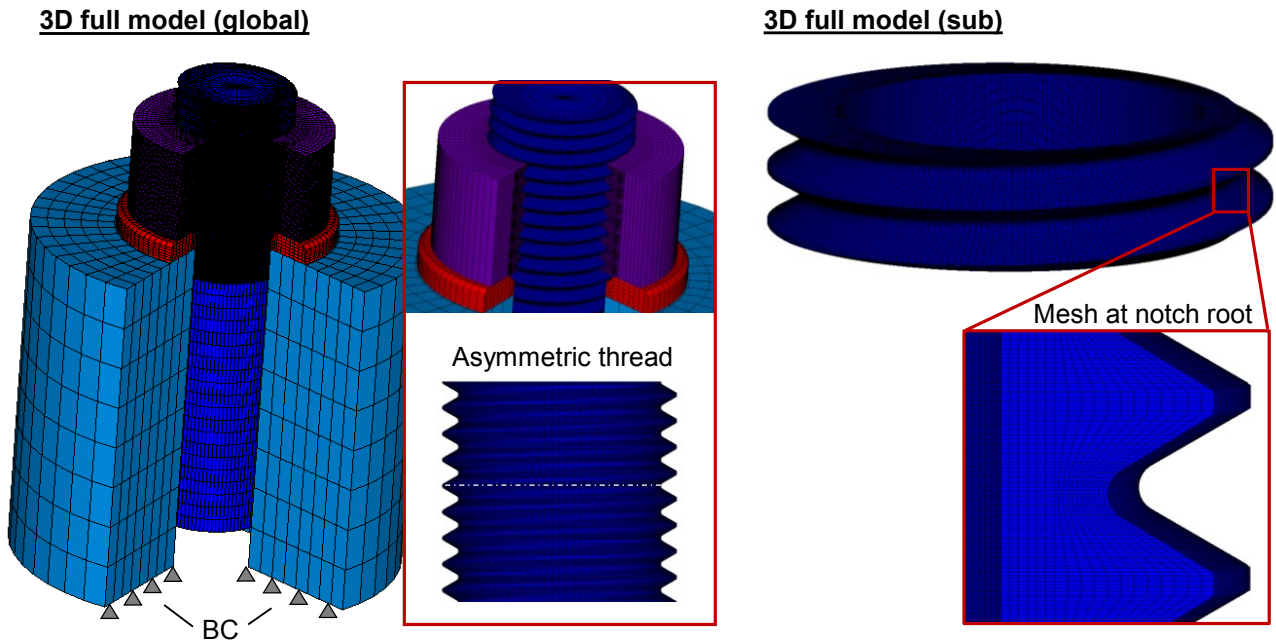


Figure 4-11: Full 3D volume element model of a M36 HV-bolt set with continuous pitch of the thread (left: global model, right: sub model of maximum loaded bolt thread area)

The base material characteristics in terms of cyclic stabilized and monotonic material curves, determined in the previously described material investigations, are implemented by a multilinear plastic material law with kinematic hardening using a sublayer formulation based on *Besseling* (1958). Plasticity is defined by the *van Mises* yield surface. To account for large deformations at high stress levels, the monotonic stress-strain relations depicted in Figure 4-2, right are transformed from “engineering” to “true” stresses and strains according to equations Eq. 4-4 and Eq. 4-5. After reaching the tensile strength  $R_m$  ideal plastic material behaviour is assumed.

$$\varepsilon_{\text{true}} = \ln(1 + \varepsilon_{\text{eng}}) \quad \text{Eq. 4-4}$$

$$\sigma_{\text{true}} = (1 + \varepsilon_{\text{eng}}) \cdot \sigma_{\text{eng}} \quad \text{Eq. 4-5}$$

Using a penalty based *Augmented Lagrangian* contact algorithm, surface-to-surface contact is established by definition of overlaying contact and target elements in the paired thread and the further contact surfaces. All models use an isotropic friction contact definition based on *Coulomb's* law. If not specified differently, the friction coefficient is set to  $\mu = 0.1$ . Especially in the non-linear analyses, the contact stiffness has a noteworthy effect on the result accuracy. Therefore, in all three modelling approaches the contact stiffness was adjusted in convergence studies to minimize the amount of penetration between contact surfaces while maintaining a numerically stable solution. The ultimately applied contact stiffness factors (FKN, see ANSYS Inc., 2016) alongside with the most relevant mesh characteristics of the applied models are given in Appendix C.1.

#### 4.3.2 Evaluation of numerical results

At the notch root surface a plane stress state develops (see Chapter 2.1.2). The damage decisive location, where fatigue crack initiation is assumed to occur, is identified under linear elastic conditions by the maximum principal notch stress concentration  $K_t$  or under elastic-plastic material conditions by the maximum principle strain  $\varepsilon_1$ . At this location the local cyclic material response is determined with the corresponding first principle stress  $\sigma_1$  (see Section 4.3.3).

To provide a comprehensive perspective of the numerically determined development of local loading conditions at the loaded bolt thread surface, the two axisymmetric models are evaluated along a result path in axial direction of the thread (Figure 4-12, left). For the full 3D model a circumferential path around the bolt thread is used, which is located at about  $30^\circ$  from the notch root towards the loaded thread flank, where the maximum linear elastic stress and elastic-plastic strain concentrations occur (Figure 4-12, right). The subsequently presented results refer to pure axial nominal loading at the bolt shaft. The impact of bending stresses is evaluated in the sensitivity studies in Section 4.5.3.

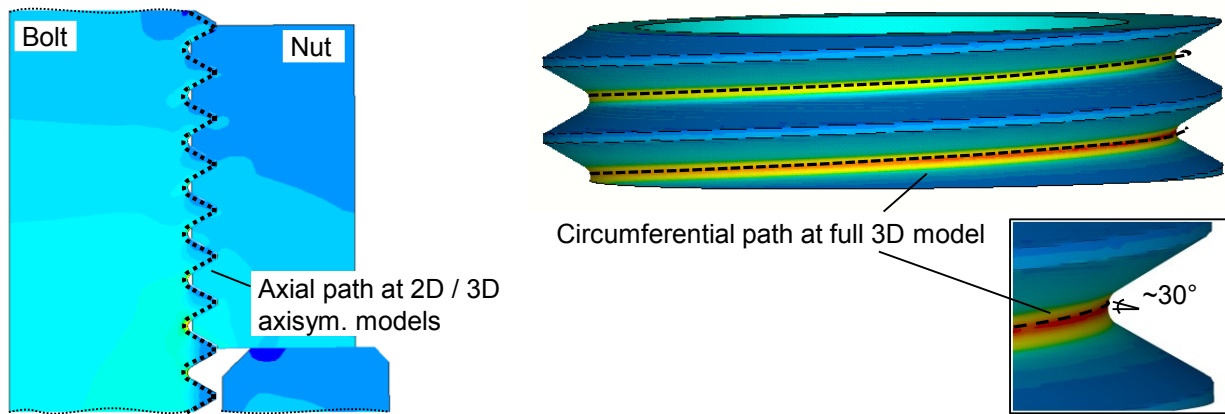


Figure 4-12: Result evaluation paths at numerical models

Linear elastic material conditions

The result comparison from calculations for a M36 HV-bolt geometry with linear elastic material behaviour is shown in Figure 4-13. The origin of the x-axis is defined at the location of the maximum stress concentration in the first load-bearing turn of the thread. Between the different modelling approaches the maximal occurring notch stress concentrations  $K_t$  closely coincide, with the full 3D model leading to a slightly lower value than the axisymmetric models. Considering the continuous thread pitch, in the vicinity of the peak value a flatter decline of the stress concentration towards the lower nut run out is visible than upwards towards the second turn. After the first full turn throughout the thread circumference the full 3D model's results fall below the second peak value of the axisymmetric models, indicating certain differences in the overall load distribution. The further development throughout the thread cannot be evaluated with the limited extent of the full 3D sub model, which had the primary purpose of assessing the fatigue decisive maximum stress and strain concentrations.

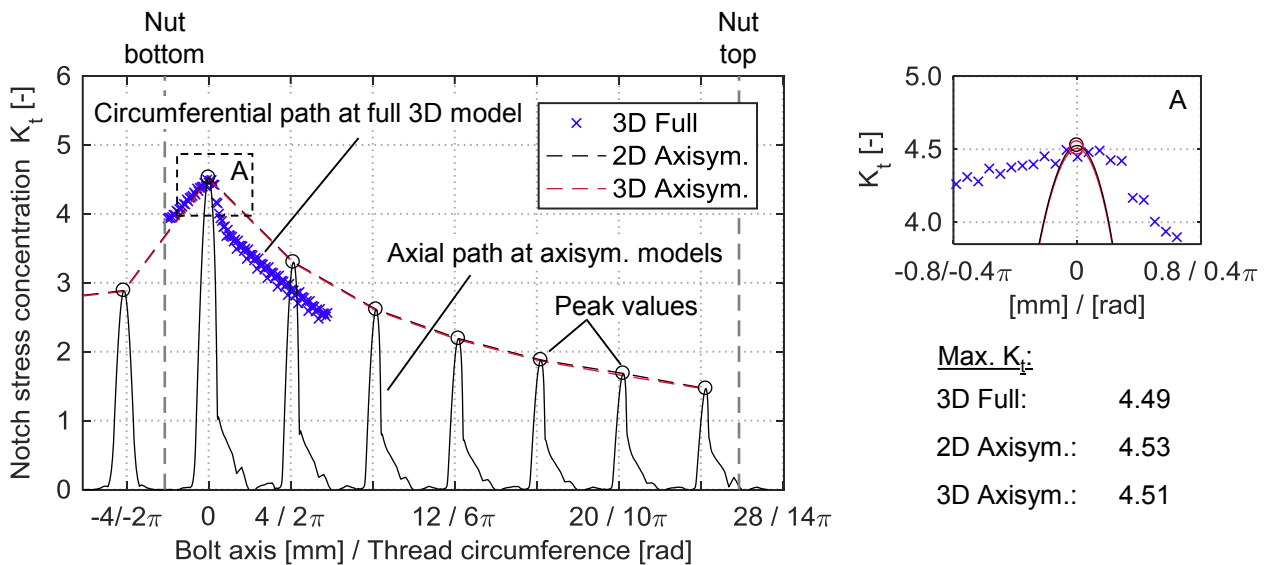


Figure 4-13: Comparison of numerical results for an M36 HV-bolt set with different modelling approaches under linear elastic material behaviour

The results depicted in Figure 4-13 further demonstrate that with the chosen circumferential mesh configuration and applied contact stiffness the axisymmetric 3D volume element extension provides an accurate approximation of the 2D model's results. As this circumstance was also approved in calculations with non-linear material implementations, the numerical set-up of the 3D axisymmetric model can be regarded as appropriate for further application in the evaluation of bending affected stress states. In the succeeding evaluations, concerning pure axial nominal loading, only the results from the 2D axisymmetric model are depicted.

#### Elastic-plastic material conditions

Figure 4-14 shows the results of path evaluations from calculations with elastic-plastic material behaviour, determined for monotonic loading conditions (Chapter 4.2.1). From the axial path evaluation of the 2D axisymmetric model only the contour of the peak values is plotted. The local strain and corresponding stress development is depicted at four different nominal stress levels at  $0.2 \cdot R_{p,0.2}$  (a),  $0.4 \cdot R_{p,0.2}$  (b),  $0.7 \cdot R_{p,0.2}$  (c) and  $0.9 \cdot R_{p,0.2}$  (d). Thereby the 0.2%-plastic strain limit corresponds to the 10.9 material class nominal value  $R_{p,0.2,nom} = 900 \text{ N/mm}^2$ .

Both numerical models show a matching load dependent stress- and strain development. While at the lowest considered load level the local strains (Figure 4-14, right) are relatively homogenous throughout the initial turns of the thread and of mostly elastic nature, a pronounced, growingly plastic strain peak develops with increasing load level. Correspondingly, at higher load levels local stresses (Figure 4-14, left) increasingly equalise throughout the thread while approaching the base material's tensile strength. In the region of the bolts nominal preload level, between 0.7 and  $0.9 \cdot R_{p,0.2}$ , local stresses change only marginally (for the upper load level lighter blue markers are used to enable a better distinction). Simultaneously, the peak strain value increases by about 50 %.

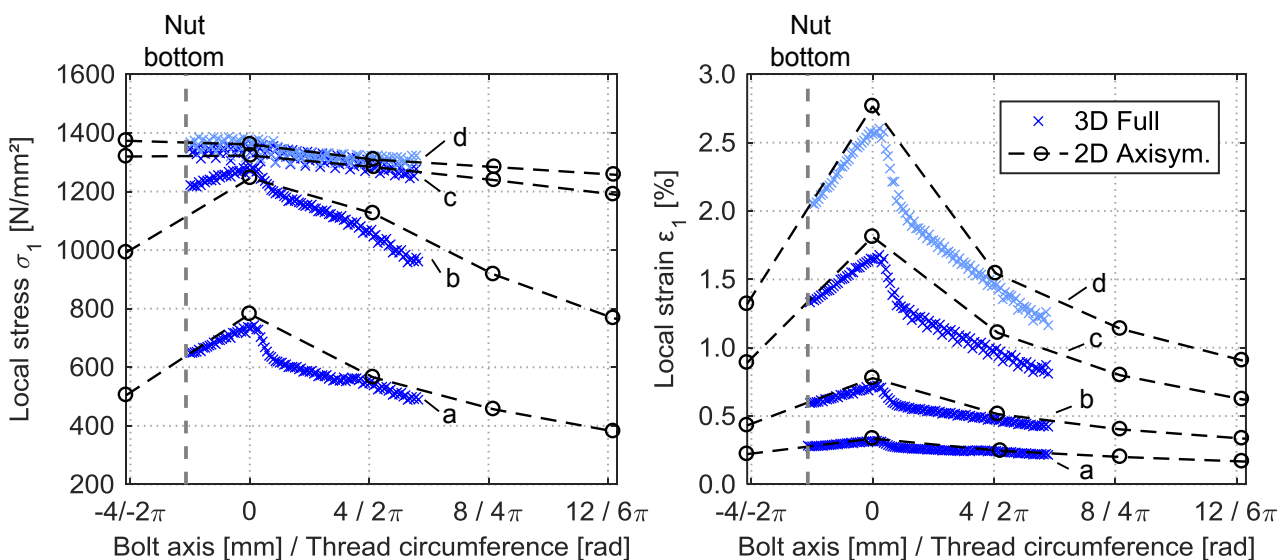


**Figure 4-14: Local stresses (left) and local strains (right) inside the paired thread of an M36 HV-bolt set resulting from calculations with 2D axisymmetric and full 3D FE-model under elastic-plastic material behaviour (monotonic loading) at nominal load levels a:  $0.2 \cdot R_{p,0.2}$ , b:  $0.4 \cdot R_{p,0.2}$ , c:  $0.7 \cdot R_{p,0.2}$ , d:  $0.9 \cdot R_{p,0.2}$**



Analogous to the linear elastic stress development in the continuous thread (Figure 4-13), elastic-plastic strains build up steadily from the lower nut run-out to a small peaking plateau and rapidly decline afterwards. Thereby, despite a close proximity of the linear elastic  $K_t$ -values, the local elastic-plastic strains from the full 3D model fall visibly below the peak values from the 2D axisymmetric model (in an order of magnitude of  $\sim 6\%$  at all represented nominal load levels).

### Result discussion

The results from the performed path evaluations are in good qualitative agreement with elastic stress measurements inside a continuous bolt thread by *Seybold* (2005) as well as the comparison of numerical determined progressions of linear elastic and elastic-plastic stresses inside an M10 bolt thread with and without continuous pitch by *Schneider et al.* (2010).

Similar to the latter mentioned study, the results presented here do not indicate that a consideration of the continuous thread pitch imposes a negative effect on the local loading conditions and thus do not confirm the corresponding observation made by *Marten* (2009). With the improved capabilities of numerical models in terms of new element technologies, refined and optimised mesh and contact definitions and the increased possibilities of performing calculations with non-linear material behaviour, the full 3D model's results exhibit an opposing tendency of slightly less fatigue critical maximum strains. The numerical results provide indication that the unilateral local confinement of the maximal loaded area inside the continuous thread rather causes a beneficial than a negative effect. This can be explained with enhanced capabilities of local stress and strain redistributions in the direct vicinity of the maximal loaded material area, which are not present in an axisymmetric model.

It needs to be pointed out that computational and modelling requirements set boundaries to the achievable mesh size in the continuous pitch of the full 3D sub-model. As the fine mesh of the notch root needs to be maintained over the entire thread turn and because of a resulting coupling of element numbers at the notch root and around the circumference, the mesh density inside the paired thread notably differentiates to the 2D model. With a rather fine mesh chosen in the latter to enable upscaling of the model to larger bolt diameters without extensive mesh adjustments, the mesh density along the notch root radius is approximately four times finer than in the full 3D sub model (see also Appendix C.1).

However, for the here analysed M36 bolt geometry a 2D model with half of the elements along the notch root radius leads to almost identical results. Even with a mesh size reduced to the order of magnitude of the mesh of the full 3D sub model, resulting stresses and strains are only marginally lower than with the original applied high mesh density and no changes of the above made interpretations could be justified. Moreover, also when considering results from full 3D models with lower mesh densities than ultimately applied, no tendency is observed that would indicate that a further refined mesh would lead to a largely increased stress and strain development. Thus, even though a slight deviation of the resulting local stresses and strains caused by a finer mesh cannot entirely precluded, the above presented observations and interpretations can be expected to remain unaffected.

All calculated local stresses and strains within the framework of this thesis are result of a load application directly to the bolt itself. As such, they aim to replicate the load situation during the experimental investigations. The strain development inside the thread of an M24 HV-bolt during tightening by rotation of the nut (necessarily using an FE model with continuous thread pitch) is investigated by *Lorenz & Stranghöner* (2016a) and (2016b). The reported local plastic strains are in an equal order of magnitude as found in the present investigation. This supports the assumption that, in its general characteristic, the obtained numerical results are also transferable to bolts subjected to rotational tightening. Still, to precisely quantify possible differences introduced by the added torque a specific comparative numerical study would be required, which is not in the focus of the thesis at hands.

#### Upscaling to larger bolt diameters

Even though, due to changes in the  $d/p$ -ratio, thread geometries are not strictly geometrically similar, an equivalent development of local loading conditions as described above for bolt size M36 can also be expected for larger HV-bolt geometries. This is verified in numerical calculations with linear elastic material behaviour. The comparison of the resulting maximum notch stress concentrations in the first load-bearing turn of the thread for large-size HV-bolts with different diameters is given in Figure 4-15. Corresponding results of path evaluations at the thread surface analogous to Figure 4-13 can be found in Appendix C.2. For all bolt diameters the results show a compliant behaviour, whereby the resulting  $K_t$ -values from the models with continuous thread pitch fall slightly below the values from the axisymmetric models. Thereby, a modest increase of stress concentration at larger bolts sizes is visible from both modelling approaches.

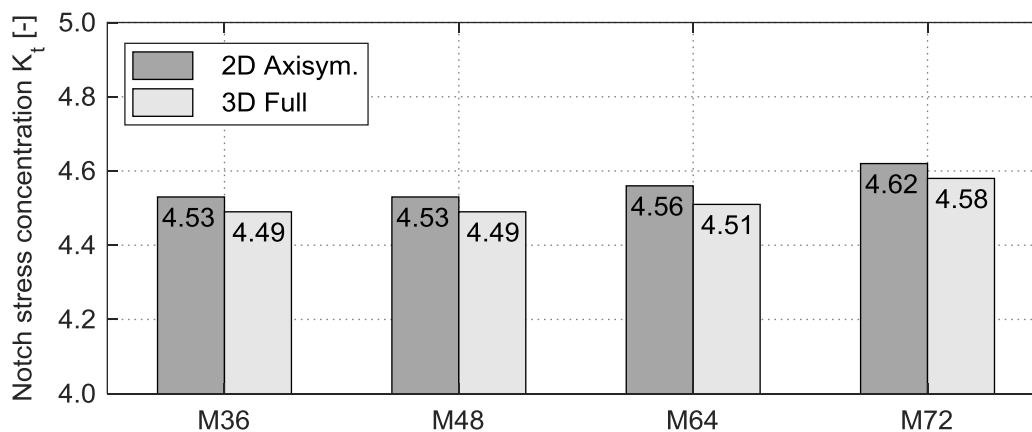


**Figure 4-15: Maximum linear elastic notch stress concentrations  $K_t$  in dependence of FE model type and bolt diameter**

In the process of upscaling the bolt dimensions in the FE models the initially used mesh configuration was maintained. Thus, while the number of elements inside the thread and around the circumference are identical, the absolute element sizes increase by a factor of about  $\sim 1.5$  to  $\sim 2$  between geometries M36 and M72. However, due to the initially chosen fine mesh configuration of the 2D axisymmetric

mode, its result accuracy remains unaffected. Furthermore, despite the previously discussed limitations of mesh density, there is no indication that the mesh scaling had a substantial effect on the quality of the obtained results from the full 3D model, either. It is therefore plausible to assume that the previously made observations for the M36 bolt geometry regarding the two different modelling approaches may also be transferred to larger bolt sizes. Correspondingly, under elastic-plastic conditions a slightly more critical local stress-strain development can be expected with an axisymmetric FE modelling approach for the entire considered diameter range.

### 4.3.3 Approximation of the local stress-strain response under cyclic loading

With the elastic-plastic nominal ( $S$ - $\varepsilon$ ) and local ( $\sigma$ - $\varepsilon$ ) stress to local strain relations from the numerical models, the cyclic local stress-strain responses at the most fatigue critical location inside the thread can be determined for a given nominal loading. As exemplified by the load histories of test results under high mean strains depicted in Figure 4-8, the mean stress as well as strain level deviates from cyclic loading without mean strain. The high preload and resulting mean stress and strain level of HV-bolts thus need to be appropriately considered when approximating the local cyclic stress-strain response.

Therefore, as illustrated in Figure 4-16 the local hysteresis under cyclic loading is synthesised from FE calculations with different material definitions. Following the procedure proposed by *Schneider* (2011) the pathway for initial loading is calculated considering monotonic material behaviour. The succeeding cyclic hysteresis after the first load reversal is determined using the cyclic stabilized stress-strain relation under consideration of the *Bauschinger* effect by use of the *Masing* model (Eq. 2-12), and it is then appended to the initial loading path. For additional consideration of possible cyclic relaxation under high mean strains the stress level of the hysteresis can be modified by the value  $\Delta\sigma_{\text{Relax}}$  in dependence of the calculated local strain amplitude according to results of the corresponding material tests (see Chapter 4.2.3).

In the technical execution of experimental fatigue investigations (see Chapter 3), the monotonic attainment of the mean load level is commonly followed by a cyclic ramp-up with increasing amplitudes until the target amplitude is reached. As in material tests transient cyclic effects especially occur during the initial load cycles, depending on the magnitude of the final target amplitude, the ramp-up already may cause cyclic softening at the notch root. At commonly high nominal mean load levels and comparatively low amplitudes this is of little significance to the resulting local loading conditions. Therefore, from technical perspective, it is a valid presupposition to suppose monotonic material conditions until reaching the upper nominal load level  $S_{\text{max}}$  for the first time, as made in the approach by *Schneider*. However, the effect can be of larger impact when assessing cyclic loading conditions at lower mean load levels, where the cyclically established amplitude forms a larger contribution to the maximum load level (as for instant present in the fatigue tests on HV-bolts M48 by *Marten*, 2009).

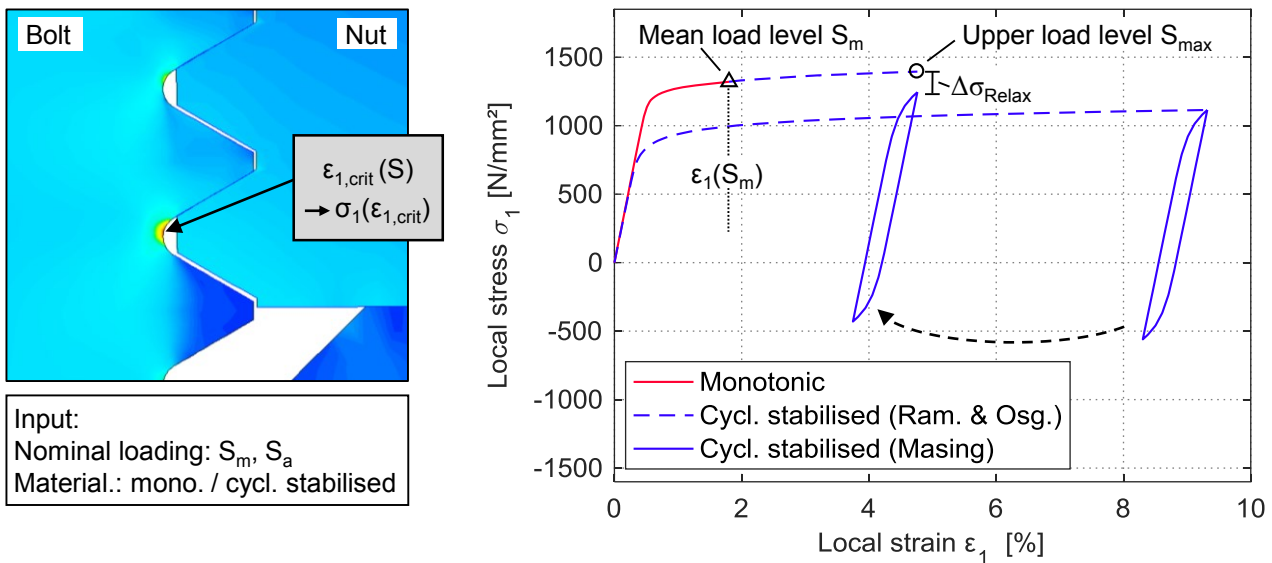


**Figure 4-16: Synthesis of local cyclic stress-strain response**

Thus, in the present investigation, to enable consideration of cyclic softening during the ramp-up phase, cyclic stabilized material behaviour according to the *Ramberg & Osgood* relation is utilized between nominal mean ( $S_m$ ) and upper load level ( $S_{max}$ ). In this way it is supposed that during the stepwise increase of amplitudes, in accordance with the established ‘material memory’ model described for example by *Haibach* (2006), after closing a hysteresis loop on the initial loading curve the stress-strain path follows the original cyclic stress-strain curve. Thereby, the cyclic increase of stresses and strains is evaluated at the basis of the strain level that is reached at the monotonic mean load  $\epsilon_1(S_m)$ .

In Figure 4-17 local hysteresis obtained with the combined approach as described above are compared at different nominal mean load levels to calculations with sole monotonic as well as sole cyclic stabilized material behaviour during initial loading. The depicted results are calculated with the axisymmetric 2D FE model for an M36 HV-bolt set of material 32CrB4 and cyclic relaxation is not considered. The unvarying nominal amplitude  $S_a$  is in a representative magnitude for the upper high cycle fatigue range.

At a regular mean load level  $S_m = 0.7 \cdot R_{p,0.2}$  (Plot A) the results from the combined approach show little deviation to a purely monotonic initial loading path, with only a slight increase of the maximum strain. This behaviour remains consistent up to a nominal mean load reduction to about half of the initial value (Plot B). When further reducing  $S_m$  the local stress at the upper nominal load  $S_{max}$  falls visibly below the calculation with sole monotonic initial loading path (Plot C). At distinctly low mean load levels, the initial loading curve from the combined approach increasingly approximates the curve with purely cyclic material behaviour (Plot D), as it is classically applied in the notch strain approach for loading conditions with low mean stress.

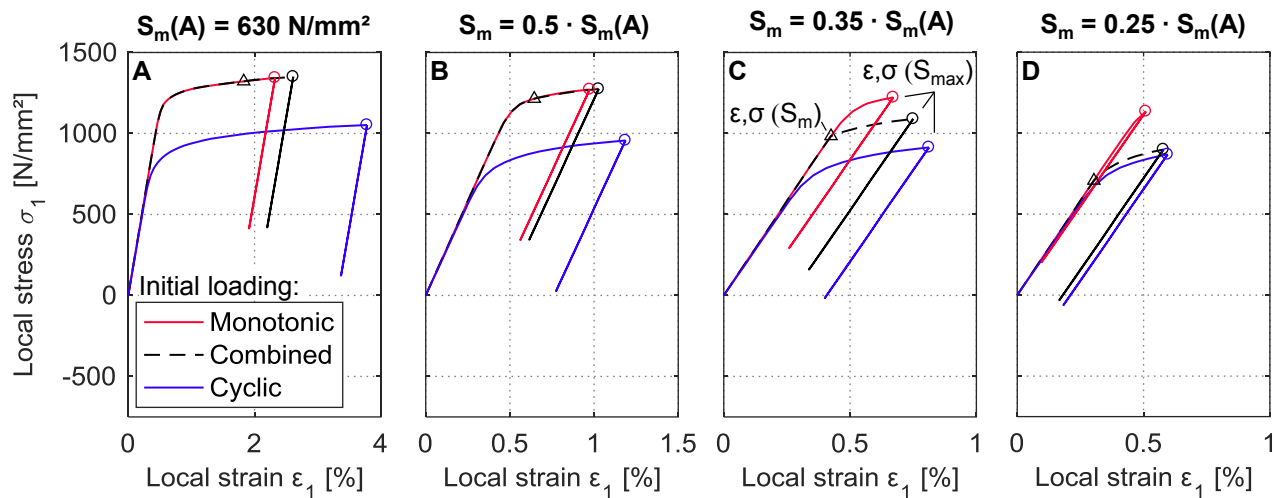


**Figure 4-17: Comparison of cyclic hysteresis with different material behaviour during initial loading at nominal stress amplitude  $S_a = 104 \text{ N/mm}^2$  and varying mean load levels (A:  $S_m = 630 \text{ N/mm}^2$ ; B:  $S_m = 0.5 \cdot S_m(A) = 315 \text{ N/mm}^2$ ; C:  $S_m = 0.35 \cdot S_m(A) = 220 \text{ N/mm}^2$ ; D:  $S_m = 0.25 \cdot S_m(A) = 157 \text{ N/mm}^2$ )**

With the described behaviour, the combined approach is eligible for analytical calculations with a monotonically achieved mean load levels of variable magnitude, as it automatically approaches the two variants with individual material behaviour and covers presumable effects of cyclic stabilization during successive build-up of cyclic amplitudes. Still, it is a strong simplification of the actual complex steadily occurring transient material effects. It may be argued that, due to the usually relatively small amplitudes during the ramp-up, little transient effects occur and hence may be overestimated by the combined approach. However, as demonstrated, the consideration of combined material behaviour during initial loading only causes a meaningful effect on the hysteresis at a combination of relatively low nominal mean load level and rather large target amplitude. Here, the purely monotonic and the combined initial loading path can be regarded as upper and lower bound of the realistically occurring load level. Thus, the combined approach is considered appropriate to investigate the potential impact of cyclic stabilization during the ramp-up at experiments at respective loading conditions.

The possibilities of direct consideration of transient material behaviour within advanced FEM material implementations is investigated by *Panic et al.* (2014). However, in order to avoid associated extensive numerical effort, they recommend the method presented by *Schneider*, and used here in slightly altered form, for a more practical application in analytical fatigue life assessment. Accordingly, with the presented methodology only two numerical calculation (i.e., with monotonic and with cyclic stabilized material behaviour) are required for one specific bolt geometry-material configuration to enable synthesising the cyclic stress-strain response for arbitrary nominal loading.

#### 4.3.4 Conclusions for application of numerical results in analytical fatigue calculations

From the performed investigations on the numerical assessment of local loading conditions the following conclusions can be drawn for application in the succeeding fatigue damage assessment:

- From comparative numerical calculations for an M36 HV-bolt set it is reliably ascertained that the application of a numerical model with continuous pitch of the thread does not lead to higher fatigue driving critical local stress or strain concentrations than calculated with an axisymmetric model. In fact, under elastic-plastic material conditions the results indicate a slightly benign plastic strain development, due to higher redistribution capabilities in the continuous thread. Performed numerical calculations with linear elastic material behaviour justify the conclusion that a similar tendency can be expected also for larger HV-bolt sizes up to diameter M72.
- From the found variations of local elastic-plastic strains between the two modelling approaches an effect on the analytically calculated fatigue strength can be expected. The actual impact of the modelling approach to the results of analytical fatigue calculations will be investigated for the example of a M36 HV-bolt geometry. The impact of the bolt diameter to the analytically calculated fatigue strength, indicated by a slight increase of linear elastic notch stress concentrations, will be further investigated using elastic-plastic axisymmetric models only.
- For the assessment of bending affected nominal stress states, a 3D axisymmetric volume element extension of a 2D plane element model provides an expedient, straightforward modelling solution which shows good agreement to its 2D counterpart under axial loading.
- The cyclic local elastic-plastic stress-strain response inside the thread is synthesized from numerical calculations with monotonic and cyclic stabilized material behaviour, as determined in the performed base material investigations. To enable consideration of possible cyclic softening effects during a cyclic ramp-up phase of fatigue experiments the initial loading path is calculated with a combination of both monotonic and cyclic material behaviour. This can be of particular significance when assessing nominal stress states with low mean load levels, as present in earlier experiments on large-size bolts published in the literature.

## 4.4 Fatigue damage assessment

### 4.4.1 Technical crack initiation

Based on the accomplishments of the previous two chapters 4.2 and 4.3, bearable load cycles of HV-bolts until technical crack initiation can be calculated with the strain-life approach. To this end, the corresponding base material's strain-life curve is evaluated with the aid of the approximated cyclic local stress-strain response. For transition of the strongly mean stress affected local loading conditions to a load level with  $R = -1$ , inherent to the strain-life curve, the following three damage parameters, described in Chapter 2.2.4, are utilized and compared:

- $P_{\text{SWT}}$  by Smith, Watson & Topper (*Smith et al.*, 1970)
- $P_{\text{M}}$  by *Narberhaus* (1999)
- $P_{\text{J}}$  by *Vormwald* (1989)

#### Damage parameter – fatigue life relations (P-life curves)

For fatigue life calculation, the strain-life curve is transformed to the respective damage parameter's P-life curve, which then can be evaluated with the P-value derived for the local cyclic stress-strain response at the thread. The stress-mechanical support effect at the notch root, caused by a decreasing stress gradient across the bolt diameter, is optionally considered by multiplication of the P-life curve with the notch sensitivity factor according to *Siebel & Stieler* (1955) and FKM-Guideline (2012). Thereby, as they are directly incorporated in the elastic-plastic FE calculations, beneficial effects from the stress relief under local plasticity are eliminated by division with the macroscopic notch sensitivity factor ( $n_p$ ) according to *Neuber* (1985), see Chapter 2.2.5. A statistical size effect is not considered at this stage.

A summary of the calculation of notch sensitivity factors according to Equations 2-22 to 2-25, for different bolt diameters and materials, can be found in Appendix E.1. For calculation of the macroscopic notch sensitivity factor an estimation of the base materials endurance limit is required. However, considering the data for the M36 bolt material 32CrB4, derived from constant amplitude tests, no meaningful deviations of the sensitivity factor arise at the relevant region of the strain-life curve at load cycles  $> 5 \cdot 10^5$ . Therefore, the value can safely be approximated. Possibilities for a more explicit estimation of the material's endurance limit are further investigated in Chapter 4.4.2.

Figure 4-18 shows the P-life curves of the three investigated damage parameters with and without consideration of the applicable notch sensitivity factor  $n_s = 1.15$  (derived from cyclic material data for the M36 bolt material 32CrB4 from constant amplitude tests). Additionally, the corresponding material test results (see section 4.2.2 and 4.2.3), transferred to their respective damage parameter values, as well as the original strain-life curve are plotted for verification.

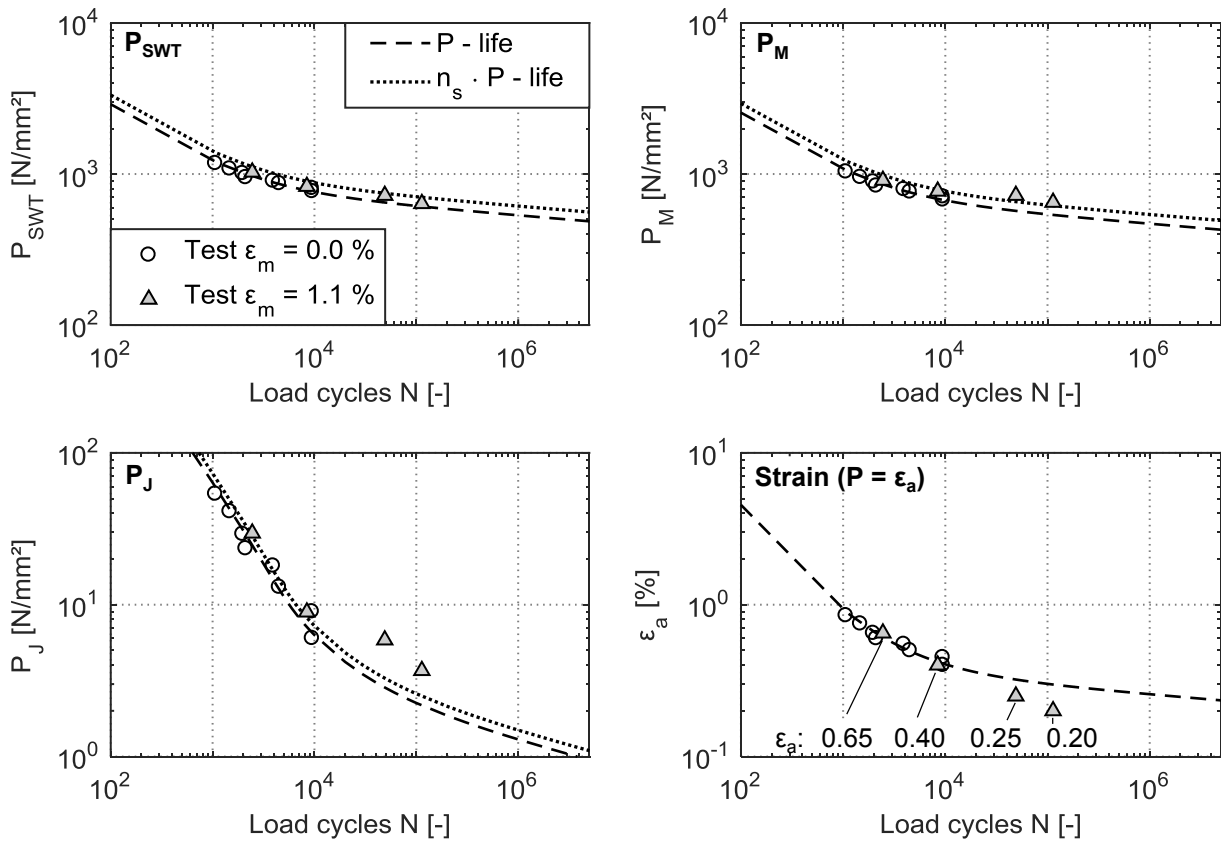


**Figure 4-18: Damage parameter fatigue life relations with and without notch sensitivity factor ( $n_s = 1.15$ ) for M36 bolt material 32CrB4 (constant amplitude tests) and comparison to damage parameter values of the corresponding material test results ( $n_s = 1.0$ ) with and without mean strain**

Damage parameter evaluation

The general development of the damage parameters' fatigue life prediction in dependence of the tensile mean stress level (i.e., their mean stress sensitivity) is illustrated in the *Haigh* diagram in Figure 4-19. The therein given mean stress dependent stress amplitudes are shown for the example of  $N = 1 \cdot 10^5$  endurable load cycles and are calculated in equivalence to the basic strain- and P-life curves ( $n_s = 1.0$ ), considering an unnotched geometry ( $K_t = 1$ ) and uniaxial loading conditions.

At the contemplated uniaxial and unnotched conditions, the  $P_{SWT}$ -parameter offers the most optimistic fatigue life prediction at the entire considered mean stress range. Still, it shows a distinguishably different behaviour to the  $P_J$ -parameter at higher mean stresses ( $R_\sigma > \sim 0.2$ ), where it exhibits a continuous reduction of the fatigue strength without threshold. In the description of the  $P_J$ -parameter, mean stress sensitivity is achieved by definition of a damage relevant segment of the hysteresis, based on theoretically opened micro crack conditions. This segment principally increases with the tensile mean stress. However, once the entire hysteresis is considered damage effective (i.e., wholly opened crack conditions are assumed) no further reduction of the fatigue strength occurs. Thus, the  $P_J$ -parameter reaches a horizontal progression at higher mean stresses and eventually the  $P_{SWT}$ -parameter falls below the  $P_J$  prediction.



At low and intermediate mean stress levels the empirical  $P_M$ -parameter shows a comparable behaviour to the  $P_J$ -parameter. At higher stress ratios, however, it predicts a strongly increasing mean stress dependent reduction of the fatigue strength. It is noted that, as the  $P_M$ -parameter formulation considers the specific notch sharpness of the structural component, with increasing  $K_t$  value ( $K_t > 1$ ) the fatigue life prediction does decrease less drastically at stress ratios  $R_\sigma > \sim 0.5$ , and it approaches a rather constantly declining progression. Still, it exhibits a notably stronger mean stress sensitivity than the other two parameters.

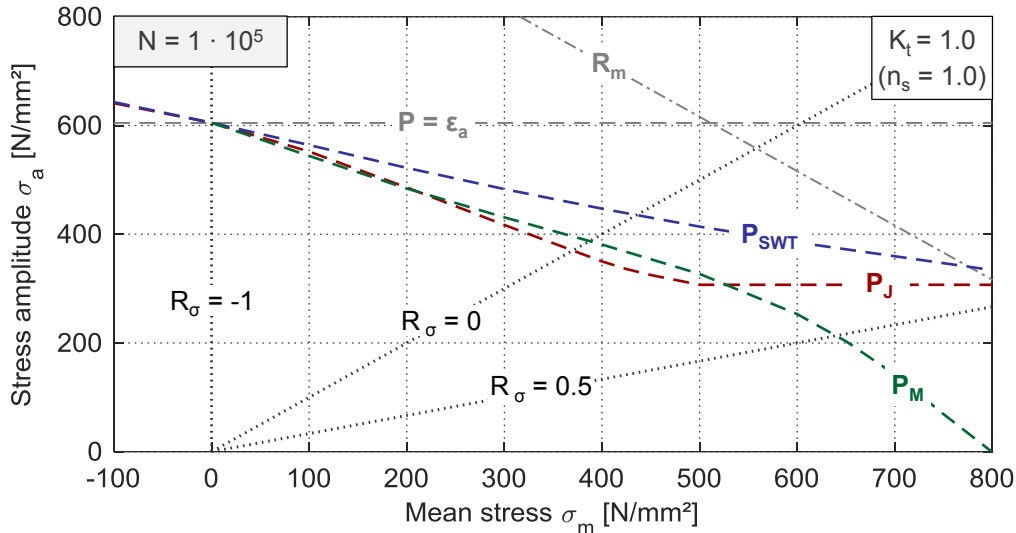


**Figure 4-19: Haigh-diagram for damage parameter development under tensile mean stress calculated for material 32CrB4 (constant amplitude tests)**

A first evaluation of the damage parameters' accuracy can be performed based on the comparison to enduring load cycles from the tests under high mean strain  $\epsilon_m = 1.1\%$ , performed by *Oechsner et al.* (2015) (see Chapter 4.2.3). As can be seen in Figure 4-18, at the lower two strain amplitudes ( $\epsilon_a = 0.2\% \rightarrow R_\sigma = 0.2$ ,  $\epsilon_a = 0.25\% \rightarrow R_\sigma = 0.01$ ) all P-parameters underestimate the actual bearable load cycles of the experiments (since the experimental values are derived from unnotched specimens the P-life curves without notch sensitivity multiplication need to be considered for the comparison). The strongest deviations result from calculations with the  $P_M$ -parameter. Comparing  $P_J$ - and  $P_{SWT}$ -parameter, the latter provided a better approximation of the experimental results, even though it is noted that the visual interpretation from the figure tends to exaggerate the actual difference due to differing slope and scaling of the two P-life curves. The found tendency complies with the P-parameter development shown in Figure 4-19. At the higher two strain amplitudes the resultant stress ratio  $R$  of the high mean strain experiments increasingly approximates a mean stress free stress state ( $\epsilon_a = 0.4\% \rightarrow R_\sigma = -0.66$ ,  $\epsilon_a = 0.65\% \rightarrow R_\sigma = -0.97$ ). Correspondingly, the calculated deviations fall into the general scatter of the material test results without mean strain and the test results are fairly well approximated also by the original strain-life curve. The precisely calculated deviations as well as a classification of the material test results in a Haigh-diagram representation is included in Appendix D.1.

Within the framework of his analytical fatigue investigation on smaller sized HV-bolts *Schneider* (2011) has made similar observations as described above, concerning the comparison of  $P_{\text{SWT}}$ - and  $P_{\text{J}}$ -life curves to high-strength bolt material test results under high mean strain. In this context he points out that, albeit generally possible, an adjustment of the  $P_{\text{J}}$  parameter's mean stress sensitivity is not expedient due to the limited number of available test results. This applies also for the present study. Moreover, local loading conditions as present at the lower two test amplitudes at  $\varepsilon_{\text{m}} = 1.1\%$  are approximately representative for the prevailing local loading conditions of the analysed preloaded bolts ( $S_{\text{m}} = 630 \text{ N/mm}^2$ ) only in the upper high cycle fatigue range, at nominal load levels  $S_{\text{a}} \approx 100\text{-}120 \text{ N/mm}^2$ . Here FE calculations lead to corresponding local stress ratios  $R_{\sigma}$  of about 0.35 to 0.20 and strain amplitudes between 0.2 and 0.25 %. At lower nominal stress levels, the calculated strain amplitudes decrease up to about  $\varepsilon_{\text{a}} \approx 0.1\%$  in the region of the experimentally determined endurance limit ( $S_{\text{a,D},50} \approx 45 \text{ N/mm}^2$ ) at distinctly larger local stress ratios  $R_{\sigma} \approx 0.7$ . Thus, the transferability of observations made from the damage parameter evaluation based on material test results at high mean strain to the succeeding analytical fatigue calculation of HV-bolts is limited to the respective load range. A collocation of the numerically calculated local loading conditions for relevant fatigue load levels of the M36 HV-bolts' S-N curve is included in Appendix D.2.

Using the presented P-life curves (material 32CrB4, cyclic material data from constant amplitude tests), analytical fatigue calculation results with the three investigated damage parameters are compared to experimental results for black (B) M36 HV-bolt sets (see Chapter 3.3) in Figure 4-20. If not indicated otherwise, in all following analytical fatigue calculations the local loading conditions at the bolt thread are determined under pure axial loads with a 2D axisymmetric FE model (see Chapter 4.3.1).

When disregarding the stress sensitivity factor and thus stress-mechanical support effect at the notch root ( $n_{\text{s}} = 1.0$ , Figure 4-20, left), both  $P_{\text{SWT}}$ - and  $P_{\text{J}}$ -parameter provide a very comparable approximation of the experimental results. Thereby, appearing contradictory to the previous damage parameter evaluation based on the material tests with high mean strain and the P-parameter development in the *Haigh*-diagram,  $P_{\text{J}}$  leads to slightly higher endurable load cycles than  $P_{\text{SWT}}$ . This is due to the fact that the consideration of the multiaxial stress state at the notch root and the evaluation of first principle stresses leads to a higher considered mean stress level than under uniaxial conditions. Given its distinct mean stress sensitivity at higher stress ratios (see Figure 4-19), this circumstance has a stronger effect on the  $P_{\text{SWT}}$ - than on the  $P_{\text{J}}$ -parameter calculation.

Only when considering the stress-mechanical support effect by use of the notch sensitivity factor ( $n_{\text{s}} = 1.15$ , Figure 4-20, right) the  $P_{\text{SWT}}$ -parameter leads to the expected overestimation of fatigue strength under high tensile mean stresses, as indicated in the literature (see also Chapter 2.2.4 and 2.2.7). Here, due to its different scaling ( $P_{\text{J}}$ -values are roughly two decimal steps lower than  $P_{\text{SWT}}$ ) and resultant lower impact by the notch sensitivity factor, the  $P_{\text{J}}$ -parameter provides a superior approximation of the experimental results. It needs to be taken into consideration that at this stage load cycles until technical crack initiation are compared to experimental load cycles until rupture. The

additional consideration of macroscopic crack propagation, which primarily affects the endurable load cycles in the upper high cycle fatigue range, is evaluated later on in Chapter 4.4.3.

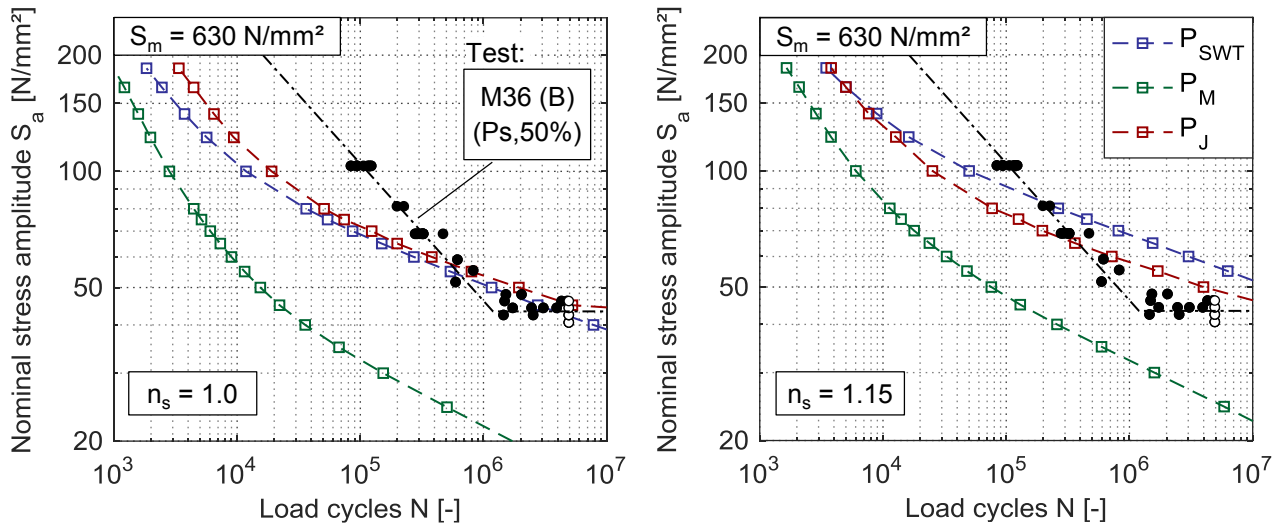


**Figure 4-20: Validation of analytical fatigue calculation results with different damage parameters for black (B) M36 HV-bolt sets (2D axisymmetric FE model) and material 32CrB4 with cyclic material data from constant amplitude tests with and without consideration of the notch sensitivity factor  $n_s$**

Analytical fatigue calculation results on large-size HV-bolts by *Marten* (2009) had indicated that at lower load levels the  $P_M$ -parameter can lead to a better approximation of the fatigue strength than  $P_{SWT}$ . This cannot be confirmed in the here applied calculation approach. Regardless of the notch sensitivity factor, the results obtained with the  $P_M$ -parameter fall notably below the experimental fatigue curve. As its development aimed for compensating underestimated mean stress effects by the  $P_{SWT}$ -parameter, it is characterized by a further increased mean stress sensitivity at high stress-ratios. As a consequence, the calculated endurable load cycles are more strongly affected by the augmented mean stress state resulting from considering principle stresses inside the thread. Moreover, the parameter is mainly substantiated on observations with less severe notch sharpness than present at the bolt thread ( $K_t \approx 4.5$ ) (see *Narberhaus*, 1999).

A less conservative estimation can be achieved when comparing the  $P_M$ -values, derived for the local loading condition of the bolt, to the original  $P_{SWT}$ -life curve, on which the empirical  $P_M$ -development is founded. This however would not be methodically consistent with the other damage parameters, as it violates the condition that the  $P$ -life can be deduced from its  $P$ -values for loading conditions with  $R=-1$ , and it implies that under mean stress free conditions the damage parameter predicts a higher fatigue strength than the original strain-life curve (see *Haigh*-diagram in Appendix E.2).

For the further investigations only the  $P_J$ - and  $P_{SWT}$ -parameter are considered.

Impact of cyclic relaxation

As described in Chapter 4.3.3, the effect of cyclic relaxation under high mean strains can be included into the analytical fatigue calculation by shifting the cyclic hysteresis downwards based on corresponding material test results. The results of analytical fatigue calculations with and without cyclic relaxation are compared in Figure 4-21. Using the linear relation, derived from the regression of the material test data for the considered bolt material 32CrB4 (Figure 4-9), relaxation is assumed to occur at strain amplitudes  $\epsilon_a \geq 0.1\%$ . Therefore, considering the  $P_{SWT}$ -parameter, the decreased mean load level causes an increase of calculated endurable load cycles, beginning at nominal stress amplitudes closely above the experimental endurance limit.

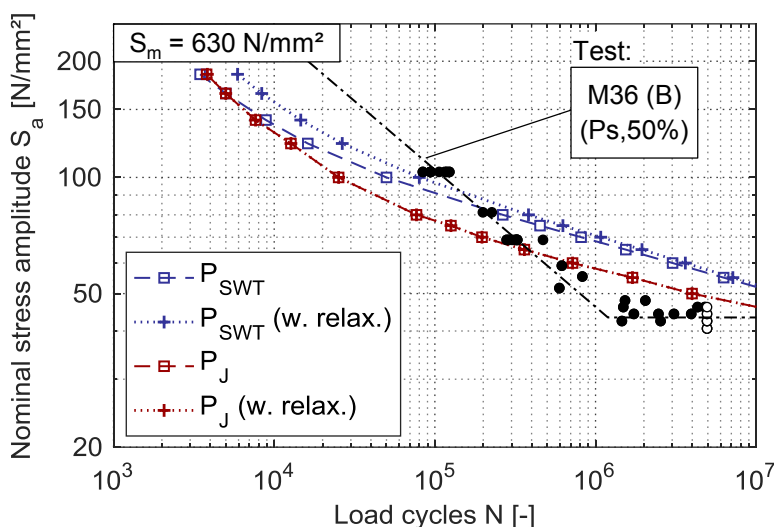


**Figure 4-21: Comparison of analytical fatigue calculations with and without consideration of cyclic relaxation (M36 HV-bolt sets, material 32CrB4, cyclic material data from constant amplitude tests, notch sensitivity factor  $n_s = 1.15$ )**

Considering the  $P_J$ -parameter, under the present high nominal mean stress at the majority of nominal load levels the calculated stress for theoretical crack closing is notably smaller than the minimum stress of the cyclic hysteresis. Consequently, the entire hysteresis is considered damage relevant, also when it is shifted downwards by the respective amount of cyclic relaxation. Hence, contrary to the  $P_{SWT}$  parameter, for the largest part of relevant load levels the calculation results with the  $P_J$ -parameter remain unaffected by the consideration of cyclic relaxation. Only at very high nominal stress amplitudes an effect can be noted. Given the relatively modest deviation present also at the  $P_{SWT}$ -parameter results, the impact of cyclic relaxation to the analytical fatigue calculation can be considered a minorly decisive factor for the considered material.

Results of analogous tests under high mean strain on a high-strength material 41Cr4 by *Schneider* (2011) have yielded slightly lower cyclic relaxation values than determined and applied above for the investigated M36 bolt material. As such, the two test series indicate that it is acceptable to neglect the effect of cyclic relaxation in analytical fatigue calculations of high-strength bolts.

Impact of test procedure for cyclic material data

Thus far, all presented analytical fatigue calculations have been performed using the cyclic material data determined with the more comprehensive method, based on constant amplitude tests. Figure 4-22 shows a comparison to calculation results with material data for the same material derived from Incremental-Step-Tests (IST). Generally, with both methods an acceptable approximation of the experimental fatigue results is achieved. Nevertheless, while at the upper high cycle fatigue range the calculation results are rather comparable, a growing deviation occurs with decreasing load level. The present deviations mainly result from the diverging progression of the strain-life curve at lower strain amplitudes (see Figure 4-7, left). Arguably, the calculation with the steeper strain-life curve progression resulting from the simplified IST based procedure leads to an even improved approximation of the experimental results. Still, the actual quality of the result approximation is yet to be evaluated in detail in the framework of load cycle calculation until rupture (Chapter 4.4.3) and evaluation of the analytical endurance limit estimation (Chapter 4.4.2). Moreover, it is noted again that the strain-life curves from both testing procedures are not conclusively justified by material tests with low strain amplitudes.

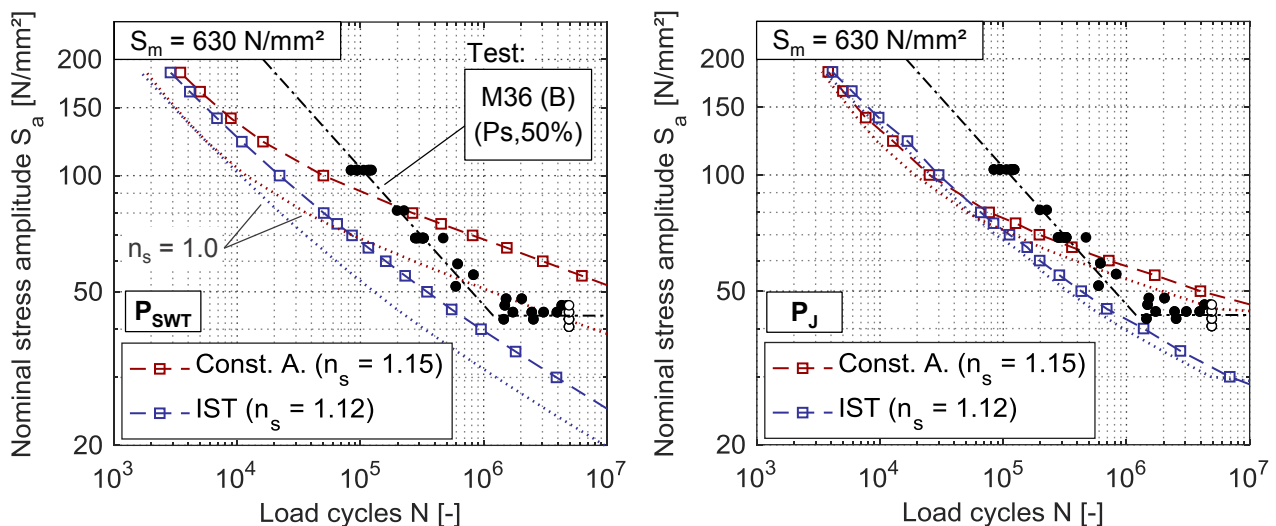


**Figure 4-22: Comparison of analytical fatigue calculation results with cyclic material data from constant amplitude test and Incremental-Step-Test (IST) (M36 HV-bolt sets, material 32CrB4)**

Concerning the cyclic stress-strain curves, at the majority of relevant nominal load levels the numerically calculated local stress-strain response inside the thread is in an order of magnitude without significant deviation between the two testing procedures (see Figure 4-7, right). However, an earlier impact of plastic strains in the cyclic stress-strain curve from IST, and hence a larger plastic strain contribution in the region of an assumed endurance limit of the material under mean stress free condition, causes an indirect effect on the calculation, as it leads to a slight reduction of the notch sensitivity factor (see Appendix E.1). This is considered in the depicted calculation results. As reference, also calculations with  $n_s = 1.0$  are plotted. While the variation of the notch sensitivity factor has a marginal impact on the calculation with the  $P_J$ -parameter, it has a noteworthy, albeit not overly

critical, effect on the result with the  $P_{SWT}$ -parameter. This highlights the already indicated sensitivity of the  $P_{SWT}$ -parameter to the notch sensitivity factor.

Impact of the FE modelling approach

It has been shown in Chapter 4.3 that the application of an FE model that considers the realistic continuous pitch of the thread leads to a slightly beneficial local plastic strain development, compared to an axisymmetric model. To evaluate the resultant impact in the analytical fatigue assessment method, firstly Figure 4-23 shows cyclic hysteresis for two relevant load levels of the S-N curve, one in the upper high cycle fatigue range ( $S_a = 100 \text{ N/mm}^2$ ) and the other close to the experimental endurance limit ( $S_a = 50 \text{ N/mm}^2$ ).

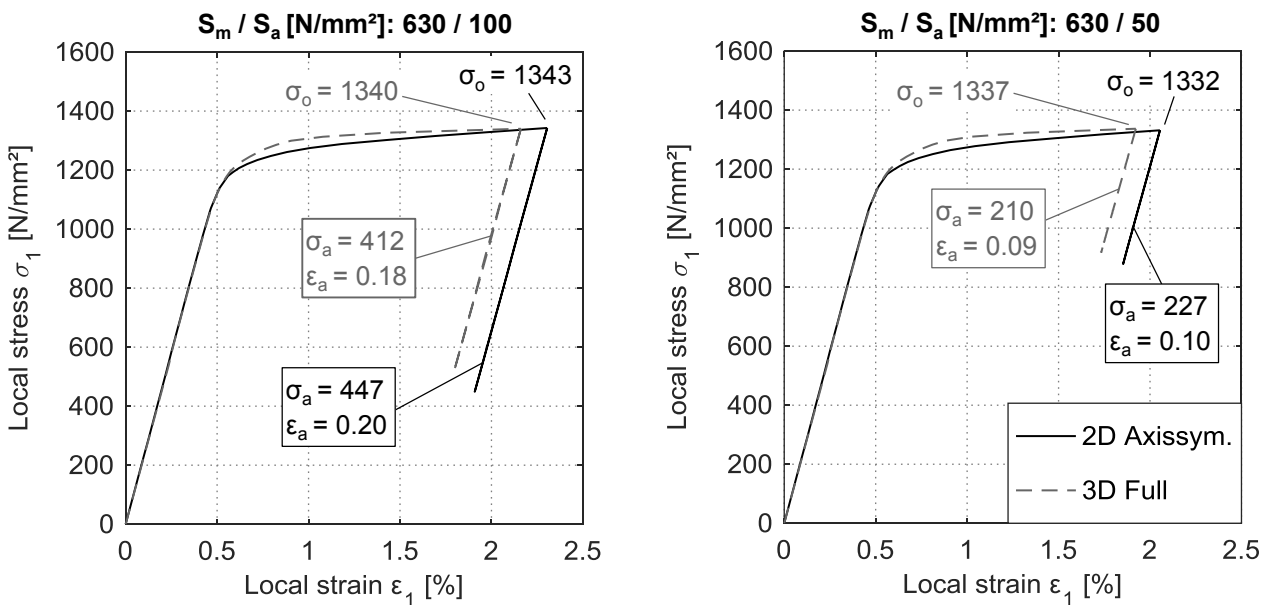


**Figure 4-23: Divergence of local cyclic hysteresis calculated with 2D axisymmetric and full 3D FE model with continuous thread pitch (M36 HV-bolt set, material 32CrB4)**

In consistency with the stress- and strain path evaluations in Figure 4-14, at the relevant high nominal mean stress ( $S_m = 630 \text{ N/mm}^2$ ) the maximum upper local stress  $\sigma_o$  is mostly unaffected by the modelling approach. However, calculations with the full 3D model lead to slightly lower strain- and resultant stress amplitudes. As illustrated by the corresponding analytical fatigue calculation results in Figure 4-24 (the close-up on the right hand side of the figure illustrates the deviations between the modelling approaches in a higher resolution), these cause a small increase of endurable load cycles, compared to the calculation with the 2D axisymmetric model. The slightly lower strain level, present in the hysteresis comparison, does not cause an effect in both damage parameter definitions.

Additionally shown in Figure 4-24 are calculation results with the 3D model with axisymmetric thread geometry, which was primarily constituted for the later investigation of bending affected stress states. Still, under the here considered purely axial nominal loading the result depiction highlights the fact that also after thorough mesh adjustment it does not exactly match the results from its 2D counterpart, using rotational symmetric boundary conditions. It can thus be presumed that the detected

result deviation, observed when using the FE model with continuous thread pitch, is caused by a combination of numerical (e.g., mesh, element and contact definitions) and geometrical reasons (i.e., enhanced capabilities of local stress and strain redistributions).

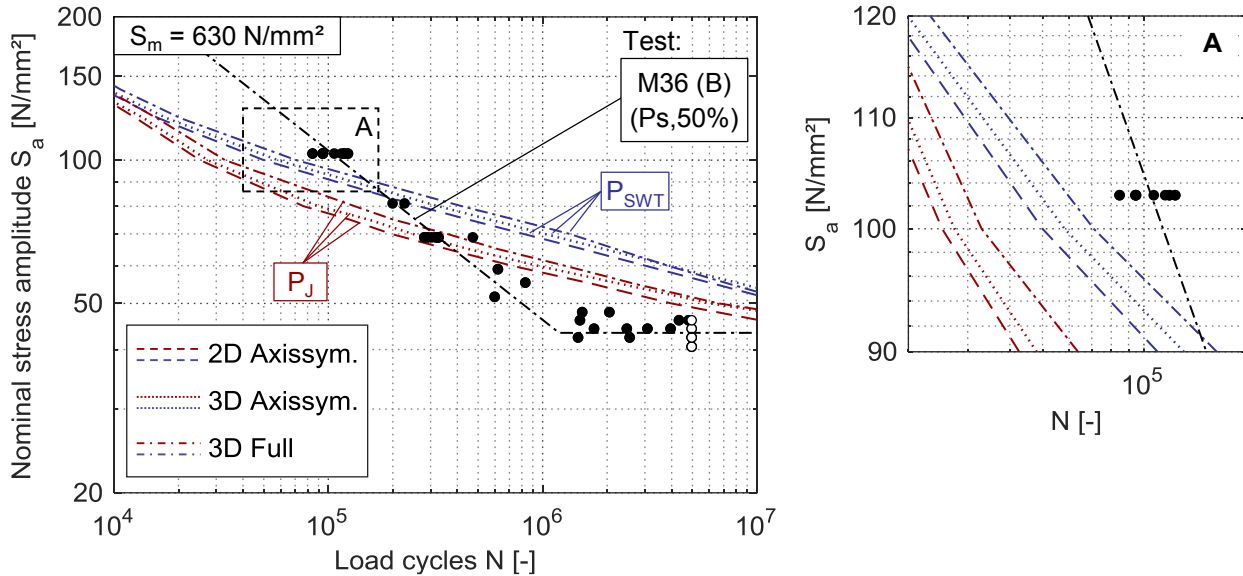


**Figure 4-24: Comparison of analytical fatigue calculations with different FE modelling approaches (M36 HV-bolt sets, material 32CrB4, cyclic material data from constant amplitude tests,  $n_s = 1.15$ )**

Considering both  $P_J$ - and  $P_{SWT}$ -parameter, the divergence obtained with the full 3D compared to the 2D axisymmetric model's results are of marginal nature and slightly less conservative. Moreover, additionally to the vastly higher modelling effort, the constitution of a numerically stable and reliable FE model with continuous thread pitch displayed a considerably higher sensitivity to numerical uncertainties. Hence, as the application of a full 3D model does not provide a significant benefit to the analytical fatigue assessment procedure, an axisymmetric modelling approach is to be preferred.

#### 4.4.2 Approximation of endurance limit

From a technical, macroscopic point of view, the occurrence of an endurance limit can be attributed to the circumstance whether or not a technical crack is initiated. Contrary to the fatigue strength in the upper high cycle fatigue range, its analytical evaluation is thus enabled with the sole application of the strain-life concept. To this end, information about the base materials' strain-related endurance limit under mean stress free conditions (henceforth denoted as strain endurance limit) is required. Within the base materials investigation in Chapter 4.2, with neither of the applied assessment procedures for determination of cyclic material properties such information was established. Still, by reasonably estimating the base materials endurance limit, the potential of predicting the bolt's endurance limit with the applied analytical approach can be assessed. This is done in the given section for the M36 HV-bolts and its base material 32CrB4.

Estimation of the base material's endurance limit

In the first place, background for the estimation can be sought in the literature from published material investigations of relevant materials, where an endurance limit was experimentally determined. This is usually done by stress- instead of strain-controlled material tests with  $R = -1$ , assuming dominantly elastic material conditions. With the determined stress endurance limit  $\sigma_{a,D}$  the associated strain amplitude  $\epsilon_{a,D}$  can then be calculated from the corresponding cyclic stress-strain relation. The knee point  $N_D$  (i.e., the load cycle number where the strain endurance limit is reached) is obtained from the material's strain-life curve. Additionally, an orientation can be obtained by referring to the FKM-Guideline (2012), which for un-notched structural steel components at axial stress with  $R = -1$  allows the calculation of the stress endurance limit in dependence of the material's tensile strength as  $0.45 \cdot R_m$ . With available cyclic material data, this can then be transferred to the strain endurance limit and associated knee point, as described above.

Within the available references in the literature for high-strength materials suitable for HV-bolts, only a limited number of studies include an adequate experimentally substantiated approximation of the endurance limit. Table 4-4 provides the obtained estimation background for strength class 10.9 and 8.8 materials with strain endurance limits and associated load cycle numbers. Additionally, the corresponding strain endurance limits calculated at the basis of the stress estimation according to the FKM-Guideline are given. The underlying cyclic material parameters are included in Appendix E.5.

**Table 4-4: Estimation of 32CrB4 material's endurance limit based on references given in the literature**

Material: (Source)	36CrB4 (1)	41Cr4 (1)	42CrMo4 (2)	41Cr4 (2)	30CrNiMo8 (2)	30CrNiMo8 (2)	<b>32CrB4</b>
Strength class	10.9			8.8			10.9
$R_m$ [N/mm <sup>2</sup> ]	1124	1121	1111	904	910	910	1116
<u>Endurance limit from material tests:</u>							<b>Estimate:</b>
$\epsilon_{a,D}$ [%]	0.242	0.259	0.272	0.197	0.231	0.218	<b>~0.22 – 0.27</b>
$N_D$ [-]	$1.4 \cdot 10^6$	$2.9 \cdot 10^6$	$1.4 \cdot 10^5$	$3.8 \cdot 10^5$	$2.0 \cdot 10^5$	$2.9 \cdot 10^6$	$\sim 2 \cdot 10^7 - 5 \cdot 10^5$
<u>Endurance limit calculated based on FKM-Guideline (2012)</u>							
$\sigma_{a,D}$ [N/mm <sup>2</sup> ]	506	504	500	407	410	410	502
$\epsilon_{a,D}$ [%]	0.248	0.246	0.242	0.233	0.203	0.201	0.242
$N_D$ [-]	$9.4 \cdot 10^5$	$9.7 \cdot 10^6$	$3.3 \cdot 10^5$	$1.2 \cdot 10^5$	$6.4 \cdot 10^5$	$3.4 \cdot 10^7$	$2.8 \cdot 10^6$
<sup>1</sup> Schneider (2011)							
<sup>2</sup> taken from materials database Boller et al. (2008), original source given in E.5							



In the juxtaposition of experimental results, the materials of strength class 10.9 tendentially exhibit a higher endurance limit than the 8.8 strength class materials. This is in general accordance with the tensile strength dependency suggested in the FKM-guideline. The calculation according to the FKM-Guideline provides an adequate approximation of the experimentally attested strain endurance limits. Still, the calculated values, even though assumed in the guideline for a survival probability of  $P_s,97.5\%$ , in some cases overestimate the experimental strain amplitude ( $P_s,50\%$ ) of the here considered high-strength materials. Considering this, a range between  $\varepsilon_a \approx 0.22 - 0.27 \%$  is contemplated a plausible estimation for the strain endurance limit of the M36 HV-bolts' 10.9 base material 32CrB4.

The evaluation of the 32CrB4 material's strain-life curve, derived from constant amplitude tests, yields associated load cycles  $N_D$  at the knee point between  $N_D \approx 2 \cdot 10^7 - 5 \cdot 10^5$ . Arguably, the higher end of this load cycle range exceeds the plausible location of the knee point, when compared to the test results of M36 HV-bolts. However, it is pointed out that in the associated load cycle range the strain-life curve follows a rather shallow progression. This causes strong changes of load cycle numbers at only slight deviations of the strain amplitude. Moreover, the exact progression of the strain-life curve at this load cycle range is uncertain because it lacks experimental justification and is extrapolated from the results at higher strain levels (see Chapter 4.2.2). The location of the knee point thus needs to be valued as a rather rough indicator for the endurance limit.

#### Application of the estimated endurance limit in the damage parameter concept

In analogy to the constitution of the damage parameter-life curves, from the strain endurance limit  $\varepsilon_{a,d}$  at  $R = -1$  corresponding endurance limit damage parameter values  $P_{J,D}$  and  $P_{SWT,D}$  can be determined. Similar to the P-life curves, for consideration of the stress-mechanical support effect, these are multiplied by the notch sensitivity factor  $n_s$ . Based on the numerically determined local cyclic stress-strain response, the nominal loading conditions ( $S_m$  and  $S_a$ ), at which the damage parameter endurance limit is reached, are determined iteratively; the obtained nominal stress amplitude designates the analytically calculated endurance limit of the bolts  $S_{a,D}$ .

The results of endurance limit calculations for the M36 HV-bolt sets, considering strain endurance limits  $\varepsilon_{a,D}$  in the previously estimated range (A: 0.27 %; B: 0.24 %; C: 0.22 %), are presented in Figure 4-25 for a nominal mean stress level  $S_m = 630 \text{ N/mm}^2$ . For the underlying strain-life curve for base material 32CrB4 cyclic material data from constant amplitude tests are used. The corresponding notch sensitivity factor  $n_s = 1.15$  is considered. Additionally, calculation results without notch sensitivity factor ( $n_s = 1.0$ ) are plotted as dashed lines.

Congruent to the earlier discussed damage parameter behaviour, under consideration of the notch sensitivity factor the  $P_{SWT}$ -parameter yields a visibly more optimistic prediction of the endurance limit than  $P_J$ . Still, also with the latter, at the highest considered material endurance limit (curve branch A) the experimentally determined endurance limit of the bolts is considerably overestimated. A better approximation is achieved from closely below mid to the lower range of the estimated strain endurance limits (branches B and C), where the analytical results coincide with the scatter band of the

experiments. Using the  $P_{SWT}$ -parameter, this is only the case starting from beneath branch C, associated to the nethermost strain amplitude of the estimation range. For both damage parameters the approximation quality improves in calculations with  $n_s = 1.0$ .

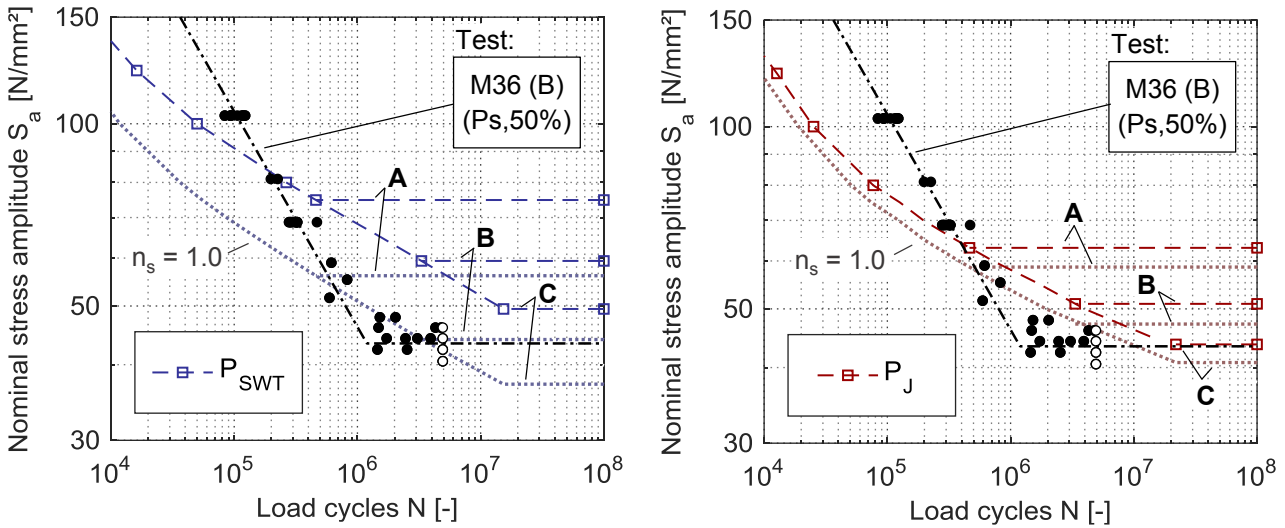


**Figure 4-25: Analytical endurance limit calculations for M36 HV-bolt sets based on estimated strain endurance limits for material 32CrB4 (A:  $\epsilon_{a,D} = 0.27\%$ , B:  $\epsilon_{a,D} = 0.24\%$ , C:  $\epsilon_{a,D} = 0.22\%$ ) and cyclic material data from constant amplitude tests (notch sensitivity factor  $n_s = 1.15$ )**

The corresponding results for the calculations considering the notch sensitivity factor are given in Table 4-5 as well as the comparison to results calculated analogously with cyclic material data from IST. A graphical representation of the latter as well as the tabulated results from the calculations without notch sensitivity factor are included in Appendix E.3.

**Table 4-5: Results of analytical endurance limit calculations for M36 HV-bolts with cyclic material data for material 32CrB4 from constant amplitude tests ( $n_s = 1.15$ ) and Incremental-Step-Tests ( $n_s = 1.12$ )**

	Material data from constant amplitude tests			Material data from Incremental-Step-Tests (IST)			Test result M36 (B) (Ps,50%)	
	(A)	(B)	(C)	(A)	(B)	(C)		
Estimated base material endurance limit $\epsilon_{a,D}$ [%]	0.27	0.24	0.22	0.27	0.24	0.22		
$S_{a,D}$ [N/mm²]	$P_{SWT}$	74.82	59.35	49.44	67.9	55.68	47.66	<b>43.36</b>
	$P_J$	63.07	50.97	43.68	71.96	58.39	50	
$N_D$ [-]	$4.6 \cdot 10^5$	$3.3 \cdot 10^6$	$2 \cdot 10^7$	$9.7 \cdot 10^4$	$2.2 \cdot 10^5$	$4.3 \cdot 10^5$	<b><math>1.2 \cdot 10^6</math></b>	

When considering the cyclic material data from IST instead of constant amplitude tests, the  $P_J$ -parameter yields noticeably higher calculation results. This is caused by the already remarked higher plastic strain contribution in the cyclic stress-strain curve at the relevant range of strain amplitudes

(see Figure 4-7). As a consequence, for a given strain endurance limit  $\epsilon_{a,D}$ , a higher damage parameter endurance limit  $P_{J,D}$  is determined (i.e., the hysteresis resulting at the given strain amplitude is associated by the parameter with a high damage effect, bearable at the endurance limit). Correspondingly, a higher endurance limit is calculated for the bolt. The impact of the lower notch sensitivity factor, equally caused by the difference in the cyclic stress-strain relation, does not compensate for this effect. On the contrary, the  $P_{SWT}$ -parameter itself is not substantially affected by the changes of the cyclic stress-strain curve. Here differences of results between the two material evaluation procedures (in terms of a reduction of the calculated endurance limits) mainly arise indirectly from the reduced notch sensitivity factor. Correspondingly, when neglecting the notch sensitivity factor, the calculation results scarcely deviate (see Appendix E.3).

Besides the discrepancies in the calculated endurance limits, due to its distinguishably steeper progression at lower strain amplitudes, the application of the strain-life curve from IST leads to sizeably reduced load cycles at the knee point  $N_D$ .

### Result discussion

As the actual strain endurance limit of the base material is unknown, no conclusive verification of the damage parameter adequacy and prediction quality is feasible. Still, from the observations made based on the estimated endurance limit range, a number of conclusions can be drawn. These are discussed in the following.

Assuming that the predicted range of the strain endurance limit is sufficiently accurate, a better approximation of the experimental results is achieved with the  $P_J$ - than with the  $P_{SWT}$ -parameter. This is dominantly caused by the already recognized high susceptibility of the latter to the notch sensitivity factor. The circumstance that the  $P_{SWT}$ -parameter yields a higher endurance limit estimation as  $P_J$  (when considering the notch sensitivity factor and cyclic material data from constant amplitude tests) is congruent with investigations from *Schneider* (2011) for smaller HV-bolts M10 and M16; even though the therein assessed discrepancy between the two parameters is not as pronounced as in the present calculations. Still, as can be observed in Figure 4-25, in calculations with  $n_s = 1.0$  the  $P_{SWT}$ -parameter provides a noticeably improved prediction of the experimental endurance limit. Likewise, also with the  $P_J$ -parameter a better approximation is visible when neglecting the notch sensitivity factor. This provides reason to presume that the common approach by *Siebel & Stieler* (1955) may overestimate the actual stress-mechanical supporting effect for the investigated large diameters and bolt dimensions. This needs to be taken into consideration in the further analytical evaluations in the course of this thesis.

Concerning the application of cyclic material data from IST, it is noted again that, in principle, the IST based determination procedure is not eligible for the determination of the base materials' endurance limits. The here performed calculations show that also in combination with an estimated or, potentially, an additionally determined endurance limit (e.g., by supplemental stress controlled material tests), its application is disputable. For both investigated damage parameters a higher plastic strain contribution in the cyclic stress-strain relation causes an effect on the calculated endurance limits of the bolts, either indirectly by the notch sensitivity factor or directly in the damage parameter

calculation. Since an earlier development of cyclic plastic strains is a recognized (albeit not compulsory) phenomenon for metals analysed in IST (see *Wagner, 2007*), the effect of the IST based cyclic stress-strain curve needs to be seen problematic for two reasons. Firstly, the presence of noteworthy plastic strains at the endurance limit contradicts the basic assumption justifying the commonly applied determination of the strain endurance limit based on stress-controlled tests. Secondly, the general concept of an endurance limit is based on the presupposition of constant amplitude loading. The consideration of material behaviour, which is distinctly characteristic for loading with variable amplitudes, is therefore limitedly qualified for the present aim of approximating the bolts endurance limit.

Contrary to the deviations between the cyclic stress-strain relations, the different progression of the strain-life curves, derived from IST and constant amplitude tests, does not affect the endurance limit prediction but only the associated load cycle number at the knee point. As the progression does, however, affect the prediction accuracy of the fatigue curve in the above transition region to the endurance limit, the location of the predicted knee points shall be briefly discussed. As mentioned earlier in this chapter, due to its shallow progression, relatively large load cycles at the knee point are derived from the material curve from constant amplitude tests in the estimated range of plausible strain endurance limits. Given its lack of experimental justification in the respective load cycle range, it may be argued that the fatigue life in the relevant region between approximately  $10^5$  and  $10^7$  load cycles is presumably overestimated to a certain degree. Contrary, considering the progression of the strain-life curve derived from IST, the calculated knee points (which are unaffected by the aforementioned limitations related to the cyclic stress-strain curve) appear rather low in comparison to the experimental results for the tested bolts (see Table 4-5). This indicates a rather conservative estimation. It needs to be concluded that presumably both of the here applied strain-life curves and thus the resultant analytical bolt-fatigue curves do not display entirely accurate the actual fatigue behaviour of the base material in the transition region to the endurance limit.

#### 4.4.3 Macroscopic crack propagation

##### Crack propagation models

Up to this stage, only load cycles until technical crack initiation have been evaluated. The additional calculation of load cycles during the macroscopic crack propagation phase enables the determination of the complete analytical S-N curves until rupture. To this end, linear elastic fracture mechanics shall be applied. Thereby, the cyclic stress intensity  $\Delta K$  at the tip of the assumed propagating crack is evaluated with *Paris' law* (Eq. 2-7).

Due to the absence of a distinct calculation model for bolted connections, an approximative model representation is required for determination of the stress intensity at the crack tip. Within the catalogue of available models, given in FKM-Guideline (2006), a round bar model provides the closest similarity to the bolt geometry (i.e., disregarding the formed thread). As suggested - and verified - by *Pyttel et al. (2008)*, an equivalent geometric representation may also be achieved using a hollow cylinder model with an inner tube radius set to  $r_i \approx 0$  (e.g.,  $r_i = 0.1$ ). The latter model provides the

additional possibility of considering a variant stress development in radial direction. Correspondingly, two eligible modelling solutions for bolted connections, as introduced by *Pyttel et al. (2008)*, are illustrated in Figure 4-26, left. Their application for the here presented investigation is subsequently described (it is noted that the here applied model numbering is vice versa to the original nomenclature in the underlying publication).

**Model 1** uses the hollow cylinder model under variable stresses with circumferential (external) surface crack according to FKM-Guideline (2006) with the nominal bolt diameter  $d = 2 \cdot r_0$ . The incorporated crack depth  $a^*$  is defined as sum of the thread depth  $h_3$  and the depth of the evolving physical crack  $a$ . Loading is applied by means of the linear elastic 1<sup>st</sup> principle stress development in radial direction  $\sigma(x)$  at the decisive maximal loaded first load-bearing turn of the thread. Thereby, only the considered physical crack is subjected to stresses, and the crack section representing the thread depth remains unloaded. The required stress gradient distribution at the fatigue decisive location (expressed by the stress concentration  $K_t = \sigma / S_{(Asp)}$ ) is derived from a linear elastic FE calculation of the investigated HV-bolt set (Figure 4-26, right).

**Model 2** uses the round bar model under constant tension with circumferential surface crack according to FKM-Guideline (2006). Similar to Model 1, the bar dimensions correspond to the nominal bolt diameter  $d = 2 \cdot r_0$ , and the incorporated crack depth  $a^* = h_3 + a$  includes the thread depth  $h_3$  as theoretical extension of the actual physical crack. However, a uniform stress development is defined conservatively over the entire incorporated crack  $a^*$  with a magnitude  $\sigma = F / \pi r_0^2$  (i.e., the nominal stress at the bolt shaft). The corresponding stress level (M2) is illustrated in Figure 4-26, right.

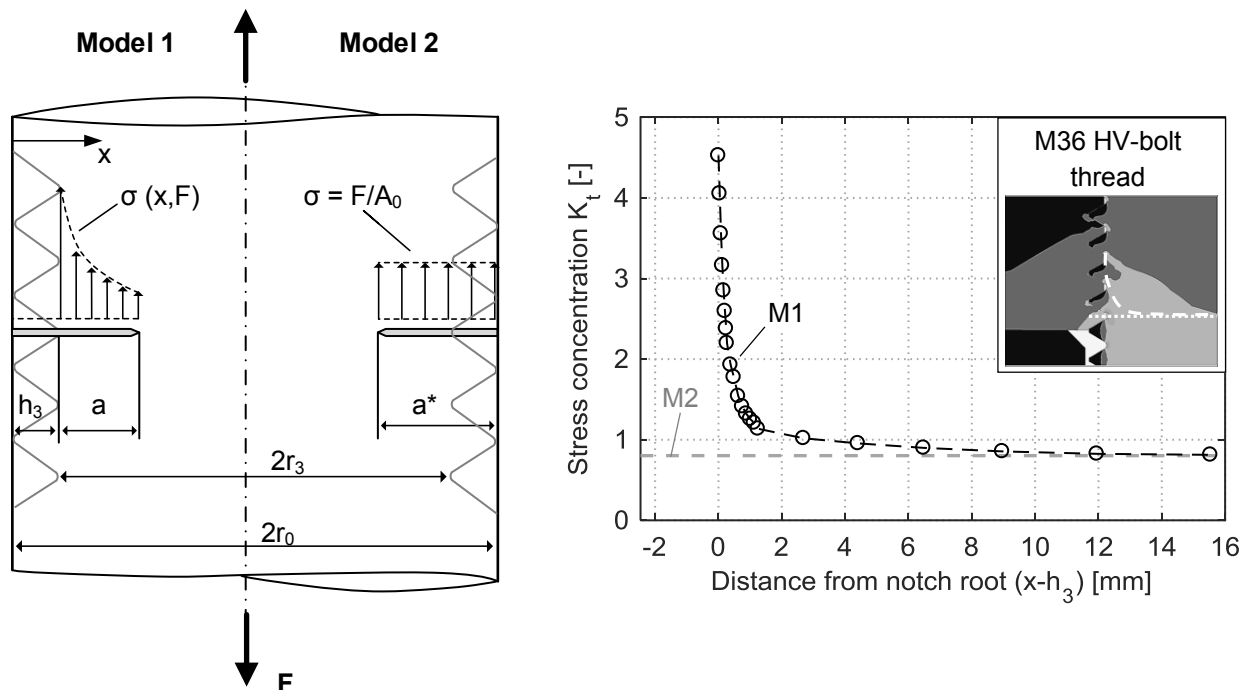


**Figure 4-26: Schematic depiction of applicable crack tip stress intensity models for threaded fasteners acc. to *Pyttel et al. (2008)* (left) and stress development at the maximal loaded turn of an M36 HV-bolt thread derived from linear elastic FE calculation (right)**

In the investigation by *Pyttel et al.* (2008) under static conditions, the consideration of the actual stress gradient at the notch in Model 1 has led to a slightly improved approximation of a numerically determined stress intensity factor  $K$  compared to Model 2. Thereby, with increasing crack depth, Model 1 has led to higher stress intensities than Model 2. The impact of the modelling approach in the calculation of the cyclic crack propagation is evaluated in the sequel.

#### Calculation of load cycles until rupture

To calculate the load cycles until rupture, a numerical integration of *Paris'* law needs to be performed, see Chapter 2.2.1. For definition of the required integration boundaries, in accordance with common conventions as well as other fracture mechanical calculations on bolts by *Kremer* (2005) and *Schneider* (2011), the incipient crack depth of the initial technical crack is assumed as  $a_i = 0.1$  mm. The final crack depth before rupture  $a_e$  is determined based on digital microscopic measurements at the fractured surfaces of the tested bolts. The measurement results are listed in Appendix F.1. For the here analysed M36 HV-bolt sets, mean values are applied for load levels in the upper high cycle fatigue range of  $a_e = 8$  mm and in the transition region to the endurance limit (nominal bolt stress levels  $S_a \leq 50$  N/mm<sup>2</sup>) of  $a_e = 12$  mm.

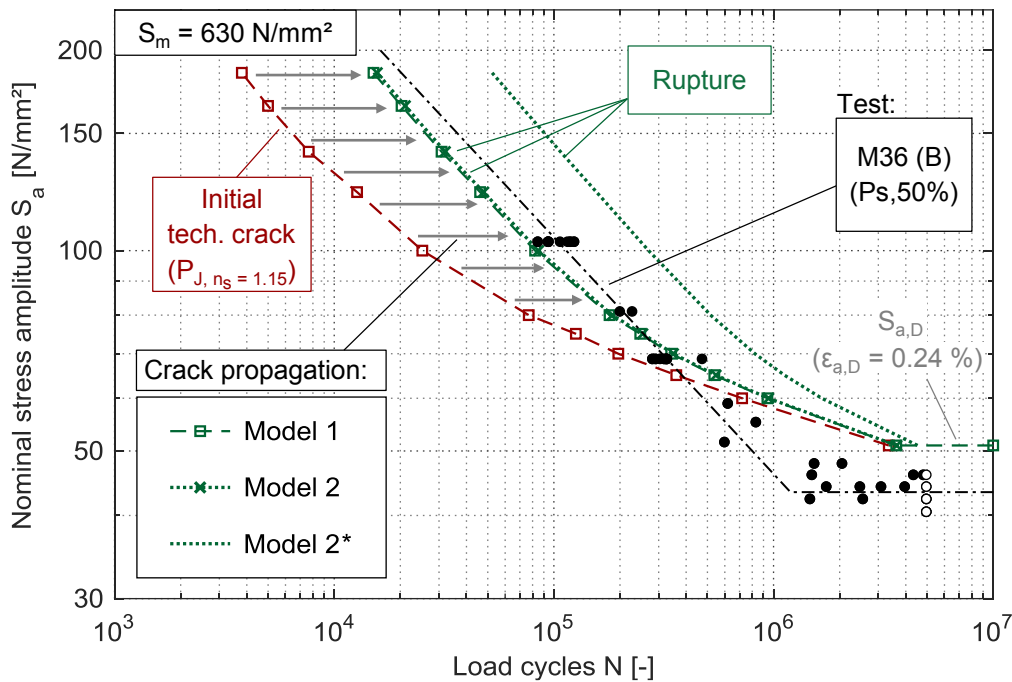
Using the two introduced models for determination of the cyclic range of the crack tip stress intensity  $\Delta K$  (i.e., calculated for a nominal stress range  $\Delta S = 2S_a$ ), numerical integration was executed with the fracture mechanics software package *FracSafe 2.1*. The material constant  $C = 2.0 \cdot 10^8$  and exponent  $m = 2.63$ , applied in the crack propagation function, correspond to a comparable high-strength material 42CrMo4 ( $R_m = 1100$  N/mm<sup>2</sup>) for a high mean stress level with stress intensity ratio  $R_k = 0.8$ . The parameters, applied in accordance with aforementioned studies on crack propagation of high strength bolts, are taken from the materials data collection in *FKM-Guideline* (2006) (defined for  $\Delta K$  in N/mm<sup>2</sup>  $\sqrt{m}$  and  $da/dN$  in mm/load cycle).

Figure 4-27 shows the comparison of resultant analytical fatigue curves with the experimental results for the investigated black M36 HV-bolt sets. Therein, load cycles until technical crack initiation are calculated with the  $P_J$  damage parameter and cyclic base material data (32CrB4) from constant amplitude tests. For the determination of the complete S-N curves until rupture, the calculated crack propagation load cycles are added to the load cycles until initial cracking. In the figure, an estimated base material endurance limit at  $\varepsilon_{a,D} = 0.24$  % ( $R = -1$ ) is considered. Distinct calculation results at selected load levels are given in Table 4-6.

With both introduced crack propagation models a good approximation of the experiment results in the upper high cycle fatigue range is achieved. Thereby, the tendentially lower estimation of the stress intensity factor with Model 2, caused by the simplified consideration of the loading conditions inside the thread, only has a minor impact on the calculated crack propagation load cycles. This was also confirmed in calculations for larger bolt diameters up to M72 (see also Chapter 4.5.1). The similarity of both models in the crack propagation calculation is noteworthy because, unlike Model 1, the numerical integration of the geometry function for the round bar model is also fairly easily achievable 'by hands' of a serious engineer in common computational scripting tools, as it has been done

for instance by *Gottlieb* (2015) in his Master's thesis. The approach may therefore be applied as approximately equivalent solution when no fracture mechanics software is available.

Still, Model 1 is to be considered more accurate because it does inherently consider the stress gradient at the thread in radial direction and, as result from a corresponding FE calculation of the complete bolt-to-nut connection, also the longitudinal stress development in the paired thread (see Figure 4-13). It is therefore applied hereinafter in the succeeding calculations.



**Figure 4-27: Comparison of analytical fatigue calculation results of load cycles until rupture with experimental results for black M36-HV bolt sets**

Additionally, in Figure 4-27 calculation results from an adaption of Model 2 (denoted as Model 2\*) are illustrated, where the model dimensions are limited to the bolt's core diameter  $d_3 = 2 r_3$  instead of the nominal shaft diameter (which is to be compensated by a corresponding modification of the applied stress level  $\sigma(M2^*) = F / \pi r_3^2$ ). While this modelling approach has been successfully applied by *Kremer* (2005) for recalculation of experimentally determined crack propagation load cycles at bolt size M8, the omission of the conservatively acting fictitious extension of the incorporated crack through the thread depth leads to a strong overestimation of fatigue life in the here presented investigation. As already the sole crack propagation load cycles determined with Model 2\* in the upper HCF notably exceed the experimentally determined load cycles until rupture (see Table 4-6), its application cannot be recommended for large-size bolts.

An analogous adaption of Model 1 ( $\rightarrow$  Model 1\*) is additionally considered in the aforementioned investigations by *Pyttel et al.* (2008). Contrary to Model 2\*, thereby the negligence of the stiffness contribution of the thread leads to increased stress intensities compared to Models 1 and 2. Due to its conservative nature it is not considered in the here presented result depiction.

**Table 4-6: Juxtaposition of analytically and experimentally determined fatigue load cycles for M36 HV-bolt sets**

Load level ( $S_m = 630 \text{ N/mm}^2$ )	Technical crack initiation	Crack propagation			Rupture	
	$P_J (n_s = 1.15)$	Model 1	Model 2	(Model 2*)	Analytical ( $P_J / \text{Model 1}$ )	Experimental M36 (B)
HCF1 $S_a = 103 \text{ N/mm}^2$	$2.36 \cdot 10^4$	$5.39 \cdot 10^4$	$5.67 \cdot 10^4$	$(2.32 \cdot 10^5)$	$7.8 \cdot 10^4$	$\approx 1 \cdot 10^5$
HCF2 $S_a = 69 \text{ N/mm}^2$	$2.42 \cdot 10^5$	$1.54 \cdot 10^5$	$1.62 \cdot 10^5$	$(6.63 \cdot 10^5)$	$4.0 \cdot 10^5$	$\approx 3 \cdot 10^5$
TDL $S_a = 50 \text{ N/mm}^2$	$3.35 \cdot 10^6$	$3.58 \cdot 10^5$	$3.78 \cdot 10^5$	$(1.52 \cdot 10^6)$	$3.7 \cdot 10^6$	$\approx 6 \cdot 10^5 - 2 \cdot 10^6$

Comparing load level wise calculated fatigue load cycles in crack initiation and crack propagation phases to the measurement results from *Kremer* (2005), the analytical calculations with Model 1 and Model 2 are in a plausible order of magnitude. Thereby, at the highest tested load horizon HCF1 the overall load cycles until rupture are substantially affected by crack propagation. The proportional contribution decreases at lower load levels and overall load cycles are increasingly dominated by technical crack initiation. Consequently, with decreasing load level the accuracy of the approximation of the experimental results depends more strongly to the previously elaborated damage parameter characteristics.

A graphical comparison of the complete S-N curves until rupture, calculated with different damage parameters and including the variant consideration of the support effect at the notch, is given in Figure 4-28. The non-conservative nature of the  $P_{SWT}$ -parameter's estimation under consideration of the notch sensitivity factor  $n_s$  is further enhanced by the additional consideration of crack propagation. Only when neglecting the support action, an acceptable approximation of the experimental results is achieved, which however is the most conservative among the considered damage parameter configurations. For the  $P_J$ -parameter, neglecting  $n_s$  leads to a slightly more conservative load cycle estimation, which causes an improved approximation of the experimental results in the transition region to the endurance limit.

Generally, also when using the cyclic material data obtained from Incremental-Step-Tests (Figure 4-29) a good analytical result quality is obtained in the upper high cycle fatigue range at both experimentally investigated load horizons. Here the overestimation of the  $P_{SWT}$ -parameter with consideration of the notch sensitivity factor is compensated by the more conservative progression of the strain-life curve and the beneficial impact of the lower  $n_s$ -value obtained with IST based material data. Due to the strain-life curve progression, at lower load levels no distinct transient development towards an endurance limit, as present in the experimental results and calculations with material data from constant amplitude tests, is displayed by the analytical results. Moreover, the earlier discussed restrictions for prediction of the actual endurance limit apply.



The depicted calculation results with cyclic material data from the two testing procedures support the previously made assumption that the base material's actual fatigue life behaviour at higher load cycles is somewhat overestimated by the strain-live curve from constant amplitude tests and underestimated by its IST based counterpart.

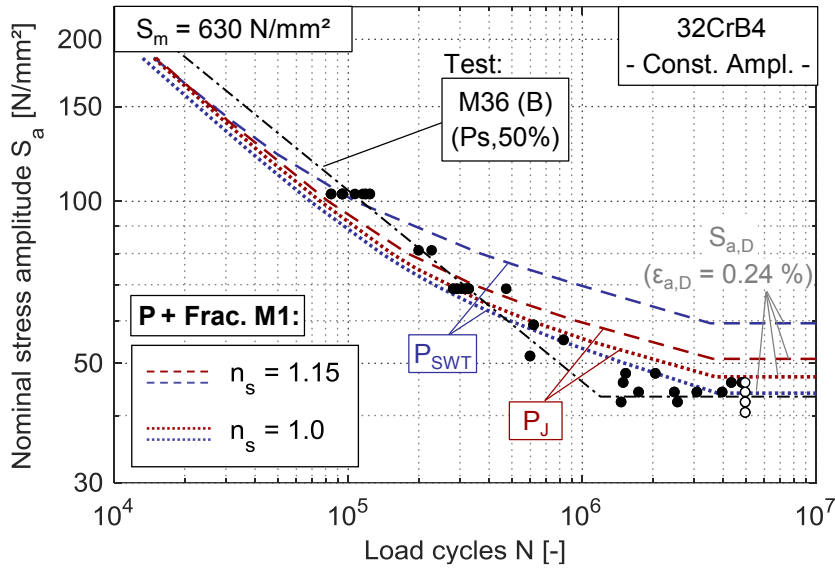


Figure 4-28: Analytical fatigue curves until rupture with different damage parameter approaches considering cyclic material data from constant amplitude tests

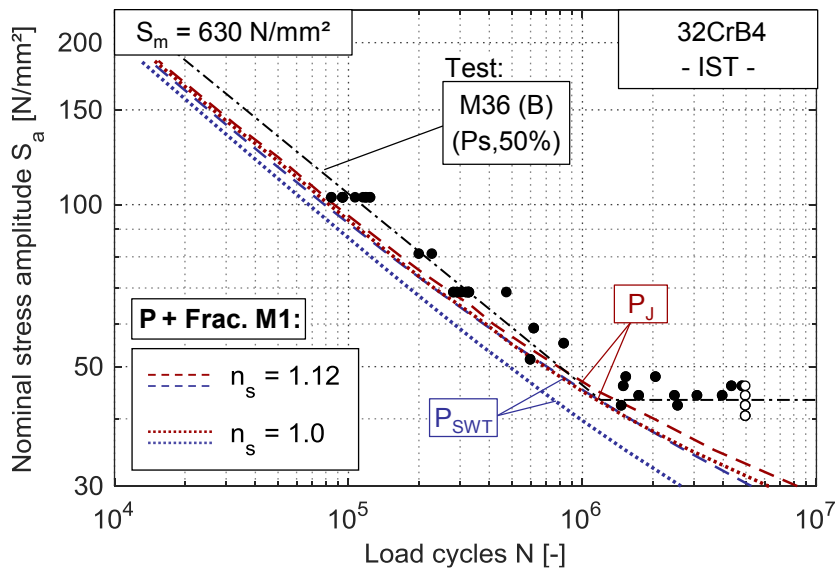
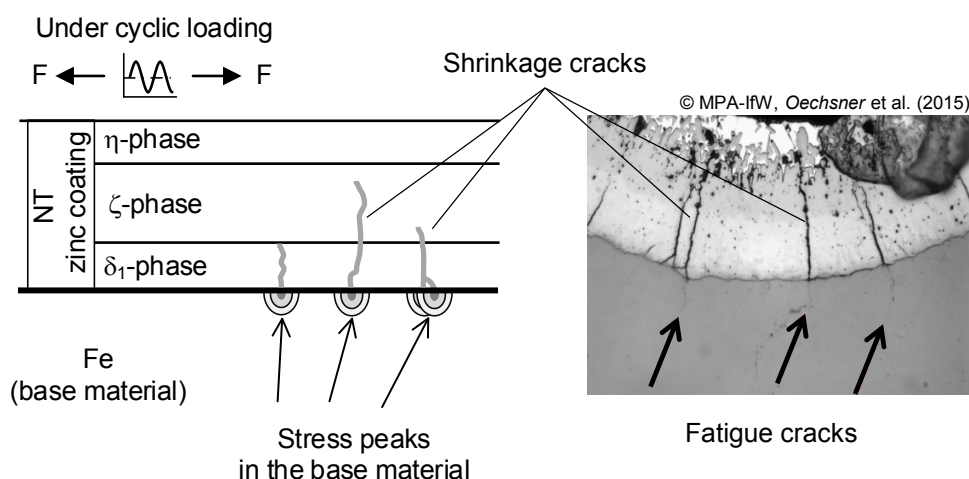


Figure 4-29: Analytical fatigue curves until rupture with different damage parameter approaches considering cyclic material data from Incremental-Step-Tests (IST)

#### 4.4.4 Consideration of the boundary-layer effect

The experimental results on M36 HV-bolt sets, presented in Chapter 3.3, have evidently shown a significant reduction of the fatigue strength caused by hot-dip galvanizing. Thus far, this behaviour is not represented in the applied calculation methodology. In order to provide a legitimate analytical approximation of the fatigue strength also for hot-dip galvanized HV-bolts, an adaption of the calculation approach is necessary, which in particular considers the effect of the boundary layer.

As elaborated in Chapter 2.1.4, for structural steel components with hot-dip galvanizing, fatigue cracks are initiated at locations where shrinkage cracks in the zinc coating reach up to the base material surface. The corresponding model assumption (derived by *Ungermann et al.*, 2015, and acknowledge for bolt-alike notch geometries by *Simonsen*, 2015 and *Oechsner et al.*, 2015) suggests that at these locations at the tips of the shrinkage cracks, microstructural stress peaks occur which under cyclic loading favour premature fatigue damage of the component (Figure 4-30).



**Figure 4-30: Model representation of the damage effect caused by galvanizing boundary layer according to *Ungermann et al.* (2015), *Simonsen* (2015) and *Oechsner et al.* (2015)**

#### Engineering models for consideration of the boundary layer effect

Generally, the relevance of surface effects on the fatigue life diminishes in the phase of technical crack propagation, see *Radaj & Vormwald* (2007). This can also be presumed for the here contemplated impact of hot-dip galvanizing. An implementation of the damage effect of the zinc coating is therefore particularly to be considered within the strain-life approach for calculation of crack initiation fatigue life. Given the complex causative damage process on microstructural level, which is not yet conclusively investigated, simplified engineering models are introduced.

In the research project “Experimental and analytical assessment of the fatigue strength of bolts with large dimensions under consideration of boundary layer effects” (*Oechsner et al.*, 2015) an adaption of the “thin surface layer model” by *Seeger & Heuler* (1984) (see Chapter 2.2.5) was pursued for integration of the effect of hot-dip galvanizing to the notch-strain approach. Thereby the general load-bearing and base material behaviour is considered unaffected by the surface layer. The assumed stress concentration at the shrinkage cracks may be incorporated by adding a supplemental load

component as virtual residual strain  $\epsilon_r$  to the bolt's relation between nominal load L (here equivalently expressed by the nominal bolt stress S) and local strain  $\epsilon$  at the fatigue critical location inside the thread, derived from the FE calculation. This procedure is illustrated as Variant 1 in Figure 4-31, left, with an exemplary chosen strain addend  $\epsilon_r = 0.75\%$ .

As the strain increment is applied constantly at all nominal load levels, the cyclic strain range after load reversal  $\Delta\epsilon$  remains unaffected, apart from an increase of the mean strain level. In the evaluation of the local stress-strain ( $\sigma$ - $\epsilon$ ) behaviour, the virtual residual strain leads to a corresponding residual stress  $\sigma_r$ , present at unloaded conditions. However, already at unmodified loading conditions the prevailing high mean stress level causes strongly plastic local deformations. The considered strain augmentation thus only leads to a marginal increase of the local stress level of the cyclic hysteresis.

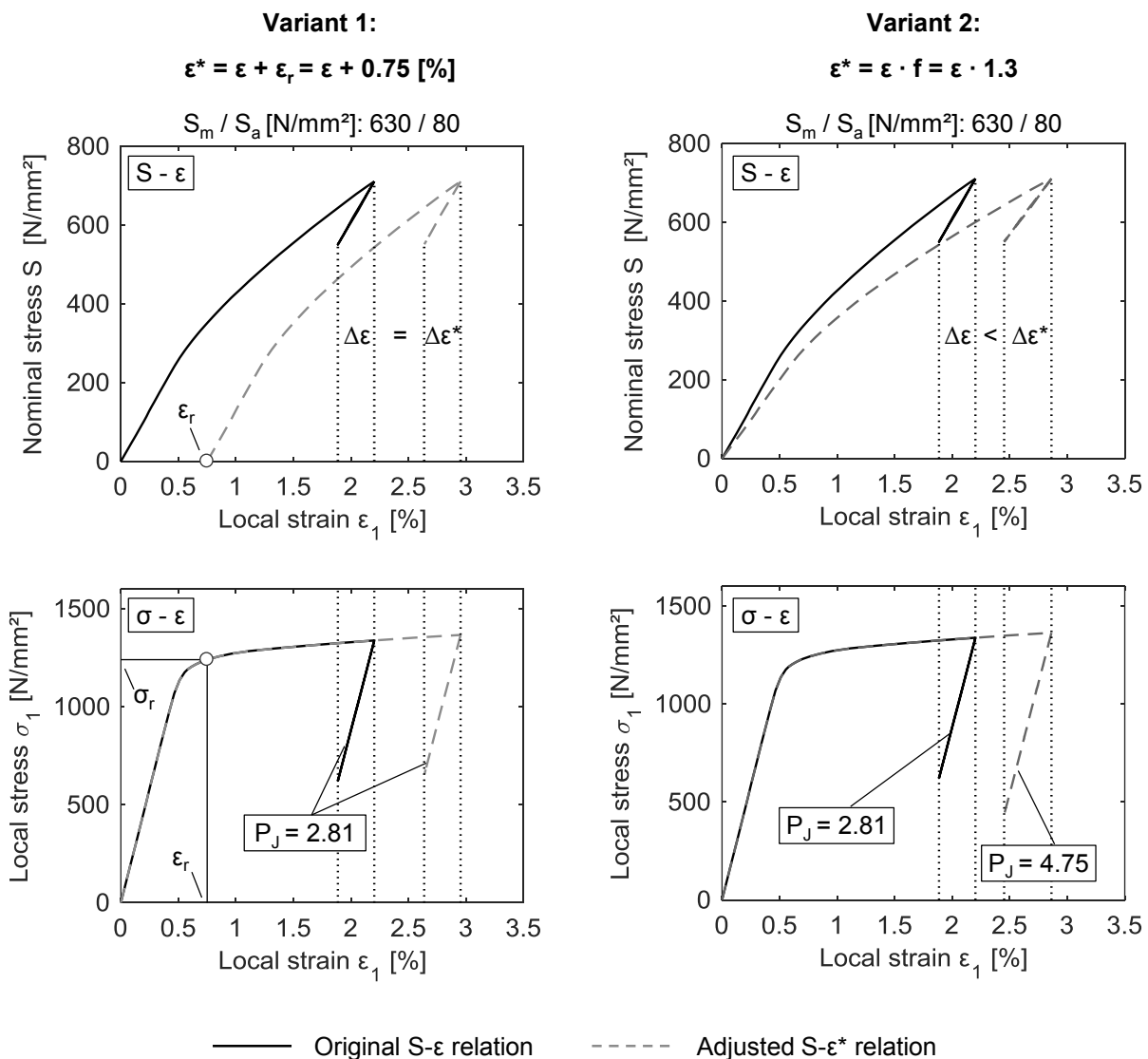


**Figure 4-31: Variants of adjusting the nominal load (S) – local strain ( $\epsilon$ ) relation for inclusion of the damage effect caused by hot-dip galvanizing to the strain-life approach**

As a consequence, due to the threshold of the mean stress sensitivity (see Chapter 4.4.1), also at the here incorporated rather large residual strain increment, no increased fatigue damage is considered by the  $P_J$ -parameter. Also using the  $P_{SWT}$ -parameter, the experimentally determined reduction of fatigue life caused by hot-dip galvanizing cannot be reproduced with strain increments  $\varepsilon_r$  in a technically reasonable order of magnitude.

Additional to the residual strain increment, the “thin surface layer model” allows the consideration of a separate local stress-strain relation (i.e., material behaviour) of the boundary layer. As illustrated in the schematic depiction of the model in Figure 2-14, for surface layers with higher strength attributes than the base material, this, at identical local strains, leads to an augmented local stress range of the surface layer. In the original application purpose of the model for surface strengthened components (see *Bruder & Seeger, 1996*), fatigue crack initiation is then considered to occur in the surface layer. However, the here investigated boundary layer is notably softer than the base material (instrumented indentation tests by *Oechsner et al., 2015* have shown hardness and elasticity values of the zinc coating of about half compared to the high strength steel base material). The actual stresses in the coating are therefore smaller than in the base material. Moreover, as previously indicated, owing to shrinkage processes, the zinc coating must be considered fully cracked already in the initial production state before cyclic loading. Thus, an explicit consideration of the boundary layer’s material behaviour is not suitable for the present application purpose. A modification of the base material’s local  $\sigma$ - $\varepsilon$  relation caused by the zinc coating cannot be regarded plausible, either.

Given the aforementioned observations, the “thin surface layer model” is not considered qualified for incorporation of the damage effect of the zinc coating to the analytical fatigue calculation with the stain-life approach.

An alternative approach for modification of the bolt’s  $S$ - $\varepsilon$  relation is illustrated as Variant 2 in Figure 4-31, right. Thereby, to incorporate the negative impact of the zinc coating to the local loading conditions, a factor  $f$  is applied to the original strains determined without boundary layer. This also results in an augmentation of the strain range  $\Delta\varepsilon$  under cyclic loading. Similar to Variant 1, the local stress-strain relation is maintained identical to the uncoated material state. However, the increased strain and likewise enhanced corresponding stress range results in a higher fatigue damage, displayed in the damage parameter evaluation ( $P_{(\varepsilon)} < P_{(\varepsilon^*)}$ ).

Different to the basic assumption of the “thin surface layer model”, in the suggested approach the load dependent occurring local strains are considered affected by the boundary layer. Thereby, rather than a contribution to the load-bearing behaviour of the surface layer, the strain augmentation may be interpreted as an additional geometrical impact. This corresponds to the aforementioned model assumption of a microscopic notch effect caused by the shrinkage cracks. As no physically substantiated estimation is obtainable, the magnitude of the considered strain enlargement factor  $f$  is adjusted solely empirically. The aspired reduction of the analytically calculated endurance limit between hot-dip galvanized and uncoated black bolts of about 20 to 25 %, indicated by the experimental results, can be achieved by introducing a strain factor  $f = 1.25 - 1.30$ . Corresponding analytical fatigue calculation results are presented in Figure 4-32 and Figure 4-33. Therein, an estimated

base material endurance limit  $\epsilon_{a,D} = 0.24 \%$  is considered (see Chapter 4.4.2) and macro-crack propagation load cycles are calculated independently of the boundary layer. Additionally to the full load cycles until rupture, analytical crack initiation fatigue curves of the galvanized bolts are plotted in the red dotted lines.

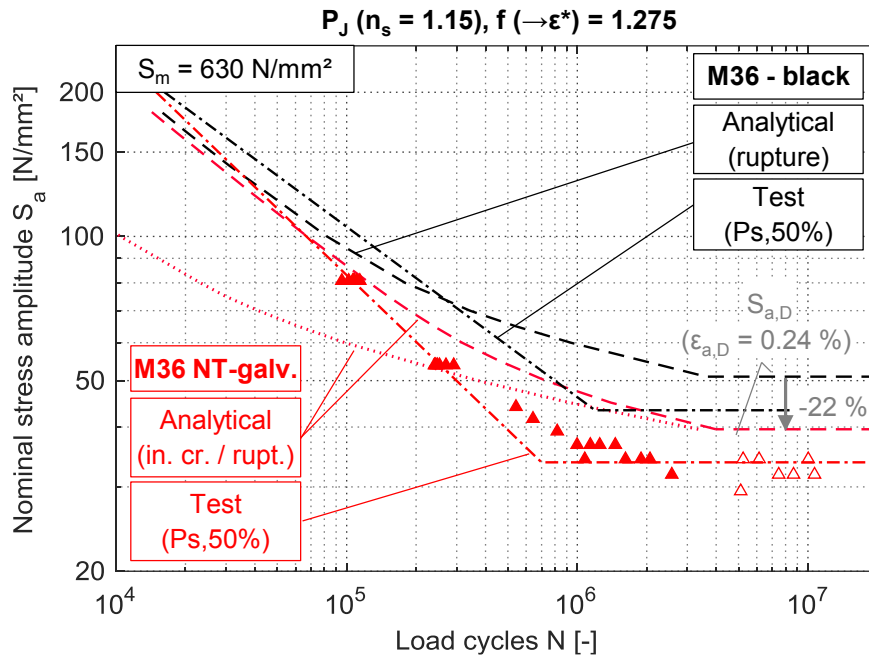


Figure 4-32: Calculation results considering the effect of hot-dip galvanizing with strain adjustment Variant 2 and  $P_J$  damage parameter ( $n_s = 1.15$ , material 32CrB4, cyclic material data from constant amplitude tests)

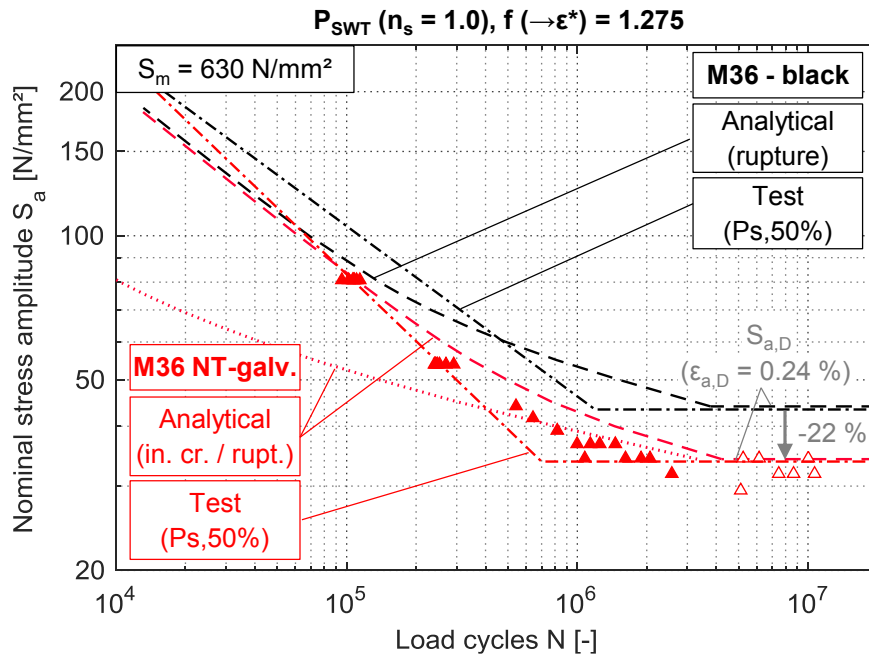


Figure 4-33: Calculation results considering the effect of hot-dip galvanizing with strain adjustment Variant 2 and  $P_{SWT}$  damage parameter ( $n_s = 1.0$ , material 32CrB4, cyclic material data from constant amplitude tests)

As can be observed from the comparison between analytical and experimental results, using the suggested approach, the effect of hot-dip galvanizing can expediently be incorporated to the calculation procedure with both  $P_J$  and  $P_{SWT}$  damage parameter. Certainly, similar to the uncoated M36 bolts, with the latter an appropriate approximation of the experimental results is only obtained when neglecting the stress-mechanical support effect ( $n_s = 1.0$ ). Based on the directly triggered endurance limit reduction, the effect of the zinc coating is extended to the upper high cycle fatigue range. Since at higher nominal load levels fatigue life is increasingly affected by macroscopic crack propagation, the calculation results with and without boundary layer consideration approximate. This tendency generally reflects the behaviour found in the experimental results. Still, contrary to uncoated bolts, including the boundary layer consideration, the analytical fatigue approximation in the upper high cycle fatigue range shows an overestimating tendency compared to the test results. Correspondingly, the deviation between uncoated and galvanized bolts at the upper tested load level is notably less severe in the analytical calculation than in the experimental results. This observation gives rise to the assumption that also the macroscopic crack propagation phase, which at this load level forms a significant contribution to the overall fatigue life, is to a certain degree affected by the zinc coating.

The accuracy of the result approximation in the transition region to the endurance limit, where fatigue life is increasingly governed by technical crack initiation, mainly depends on the applied damage parameter approach and the earlier discussed influence of the strain-life curve progression. Additional calculation results with the  $P_J$ -parameter under negligence of the notch sensitivity factor and with the more conservative strain-life curve from IST are included in Appendix E.4. In both calculations, the reduction of crack initiation load cycles leads to an improvement of results in the TEL as well as at the lower tested load level in the upper HCF. A similar tendency is observable in the comparison between the depicted calculation results in Figure 4-32 and Figure 4-33.

Alternatively, instead of adjusting the local loading conditions, an equivalent calculation result can be achieved by reducing the applied damage parameter – fatigue life relation ( $P$ -life curve). Thereby, an additional modification factor is to be considered in analogy to the notch sensitivity factor  $n_s$  ( $n_{total} = n_{zinc} \cdot n_s$ , with  $n_{zinc} < 1.0$ ). This approach is emblematic for an alternative interpretation of the underlying damage mechanism, where the zinc coating is assumed to affect the fatigue load-bearing capability of the base material, rather than the local loading conditions. However, thereby different correction factors are required for the two considered damage parameters ( $\Delta S_{a,D} = 20\% \rightarrow n_{zinc}(P_J) \approx 0.6$ ;  $n_{zinc}(P_{SWT}) \approx 0.9$ ). The here applied load dependent procedure provides the advantage that an identical strain adjustment factor  $f$  causes an equivalent effect on the calculation results with both damage parameters.

#### Discussion of the boundary layer impact in the macroscopic crack propagation phase

It can be presupposed that the principle macro-crack propagation behaviour of uncoated and hot-dip galvanized bolts with the same base material is largely equivalent. However, the shape of the propagating crack verifiably variates in dependence of the boundary layer. *Kremer* (2005) for electrochemical galvanized bolts as well as *Eder et al.* (2018) for hot-dip galvanized bolt-alike notched specimens report of tendentially more crescent- (i.e., circumferential) rather than half-moon-shaped

fracture surfaces, compared to the uncoated counterparts. The same tendency can be observed from the fracture surfaces of the tested bolts of the here present study (see Appendix F.1). Moreover, compliantly with the results from *Kremer*, for all boundary layer states fracture surfaces show a more pronounced circumferential tendency with increasing loading (*Eder et al.* performed tests at only one load level).

*Eder et al. (2018)* point out that according to *Milella (2013)* a more crescent-shaped beach mark pattern and resultant fracture surface can be associated with increasingly severe stress concentrations, whereas at milder stress concentrations a more levelled beach mark progression develops (see Figure 4-34). The varying fracture surface development can be attributed to the abundance of occurring incipient surface cracks under cyclic loading in the base material at the notch root. These observations correlate with the boundary layer and load level dependent fracture surface tendency of the experiments, described above.

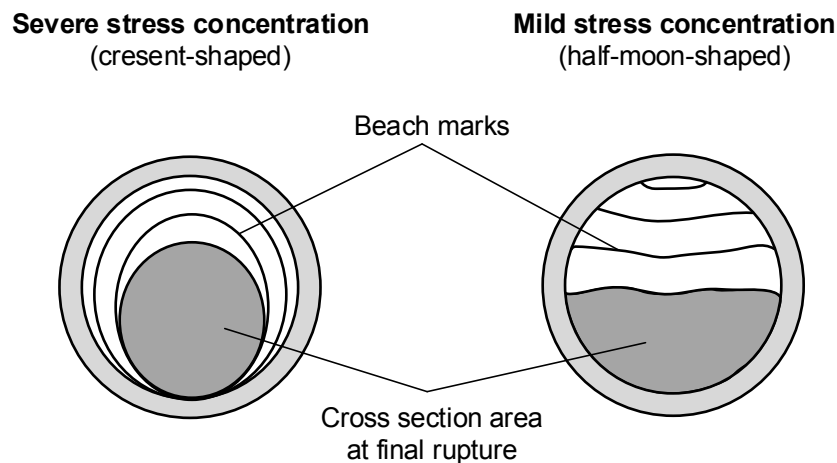


**Figure 4-34: Schematic illustration of fracture surfaces after fatigue crack propagation of round notched specimens following severe (left) and mild (right) stress concentrations; adapted from *Eder et al. (2018)* and *Milella (2013)***

The described crack shape variation may be considered in the analytical calculation of macro-crack propagation by means of the crack depth to width ratio  $a/c$ , for instance in a semi-elliptical surface crack model according to FKM-Guideline (2006), as suggested by *Kremer (2005)*. Thereby, a more strongly circumferential crack shape and correspondingly considered crack width  $c$  causes a reduction of crack propagation load cycles. However, the consideration of a fully circumferential surface crack, as hypothesised in the numerically validated crack propagation model applied in the presented calculations (see Chapter 4.4.3), already implies a theoretical unfavourable limit state of the actually present single-sided crack initiation. A crack shape dependent adaption is thus not appropriate in the approximative geometry model.

It needs to be acknowledged that the here applied macro-crack propagation calculation, using an approximative crack propagation model and assumed material parameters, designates a rather general estimation approach. It aims for a manageable practical applicability based on technically available model assumptions. Investigations of advanced crack propagation calculation methods of bolts

including numerically aided crack propagation functions, as performed for instance by *Olveda et al. (2014)* and *Stranghöner et al. (2018)*, were not in the scope of the present dissertation. In the further development of such models the specific crack shape adaption for consideration of the surface layer impact is advisable.

## 4.5 Extended sensitivity studies

Up to this point, the elaborated analytical fatigue assessment procedure was solely validated and adjusted on the basis of the experiments on M36 HV-bolts, under axial loading, with nominal preload, and with the respective set of material data from the original bolt material. In this conclusive chapter the validation is extended to an increased framework of boundary conditions. In a first step, the induced effect by variations of the bolt geometry, and in particular by an increased bolt diameter, is evaluated. Secondly, the importance of knowledge about material data determined for the original bolts' base material is assessed. Finally, the effect of varying loading conditions is evaluated. In this context, the scope of experimental validation is extended to the test results of black and hot-dip galvanized M64 HV-bolts as well as test results of M48 HV-bolt from the literature.

### 4.5.1 Impact of the bolt geometry

As elaborated in the state of the art of this dissertation, size effects, which influence the fatigue strength of HV-bolts, may arise from a variety of different origins (see Chapter 2.1.4). Contrary to the performed experimental investigations, the analytical calculation procedure, within boundaries, provides opportunity for isolated assessment of different size effects. Thus, to distinctly investigate the impact of geometry dependent variations which arise at bolts with increased diameters, possibly differing base material characteristics are disregarded at this stage, and analytical calculations are performed with identical base material data. In the sequel, firstly the sole geometrical impact of increased bolt diameters is evaluated. Secondly, the potential statistical size effect is assessed.

#### Geometrical size effects

Due to the normatively standardized thread geometries, which at different bolt diameters are not geometrically similar, a potential geometrical impact on the fatigue strength arises from the specific diameter dependent notch geometry. Figure 4-35 shows the development of the ratio between nominal bolt diameter  $d$  and thread pitch  $p$ , as indicator for the geometrical sharpness of the introduced notch. They are compared to the calculated linear elastic stress concentration factors at the notch root derived with 2D axisymmetric FE models (see Chapter 4.3.2).

A further diameter dependent impact is imposed by the stress-gradient in lateral direction from the notch root and the correlating support effect provided by the lesser loaded surrounding material. The normalised lateral stress developments from linear elastic FE calculations, starting at the most critically loaded location at the notch root, are illustrated in Figure 4-36 (expressed by the related notch stress concentration  $K_t / K_{t,max}$ ). Jointly, the thereof derived related stress gradients  $\chi^*$  and stress-mechanical support numbers  $n_s$ , calculated with the approach by *Siebel & Stieler (1955)* (see Chap-



ter 2.2.5 as well as Appendix E.1), are given. The thereby considered material dependent macroscopic notch sensitivity factor  $n_p$  is identical for all diameters. Additionally to the here investigated large-size diameters, the graphic shows the results for smaller bolt size M16, for comparison.

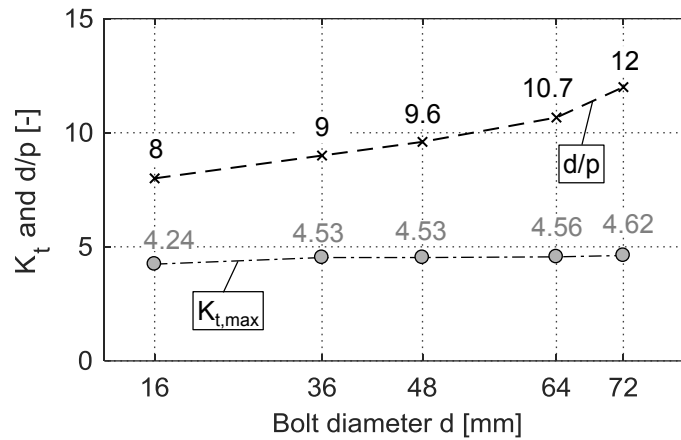


**Figure 4-35: Comparison of notch sharpness expressed by the  $d/p$ -ratio and resulting notch effect expressed by the linear elastic notch stress concentration  $K_t$  in dependence of the bolt diameter**

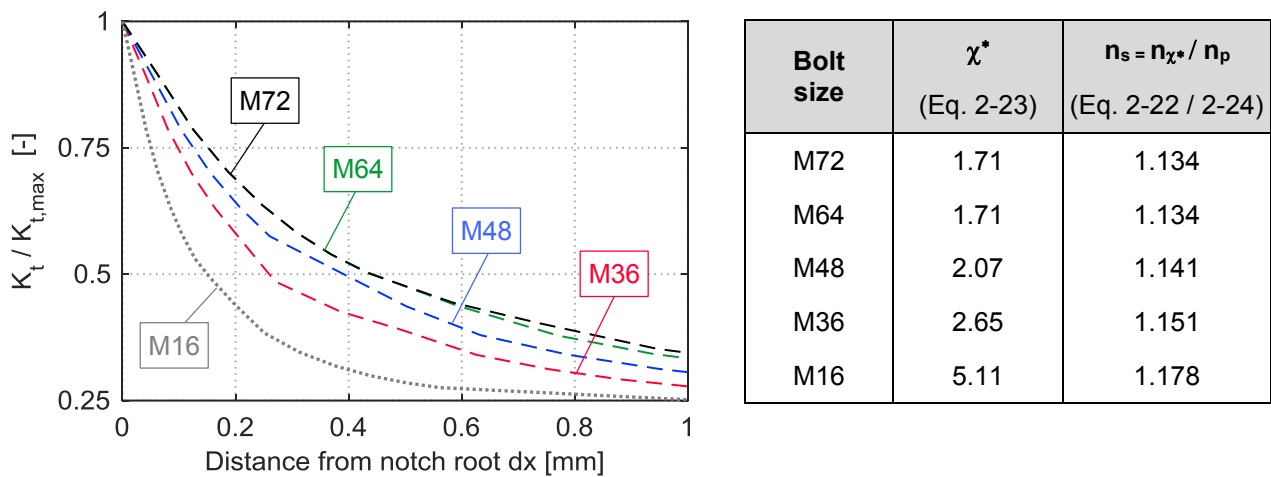


**Figure 4-36: Stress gradients and corresponding notch sensitivity factors in dependence of the bolt diameter**

In order to quantify the impact of the two mentioned geometry dependent effects, Figure 4-37 shows analytical fatigue calculation results for large-size HV-bolts between diameters M36 and M72. Results are shown separately for the upper HCF (left) and the endurance limit (right). Crack initiation load cycles are calculated with the  $P_J$  damage parameter and cyclic material data from constant amplitude tests for material 32CrB4. For approximation of the bolts' endurance limit a base material strain endurance limit  $\epsilon_{a,D} = 0.24\%$  is assumed (see Chapter 4.4.2).

From the calculation results without consideration of the notch sensitivity factor ( $n_s = 1.0$ ) the particular impact of the variant thread geometries can be assessed. As visible in Figure 4-35, despite the notable increase of the  $d/p$ -ratio, the actual resultant notch stress concentrations deviate only slightly from bolt diameter M36 upwards. Correspondingly, only a fractional reduction of endurance limits

related to thread geometry is present in the analytical calculations. It can therefore be concluded that for the investigated diameter range between M36 and M72 no relevant impact is imposed on the bolts' fatigue strength by the variant thread characteristics.

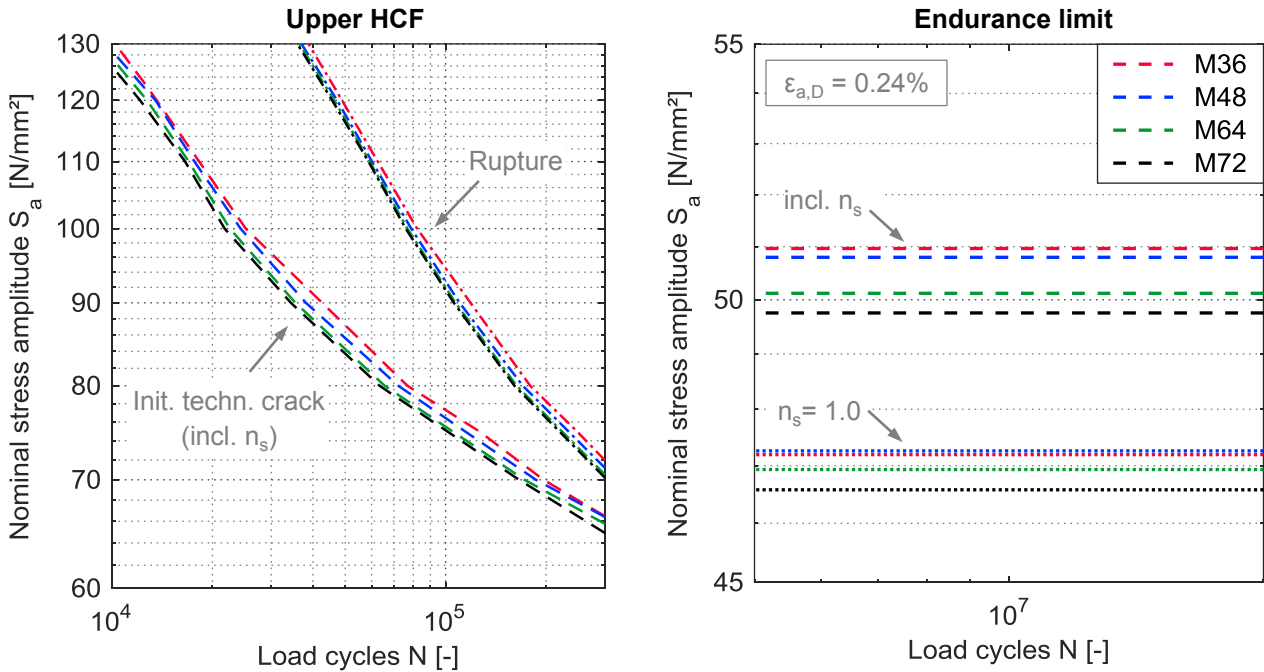


**Figure 4-37: Comparison of analytical fatigue calculation results for HV-bolt sets with different diameters ( $S_m = 630 \text{ N/mm}^2$ ,  $P_J$  damage parameter, material 32C4B4, cyclic material data from constant amplitude tests)**

Regarding the stress-mechanical size effect, it can be observed in Figure 4-36 that the linear elastic stress gradient significantly decreases from smaller bolt size M16 up to the large-diameter range between M36 and M72. Correspondingly, under elastic-plastic conditions a stronger development of plastic strains in the material adjacent to the notch root must be expected with increasing bolt diameter, thus reducing the support action. While between diameters M36 and M48 still a notable variation of the stress gradient is present, from bolt diameter M48 upwards the reduction tendency perceptibly diminishes. Between diameters M64 and M72 no further depletion occurs. The described tendency is reflected in the corresponding notch sensitivity factors  $n_s$ . However, in the analytical calculation of the endurance limit (Figure 4-37, right), apart from the given general enlargement of the calculated fatigue strength, the additional inclusion of the diameter dependent notch sensitivity factor only causes a marginally stronger deviation between the considered diameters than imposed by the notch geometry itself. As the deviation of calculated endurance limits between bolt size M36 and M72 is little more than  $1 \text{ N/mm}^2$ , the impact indicated by the here considered calculations with the  $P_J$ -parameter is negligible. From the previous investigations in Chapter 4.4 it is evident that an assessment with the  $P_{SWT}$ -parameter, which is not depicted here, would result in a notably stronger diameter related impact of the stress-gradient. However, considering the thus far performed studies, it must be assumed that the effect of the stress-mechanical support number is strongly overestimated and thus not properly reflected in calculations with the  $P_{SWT}$ -parameter.

In the upper HCF (Figure 4-37, left) the calculated load cycles until technical crack initiation are subjected to a reduction of about 15 % between bolt sizes M36 and M72 by the combined effect of notch geometry and support action. However, this somewhat stronger deviation than found for the endurance limit largely resolves in the final fatigue curves until rupture and the additional consideration of macro-crack propagation.

When using the crack propagation Model 1 presented in Chapter 4.4.3, the diameter dependent stress gradient is inherently included in the calculation by the applied radial stress development throughout the bolt diameter (equivalent to the stress development used for determination of the stress-mechanical support effect in Figure 4-36). In all calculations the assumed initial crack depth is maintained equally to  $a_i = 0.1\text{mm}$ . The final crack depths, required for the calculations, are estimated, based on the microscopic measurements of the fracture surfaces of the tested M36 and M64 bolts (see Appendix F.1). As the final crack depth has a minor impact on the calculated load cycles, these approximative values can be considered sufficiently accurate. With only about 4 % reduction of calculated crack propagation load cycles between diameters M36 and M72, no significant impact of the diameter is indicated by the applied crack propagation calculation. This is reflected in the final load cycles until rupture. Thereby, in accordance with the described diameter dependent behaviour of the stress gradient, the visible slight reduction tendency for the most part arises between bolt size M36 and M48. It resolves at further increased diameters. Since no major effect is imposed by the diameter related stress gradient, as previously indicated in Chapter 4.4.3, crack propagation load cycles in a similar order of magnitude may also be calculated with the simplified crack propagation Model 2.

The results show that neither changes of the thread geometry nor the stress gradient, resultant from an increased bolt diameter, need to be expected to cause a major reduction of the fatigue strength. In the comprehensive validation, performed in the previous Chapter 4.4, it was shown that equally to the  $P_{\text{SWT}}$  damage parameter also with the above considered  $P_J$ -parameter a better approximation of the experimental results is achieved when disregarding the support number  $n_s$  and thus the stress-mechanical size effect. As the here applied approach by *Siebel & Stieler (1955)* was mainly derived for the purpose of assessing smaller dimension components than in the present case, it is probable that for the given magnitude of considered diameters the actually present support effect and its beneficial implication are overestimated. When using the alternative approach given in FKM-Guideline (2012) for calculation of a stress-gradient dependent notch sensitivity factor, for all here considered bolt diameters (including M16) the calculation yields a value  $n = 1$ . This supports the previously stated assumption.

#### Statistical size effect

The statistical size effect considers the increased probability of fatigue-relevant material defects to emerge at larger structural components. As the initial formation of a microscopic fatigue crack is mainly a surface related process, the statistical assessment may usually be affiliated to the contemplation of the highly stressed surface area of the investigated structural component (rather than material volume). Accordingly, by evaluation of a *Weibull*-distribution (aka., “weakest-link model”) the

statistical size effect may be incorporated to the strain-life concept with the statistical notch sensitivity factor  $n_w$  according to Equation 4-6 (see *Vormwald & Seeger, 2015; FKM-Guideline, 2012*). Thereby, the surface area of the reference material specimen  $A_{ref}$  is related to the critically loaded surface area of the investigated component  $A_\sigma$ . According to FKM-Guideline (2012), for structural steel the *Weibull* exponent may be estimated to  $k_w \approx 30$ .

$$n_w = \left( \frac{A_{ref}}{A_\sigma} \right)^{\frac{1}{k_w}} \tag{Eq. 4-6}$$

While for the application of the weakest-link model in the present investigation the applicable reference surface area is distinctly given by the dimensions of the base materials specimens, the approximation of the bolts critical surface area is fairly ambiguous. In the literature it is referred to a section of the structural component with more than 90-95 % of the maximum principle stress being an appropriate approximation basis (see *Sonsino, 1993*). A corresponding surface area can be determined with the aid of linear elastic FE calculations. To avoid an overestimation of the actual physically present critical surface area, it is essential to consider the continuous pitch of the thread in the FE model (see Chapter 4.3). For the here investigated large-size HV-bolt sets the numerical calculations yield a critical loaded surface area inside the thread with at least 95 % of the maximum principle stress ( $K_{t,95\%}$ ) with an extension over roughly a quarter of the bolts circumference ( $1/2 \pi$ ) and a height of about half of the bolts notch radius ( $1/2 R$ ). Neglecting the curvature of the notch root, the critical surface area  $A_{95\%}$  may therefore be analytically approximated by assessing a cylindrical surface section with the bolts core diameter  $d_3$  (see Figure 4-38, left). Considering a critical surface with at least 90% of the maximum stress concentration, the surface area doubles to approximately half of the bolts circumference ( $A_{90\%} \approx 2 \cdot A_{95\%}$ ). For the present investigation it is suspected that the stronger confinement of the fatigue critical area inside the thread represented by the lower bound of the surface area estimation ( $A_{95\%}$ ) reflects a more appropriate approximation of the actual physical conditions.

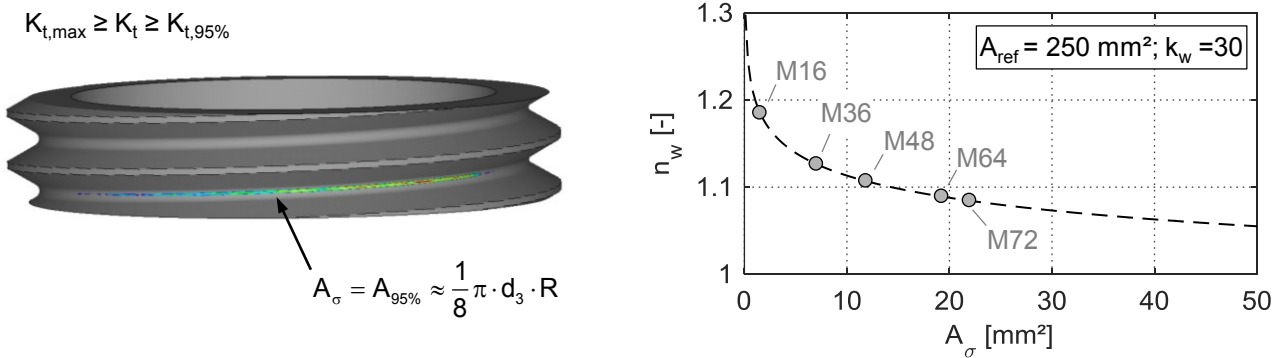


**Figure 4-38: Approximation of the critically loaded surface area at the bolt thread with a 3D FE model (left) and development of the statistical size effect acc. to Eq. 4-6 (right)**

Figure 4-38, right shows the development of the statistical notch sensitivity factor  $n_w$  in dependence of a critical surface area  $A_\sigma$  and corresponding HV-bolt diameter on the basis of the specimen size

from the cyclic material tests under constant amplitude loading (CA; cylindrical section with  $d = 4 \text{ mm}$  and  $h = 20 \text{ mm}$ ). The corresponding values are given in Table 4-7. Therein, additionally the resulting notch sensitivity factor derived for the differently sized material specimens used for the Incremental-Step-Tests are included (IST; cylindrical section with  $d = 8 \text{ mm}$  and  $h = 25 \text{ mm}$ ).

**Table 4-7: Critical surface areas and corresponding notch sensitivity factors for expression of the statistical size effect**

Bolt size	$A_{95\%}$ [mm <sup>2</sup> ]	$n_w$	
		CA ( $A_{ref} = 250 \text{ mm}^2$ )	IST ( $A_{ref} = 630 \text{ mm}^2$ )
M72	21.98	1.084	1.118
M64	19.26	1.089	1.123
M48	11.87	1.107	1.142
M36	7.05	1.126	1.162
M16	1.54	1.185	1.222

Despite the significantly larger overall dimensions, the critical surface areas at the bolt threads are substantially smaller than the specimens' reference areas. Thus, analogously to the stress-mechanical notch sensitivity factor, the consideration of the statistical size effect causes an increase of the analytically calculated fatigue strength. The associated effects are in a comparable order of magnitude. However, when considering the material data from CA tests, they are on a slightly lower level. Moreover, as can be observed by the comparison of Figure 4-39 and Figure 4-37, a slightly stronger diameter related impact is imposed by the statistical than by the stress-mechanical size effect.

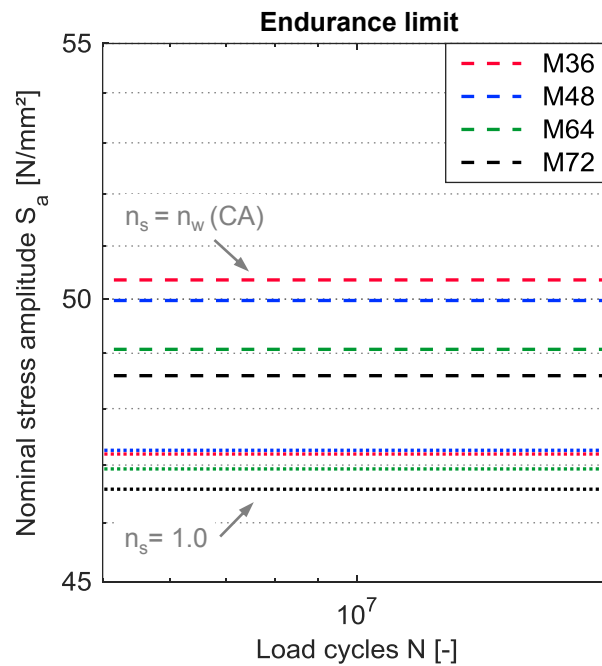


**Figure 4-39: Diameter dependent analytical calculation of the endurance limit under consideration of the statistical size effect ( $S_m = 630 \text{ N/mm}^2$ ,  $P_J$  damage parameter, material 32C4B4, cyclic material data from constant amplitude tests)**

Nonetheless, as can be observed in Figure 4-38, right, in the investigated large-size diameter range the applicable *Weibull*-distribution reaches a relatively shallow progression. Thus, the divergence of the calculated endurance limits between bolt diameters remains small. When using a critical surface area  $A_{90\%}$  the analytically determined fatigue strengths further approximate the calculation results without notch sensitivity factor ( $n_s = 1$ ).

It can be concluded that, such as the two previously evaluated diameter related impact factors, also the statistical size effect (in terms of the effect of an increasing bolt diameter) only minorly influences the crack initiation fatigue life of large-size HV-bolts. This is in accordance with the general observations regarding the statistical size effect of high strength steel components by *Böhm & Heckel* (1982) (see Chapter 2.1.4). Nevertheless, a possible combined consideration of statistical and stress-mechanical notch sensitivity factor in the analytical fatigue calculation according to Equation 2-25 would lead to a further overestimation of the experimental fatigue strength of the tested HV-bolts. As discussed above, the occurrence of a pronounced stress-mechanical size effect at large-size bolt diameters is questionable. It is thus to be preferred to use a support number  $n_s$  constituted solely by the statistical size effect, which may gain relevance in dependence of the size of the reference material specimens. Moreover, the statistical size effect becomes of notable significance in the analytical fatigue calculation of smaller bolt diameters (see Figure 4-38, right). However, given the small potential impact, for the here investigated bolt sizes neglecting both stress-mechanical as well as statistical size effect can be regarded acceptable.

It is plausible that statistical ramifications, for instance due to a higher density of microstructural voids at larger component sizes, may also influence to a certain degree the fatigue life during macroscopic crack propagation. However, after initiation of the technical crack the here applied surface related weakest-link model cannot readily be transferred to the succeeding macro-crack propagation phase. Thus, in the present investigation no statistical effect is incorporated in the analytical calculation of load cycles during macro-crack propagation.

#### 4.5.2 Impact of the bolt material

In the present section the potential impact on the analytical fatigue assessment of deviating cyclic material data, derived for different high-strength bolt materials, shall be assessed. In the framework of the present dissertation, comparison background for bolt material data was only acquired with the simplified evaluation method based on Incremental-Step-Tests (IST). Therefore, in the first instance a comparison is carried out using cyclic material data given in the literature for different materials derived with the more convincing test procedure with constant amplitudes (CA), as it was utilized here solely for the M36 bolts' material 32CrB4. For the juxtaposition, only cyclic material data of materials with similar strength properties (strength class 10.9) and with comprehensive experimental background, which includes a determined strain endurance limit, are considered. Additionally, the analytically estimated set of cyclic material data provided by the Uniform Material Law (UML) by *Bäumel & Seeger* (1990) is included in the evaluation. The estimation is based on the static material properties of the M36 bolt material 32CrB4. Thereby, as for the 32CrB4 material itself, the strain endurance limit is assumed to  $\epsilon_{a,d} = 0.24 \%$  (see Chapter 4.4.2).

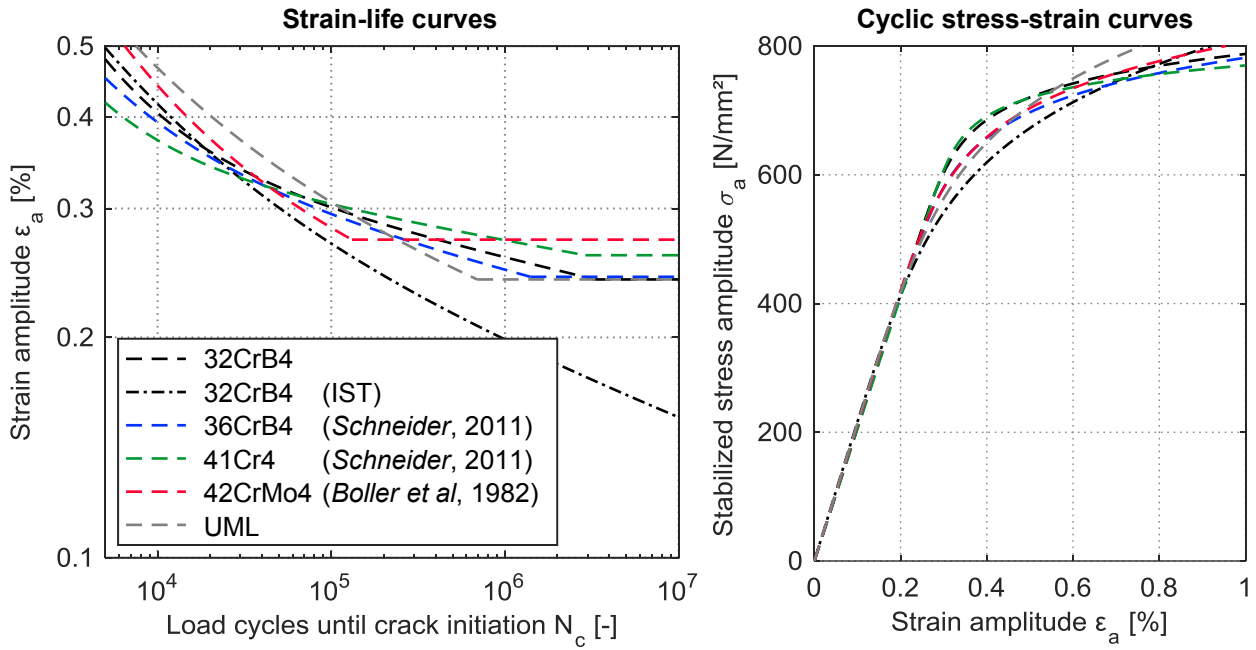


Figure 4-40: Comparison of cyclic material curves for high-strength steels given in the literature

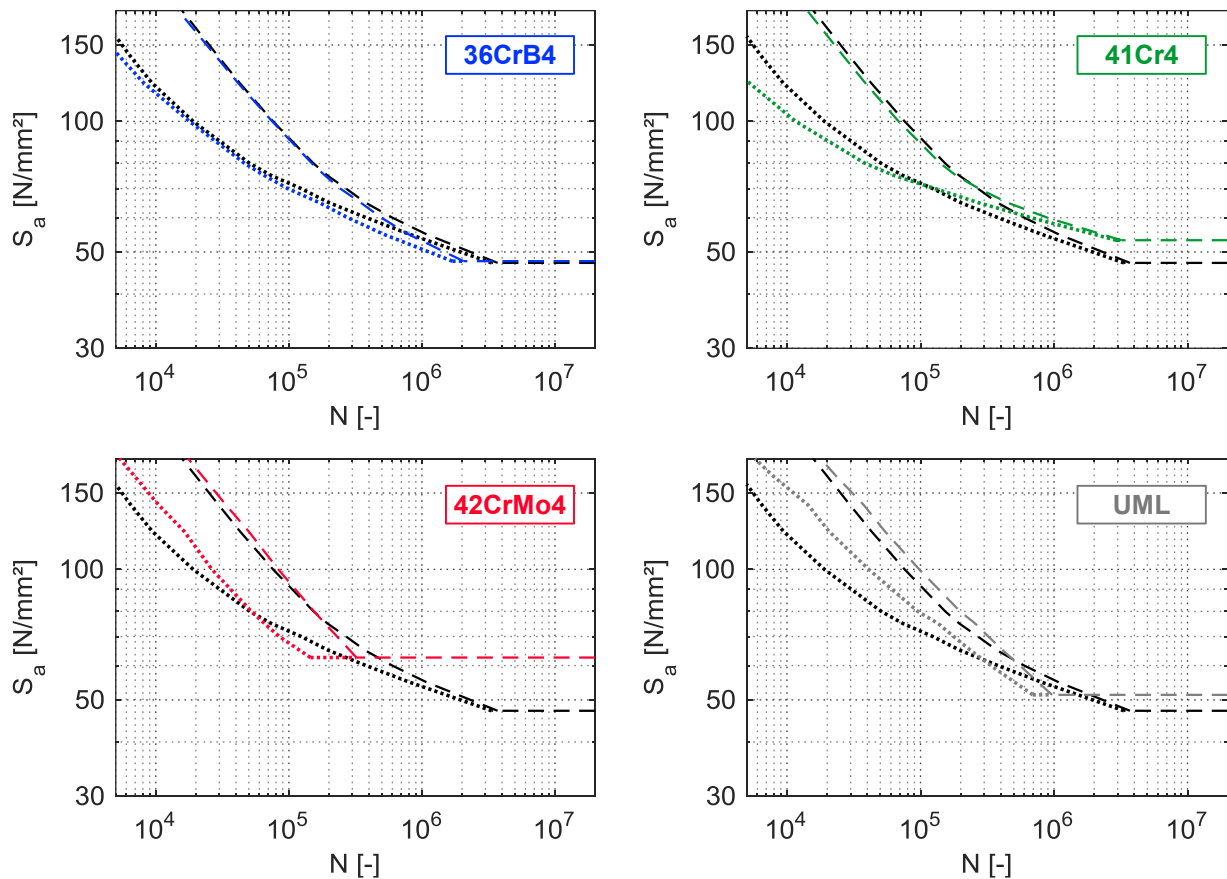


Figure 4-41: Individual comparison of analytical fatigue calculations for M36 bolts ( $S_m = 630$  N/mm<sup>2</sup>,  $P_j$  damage parameter,  $n_s = 1.0$ ) with original 32CrB4 material data from constant amplitude tests (black lines) to calculations with material data from the literature (dotted lines: crack initiation; dashed lines: rupture)

The cyclic material curves of the considered materials are shown in Figure 4-40, together with the curves for the original M36 bolt material 32CrB4 as well as the thereof derived UML. The underlying cyclic material parameters are included in Appendix E.5. Additionally, the 32CrB4 material curves derived from IST are plotted as reference. Below, in Figure 4-41, the results of analytical fatigue calculations for the M36 HV-bolt geometry with different cyclic material data (coloured lines) are compared individually to the results with the original bolt material's data from CA tests (black lines). All calculations consider identical crack propagation load cycles. The decisive benchmark criterion for the comparison are therefore the crack initiation load cycles depicted in dotted lines and the calculated endurance limits.

Within the here considered sample of materials a good agreement and close similarity of load cycles in the upper high cycle fatigue range (HCF) is achieved with the most resembling alloy specification 36CrB4. The good compliance of cyclic material characteristics also indicates that the strain endurance limit approximation of the original bolt material is appropriately chosen. For the two further considered material alloys notably stronger deviations occur. Thereby, the variations of calculated load cycles in the upper HCF are essentially precipitated by the different progressions of the materials' strain-life curves. At relevant fatigue loading conditions, calculated strain amplitudes at the notch root are mostly restricted to the linear region of the cyclic stress-strain curves, with close resemblance of all considered materials. Only at high nominal stress amplitudes and in a fatigue life range of  $N < \approx 10^4$ , noteworthy plastic deformations may occur in the cyclic hysteresis. Thus, a material specific impact of the cyclic stress-strain curve is restricted to this area. Moreover, as discussed in Chapter 4.4.2 on the example of the IST based cyclic material curves, an earlier development of plastic deformations under cyclic loading may affect the analytical calculation of the endurance limit. However, the discrepancies between the considered materials in the upper region of the cyclic stress-strain curves are notably less pronounced than precipitated by the material testing procedure with variable amplitudes. At the here considered high mean stress level ( $S_m = 630 \text{ N/mm}^2$ ) a possible impact on the calculation procedure from the monotonic material behaviour may effectively arise only from the slightly varying strength limit  $R_m$ , which affects the upper and thus the mean stress level of the cyclic hysteresis. However, also with the presumably overestimated mean stress sensitivity of the  $P_{\text{SWT}}$  damage parameter, only a slight impact is imposed upon the calculation results. With the here applied  $P_J$ -parameter the given changes of monotonic material behaviour between high-strength materials do not affect the calculation.

A significant deviation of analytical fatigue results in the upper HCF, to an extent that also a notable shift of calculated load cycles until rupture is visible, occurs in the calculation with the UML. Moreover, even though an identical strain endurance limit is considered, the analytically calculated endurance limit is raised by the impact of the cyclic stress-strain curve.

Despite the limited evaluation background, which originates from the lack of comprising experimentally substantiated material data, the presented comparison in Figure 4-40 convincingly illustrates that cyclic material data between materials with comparable strength characteristics are only limitedly transferable. This especially concerns the strain-fatigue behaviour, for which changes may have



a notable effect on the analytically estimated fatigue life. The given material assessment indicates that a better compliance might be suspected at resembling or identical alloy specifications. Obviously, this supposition requires further validation. It must also be considered that a general scatter of cyclic material properties is likely to arise due to the specific production as well as testing condition, regardless of the specific alloy specification. Thus, generally, knowledge about the specific cyclic material characteristics is crucial for an appropriate analytical fatigue assessment. To gain knowledge about the transferability of cyclic material properties, an extension of the presently given background of meaningful cyclic material data for high-strength bolt materials is required. Due to differences in the methodical analytical calculation approach, the objections by *Marten* (2009) against the application of the UML for calculation of preloaded bolts cannot directly be transferred to the here applied procedure. Nonetheless, the given comparative calculation emphasizes that the UML cannot be regarded as a reliable approximation tool. It needs to be considered as a very rough approximation of the actual material behaviour and may lead to significant deviations of results compared to the actual bolt material.

The compositions of the above considered material alloys are primarily representative for production of HV-bolts with diameters smaller or equal M36. Due to production reasons, for larger diameters commonly superior quality alloys with combined proportions of chromium (Cr), nickel (Ni) and molybdenum (Mo) are used. The simplified IST based material tests, described in 4.2.2, have generally revealed a good resemblance of cyclic material behaviour between the investigated bolts M36 and M64 (30CrNiMo8) as well as M48 (34CrNiMo6) by *Marten* (2009). The most pronounced deviation of strain-life curves occurs between the M36 and M64 bolt material (see Figure 4-7). Therefore, the impact of the actual bolt material to the analytically calculated fatigue strength of the M64 bolts is evaluated in Figure 4-42, on the example of the NT-galvanized specimens.

In the analytical calculation the strain enhancement factor  $f = 1.275$ , introduced in Chapter 4.4.4 for consideration of the boundary layer effect by hot-dip galvanizing, is incorporated. Additionally to the results of the M64 HV-bolts, the median S-N curve ( $P_{s,50\%}$ ) for the NT-galvanized M36-HV-bolts is depicted in grey colour for comparison purposes. Since with the IST based material data no conclusions regarding the endurance limit are feasible, only the upper HCF is considered in the analytical calculations.

The analytical results exhibit only a minor deviation of calculated crack initiation load cycles and hence confirm the comparability of underlying cyclic material properties. Given the good compliance between the CA and IST based strain-life curves in the upper HCF, observed for M36 bolt material 32CrB4, as well as the validation of the two testing procedures given by *Vormwald & Seeger* (1988), it is assumed that an adequate comparability may also be suspected for the unknown strain-life behaviour of the M64 as well as the M48 bolt materials at constant amplitude loading. As elaborated beforehand, for a comprehensive analytical fatigue calculation, which extends to the transition region and the endurance limit, material data from IST is not appropriate. Hence, for the present studies it is assumed legitimate to use the 32CrB4 material data from CA test as good approximation also in analytical fatigue calculations of the experimentally investigated bolts with diameters M64 and M48.

As a consequence, similar to the geometrical impact factors, investigated in the previous chapter 4.5.1, the analytical calculations do not suggest a significant “material-technological” size effect in the crack initiation phase. However, due to the lack of a meaningful fracture mechanical material data basis, the impact of material dependent crack propagation parameters cannot be evaluated. The investigation results indicate that the attested reduction of the experimental fatigue strength between the tested NT hot-dip galvanized M36 and M64 bolts in the upper HCF (see Figure 4-42) is predominantly attributable to a reduction of bearable load cycles in the macroscopic crack propagation phase.

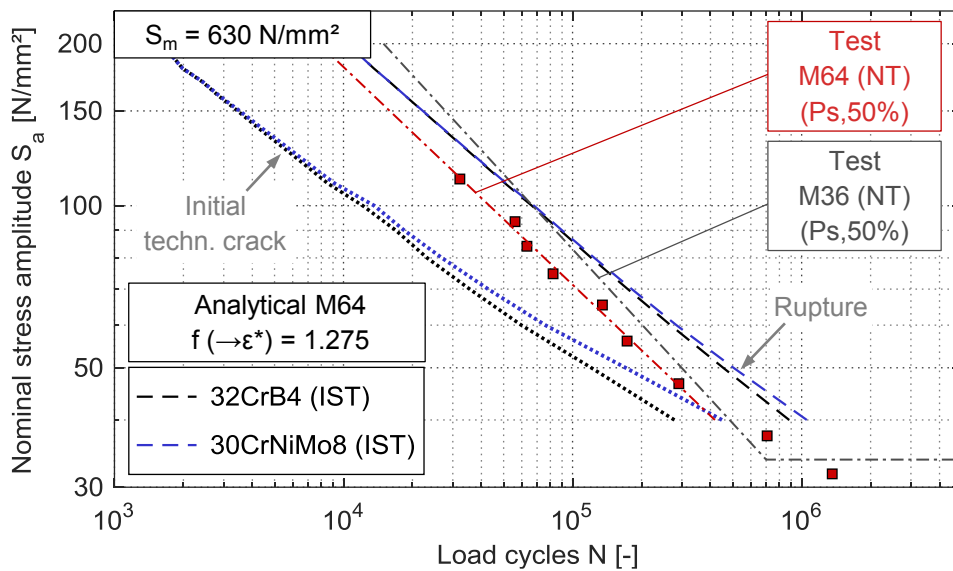


Figure 4-42: Impact of the bolt material in the analytical fatigue calculation of the M64 HV-bolt sets ( $P_J$  damage parameter,  $n_s = 1.0$ )

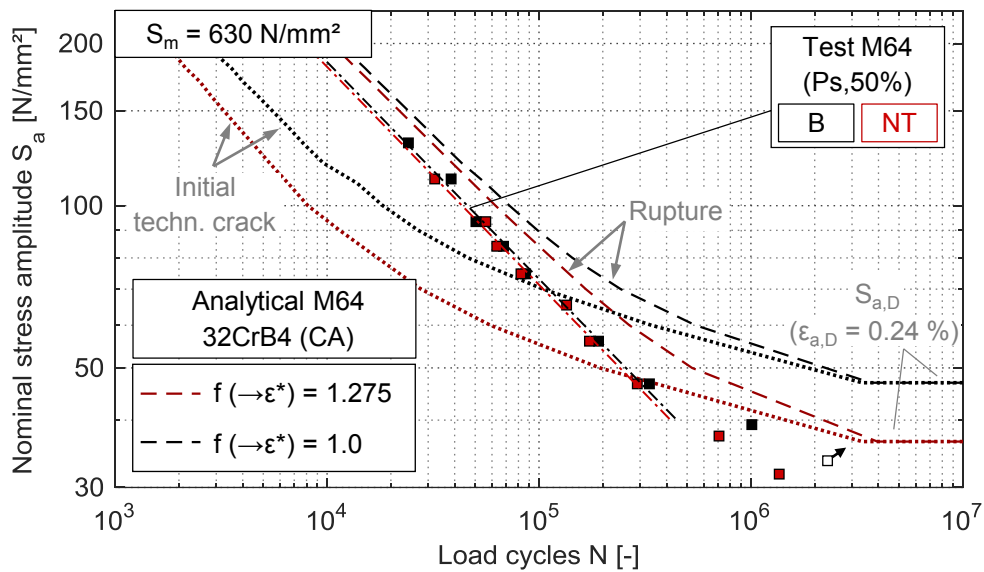


Figure 4-43: Comparison of analytical fatigue calculations for M64 HV-bolts (B, NT) with and without consideration of the strain enhancement factor to experimental results ( $P_J$  damage parameter,  $n_s = 1.0$ )

Nevertheless, the result comparison illustrated in Figure 4-43 shows that only with consideration of a strain enhancement factor in the strain-life concept an acceptable approximation of the experimental results is achieved. Without application of the strain factor, the fatigue strength, especially at lower load levels, is clearly overestimated. Thus, for the black M64 bolts also a reduction of crack initiation load cycles compared to their diameter M36 counterparts needs to be assumed.

Additionally to the variation of the materials, sensitivity studies were performed where the friction coefficient inside the paired thread was varied from the here regularly applied value  $\mu = 0.1$ . Thereby, in accordance with analogous analytical investigations by *Seybold* (2005) and *Marten* (2009), at axial loading conditions only a marginal impact was observed. In fact, with the here applied 2D axisymmetric FE-model, as refined implementation from the model used by *Marten*, an even smaller impact is indicated. Even with an increased friction coefficient  $\mu = 0.3$ , which can be considered close to the theoretical upper end for a completely degreased steel to steel contact surface (see *Kloos & Thomala*, 1979), only a marginally increased notch sensitivity factor of  $K_t = 4.60$  is derived (compared to  $K_t = 4.56$  for  $\mu = 0.1$ , see Chapter 4.3.2). In an analytical fatigue calculation, considering both crack initiation and macro crack propagation, this leads to an irrelevant effect. The calculated S-N curves are almost identical to the results shown in Figure 4-43.

Consequently, given the obtained results of this and the previous section, the analytical fatigue investigations do not suggest that either a base material related or a geometrically imposed impact factor was causative for the low fatigue strength of the tested black M64 HV-bolts. Likewise, an increased friction coefficient, due to variant lubrication characteristics inside the thread, is not indicated as plausible justification.

### 4.5.3 Impact of loading conditions

#### Preload level

Finally, the sensitivity of the analytical fatigue assessment procedure to loading conditions shall be assessed. To this end, firstly, the impact of the preload level in analytical fatigue calculations with  $P_J$  and  $P_{SWT}$  damage parameters is evaluated in Figure 4-44. The analytical calculations are plotted in comparison to the fatigue test results from *Marten* (2009) on HV-bolts M48, which were executed at reduced mean load level  $S_m \approx 0.15 R_{p0.2}$ . As only NT hot-dip galvanized bolts were tested, the analytical results consider the introduced strain enhancement factor  $f = 1.275$ . Cyclic properties from constant amplitude tests for material 32CrB4 with endurance limit estimation were used. The considered load levels are restricted to nominal stress-ratios  $R > 0$  (for the lowest depicted mean load levels the nominal stress range varies between  $R \approx 0.6$  at the endurance limit and  $R \approx 0.1$  in the top region of the upper HCF). Due to the limitations of comparable macro-crack propagation material constants for corresponding stress-ratios, load cycles until rupture were only calculated for the nominal mean stress level  $S_m = 0.7 R_{p0.2}$ .

To accurately capture the assumable local loading conditions at the thread caused by the experimental load application, the initial loading path is calculated with the combined material consideration

approach, described in Chapter 4.3.3. Thereby, monotonic material conditions are assumed up to the nominal mean stress level  $S_m$ . For consideration of presumable cyclic relaxation effects during the following cyclic ramp up phase, cyclic stabilized material behaviour is supposed between  $S_m$  and upper load level  $S_{max}$ . As discussed in Chapter 4.3.3, the applied approach for calculation of the initial loading path notably affects the resulting mean load of the cyclic hysteresis at reduced nominal preloads (see also Figure 4-17).

The calculations confirm that, similar to the bolts of diameter M36 and M64, a good analytical approximation is also achieved to the experimental results of the M48 HV-bolts at reduced mean load level, if the  $P_J$  damage parameter is used (Figure 4-44, left). Due to the previously discussed mean stress dependent characteristics of the damage parameter (see Chapter 4.4.1), no deviations of the calculation results occur at considered mean stresses between 0.7 and approximately  $0.25 R_{p,0.2}$  (the coinciding crack initiation fatigue curves are therefore depicted in identical colouring). At mean load level  $0.15 R_{p,0.2}$  the analytical calculation predicts an incipient beneficial impact on the crack initiation fatigue life at higher load levels, as an effect of the lower part of the cyclic hysteresis falling below the theoretical crack opening stress considered in the  $P_J$ -parameter definition. Only at further decreased mean stress (not illustrated) the increase of analytically predicted fatigue life extends to lower load levels and eventually to the endurance limit (approx.  $0.1 R_{p,0.2}$ ). However, it needs to be considered that due to manufacturing tolerances at the actual bolt-to-nut assembly, at very low stress-ratios a presumable positive material damage behaviour can be superimposed by negative effects of an insufficient stress distribution inside the paired thread. Correspondingly, *Schneider* (2011) found that endurance limit estimations with the strain-life approach overestimate the experimental results of threaded fasteners of experiments with constant low nominal stress-ratio  $R = 0.1$ .

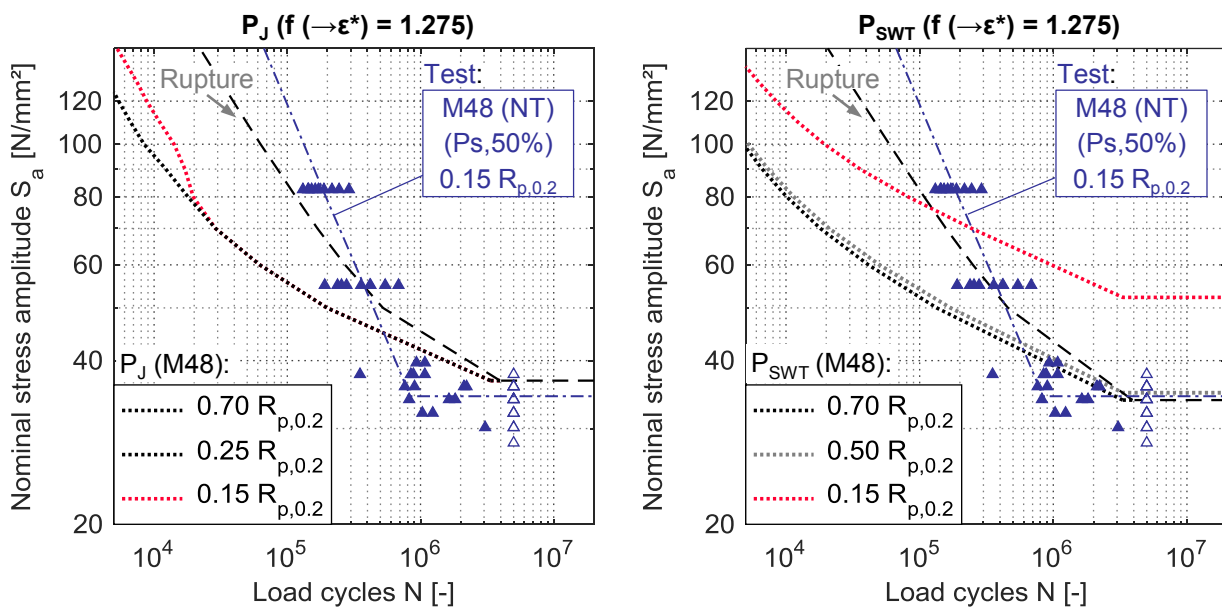


**Figure 4-44: Comparison of analytical fatigue calculations with different mean load levels to experimental fatigue results from *Marten* (2009) on NT-galvanized M48 HV-bolt sets ( $n_s = 1.0$ , material 32CrB4 (CA),  $\epsilon_{a,d} = 0.24$  %; left:  $P_J$ -parameter; right:  $P_{SWT}$ -parameter)**

For the here considered range of mean stress levels, the analytical calculations with the  $P_J$ -parameter reflect well the collated findings from experimental investigations in the literature for residual stress free bolts, rolled before heat treatment (see Chapter 2.1.4). They confirm that no substantial impact on the endurance limit is to be expected and that an impact is limited to the upper HCF, especially at higher load levels. It needs to be assumed that a beneficial effect of a reduced mean load will likewise occur in the macroscopic crack propagation phase. Correspondingly, contrary to the comparison with NT-galvanized M36 bolts tested at regular preload (Chapter 4.4.4), the analytically calculated load cycles until rupture at mean load level  $S_m = 0.7 R_{p,0.2}$  underestimate the experimental results at  $S_m \approx 0.15 R_{p,0.2}$ , especially at the upper tested load horizon.

At increased mean load levels compared to the conventional nominal preload, the analytical fatigue assessment procedure does not indicate an effect on the crack initiation fatigue life. Calculations with the  $P_J$ -parameter yield similar results with mean load level 0.9 as with  $0.7 R_{p,0.2}$ . This, however, is contradictory to experimental investigations by *Schneider* (1992) as well as *Weber* (2010), which both found a tendential reduction of the endurance limit at this very high mean load level range. It was validated in this dissertation that no substantial impact on the local hysteresis' stress level, and accordingly to the damage calculation, occurs as a consequence of an increased mean load level above  $0.7 R_{p,0.2}$ . However, demonstrably, the local strains at the maximal loaded turn of the thread significantly increase (see Figure 4-14). It can be assumed that the expansion of plastic deformations inside the thread may lead to a reduction of the support action at the notch root as well as possibly an enlargement of the fatigue critical area prone to crack initiation. Both related effects (i.e., stress-mechanical and statistical size effect) have been demonstrated to be mostly insignificant for the here considered bolt diameters. This circumstance provides basis for the assumption that the impact of high preload levels is less pronounced at large-size bolts than for the smaller bolt sizes, which were subject of investigation in the aforementioned studies in the literature. Still, further experimental validation in fatigue tests under high mean load level is indispensable for validation of this hypothesis.

Contrary to the calculations with the  $P_J$  damage parameter, the application of the  $P_{SWT}$ -parameter (Figure 4-44, right) leads to a strong overestimation of the experimentally determined fatigue strength at the reduced mean load level  $0.15 R_{p,0.2}$ . Evidently, the mean stress sensitivity of the damage parameter does not accurately describe the actual physical mean stress dependent behaviour of the bolts and anew, similar to its unrealistic susceptibility to the notch sensitivity factor, the  $P_{SWT}$ -parameter is proven overly sensitive. Thus, despite its generally good approximation of the fatigue strength at regular mean load level and notch sensitivity factor  $n_s = 1.0$ , its suitability for application in an analytical fatigue assessment of HV-bolts must be regarded as very limited.

### Bending impact

Unlike the conventional experimental set-up for bolt fatigue tests, the prevailing axial stresses of HV-bolts in L-shaped ring-flanges are systematically superimposed by eccentricity resultant bending stresses. The actually occurring magnitude of these stresses strongly varies in dependence of the flange geometry as well as preload and flange imperfections. With the purpose of illustrating the general effect of a combined stress state on the bolts' fatigue behaviour, the loading situation is emulated here in a simplified way. Corresponding analytical fatigue calculations with the  $P_J$  damage parameter, using a 3D axisymmetric FE-model (see Chapter 4.3.1) are illustrated in Figure 4-45. The two considered bending affected load situations are simulated in a way that the nominal stress at the bolt shaft is formed proportionally by 25 / 75 % bending / axial stresses (dotted blue line) and 50 / 50 % bending / axial stresses (dotted red line), respectively. Thereby, the bending stresses are included only in the cyclic hysteresis. In the initial loading path, representing the monotonic preloading process, still purely axial loading conditions are maintained.

The analytical calculations (including the strain enhancement factor  $f = 1.275$ ) are plotted in comparison to experimental results for NT-galvanized M48 HV-bolt sets tested under pure cyclic bending loading, published by *Schaumann & Marten* (2008). Similar to the analytical calculations, the established mean stress during the experiments can be considered purely axial. The experimental mean load level was approximately  $0.4 R_{p,0.2}$ , which is within the previously identified range without impact on the analytical calculation results with the  $P_J$  damage parameter. Due to the preload, the bolts were always maintained entirely under tension during the experiments. It is noted that the symbolic illustration of the loading condition in Figure 4-45 is thus representative only for the applied cyclic loading.

Additionally, the corresponding results for the axially loaded M48 bolts by *Marten* (2009), which were established in the same test series and with identical bolt production batches, as well as the analytical calculation results at pure axial loading are plotted as reference. Pure cyclic bending loading had to be omitted in the analytical calculations because of numerical restrictions.

For a valid comparison, all shown results, both analytical and experimental, need to be representative for fatigue failure at an identical location (i.e., in the first load bearing turn of the thread). In the analytical calculations this is secured by the circumstance that at the considered loading conditions the maximum stress and strain concentration at the paired thread still notably exceeds the further existing local peaks, for example under the bolt head or at the shaft transition. In the experimental investigations by *Schaumann & Marten* (2008) under bending loading a notable number of specimens failed due to fatigue crack initiation under the bolt head, whereby the location of the failure was strongly dependent on the bolt manufacturer. Compliantly with the evaluation approach suggested by *Schaumann & Marten* for the comparison of fatigue test results with varying failure location, in the below depicted illustration of bending fatigue test results only specimens from one production batch are included, where the occurrence of fatigue failure was restricted to the first load-bearing turn of the thread. When contemplating the entire test series, including additional specimens from two further bolt manufactures which mainly showed failures under the bolt head, a significantly

larger scatter of results occurs. Thereby the resultant mean value of the endurance limit for combined consideration of the failure locations lies below the here depicted value but still above the experimental endurance limit for axial loading.

It is noted that, unlike the axial load fatigue tests, the experiments under bending were aborted when the initiation of a fatigue crack of a magnitude noticeable by the resonance testing facility was detected, and not at full or directly impending rupture of the specimens. In the upper HCF the two depicted experimental S-N curves are therefore only limitedly comparable. In the analytical assessment of macro-crack propagation the consideration of bending stresses would generally be feasible by corresponding adjustment of the applied specific stress distribution along the crack. The applied auxiliary crack propagation model from *Pyttel et al. (2008)* was, however, only numerically validated and confirmed for pure axial loading. It is thus refrained from calculating full load cycles until rupture and only analytical crack initiation load cycles determined with the strain-life approach are shown. Nevertheless, direct comparability between analytical and experimental results under bending in the upper HCF cannot be granted either because the experimentally detected crack size needs to be assumed larger than the considered technical crack size of 0.1 mm in the calculations. The main benchmark criterion for a result evaluation is thus the endurance limit, which remains unaffected by the aforementioned restraints. Still, results are also depicted for the upper HCF for informative purposes.

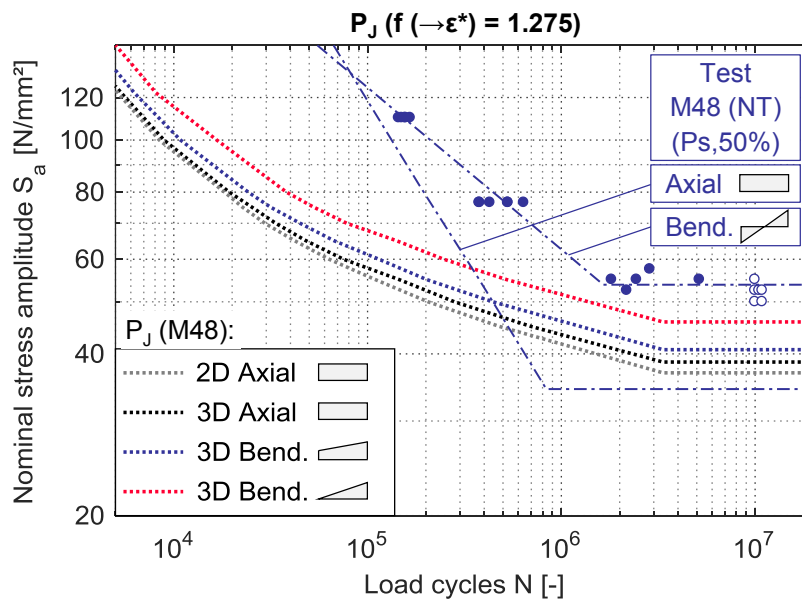


**Figure 4-45: Comparison of analytical fatigue calculations under axial loads with and without bending influence ( $P_J$ -parameter,  $n_s = 1.0$ , material 32CrB4 (CA),  $\epsilon_{a,d} = 0.24\%$ ) to experimental results for NT-galvanized M48 HV-bolt sets under pure axial and pure bending cyclical loading from *Marten (2009)* and *Schaumann & Marten (2008)* for crack initiation in the first load-bearing turn of the thread**

From the comparison between analytical results in Figure 4-45 with different loading conditions it can be confirmed that the expected beneficial effect of bending to the fatigue strength is reasonably represented by the calculation procedure. Thereby, with increasing bending contribution to the nominal stress state, the calculated endurance limit is noticeably elevated compared to a calculation at

pure axial loading. It needs to be considered that, as indicated previously, for pure axial stresses the application of the 3D FE model representation for determination of the notch strains leads to a slight increase of the calculated fatigue strength compared to the application of a 2D axisymmetric model (depicted as reference in the grey dotted line). This numerical impact is presumed to be also included in the bending affected calculations in a similar order of magnitude. Thus, a valid qualification of the isolated impact of bending can be performed by comparison to the calculation results under axial loading using the equivalent 3D axisymmetric FE model.

In the calculation with 25 % bending contribution to the nominal stress, only a minor elevation of the calculated endurance limit compared to the analytical result with axial loads of a factor  $S_{a,d,bend} / S_{a,d,ax} \approx 1.05$  occurs. The beneficial impact noticeably increases at the calculation with 50 % bending impact on an endurance limit elevation of approximately 1.2. From the depicted experimental test results, restricted to the comparison between bolts with dominating failure location in the first load-bearing turn of the thread, an increased endurance limit of bolts tested under pure cyclic bending (100 %) of a factor of 1.5 was determined. The analytical results are therefore in good quantitative agreement with the experimental findings. From the calculations, it can be noticed that the beneficial impact on the fatigue strength does not increase linearly with the bending contribution in the nominal loading but distinctly develops at larger bending impact. Concerning HV-bolts in ring-flanges, the actual bending impact can be presumed relatively small to the here considered stress states. Thus, the expectable fatigue strength may be assumed very comparable to pure axial loading conditions and a potential beneficial impact caused by the loading situation needs to be considered as mostly insignificant.

The distribution of linear elastic stresses along the thread of the 3D axisymmetric FE model, which correlates with the development of elastic-plastic strains, is presented in Figure 4-46. The considered loading conditions are similar to the analytical calculation in Figure 4-45. Visibly, under bending influence a less severe stress concentration develops in the first load-bearing turn. Simultaneously, stress re-distributions are indicated by increasing concentrations in the last loaded turn and the free loaded thread. In accordance with the observations made with the analytical fatigue calculation results, a substantial decrease of the maximum notch stress concentration  $K_t$  only occurs at the stress state with larger bending contributions. At a stress state with only 25% bending impact, the stress development barely deviates from purely axial loading.

As further potential causes for the improvement of the fatigue strength with increasing bending impact, a stronger stress-mechanical support effect can be suspected. The latter may originate from a tendentially lower stress gradient in radial direction from the notch root, arising at bending affected compared to pure axial loading. However, for the here analytically evaluated loading situation with the largest bending impact (50 %), no significant differences of the stress gradient in the direct vicinity of the notch root occur compared to the calculation with axial loading (see Figure 4-36). Thus, similar to the axially loaded bolts, the support effect due to the stress gradient may be regarded as



negligible also under a bending affected stress state. It is thus not considered to significantly contribute to the improved fatigue strength. Correspondingly, in all calculations, depicted in Figure 4-45, the support number was maintained as  $n_s = 1.0$ .

In conclusion, the improved fatigue strength evoked by bending, at large-size bolts is dominantly attributable to the changing stress distribution inside the thread. For small bolts, where the stress-gradient is considered to impose a stronger impact, an additional beneficial effect may occur. Moreover, an impact of a changing critical loaded surface area (i.e., statistical size effect) is thinkable.

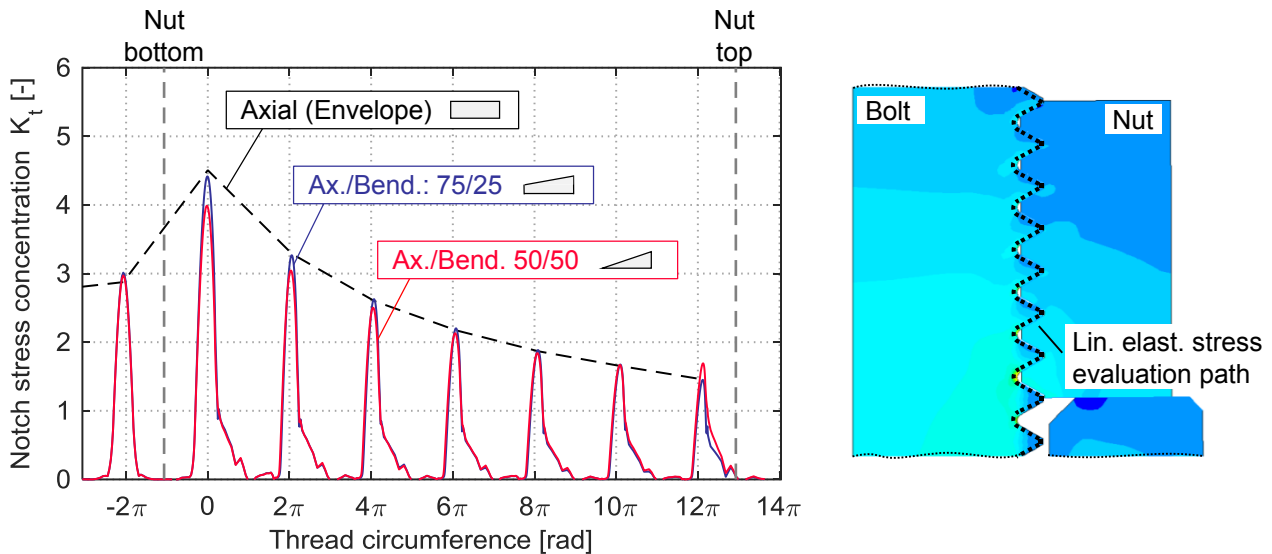


**Figure 4-46: Distribution of linear elastic notch stress concentration along the thread at purely axial and bending affected nominal loading calculated with axisymmetric 3D FE model**

#### 4.6 Findings

The previous chapter contained thorough investigations on the analytical fatigue assessment of large-size HV-bolts. The applied methodology was based on the established strain-life approach and supplemented by linear elastic fracture mechanics calculations. With the fundamental background of earlier works, a further development for the application to large-size HV-bolts was systematically elaborated. Moreover, the refined methodology was used to exemplary assess specific fatigue-relevant characteristics, such as size effects, material impacts and loading conditions. Even though such investigations can hardly substitute entirely comprehensive experimental investigations, they provide valuable insights with drastically reduced monetary and temporally efforts.

In the sequel, the most relevant findings are summarised which concern both the general application conditions of the evaluation method as well as conclusions regarding large-size bolt fatigue.

##### Provision of base material data

Comparative calculations with varying sets of material data have highlighted that knowledge about the actual base material's cyclic behaviour is crucial for an accurate analytical fatigue assessment. This mainly concerns the strain amplitude – fatigue life relation. Material data derived from a condensed testing procedure with strain-controlled Incremental-Step-Tests, instead of a comprehensive

constant amplitude test series, can provide a reasonable basis for fatigue life calculations in the upper high cycle fatigue range. However, they disqualify for any conclusions regarding the endurance limit, also if the latter is explicitly determined by supplemental stress-controlled tests.

Based on cyclic material data from strain-controlled constant amplitude tests, which were limited to the high upper high cycle fatigue range, a reasonably accurate approximation of the tested HV-bolts' endurance limit could be achieved by appropriately estimating the base material's strain endurance limit. Still, the full potential of the comprehensive material testing procedure may only be exploited, when constant amplitude material tests are also extended to a higher load cycle range and the material's endurance limit is experimentally verified. If the extended testing efforts associated with such tests are embraced, a strongly improved quality of analytical results obtained with the strain-life approach can be expected.

The analytical investigations have indicated that the effect of cyclic mean stress relaxation at high mean strains has a minor effect on the fatigue strength of preloaded HV-bolts. It may therefore be considered acceptable to neglect the effect in analytical calculations. Compared to the accurate experimental verification of the strain-life behaviour at loading conditions with  $R = -1$ , the execution of base material tests with high mean strains for investigation of cyclic relaxation can be regarded secondary.

For the application of linear elastic fracture mechanics, solely standard material parameters from the literature were applied. Since in the upper high cycle fatigue range fatigue characteristics of HV-bolts can be considered strongly affected by macro-crack propagation, it is recommendable to take actual fracture mechanical properties of customary HV-bolt base materials into closer consideration.

### **Numerical assessment of local loading conditions**

It was verified that for large-size HV-bolt sets the consideration of the actually given continuous pitch of the bolt thread within a 3D numeric implementation does not result in a more severe fatigue critical stress and strain development inside the paired thread, compared to an axisymmetric modelling approach. Instead, the results suggest an improved stress redistribution capability when the continuous thread pitch is incorporated. Resultant slightly lower stress and strain peaks inside the thread lead to an increased fatigue life estimation in the analytical fatigue calculation. However, a 3D model implementation is considerably more sensitive to numerical modelling characteristics than a 2D axisymmetric model and requires extensive numerical adjustment studies. It is therefore advisable to favour a 2D axisymmetric FE modelling approach for the assessment of local loading conditions of large-size HV-bolts. If the analysis requires the consideration of the continuous pitch (e.g., when assessing stress states under rotational tightening), corresponding FE models need to be evaluated with high diligence. For the consideration of bending affected stress states, the application of a rotational symmetric extension of a 2D plane element to a 3D volume element model can be regarded a suitable simplified modelling approach. However, also here the aforementioned remarks apply. Still, at all modelling approaches numerical sensitivity studies to mesh and contact definitions are indispensable.

### Analytical fatigue damage assessment

Among three investigated damage parameters, the  $P_J$ -parameter by *Vormwald* (1989) has proven vastly superior for the assessment of fatigue damage until technical crack initiation of preloaded, large-size HV-bolts. Contrary, due to its pronounced mean stress sensitivity at the relevant notch sharpness and loading conditions, the popular  $P_{SWT}$ -parameter needs to be regarded limitedly suitable. Especially at calculations with mean stresses, reduced from the nominal preload level, calculations with the  $P_{SWT}$ -parameter lead to unrealistic results. Moreover, it shows overly sensitive to a possibly incorporated notch sensitivity factor. Even though earlier studies had indicated certain potentials, the  $P_M$ -parameter by *Narberhaus* (1999) can be considered unqualified for the application in the here presented evaluation methodology for large-size HV-bolts.

A notch sensitivity factor can be used to incorporate both stress-mechanical and statistical size effects to the analytical calculations. However, the performed evaluations suggest that a stress-mechanical support action has an insignificant effect at the diameter range  $\geq M36$  and hence superior results are achieved when the corresponding notch sensitivity factor is maintained at  $n = 1.0$ . Also a statistical size effect, incorporated based on a weakest-link model and the relation of fatigue critical surface areas, only has a small impact on the here considered large-size diameter range. In the present study it is therefore found acceptable to likewise disregard the effect in the analytical fatigue calculation for improvement of results. However, generally its actual magnitude, when incorporated into the strain-life approach, also depends on the size of the specimens, used for determination of base material data. It is thus recommended to generally analyse the potential impact constituted by the statistical size effect. If found appropriate, a notch sensitivity factor may then be constituted by the statistical rather than the conventionally applied stress-mechanical consideration. The statistical size effect also gains importance at bolt diameters smaller than contemplated in the here presented study.

For fatigue calculations of hot-dip galvanized HV-bolts, the originally applied calculation methodology needs to be modified. To incorporate the complex damage mechanism considered decisive for the negative effect of hot-dip galvanizing, a simplified engineering model is suggested. Thereby, an empirically defined enhancement factor is applied to the local strain development, numerically determined for conditions without boundary layer. The strain enhancement factor leads to increased stress and strain ranges of the hysteresis compared to uncoated conditions at identical nominal loading, and thus a larger damage effect. The procedure is in accordance with the hypothesis, introduced in the literature, that a microscopic stress concentration effect at shrinkage cracks in the zinc layer is causative for the impact on the fatigue strength.

The application of simplified analytical crack propagation models combined with established material parameters for the application to HV-bolts has proven an appropriate auxiliary tool for the estimation of full load cycles until rupture. Among potential models, a hollow cylinder representation under variable stress with circumferential surface crack, as suggested by *Pyttel et al.* (2008), can be considered most appropriate. However, in the absence of fracture mechanics software for numerical integration of the geometry function, a simplified round bar model at constant tension can be regarded

an acceptable alternative. Nonetheless, the here applied simplified and strongly generalized methodology for application of linear elastic fracture mechanics to large-size HV-bolts lacks potential for systematic evaluation of fatigue-relevant impact factors in the macro-crack propagation phase. Thus, for a more accurate analytical assessment in the upper high cycle fatigue range, especially at high load levels, advanced, numerically aided crack propagation models are necessary. Thereby, for instance, differently shaped fracture surfaces may be incorporated, which can be supposed to introduce an impact of hot-dip galvanizing to the endurable load cycles also in the macro-crack propagation phase.

### **Impact factors on large-size bolt fatigue**

Performed sensitivity studies suggest that in the large-size diameter range between M36 and M72 no significant size-effect is introduced by either, the variant notch geometry of the thread or the stress-mechanical support action related to the stress gradient. Likewise, no pronounced statistical impact needs to be expected. Neither of these factors may thus plausibly be assumed causative for the found discrepancies of the fatigue strength between M36 and M64 bolts in the experimental investigations.

In general, variant cyclic material properties of high-strength bolt materials can be considered to potentially introduce relevant scatter of endurable load cycles. However, between HV-bolts with diameters M36 and M64, experimentally investigated within the framework of this dissertation, rather comparable base material properties were confirmed, at least for the crack initiation phase. However, it needs to be presupposed that the reduction between normal temperature hot-dip galvanized bolts with diameters M36 and M64, present in the upper high cycle fatigue range, is dominantly caused by varying macro-crack propagation characteristics. Here, potential impact factors need to be further investigated.

Concerning the severe reduction of fatigue strength found for uncoated, black M64 HV-bolts an impact in both macro-crack propagation and crack initiation phase needs to be supposed. Given the previously described findings, neither a geometrical nor a material related impact can be assumed decisive. Likewise, potentially altered friction properties inside the thread were not indicated as plausible explanation. Thus, also after the analytical investigations, the exact cause for the obtained reduction of fatigue strength remains uncertain.

Presupposing an appropriate mean stress dependent damage assessment of the  $P_J$ -parameter, the analytical calculations indicate that crack initiation load cycles (and thus endurance limit) of large-size HV-bolts are mostly unaffected by the mean stress level above approximately  $0.15 R_{p,0.2}$ . However, in the upper HCF an additional mean stress impact needs to be expected during macro-crack propagation. Similar to the mean stress level, the experimentally acknowledged beneficial impact of bending on the fatigue strength of HV-bolts is reflected well in the analytical calculation. However, a significant effect is only introduced at pronounced bending contributions. At superimposed stress states which are substantially dominated by axial loading, as expectable in conventional flange geometries, the fatigue resistance is to be supposed very similar to purely axial loading conditions.



## **5 Summary and Future Research**

### **5.1 Summary**

The fatigue safety of large-size bolting assemblies in ring-flange connections is of fundamental importance for the structural integrity of support structures for wind turbines. Prior to the research presented in this dissertation, the cyclic load bearing characteristics of HV-bolt systems were not properly verified for the range of large diameters, commonly used in practical application. Experimental knowledge about the impact of the bolt diameter on the fatigue strength, especially under loading conditions with representative high mean stress level, was missing. Moreover, the impact of hot-dip galvanizing, required for corrosion protection, was not conclusively quantified.

The review of the state of the art acknowledged that the validation of the design assumptions used for dimensioning of large-size bolting assemblies was primarily provided by a sole fatigue test series on HV-bolts of diameter M48. Even though comprehensive, the respective tests were performed at a substantially reduced mean load level, compared to the nominal preload. This had imposed insecurities regarding the transferability to the actual loading conditions. Comprising tests on specimens from multiple manufactures, the investigations still provided a fundamental groundwork for the here presented extended investigations. Apart from the mentioned study, further knowledge about specific fatigue characteristics of HV-bolts was mostly established in investigations on substantially smaller diameters than applied in today's modern support structures for wind turbines. This is due to the fact that fatigue testing on large-size HV-bolts, especially at representative mean load level, are cost and time consuming because of the high required testing loads. Therefore, analytical fatigue assessment methods, in particular the strain-life concept supplemented by linear elastic fracture mechanics, were contemplated in the here presented research as potentially capable additions to essential experimental investigations. Consequently, the performed research had two major aims. The first was the extension of the experimental validation of the HV-bolts' fatigue characteristics to the large-size diameter range at representative loading conditions. Secondly, but equally significant, was the methodical investigation of an analytical fatigue assessment procedure that is suitable for the evaluation of specific fatigue-relevant impact factors.

To appropriately supplement the hitherto available experimental background, a systematic testing program was implemented, consisting of three different steps. Firstly, a fundamental baseline was established by an extensive test series with more than 100 individual test runs on HV-bolt sets of diameter M36. Secondly, the experimental scope was extended to bolts with very large diameter M64, representative for the upper range of commonly applied HV-bolt sizes. Due to the high technical requirements, this test series was performed with a reduced number of specimens compared to the M36 tests. Thirdly, the two aforementioned test series performed at constant amplitude loading were supplemented by tests on M36 HV-bolts with variable amplitude loading sequences, to evaluate the bolts' fatigue performance at less academic and more service-alike loading conditions. All mentioned tests were performed at representative high mean load level at designated pure axial loading. Moreover, the impact of the boundary layer effect was investigated by including tests in all series on uncoated, black as well as hot-dip galvanized specimens.

The tests revealed a substantial impact of hot-dip galvanizing on the fatigue performance, which was equivalently attested at constant as well as variable amplitude loading. The magnitude of the effect was quantified for the M36 HV-bolts at constant amplitude loading with a reduction of the endurance limit of approximately 20 %, compared to uncoated conditions. Moreover, a notable decrease of the fatigue strength was also imposed in the upper high cycle fatigue range. The cause for the negative impact is presumably attributable to shrinkage cracks in the zinc boundary layer that lead to a premature fatigue crack initiation. However, the superior fatigue performance of uncoated specimens was not confirmed on the tested M64 HV-bolts. Here, the fatigue strength of black and hot-dip galvanized bolts was found at an almost identical level, owing to a considerable reduction of the fatigue strength between uncoated M36 and M64 HV-bolts. Thus, without the aid of further systematic investigations of potential causes, a superior fatigue classification in the design of large-size HV-bolts without corrosion protection needs to be questioned. Even though significantly less pronounced, a slight reduction of fatigue strength was also observed between the tested M36 and M64 bolts with hot-dip galvanizing boundary layer, which was increasingly pronounced at higher load levels. However, the found discrepancies could not conclusively be ascribed to the increased bolt diameter. Instead, the variant production chain and manufacturer as well as loading frequency might likewise have had a pivotal effect.

Despite the variations between the experimentally determined fatigue strengths, the secure coverage given by the fatigue classification of HV-bolts in the detail catalogue of the Eurocode 3 (FAT50) was confirmed for all tested bolt configurations. Thereby, considering the extended experimental background, the necessity of a further reduction of the fatigue class was indicated for bolt sizes larger than M36. However, the corresponding diameter reduction function applied in the Eurocode appeared conservative. Furthermore, the tests performed at variable amplitude loading indicated a notable underestimation of fatigue life at lower fatigue load levels, introduced by the considered damage accumulation hypothesis in the Eurocode 3. Recommendations for a less conservative service-life assessment given in the mechanical engineering guideline VDI 2230 could be confirmed by the here presented investigations. However, for any fatigue life verification of large-size HV-bolts subjected to amplitudes above the endurance limit with the S-N curves provided by the guideline, a shift of the knee-point to  $1 \cdot 10^6$  load cycles at a maintained endurance limit is indispensable to securely cover the experimental results.

In the systematic analytical investigations, the application of the strain-life concept to preloaded large-size HV-bolts was thoroughly evaluated and refined. For the studies, cyclic material parameters, determined on specimens from the core of the experimentally investigated M36 HV-bolts, served as the primary material data base. These parameters were established in strain-controlled constant amplitude material tests. Moreover, to extend the possibilities for validation of analytical calculation results, further cyclic material data was determined for the base materials of the tested M64 bolts as well as for bolts from the earlier test series on M48 HV-bolts. To reduce material testing efforts, in these tests an abbreviated testing procedure based on Incremental-Step-Tests was used. Thus, to enable a direct comparison of the two procedures, an additional set of material parameters was established for the M36 bolts' base material as well.

The provision of cyclic material data from the applied abbreviated testing procedure could be verified as a suitable alternative for the calculation of load cycles in the upper high cycle fatigue range. For the analytical evaluation of the endurance limit, however, comprehensive cyclic material data from constant amplitude material tests are indispensable. Despite lacking material test data in the relevant high load cycle range, in the present study an acceptable estimation of the material's strain endurance limit could be achieved based on relevant data from the literature. However, material specific results of elaborate material tests in the high load cycle range are expected to further improve the significance of analytical fatigue evaluation results.

For the determination of the local cyclic loading conditions in the paired thread with the aid of numerical methods, an axisymmetric finite element implementation was confirmed as a preferable modelling approach. In this context, it was verified that for a range of diameters between M36 and M72 no fatigue critical local stress and strain augmentations are imposed by a more elaborate, and likewise numerically sensitive, finite element implementation with consideration of the continuous thread pitch. For the final constitution of the cyclic hysteresis resulting from the nominal outer loading, monotonic material behaviour was considered along the initial loading path up to the nominal mean load. Afterwards cyclic stabilized material conditions were assumed.

Different damage parameters were evaluated for the necessary transformation of the damage contribution implied by the strain-based material data to the strongly mean stress affected cyclic loading conditions at the bolt thread. Thereby, the  $P_J$  damage parameter was identified as strongly preferable to the popular  $P_{SWT}$ - and the  $P_M$ -parameter, its empirical modification. To enable analytical fatigue calculations of crack initiation load cycles not only for uncoated but also for hot-dip galvanized HV-bolts, an engineering approach was introduced and verified to include the presumed complex damage mechanism induced by the zinc boundary layer in a simplified, manageable manner. Thereby, a strain-enhancement factor was applied to the numerically determined relation between outer loading and local strains. The magnitude of the factor was empirically calibrated, based on the experimentally quantified variation of the M36 bolts' endurance limit with undisturbed black and galvanized boundary layers.

Finally, to enable an appropriate comparison between the analytical and experimental fatigue strengths, macroscopic crack propagation load cycles were calculated additionally, with the aid of linear elastic fracture mechanics. To this end, established generalized analytical models and fracture mechanics material parameters were used.

As such, with the elaborated fatigue assessment procedure good approximations to all considered experimental test series on M36 and M64 HV-bolts at nominal mean load level as well as M48 HV-bolts at reduced mean load level were achieved. This also implied calculations with superimposed axial and bending loading. A beneficial impact of bending on the fatigue strength of the bolts, as acknowledged in the literature, was indicated by the analytical calculations to occur in a non-linear manner and only at pronounced bending contributions.



Potential size-effects were individually evaluated in terms of geometrical as well as statistical ramifications of an increased bolt diameter. For neither of these factors, the performed investigations indicated a meaningful impact on the fatigue strength for bolt diameters above M36. These findings corroborated the supposition, that the found differences between the experimentally investigated M36 and M64 HV-bolts were not primarily induced by diameter related effects.

## 5.2 Recommendations and future research

The experimental and analytical investigations in this dissertation indicated that the fatigue strength of large-size HV-bolt sets between the diameters M36 and M72 is not critically affected by geometrical or statistical diameter related impacts. Instead, found discrepancies between the available experimental investigation can probably be ascribed to generally scattering impact factors, as for instance the specific material properties, production chain and testing conditions. Given the achieved extended experimental background, a superior fatigue classification of large-size HV-bolts into another than the presently designated fatigue class FAT 50 of the Eurocode 3 is not justified. However, the obtained results evidently indicate that the incorporated steadily decreasing diameter reduction function of the Eurocode notably underestimates the fatigue strength of bolts with diameters  $> M48$ . It is thus recommended to seek for an adaption of the reduction function in order to avoid an overly conservative design. To this end, the exclusion of further reductions of the design fatigue class from diameter M48 upwards can be regarded as an appropriate modification. A reasonable range of aforementioned potential scattering impacts is already included in the existing experimental background for large-size HV-bolts because of the multitude of tests on bolts from variant manufactures and at different test stands. Still, further designated fatigue tests, which include the evaluation of the endurance limit of HV-bolts with very large diameters M64 or M72, could corroborate the proposed adaption.

A further potential of resolving given conservatisms in the design assumptions is indicated by adapting the applied damage accumulation hypothesis and the corresponding standardized S-N curve progression of the Eurocode 3 at load cycles below the endurance limit. Obviously, to this end, conclusive validation, required for an appropriate adaption, is lacking because of missing experimental background in the very high load cycle range between  $10^8$  and  $10^9$ , occurring during the service life of wind turbines. A systematic testing program, using modern resonance technology for experiments at constant amplitudes, supplemented by variable amplitude loading tests reaching into the relevant very high load cycle range could provide remedy in this regard. Even though such tests are highly elaborate, a potential correction of the applied damage accumulation hypothesis would significantly assist an economical service-life design.

Considering the two aforementioned factors, it needs to be assumed that with the presently applied design approach the fatigue life of large-size HV-bolts in ring-flanges is underestimated. This tendency is still increased by the commonly considered further reduction of the fatigue class, due the negligence of bending stresses in the stress transfer function between tower shell and bolts. A strong potential for a more economical design therefore also lies within the adaption of the underlying bolt

stress assessment approach, in order to enable a superior utilization of the bolt's actual fatigue capacity. In this context, the appropriate handling of flange imperfections and the secured ascertainment of the required preload need to be considered as equally significant as the fatigue strength of the bolts itself.

Analytical fatigue assessment methods have the potential to assist the required further development of the overall fatigue assessment approach of bolts in ring-flanges. In this regard, it is recommended to further evaluate the potential accuracy of the strain-life approach, when the progression of the base material's strain-life curve at high load cycle numbers, including the strain endurance limit, is experimentally ascertained. Moreover, advanced numerically aided macro-crack propagation models and individually determined fracture mechanics material parameters have great potentials to increase the accuracy of the analytical prediction in the upper high cycle fatigue range. Extended numerical models could then be used to assess the bolts' fatigue capacity under the actually occurring loading conditions within geometrically variable L- or T-shaped flanges.

For the accurate physical description of the boundary layer effect of hot-dip galvanizing as well as its incorporation into the analytical assessment approach apart from simplified engineering models, further advanced fundamental research is required.



## 6 References

### 6.1 Standards and technical guidelines

ASTM E739 (2010): Standard practice for statistical analysis of linear or linearized stress-life (S-N) and strain-life (e-N) fatigue data, ASTM International, November 2010.

BS 7608:2014+A1:2015 (2014): Guide to fatigue design and assessment of steel products, British Standards Institution, March 2014.

DAST - Guideline 022 (2009): Feuerverzinken von tragenden Stahlbauteilen [Hot-dip galvanizing of load-bearing steel components], Deutscher Ausschuß für Stahlbau DAST, December 2009 (in German).

DAST - Guideline 021 (2013): Schraubenverbindungen aus feuerverzinkten Garnituren M39 bis M72 entsprechend DIN EN 14399-4, DIN EN 14399-6 [Bolting assemblies with hot-dip galvanized sets M39 to M72 pursuant DIN EN 14399-4, DIN EN 14399-6], Deutscher Ausschuß für Stahlbau DAST, September 2013 (in German).

DSV-GAV (2009): Richtlinie für die Herstellung feuerverzinkter Schrauben [Guideline for production of hot-dip galvanized bolts], Deutscher Schraubenverband - Gemeinschaftsausschuss Verzinken, July 2009 (in German).

DIBt (2012): DIBt-Richtlinie für Windenergieanlagen – Einwirkungen und Standsicherheitsnachweise für Turm und Gründung [Guideline for wind turbines - Loading and verification of structural stability of tower and foundation], Deutsches Institut für Bautechnik (DIBt), 2012 (in German).

DIN 969 (1997): Verbindungselemente mit Gewinde - Schwingfestigkeitsversuch bei Axialbelastung - Prüfverfahren und Auswertung der Ergebnisse [Threaded fasteners - Axial load fatigue testing - Test methods and evaluation of results], DIN Deutsches Institut für Normung e.V., December 1997 (in German).

DIN EN 10083-3 (2007): Steels for quenching and tempering - Part 3: Technical delivery conditions for alloy steels; German version, DIN Deutsches Institut für Normung e.V., January 2007.

DIN EN ISO 1461 (2009): Hot dip galvanized coatings on fabricated iron and steel articles - Specifications and test methods (ISO 1461:2009); German version, DIN Deutsches Institut für Normung e.V., October 2009.

DIN EN 1993-1-9 (2010): Design of steel structures – Part 1-9: Fatigue; German version, DIN Deutsches Institut für Normung e.V., December 2010.

DIN EN 1993-1-8/NA:2010-12 (2010): National Annex – Nationally determined parameters – Eurocode 3: Design of steel structures – Part 1-8: Design of joints; German version, DIN Deutsches Institut für Normung e.V., December 2010.

- DIN EN 1090-2:2011-10 (2011): Execution of steel structures and aluminium structures - Part 2: Technical requirements for steel structures; German version, DIN Deutsches Institut für Normung e.V., October 2011.
- DIN EN ISO 898-1 (2013): Mechanical properties of fasteners made of carbon steel and alloy steel - Part 1: Bolts, screws and studs with specified property classes - Coarse thread and fine pitch thread (ISO 898-1:2013); German version, DIN Deutsches Institut für Normung e.V., May 2013.
- DIN EN 14399-4 (2015): High-strength structural bolting assemblies for preloading - Part 4: System HV - Hexagon bolt and nut assemblies; German version, DIN Deutsches Institut für Normung e.V., April 2015 (in German).
- DIN EN ISO 6892-1 (2017 and 2009): Metallic materials - Tensile testing - Part 1: Method of test at room temperature (ISO 6892-1:2016 and 2009); German versions, DIN Deutsches Institut für Normung e.V., February 2017 and December 2009.
- DIN EN 10263-4 (2018): Steel rod, bars and wire for cold heading and cold extrusion – Part 4: Technical delivery conditions for steels for quenching and tempering; German version, DIN Deutsches Institut für Normung e.V., February 2018.
- DIN 18088-3 (2019): Tragstrukturen für Windenergieanlagen und Plattformen – Teil 3: Stahlbauten [Structures for wind turbines and platforms – Part 3: Steel structures], DIN Deutsches Institut für Normung e.V., January 2019 (in German).
- DNVGL-ST-0126Standard (2016): Support structures for wind turbines, DNV GL AS, April 2016.
- FKM-Guideline (2006): Bruchmechanischer Festigkeitsnachweis für Maschinenbauteile [Fracture mechanics proof of strength for engineering components]; German version, 3, Forschungskuratorium Maschinenbau, Verband Deutscher Maschinen- und Anlagenbau, 2006 (in German).
- FKM-Guideline (2012): Rechnerischer Festigkeitsnachweis für Maschinenbauteile aus Stahl, Eisen- und Aluminiumwerkstoffen [Analytical strength assessment of components made of steel, cast iron and aluminum materials in mechanical engineering]; German version, 6, Forschungskuratorium Maschinenbau, Verband Deutscher Maschinen- und Anlagenbau, 2012 (in German).
- GL Guideline (2012): Guideline for the Certification of Offshore Wind Turbines, Germanischer Lloyd Industrial Services GmbH (now DNV GL AS), December 2012.
- VDI Guideline 2230 (2015): Part 1: Systematic calculation of highly stressed bolted joints - Joints with one cylindrical bolt, Verein Deutscher Ingenieure (VDI), 2015-11.

## 6.2 Books, articles and handbooks

Agatonović, P. (1973): Verhalten von Schraubenverbindungen bei zusammengesetzter Betriebsbeanspruchung [Behaviour of bolting assemblies under combined service loading]. Dissertation, Technische Universität Berlin (in German).

Al Shamaa, D. (2015): Probabilistische Betrachtung der Schadensakkumulation für stählerne Schweißverbindungen [Probabilistic assessment of damage accumulation for steel welded joints]. Dissertation, Technische Universität Berlin, Institut für Bauingenieurwesen, Shaker, Aachen, Germany (in German).

Alt, A. (2005): Dauerfestigkeitsprüfung und Dauerfestigkeit von Schraube-Mutter-Verbindungen unter kombinierter Zug- und Biegebelastung [Endurance limit and endurance limit testing of bolt-nut connections under combined tensile- and bending loading]. Dissertation, Technische Universität Berlin, VDI Verlag, Düsseldorf, Germany (in German).

Alt, A.; Mertens, H.; Arz, U.; Blessing, L.; Berger, C. (2007): Schwingfestigkeit von Schraube-Mutter-Verbindungen [High cycle fatigue of bolted connections]. In *Materialwissenschaft und Werkstofftechnik* 38, No. 5, pp. 402–409 (in German).

Bannantine, J. A.; Comer, J. J.; Handrock, J. L. (1990): Fundamentals of metal fatigue analysis, Prentice Hall, Englewood Cliffs, USA.

Bargel, H.-J.; Schulze, G. (2012): Werkstoffkunde [Materials Science], 11<sup>th</sup> Edition, Springer Vieweg, Berlin, Germany (in German).

Bäumel, A.; Seeger, T. (1990): Materials Data for Cyclic Loading, Supplement 1, Elsevier, Amsterdam, Netherlands.

Bercea, N. L. (2001): Entwicklung eines internettauglichen Programmsystems zur Berechnung von Schraubenverbindungen [Development of an application software for calculation of bolted connections suitable for internet application]. Dissertation, ETH Zürich, VDI Verlag, Düsseldorf, Germany (in German).

Berger, C.; Schaumann, P.; Stolle, C.; Marten, F. (2008): Ermüdungsfestigkeit hochfester Schrauben großer Abmessungen [Fatigue of high-strength bolts with large dimensions]. Final report, research project AiF 14728 N (in German).

Besseling, J. F. (1958): A theory of elastic, plastic, and creep deformations of an initially isotropic material showing anisotropic strain-hardening, creep recovery, and secondary creep. In *ASME Journal of Applied Mechanics* 25, pp. 529–536.

Böhm, J.; Heckel, K. (1982): Die Vorhersage der Dauerschwingfestigkeit unter Berücksichtigung des statistischen Größeneinflusses [The prediction of the fatigue strength with regard to the statistical size effect]. In *Zeitschrift für Werkstofftechnik* 13, No. 4, pp. 120–128 (in German).

Boller, C.; Seeger, T. (1987): Materials Data for Cyclic Loading, Part B: Low-Alloy Steels, Elsevier, Amsterdam, Netherlands.

- Bruder, T.; Seeger, T. (1996): Fatigue analysis for surface-strengthened notched specimens using the local strain approach. In *Fatigue 96, Proceedings of the 6th International Fatigue Congress, Vol. 2*, pp. 1327–1332.
- Christ, H.-J. (1991): Wechselverformung von Metallen [Cyclic deformation of metals], Springer, Berlin, Heidelberg, Germany (in German).
- Clormann, U. H.; Seeger, T. (1986): Rainflow-HCM. Ein Zählverfahren für Betriebsfestigkeitsnachweise auf werkstoffmechanischer Grundlage [Rainflow-HCM. A counting method for fatigue strength evaluation based on material behaviour]. In *Stahlbau* 55, No. 3, pp. 65–71 (in German).
- D'Agostino, R. B. (1986): Goodness-of-fit techniques, 1<sup>st</sup> Edition, Marcel Dekker Inc., New York, USA.
- Dixon, W. J.; Mood, A. M. (1948): A method for obtaining and analyzing sensitivity data. In *Journal of the American Statistical Association* 43, No. 241, pp. 108–126.
- Dowling, N. E. (1987): J-integral estimates for cracks in infinite bodies. In *Engineering Fracture Mechanics* 26, No. 3, pp. 333–348.
- Dragoni, E. (1997): Effect of thread pitch on the fatigue strength of steel bolts. In *Proceedings of the Institution of Mechanical Engineers Part C* 221, No. 8, pp. 591–600.
- Dünel, V. (1999): Schwingfestigkeit von Schraubenverbindungen – Optimierte Versuchsdurchführung und deren Anwendung bei der Untersuchung von Randschicht- und Oberflächenzuständen [Fatigue strength of bolting assemblies – optimised test execution and evaluation for the assessment of boundary layer and surface conditions]. Dissertation, Technische Universität Darmstadt, Fachbereich Maschinenbau, Shaker, Aachen, Germany (in German).
- Eder, M. A.; Haselbach, P. U.; Mishin, O. V. (2018): Effects of coatings on the high-cycle fatigue life of threaded steel samples. In *Journal of Materials Engineering and Performance* 27, No. 6, pp. 3184–3198.
- el Dsoki, C.; Nieslony, A.; Kaufmann, H.; Krug, P. (2008): Neue Auswertungsmethode zur Bestimmung der Kennwerte der Dehnungswöhlerlinie und der Spannungs-Dehnungs-Kurve unter Berücksichtigung der Kompatibilität [New method for evaluation of the Manson-Coffin-Basquin and Ramberg-Osgood equations with respect to compatibility]. In *Materialwissenschaft und Werkstofftechnik* 39, No. 11, pp. 806–815 (in German).
- Erdogan, F.; Ratwani, M. (1970): Fatigue and fracture of cylindrical shells containing a circumferential crack. In *International Journal of Fracture Mechanics* 6, No. 4, pp. 379–392.
- Feldmann, H. (1981): Spannungsberechnung an Schraube-Muttern-Gewinden mittels der Methode der Finiten Elemente [Stress calculation at bolt-nut threaded fasteners by use of the finite element method]. Dissertation, Technische Universität Braunschweig, Fakultät für Maschinenbau und Elektrotechnik (in German).

- Feldmann, M.; Naumes, J.; Pak, D. (2011): Zum Lastverformungsverhalten von Schrauben in vorgespannten Ringflanschverbindungen mit überbrückten Klaffungen im Hinblick auf die Ermüdungsvorhersage [Load-deformation behaviour of preloaded bolts in ring-flange connections with bridged gaps with regard to a fatigue behaviour prediction]. In *Stahlbau* 80, No. 1, pp. 21–29 (in German).
- Forman, R. G.; Kearney, V. E.; Engle, R. M. (1967): Numerical analysis of crack propagation in cyclic-loaded structures. In *Journal of Basic Engineering, Transactions of the ASME* 89, pp. 459–463.
- Gottlieb, G. E. (2015): Bewertung der Ermüdungsfestigkeit feuerverzinkter HV-Schrauben auf Grundlage örtlicher Beanspruchungen [Fatigue assessment of hot-dip galvanized HV-bolts based on local stresses and strains]. Master's thesis, Leibniz Universität Hannover, Institut für Stahlbau (in German, unpublished).
- Gudehus, H.; Zenner, H. (1999): Leitfaden für eine Betriebsfestigkeitsrechnung - Empfehlungen zur Lebensdauerabschätzung von Maschinenbauteilen [Guideline for a service life fatigue calculation - recommendations for the service life estimation of machine engineering components], 4<sup>th</sup> Edition, Verlag Stahleisen, Düsseldorf, Germany (in German).
- Haibach, E. (1970): Modifizierte lineare Schadensakkumulationshypothese zur Berücksichtigung des Dauerfestigkeitsabfalls mit fortschreitender Schädigung [Modified hypothesis of linear damage accumulation for consideration of reduction of the endurance limit with progressing damage]. Technical Report 50, Fraunhofer-Institut für Betriebsfestigkeit, Darmstadt (in German).
- Haibach, E. (2006): Betriebsfestigkeit - Verfahren und Daten zur Bauteilberechnung [Fatigue strength - Procedures and data for calculation of structural components], 3<sup>rd</sup> Edition, Springer, Berlin, Heidelberg, Germany (in German).
- Hertel, O. (2016): Prognose der Anrisslebensdauer gekerbter Bauteile bei mehrachsiger nichtproportionaler Betriebsbelastung [Prediction on crack initiation fatigue life of notched components under multi-axial non-proportional loading]. Dissertation, Technische Universität Darmstadt, Institut für Stahlbau und Werkstoffmechanik (in German).
- Hertel, O.; Vormwald, M. (2014): Multi-axial fatigue assessment based on a short crack growth concept. In *Theoretical and Applied Fracture Mechanics* 73, pp. 17–26.
- Hobbs, J. W.; Burguete, R. L.; Patterson, E. A. (2003): Investigation into the effect of the nut thread run-out on the stress distribution in a bolt using the finite element method. In *Journal of Mechanical Design* 125, No. 3, pp. 527–532.
- Hück, M. (1983): Ein verbessertes Verfahren für die Auswertung von Treppenstufenversuchen [An improved method for the evaluation of staircase tests]. In *Zeitschrift für Werkstofftechnik* 14, No. 12, pp. 406–417 (in German).
- Hück, M.; Bergmann, J.; Schütz, W. (1988): Relative Miner-Regel [Relative Miner's-rule]. In *Gemeinschaftsarbeit PKW-Industrie/IABG*, No. TF-2022 (in German).



- Jakubowski, A. (2003): Ermüdungssichere Bemessung geschraubter Ringflanschstöße in turmartigen Stahlbauten unter besonderer Berücksichtigung von Flanschimperfektionen [Fatigue-proof design of bolted ring-flanges in structural steel towers under particular consideration of flange imperfections]. Dissertation, Universität Essen, Institut für Stahlbau, Cuvillier, Göttingen, Germany (in German).
- Kaiser, B.; Beyer, S.; Dünkel, V.; Schneider, W. (1995): Schraubenverbindungen – Beanspruchungsverteilung unter ruhender und schwingender Belastung [Bolted connections - Load distribution under steady and cyclic loading]. In *Materialprüfung* 37, No. 1/2, pp. 14–18 (in German).
- Kampf, M. (1997): Dauerhaltbarkeit von Schrauben unter kombinierter Zug- und Biegebelastung [Endurance limit of bolts under combined axial and bending loading]. Dissertation, Technische Universität Berlin, Institut für Maschinenkonstruktion (in German).
- Kielbus, N.; Abe, H. (2016): Bewertung der Ermüdungsfestigkeit großer HV-Schrauben unter Betriebsbeanspruchung mit variablen Amplituden [Evaluation of the fatigue strength of large-size HV-bolts under service-loading conditions with variable amplitudes]. Seminar paper, Leibniz Universität Hannover, Institut für Stahlbau (in German, unpublished).
- Kloos, K. H.; Thomala, W. (1979): Zur Dauerhaltbarkeit von Schraubenverbindungen [On the endurance limit of bolted connections]. In *Ribe Blauheft*, Nr. 22 (Sonderausdruck aus "Verbindungstechnik" 11. Jahrgang) (in German).
- Kloos, K.-H. (1976): Einfluss des Oberflächenzustandes und der Probengröße auf die Schwingfestigkeitseigenschaften [Influence of boundary layer and specimen size to fatigue]. In *VDI-Bericht Nr. 268*, pp. 63–76 (in German).
- Koenigsmann, W.; Vogt, G. (1981): Dauerfestigkeit von Schraubenverbindungen großer Nenndurchmesser [Endurance limit of bolted connections with large nominal diameters]. In *Konstruktion im Maschinen-, Apparate- und Gerätebau* 33, No. 6, pp. 219–231 (in German).
- Kremer, U. (2005): Rissbildung und Rissfortschritt an Schraubenverbindungen unter schwingender Beanspruchung [Crack initiation and crack propagation for bolted connections under cyclic loading]. Dissertation, Technische Universität Darmstadt, Fachgebiet und Institut für Werkstoffkunde, Shaker, Aachen, Germany.
- Kuperus, A. (1974): The fatigue strength of tensile loaded tightened H.S.F.G. (High Strength Friction Grip) bolts. Research report 6-74-4, Stevin Laboratory, TU Delft.
- Lacher, G. (1986): Zeit- und Dauerfestigkeit von schwarzen und feuerverzinkten hochfesten Schrauben M20 der Festigkeitsklasse 10.9 unter axialer Beanspruchung [High-cycle fatigue strength and endurance limit of black and hot-dip galvanized high-strength bolts M20 of strength class 10.9 under axial loading]. In *Bauingenieur* 61, pp. 227–233 (in German).
- Landgraf, R. W.; Chernenkoff, R. A. (1988): Residual stress effects on fatigue of surface processed steels. In *Champoux, R. L., Kapp, J. A. u. Underwood, J. H. (Hrsg.): Analytical and Experimental Methods for Residual Stress Effects in Fatigue*, ASTM International, pp. 1–12.

- Landgraf, R. W.; Morrow, J. D.; Endo, T. (1969): Determination of the cyclic stress-strain curve. In *Journal of Materials* 4, pp. 176–188.
- Lorenz, C.; Stranghöner, N. (2016a): Numerical simulation of the preloading procedure of bolted assemblies considering plastic material behaviour. Insights and Innovations in Structural Engineering, Mechanics and Computation: Proceedings of the Sixth International Conference on Structural Engineering, Mechanics and Computation, Cape Town, South Africa, pp. 498–503.
- Lorenz, C.; Stranghöner, N. (2016b): Numerische Simulation des Anziehverhaltens von Schraubverbindungen unter Berücksichtigung des plastischen Materialverhaltens [Numerical simulation of the preloading procedure of bolted assemblies considering plastic material behaviour]. In *Stahlbau* 85, No. 7, pp. 451–458 (in German).
- Maaß, P.; Peißker, P. (2008): Handbuch Feuerverzinken [Handbook hot-dip galvanizing], 3<sup>rd</sup> Edition, WILEY-VHC, Weinheim, Germany (in German).
- Manson, S. S. (1965): Fatigue: A complex subject - Some simple approximations. In *Experimental Mechanics* 5, pp. 193–226.
- Marines, I.; Bin, X.; Bathias, C. (2003): An understanding of very high cycle fatigue of metals. In *International Journal of Fatigue* 25, No. 9-11, pp. 1101–1107.
- Marten, F. (2009): Zur Ermüdungsfestigkeit hochfester großer Schrauben [On fatigue resistance of high-strength large-size bolts]. Dissertation, Leibniz Universität Hannover, Institut für Stahlbau, Shaker, Aachen, Germany (in German).
- Masing, G. (1926): Eigenspannungen und Verfestigung beim Messing [Residual stresses and hardening of brass]. Proceeding of the 2nd International Conference of Applied Mechanics, Zürich, Switzerland, pp. 332-335 (in German).
- Mauch, H. (1999): Statistische Methoden zur Beurteilung von Bauteillebensdauer und Zuverlässigkeit und ihre beispielhafte Anwendung auf Zahnräder, Forschungsvorhaben Nr. 304 "Lebensdauerstatistik" [Statistical methods for assessment of service life and reliability and its exemplary application to gear wheels]. Final report, research project AiF-Nr. 11154/N, TU Clausthal, FVA-Forschungsberichte 1997-1999 (in German).
- Milella, P. P. (2013): Fatigue and corrosion in metals, Springer, Milan, Italy.
- Miner, A. M. (1945): Cumulative damage in fatigue. In *Journal of Applied Mechanics* 67, No. 12, pp. 159–164.
- Morrow, J. D. (1965): Cyclic plastic strain energy and fatigue of metals. In *Internal Friction, Damping and Cyclic Plasticity*, American Society of Testing and Materials, ASTM STP 387, pp. 45–87.
- Narberhaus, S. (1999): Untersuchungen zum Einfluß hoher Zug-Mittelspannungen auf die Schwingfestigkeit [Investigation on the effect of high tensile mean stresses to material fatigue]. Dissertation, Technische Universität Clausthal, Institut für Maschinelle Anlagentechnik und Betriebsfestigkeit (in German).

- Neuber, H. (1961): Theory of stress concentration for shear-strained prismatical bodies with arbitrary nonlinear stress-strain law. In *Transactions of the ASME, Journal of Applied Mechanics* 28, pp. 544–550.
- Neuber, H. (1985): Kerbspannungslehre [Notch stress theory], 3<sup>rd</sup> Edition, Springer, Berlin, Heidelberg, Germany (in German).
- Newman, J. C. (1984): A crack opening stress equation for fatigue crack growth. In *International Journal of Fracture* 24, pp. R131–R135.
- Oechsner, M.; Beyer, J.; Olveda, D.; Vormwald, M.; Beier, H. T.; Panic, D. (2014): Örtliche Bewertung der Schwingfestigkeit von Gewindeverbindungen II [Local fatigue assessment of threaded fasteners II]. Final report, FKM-project No. 297, Heft 322, Forschungskuratorium Maschinenbau e.V. (FKM) (in German).
- Oechsner, M.; Beyer, J.; Simonsen, F.; Schaumann, P.; Eichstädt, R. (2015): Experimentelle und rechnerische Bewertung der Betriebsfestigkeit von Schrauben großer Abmessung im Stahlbau unter Berücksichtigung von Randschichteinflüssen [Experimental and analytical assessment of the fatigue strength of bolts with large dimensions under consideration of boundary layer effects]. Final report, Research project P925/IGF-Nr.486 ZN, Forschungsvereinigung Stahlanwendung FOSTA e.V. (in German).
- Olveda, D.; Wuttke, U.; Oechsner, M.; Panic, D.; Beier, H. T.; Vormwald, M. (2014): Assessment of screws with local concepts. Proceedings of 4th Symposium on Structural Durability in Darmstadt (SoSDiD), Darmstadt, Germany, pp. 109–128.
- Otaki, H. (1979): Spannungsverteilung im Gewindegrund der Schraube einer Schraube-Mutterverbindung [Stress distribution inside the bolt thread of a bolt-nut fastener]. In *Konstruktion im Maschinen-, Apparate- und Gerätebau* 33, No. 3, pp. 121–126 (in German).
- Panic, D.; Beier, T. H.; Vormwald, M. (2014): Damage assessment of threaded connections based on an advanced material model and local concepts. In *Procedia Engineering* 74, pp. 119–128.
- Paris, P.; Erdogan, F. (1963): A critical analysis of crack propagation laws. In *Journal of Basic Engineering (ASME)* 85, pp. 528–533.
- Paris, P. C. (1962): The growth of cracks due to variations in load. Ph. D Thesis, Lehigh University Bethlehem, Pennsylvania.
- Pyttel, B.; Schwerdt, D.; Berger, C. (2011): Very high cycle fatigue – Is there a fatigue limit? In *International Journal of Fatigue* 33, No. 1, pp. 49–58.
- Pyttel, B.; Varfolomeyev, I.; Berger, C. (2008): Praktische Anwendung der FKM-Richtlinie "Bruchmechanischer Festigkeitsnachweis für Maschinenbauteile" [Practical application of FKM-Guideline "Fracture Mechanics Proof of Strength for Engineering"]. 40. Tagung des DVM-Arbeitskreises Bruchvorgänge (conference proceedings), Universität Stuttgart, pp. 25-39 (in German).

- Radaj, D.; Sonsino, C. M.; Fricke, W. (2006): Fatigue assessment of welded joints by local approaches, 2<sup>nd</sup> Edition, Woodhead Publishing, Cambridge, UK.
- Radaj, D.; Vormwald, M. (2007): Ermüdungsfestigkeit - Grundlagen für Ingenieure [Fatigue strength - basics for serious engineers], 3<sup>rd</sup> Edition, Springer, Berlin, Heidelberg, Germany (in German).
- Ramberg, W.; Osgood, W. R. (1943): Description of stress-strain curves by three parameters. National Advisory Committee for Aeronautics (NACA), Technical Report No. 902.
- Schaumann, P.; Eichstädt, R. (2015): Fatigue Assessment of High-Strength Bolts with Very Large Diameters in Substructures for Offshore Wind Turbines. Proceedings of the 25th International Ocean and Polar Engineering Conference (ISOPE), Kona, USA, pp. 260-267.
- Schaumann, P.; Eichstädt, R. (2016): Fatigue strength of preloaded hot-dip galvanized bolt assemblies with very large diameters. Insights and Innovations in Structural Engineering, Mechanics and Computation: Proceedings of the Sixth International Conference on Structural Engineering, Mechanics and Computation, Cape Town, South Africa, pp. 578-584.
- Schaumann, P.; Eichstädt, R.; Stang, A. (2018): Advanced performance assessment methods for high-strength bolts in ring-flange connections. In *Stahlbau* 87, No. 5, pp. 446–455.
- Schaumann, P.; Marten, F. (2008): Experimentelle Ermittlung von Wöhlerlinien großer Schrauben [Experimental determination of S-N curves for large-size bolts]. Final report, research project ZP 52-5- 16.125-1231/06, Deutsches Institut für Bautechnik (DIBt) (in German).
- Schaumann, P.; Marten, F. (2009): Fatigue resistance of high-strength bolts with large diameters. Proceedings of the International Symposium for Steel Structures (ISSS), Seoul, South Korea.
- Schneider, R. (2011): Örtliche Bewertung der Schwingfestigkeit von Gewindeverbindungen [Local assessment of fatigue of connections with threaded fasteners]. Dissertation, Technische Universität Darmstadt, Fachgebiet und Institut für Werkstoffkunde (in German).
- Schneider, R.; Wuttke, U.; Berger, C. (2010): Örtliche Bewertung der Schwingfestigkeit von Gewindeverbindungen [Local fatigue assessment of threaded fasteners]. Final report, research project AIF 15395N, Technische Universität Darmstadt, Fachgebiet und Institut für Werkstoffkunde (in German).
- Schneider, W. (1992): Beanspruchung und Haltbarkeit hochvorgespannter Schraubenverbindungen [Loads and durability of highly preloaded bolt assemblies]. Dissertation, Technische Hochschule Darmstadt, Fachbereich Maschinenbau (in German).
- Schütz, H. (1974): Schwingfestigkeit von Werkstoffen [Fatigue resistance of materials]. In *VDI-Berichte*, No. 214, pp. 45–47 (in German).
- Sedlacek, G.; Hobbacher, A.; Schleich, J. B.; Nussbaumer, A.; Maddox, S. J.; Brozzetti, J. et al. (2003): EN 1993-1-9, Background document to EN 1993-1-9. Draft version (unpublished).
- Sedlacek, G.; Hobbacher, A.; Schleich, J. B.; Nussbaumer, A.; Maddox, S. J.; Brozzetti, J. et al. (2007): EN 1993-1-9, Background document to EN 1993-1-9 (unpublished).

- Seeger, T.; Heuler, P. (1984): Ermittlung und Bewertung örtlicher Beanspruchungen zur Lebensdauerabschätzung schwingbelasteter Bauteile [Determination and assessment of local stresses and strains for the fatigue life prediction of structural components under cyclic loading]. Research report FF-20/1984, Technische Universität Darmstadt, Fachgebiet Werkstoffmechanik (in German).
- Seidel, M. (2001): Zur Bemessung geschraubter Ringflanschverbindungen von Windenergieanlagen [On design of bolted ring-flange connections of wind turbines]. Dissertation, Leibniz Universität Hannover, Institut für Stahlbau, Shaker, Aachen, Germany (in German).
- Seybold, R. (2005): Finite-Elemente-Simulation örtlicher Beanspruchungen in Schraubengewinden [Finite-element-simulation of local stresses and strains in threads]. Dissertation, Technische Universität Darmstadt, Fachgebiet und Institut für Werkstoffkunde, Shaker, Aachen, Germany (in German).
- Siebel, E.; Stieler, M. (1955): Ungleichmäßige Spannungsverteilung bei schwingender Beanspruchung [Irregular stress distribution at cyclic loading]. In *VDI-Zeitschrift* 97, No. 5, pp. 121–126 (in German).
- Simonsen, F. (2015): Der Einfluss von zinkbasierten Korrosionsschutzsystemen auf die zyklische Beanspruchbarkeit von Bauteilen aus Stahl [Influence of zinc-based corrosion protection systems on the fatigue resistance of structural steel components]. Dissertation, Technische Universität Darmstadt, Fachgebiet und Institut für Werkstoffkunde, Shaker, Aachen, Germany (in German).
- Smith, K. N.; Watson, P.; Topper, T. H. (1970): A stress-strain function for the fatigue of metals. In *Journal of Materials* 5, No. 4, pp. 767–778.
- Socie, D. F.; Marquis, G. B. (2000): *Multiaxia Fatigue*, SAE International, Warrendale, USA.
- Sonsino, C. M. (1993): Zur Bewertung des Schwingfestigkeitsverhaltens von Bauteilen mit Hilfe örtlicher Beanspruchungen [Evaluation of components fatigue behaviour on the basis of local strains and stresses]. In *Konstruktion* 45, No. 1, pp. 25–33 (in German).
- Sonsino, C. M. (2005): "Dauerfestigkeit" - Eine Fiktion ["Endurance limit" - A Fiction]. In *Konstruktion*, No. 4, pp. 87–92 (in German).
- Sonsino, C. M. (2008): Betriebsfestigkeit - Eine Einführung in die Begriffe und ausgewählte Bemessungsgrundlagen [Fatigue safety – An introduction into denotations and selected design principles]. In *Materialprüfung* 50, No. Heft 1/2, pp. 77–90 (in German).
- Steppeler, S. (2014): Zum Ermüdungsverhalten von Stumpfnahverbindungen bei sehr hohen Lastwechselzahlen [On fatigue behaviour of butt weld connections under very high load cycle numbers]. Dissertation, Leibniz Universität Hannover, Institut für Stahlbau, Shaker, Aachen, Germany (in German).
- Stranghöner, N.; Jungbluth, D.; Hüller, V.; Machura, G. (2016): Anziehen von geschraubten Verbindungen nach Eurocode 3 und DIN EN 1090-2 [Tightening of bolted connections according to Eurocode 3 and DIN EN 1090-2]. In *Stahlbau* 85, No. 5, pp. 327–335 (in German).

- Stranghöner, N.; Lorenz, C.; Feldmann, M.; Citarelli, S.; Bleck, W.; Münstermann, S.; Brinnel, V. (2018): Spröbruchverhalten hochfester Schrauben großer Abmessungen bei tiefen Temperaturen [Brittle fracture of high-strength bolts of large diameters at low temperatures]. In *Stahlbau* 87, No. 1, pp. 17–29 (in German).
- Thomala, W. (1978): Beitrag zur Dauerhaltbarkeit von Schraubenverbindungen [Contribution to endurance strength of bolted connections]. Dissertation, Technische Hochschule Darmstadt, Fachbereich Maschinenbau (in German).
- Ungermann, D.; Rademacher, D.; Oechsner, M.; Landgrebe, R.; Adelman, J.; Simonsen, F.; Friedrich, S.; Lebelt, P. (2014): Feuerverzinken im Stahl- und Verbundbrückenbau [Hot-dip galvanizing in steel and composite bridge construction]. Final report, ZUTECH research project P 835/06/2010 / IGF.-No. 351, Forschungsvereinigung Stahlanwendung FOSTA e.V. (in German).
- Ungermann, D.; Rademacher, D.; Oechsner, M.; Simonsen, F.; Friedrich, S.; Lebelt, P. (2015): Feuerverzinken im Brückenbau - Teil 1: Zum Einsatz feuerverzinkten Baustahls bei zyklisch beanspruchten Konstruktionen [Hot-dip galvanizing in bridge construction – Part 1: Using hot-dip galvanized mild steel for cyclic loaded structures]. In *Stahlbau* 84, No. 1, pp. 2–9 (in German).
- Unglaub, J.; Reininghaus, M.; Thiele, K. (2015): Zur Ermüdungsfestigkeit von feuerverzinkten Zugstäben mit Endgewinden [Fatigue of tension rods with hot dipped galvanized threads]. In *Stahlbau* 84, No. 8, pp. 584–588 (in German).
- Valtinat, G. (1994): Schwingfestigkeit von hochtemperaturverzinkten HV-Schrauben, die bis in den plastischen Bereich angezogen sind (Fatigue strength of high temperature hot-dip galvanized HV-bolts, which are preloaded up to the plastic range). Bericht Nr. 128 des Gemeinschaftsausschuß Verzinken e.V., Forschungsvorhaben GAV-Nr. FD 19 (in German).
- Vormwald, M. (1989): Anrisslebensdauervorhersage auf Basis der Schwingbruchmechanik für kurze Risse [Prediction of crack initiation life based on cyclic fracture mechanics for short cracks]. Dissertation, Technische Hochschule Darmstadt, Institut für Stahlbau und Werkstoffmechanik (in German).
- Vormwald, M.; Heuler, P.; Krae, C. (1994): Spectrum fatigue life assessment of notched specimens using a fracture mechanics based approach. In *Automation in Fatigue and Fracture: Testing and Analysis*, pp. 221–240.
- Vormwald, M.; Seeger, T. (1988): Nutzung der Anrisschwingspielzahl beim Incremental-Step-Test zur Abschätzung der Werkstoffwöhlerlinie [Use of the crack initiation life of the incremental step test to estimate a material's constant-amplitude fatigue life curve]. In *Materialprüfung* 30, No. 11-12, pp. 368–373 (in German).
- Vormwald, M.; Seeger, T. (2015): Betriebsfestigkeit auf Grundlage örtlicher Beanspruchungen [Fatigue safety based on local loading conditions]. Seminar documents, Technische Universität Darmstadt, Fachgebiet Werkstoffmechanik (in German).

- Wächter, M. (2016): Zur Ermittlung von zyklischen Werkstoffkennwerten und Schädigungsparameterwöhlerlinien [On determination of cyclic material parameters and damage parameter Woehler-curves]. Dissertation, Technische Universität Clausthal, Fakultät für Mathematik/Informatik und Maschinenbau (in German).
- Wagener, R. W. (2007): Zyklisches Werkstoffverhalten bei konstanter und variabler Beanspruchungsamplitude [Cyclic material behaviour at constant and variable amplitude loading]. Dissertation, Technische Universität Clausthal, Institut für Maschinelle Anlagentechnik und Betriebsfestigkeit (in German).
- Wang, Q.; Khan, M. K.; Bathias, C. (2012): Current understanding of ultra-high cycle fatigue. In *Theoretical and Applied Mechanics Letters* 2, No. 3, Article 031002.
- Weber, J. O. (2010): Beitrag zur betriebsfesten Auslegung von Schraubenverbindungen auf Grundlage moderner Betriebsfestigkeitskonzepte [Contribution to service-life fatigue design of bolted connection based on modern fatigue concepts]. Dissertation, Technische Universität Darmstadt, Fachgebiet Werkstoffmechanik, Shaker, Aachen, Germany (in German).
- Weibull, W. (1949): A statistical representation of fatigue in solids. In *Transactions of the Royal Institute of Technology, Stockholm* 27.
- Wiegand, H.; Kloos, K. H.; Thomala, W. (2007): Schraubenverbindungen - Grundlagen, Berechnung, Eigenschaften, Handhabung [Bolting assemblies - Fundamentals, Calculation, Characteristics, Handling], 5<sup>th</sup> Edition, Springer, Berlin, Heidelberg, Germany (in German).
- Wiegand, H.; Strigens, P. (1970): Die Haltbarkeit von Schraubenverbindungen mit Feingewinden bei wechselnder Beanspruchung [The durability of bolted connections with fine thread at alternating loads]. In *Industrie Anzeiger* 91, No. 91, pp. 2139–2144 (in German).
- Zenner, H.; Liu, J. (1992): Vorschlag zur Verbesserung der Lebensdauerabschätzung nach dem Nennspannungskonzept [Improved life time prediction by means of the nominal stress concept]. In *Konstruktion* 44, No. 1, pp. 9–17 (in German).

### 6.3 Product information and data sources

ANSYS Inc. (2016): Version 17.2 Documentation, SAS IP, Inc.

Boller, C.; Seeger, T.; Vormwald, M. (2008): Materials Database for Cyclic Loading, Fachgebiet Werkstoffmechanik, Technische Universität Darmstadt, Available online at [http://www.werkstoffmechanik.tu-darmstadt.de/materials\\_database/index.de.jsp](http://www.werkstoffmechanik.tu-darmstadt.de/materials_database/index.de.jsp), checked on 30.10.2017.

**Note:**

The previously presented list of references includes literature in both German and English language. German titles are supplemented with English translations to maintain comprehensibility to non-German readership. Where available, official translations presented in the context of the respective references are used. Otherwise, the translations are provided by the author in the best of his knowledge.





## 7 Lists

### 7.1 List of Figures

Figure 1-1: Ring-flange connection in wind turbine support structure (left) and HV-bolt sets with large diameters (right).....	1
Figure 2-1: Segment approach for the design of ring-flange connections acc. to <i>Seidel</i> (2001) (left) and schematic depiction of load transfer behaviour considering preload and flange imperfections acc. to <i>Schaumann et al.</i> (2018) (mid and right).....	6
Figure 2-2: Schematic stress distribution and usual range of $K_t$ and $K_f$ for a bolt-to-nut connection (left) and three-axial stress state in the cross-section of a notched specimen (right) acc. to <i>Wiegand et al.</i> (2007).....	7
Figure 2-3: Phases of the metallurgical fatigue process acc. to <i>Radaj et al.</i> (2006).....	8
Figure 2-4: Characteristic values of a harmonic, constant amplitude loading (left) and schematic progression of an S-N curve (right; adapted from <i>Gudehus &amp; Zenner, 1999</i> and <i>Radaj &amp; Vormwald, 2007</i> ).....	10
Figure 2-5: Schematic depiction of a load collective in discrete and continuous form (left) and fatigue-life curve and variants of the <i>Miner</i> hypothesis (original, elementary and modified form proposed by <i>Haibach, 1970</i> ) (right).....	12
Figure 2-6: Schematic depiction of fatigue crack initiation of hot-dip galvanizes structural components acc. to <i>Ungermann et al.</i> (2015).....	18
Figure 2-7: Normative S-N curves from EC 3 and VDI 2230 (left) and reference value of fatigue curves at $N = 2 \cdot 10^6$ load cycles as a function of bolt diameter (right).....	21
Figure 2-8: Equivalence of critical material volume at notch root and unnotched specimen acc. to <i>Bannantine et al.</i> (1990) (left) and denotations at hysteresis of local stresses and strains acc. to <i>Haibach</i> (2006) (right).....	24
Figure 2-9: Schematic depiction of fatigue crack growth rate curve (adapted from <i>Haibach, 2006</i> ).....	25
Figure 2-10: Schematic depiction of strain-life curve with elastic and plastic parts in dependence of hysteresis shape (left) and cyclic stress-strain curve as conjunction of peak values of stabilized cyclic hysteresis loops for material with cyclic softening behaviour (right) (adapted from <i>Bannantine et al., 1990</i> ).....	26
Figure 2-11: Transient material effects under strain controlled loading acc. to <i>Christ</i> (1991).....	28
Figure 2-12: Definitions for the damage parameter $P_J$ acc. to <i>Haibach</i> (2006).....	33
Figure 2-13: Schematic depiction of elastic stress gradient for calculation of the stress-mechanical support effect (left) and macroscopic support effect by plastic stress relief (right) acc. to <i>Vormwald &amp; Seeger</i> (2015).....	35

Figure 2-14: “Thin surface layer model” acc. to <i>Seeger &amp; Heuler</i> (1984).....	36
Figure 3-1: Investigated HV-bolt sets with different boundary layers (B: uncoated black; NT: normal temperature hot-dip galvanized; HT: high temperature hot-dip galvanized) ...	44
Figure 3-2: Test set-up for M36 HV-bolt tests under constant amplitude loading in electromotive resonance testing machine .....	45
Figure 3-3: Evaluation scheme of results in the TEL with the staircase method for black M36 HV-bolts .....	49
Figure 3-4: Alternative result evaluation in the TEL for black M36 HV-bolts with reduced sample size .....	50
Figure 3-5: Statistic scatter band and test results in the TEL for black M36 HV-bolts with full sample (left) and reduced sample (right).....	51
Figure 3-6: Test results in the upper HCF for black M36 HV-bolt .....	52
Figure 3-7: Percentile S-N curves for black M36 HV-bolts; left: without RRO; right: with RRO ....	53
Figure 3-8: Evaluation scheme of results in the TEL with the staircase method for NT-galvanized M36-HV bolts .....	54
Figure 3-9: Scatter band and results of the statistic evaluation in the TEL for NT-galvanized M36 HV-bolts .....	55
Figure 3-10: Test results in the upper HCF for NT-galvanized M36 HV-bolt .....	55
Figure 3-11: Percentile S-N curves and characteristic values for NT-galvanized M36 HV-bolts (with consideration of RRO) .....	56
Figure 3-12: High temperature hot-dip galvanized M36 HV-bolt sets with irregular failure locations at the shaft and under the bolt head.....	57
Figure 3-13: Regular evaluation scheme of results in the TEL with the staircase method for HT-galvanized M36-HV bolts and limit load cycle number $N_{lim} = 5 \cdot 10^6$ .....	58
Figure 3-14: Alternative evaluation scheme of results in the TEL with the staircase method for HT-galvanized M36-HV bolts and limit load cycle number $N_{lim} = 9 \cdot 10^6$ .....	58
Figure 3-15: Statistic scatter band and test results in the TEL for HT-galvanized M36 HV-bolts (limit load cycle number $N_{lim} = 5 \cdot 10^6$ ) .....	59
Figure 3-16: Test results in the upper HCF for HT-galvanized M36 HV-bolt .....	60
Figure 3-17: Percentile S-N curves and characteristic values for HT-galvanized M36 HV-bolts (with consideration of RRO) .....	61
Figure 3-18: Comparison of test results of M36 HV-bolts with different boundary layers .....	62
Figure 3-19: Test set-up for M64 HV-bolt tests under constant amplitude loading in servo-hydraulic testing machine.....	64

Figure 3-20: Test results and percentile S-N curves for black M64 HV-bolts (left: full results; right: excerpt (A) of the reference load horizon with modified test point M64-B*).....	66
Figure 3-21: Test results and percentile S-N curves for NT-galvanized M64 HV-bolts (left: full results; right: excerpt (A) of the reference load horizon with modified test point M64-NT*) .....	66
Figure 3-22: Comparison of test results of M64 HV-bolts with different boundary layers .....	68
Figure 3-23: Comparison of test results of M64 and M36 HV-bolt sets with uncoated, black (left) and NT hot-dip galvanized (right) boundary layer configuration.....	68
Figure 3-24: Derivation of an experimental load collective from the continuous <i>Gauss</i> collective in normalized representation ( $S_{a,i} / S_{a,max}$ ).....	72
Figure 3-25: Load sequence of variable amplitude tests in normalized representation derived from partial load collective.....	73
Figure 3-26: Classification and comparison of fatigue test results at variable amplitude loading of M36 HV-bolt sets with different boundary layer configurations .....	74
Figure 3-27: Comparison of experimental results on uncoated black M36 and M64 HV-bolt sets with normative S-N curves from EC 3 and VDI 2230 .....	77
Figure 3-28: Comparison of experimental results for hot-dip galvanized M36, M48 and M64 HV-bolt sets with normative S-N curves from EC 3 and VDI 2230 .....	77
Figure 3-29: Evaluation of test results by linear regression of logarithmic load cycle numbers with fixed slope of S-N curve for NT hot-dip galvanized HV-bolt sets of diameter M36 (a), M48 (b) and M64 (c) .....	79
Figure 3-30: Evaluation of the diameter dependent fatigue strength reduction considered in EC 3 based on experimental results by reference to the characteristic fatigue strength $\Delta S_c$ (nominal stress range) .....	80
Figure 3-31: Evaluation of the diameter dependent fatigue strength reduction considered in VDI 2230 based on experimental results by reference to the endurance limit $S_{a,D}$ (nominal stress amplitude) .....	82
Figure 3-32: Comparison of test results of NT-galvanized M36 HV-bolts at variable amplitudes to damage calculations with different adaptations of <i>Miner's</i> rule based on the experimental S-N curve.....	84
Figure 3-33: Comparison of test results of hot-dip galvanized M36 HV-bolts (NT and HT) at variable amplitudes to damage calculations with normative design S-N curves .....	85
Figure 4-1: Schematic illustration of the applied analytical fatigue assessment methodology .....	90
Figure 4-2: Means and scatter of materials strength values (left) and selected representative monotonic stress-strain relations (right) of investigated bolt materials.....	93

Figure 4-3: Cyclic material curves of M36 bolt material 32CrB4 derived from strain-controlled tests with constant amplitudes by <i>Oechsner et al.</i> (2015); left: strain-life curve; right: cyclic stress-strain curve.....	95
Figure 4-4: Load sequences of Incremental-Step-Tests .....	95
Figure 4-5: Stress-strain path of the first loading block (left) and a stabilized loading block at $1/2 N_c$ (right) from IST for M36 bolt material 32CrB4 (specimen extracted from black bolt) with $\varepsilon_{max} = 1.2 \%$ .....	96
Figure 4-6: Fatigue results of IST at different strain levels in terms of endurable blocks until crack initiation and corresponding load cycles as input for determination of strain-life curve.....	97
Figure 4-7: Comparison of cyclic material curves .....	98
Figure 4-8: Stress-strain histories from tests on M36 bolt material 32CrB4 with high mean strain $\varepsilon_m = 1.1 \%$ performed by <i>Oechsner et al.</i> (2015) .....	100
Figure 4-9: Results of strain-controlled tests under high mean strain $\varepsilon_m = 1.1 \%$ for M36 bolt material 32CrB4 according to <i>Oechsner et al.</i> (2015).....	100
Figure 4-10: Axisymmetric finite element models of a M36 HV-bolt set (left: 2D plane element model, right: 3D rotational volume element extension).....	104
Figure 4-11: Full 3D volume element model of a M36 HV-bolt set with continuous pitch of the thread (left: global model, right: sub model of maximum loaded bolt thread area) ..	104
Figure 4-12: Result evaluation paths at numerical models .....	106
Figure 4-13: Comparison of numerical results for an M36 HV-bolt set with different modelling approaches under linear elastic material behaviour .....	106
Figure 4-14: Local stresses (left) and local strains (right) inside the paired thread of an M36 HV-bolt set resulting from calculations with 2D axisymmetric and full 3D FE-model under elastic-plastic material behaviour (monotonic loading) at nominal load levels a: $0.2 \cdot R_{p,0.2}$ , b: $0.4 \cdot R_{p,0.2}$ , c: $0.7 \cdot R_{p,0.2}$ , d: $0.9 \cdot R_{p,0.2}$ .....	107
Figure 4-15: Maximum linear elastic notch stress concentrations $K_t$ in dependence of FE model type and bolt diameter .....	109
Figure 4-16: Synthesis of local cyclic stress-strain response.....	111
Figure 4-17: Comparison of cyclic hysteresis with different material behaviour during initial loading at nominal stress amplitude $S_a = 104 \text{ N/mm}^2$ and varying mean load levels (A: $S_m = 630 \text{ N/mm}^2$ ; B: $S_m = 0.5 \cdot S_m(A) = 315 \text{ N/mm}^2$ ; C: $S_m = 0.35 \cdot S_m(A) = 220 \text{ N/mm}^2$ ; D: $S_m = 0.25 \cdot S_m(A) = 157 \text{ N/mm}^2$ ) .....	112

Figure 4-18: Damage parameter fatigue life relations with and without notch sensitivity factor ( $n_s = 1.15$ ) for M36 bolt material 32CrB4 (constant amplitude tests) and comparison to damage parameter values of the corresponding material test results ( $n_s = 1.0$ ) with and without mean strain .....	115
Figure 4-19: <i>Haigh</i> -diagram for damage parameter development under tensile mean stress calculated for material 32CrB4 (constant amplitude tests).....	116
Figure 4-20: Validation of analytical fatigue calculation results with different damage parameters for black (B) M36 HV-bolt sets (2D axisymmetric FE model) and material 32CrB4 with cyclic material data from constant amplitude tests with and without consideration of the notch sensitivity factor $n_s$ .....	118
Figure 4-21: Comparison of analytical fatigue calculations with and without consideration of cyclic relaxation (M36 HV-bolt sets, material 32CrB4, cyclic material data from constant amplitude tests, notch sensitivity factor $n_s = 1.15$ ).....	119
Figure 4-22: Comparison of analytical fatigue calculation results with cyclic material data from constant amplitude test and Incremental-Step-Test (IST) (M36 HV-bolt sets, material 32CrB4) .....	120
Figure 4-23: Divergence of local cyclic hysteresis calculated with 2D axisymmetric and full 3D FE model with continuous thread pitch (M36 HV-bolt set, material 32CrB4).....	121
Figure 4-24: Comparison of analytical fatigue calculations with different FE modelling approaches (M36 HV-bolt sets, material 32CrB4, cyclic material data from constant amplitude tests, $n_s = 1.15$ ).....	122
Figure 4-25: Analytical endurance limit calculations for M36 HV-bolt sets based on estimated strain endurance limits for material 32CrB4 (A: $\epsilon_{a,D} = 0.27\%$ , B: $\epsilon_{a,D} = 0.24\%$ , C: $\epsilon_{a,D} = 0.22\%$ ) and cyclic material data from constant amplitude tests (notch sensitivity factor $n_s = 1.15$ ).....	125
Figure 4-26: Schematic depiction of applicable crack tip stress intensity models for threaded fasteners acc. to <i>Pyttel et al.</i> (2008) (left) and stress development at the maximal loaded turn of an M36 HV-bolt thread derived from linear elastic FE calculation (right) .....	128
Figure 4-27: Comparison of analytical fatigue calculation results of load cycles until rupture with experimental results for black M36-HV bolt sets .....	130
Figure 4-28: Analytical fatigue curves until rupture with different damage parameter approaches considering cyclic material data from constant amplitude tests .....	132
Figure 4-29: Analytical fatigue curves until rupture with different damage parameter approaches considering cyclic material data from Incremental-Step-Tests (IST).....	132

- Figure 4-30: Model representation of the damage effect caused by galvanizing boundary layer according to *Ungermann et al. (2015)*, *Simonsen (2015)* and *Oechsner et al. (2015)* ..... 133
- Figure 4-31: Variants of adjusting the nominal load ( $S$ ) – local strain ( $\epsilon$ ) relation for inclusion of the damage effect caused by hot-dip galvanizing to the strain-life approach..... 134
- Figure 4-32: Calculation results considering the effect of hot-dip galvanizing with strain adjustment Variant 2 and  $P_J$  damage parameter ( $n_s = 1.15$ , material 32CrB4, cyclic material data from constant amplitude tests) ..... 136
- Figure 4-33: Calculation results considering the effect of hot-dip galvanizing with strain adjustment Variant 2 and  $P_{SWT}$  damage parameter ( $n_s = 1.0$ , material 32CrB4, cyclic material data from constant amplitude tests) ..... 136
- Figure 4-34: Schematic illustration of fracture surfaces after fatigue crack propagation of round notched specimens following severe (left) and mild (right) stress concentrations; adapted from *Eder et al. (2018)* and *Milella (2013)* ..... 138
- Figure 4-35: Comparison of notch sharpness expressed by the  $d/p$ -ratio and resulting notch effect expressed by the linear elastic notch stress concentration  $K_t$  in dependence of the bolt diameter..... 140
- Figure 4-36: Stress gradients and corresponding notch sensitivity factors in dependence of the bolt diameter..... 140
- Figure 4-37: Comparison of analytical fatigue calculation results for HV-bolt sets with different diameters ( $S_m = 630 \text{ N/mm}^2$ ,  $P_J$  damage parameter, material 32C4B4, cyclic material data from constant amplitude tests) ..... 141
- Figure 4-38: Approximation of the critically loaded surface area at the bolt thread with a 3D FE model (left) and development of the statistical size effect acc. to Eq. 4-6 (right)..... 143
- Figure 4-39: Diameter dependent analytical calculation of the endurance limit under consideration of the statistical size effect ( $S_m = 630 \text{ N/mm}^2$ ,  $P_J$  damage parameter, material 32C4B4, cyclic material data from constant amplitude tests) ..... 144
- Figure 4-40: Comparison of cyclic material curves for high-strength steels given in the literature 146
- Figure 4-41: Individual comparison of analytical fatigue calculations for M36 bolts ( $S_m = 630 \text{ N/mm}^2$ ,  $P_J$  damage parameter,  $n_s = 1.0$ ) with original 32CrB4 material data from constant amplitude tests (black lines) to calculations with material data from the literature (dotted lines: crack initiation; dashed lines: rupture) ..... 146
- Figure 4-42: Impact of the bolt material in the analytical fatigue calculation of the M64 HV-bolt sets ( $P_J$  damage parameter,  $n_s = 1.0$ )..... 149

- 
- Figure 4-43: Comparison of analytical fatigue calculations for M64 HV-bolts (B, NT) with and without consideration of the strain enhancement factor to experimental results ( $P_J$  damage parameter,  $n_s = 1.0$ ) ..... 149
- Figure 4-44: Comparison of analytical fatigue calculations with different mean load levels to experimental fatigue results from *Marten* (2009) on NT-galvanized M48 HV-bolt sets ( $n_s = 1.0$ , material 32CrB4 (CA),  $\epsilon_{a,d} = 0.24\%$ ; left:  $P_J$ -parameter; right:  $P_{SWT}$ -parameter) ..... 151
- Figure 4-45: Comparison of analytical fatigue calculations under axial loads with and without bending influence ( $P_J$ -parameter,  $n_s = 1.0$ , material 32CrB4 (CA),  $\epsilon_{a,d} = 0.24\%$ ) to experimental results for NT-galvanized M48 HV-bolt sets under pure axial and pure bending cyclical loading from *Marten* (2009) and *Schaumann & Marten* (2008) for crack initiation in the first load-bearing turn of the thread ..... 154
- Figure 4-46: Distribution of linear elastic notch stress concentration along the thread at purely axial and bending affected nominal loading calculated with axisymmetric 3D FE model.. 156



## 7.2 List of Tables

Table 3-1:	Basic characteristics of performed fatigue test series on HV-bolts .....	45
Table 3-2:	Summary of test program for constant amplitude tests on M36 HV-bolt sets.....	48
Table 3-3:	Results of the statistic evaluation in the TEL for black M36 HV-bolts .....	51
Table 3-4:	Results of statistical evaluation in the upper HCF for black M36 HV-bolts.....	53
Table 3-5:	Characteristic values of percentile S-N curves for black M36 HV-bolts .....	54
Table 3-6:	Results of statistical evaluation in the upper HCF for NT-galvanized M36 HV-bolts ..	56
Table 3-7:	Results of statistic evaluation in the TEL for HT-galvanized M36 HV-bolts considering different limit load cycle number $N_{lim}$ .....	59
Table 3-8:	Results of statistical evaluation in the upper HCF for HT-galvanized M36 HV-bolts ..	60
Table 3-9:	Summary of testing program for constant amplitude tests on M64 HV-bolt sets .....	65
Table 3-10:	Results of statistic evaluation of M64 fatigue tests in high cycle fatigue range for reference load level $\bar{S}_a = 50 \text{ N/mm}^2$ .....	67
Table 3-11:	Summary of testing program for variable amplitude tests on M36 HV-bolt sets, performed at the Chair and Institute for Material Science, Technische Universität Darmstadt .....	73
Table 4-1:	Examined high-strength bolt materials and number of considered specimens for monotonic and cyclic material tests.....	92
Table 4-2:	Summary of monotonic material parameters from tensile tests (mean values).....	94
Table 4-3:	Cyclic material parameters from strain controlled tests without mean strain ( $\epsilon_m = 0$ ) .	98
Table 4-4:	Estimation of 32CrB4 material's endurance limit based on references given in the literature.....	123
Table 4-5:	Results of analytical endurance limit calculations for M36 HV-bolts with cyclic material data for material 32CrB4 from constant amplitude tests ( $n_s = 1.15$ ) and Incremental-Step-Tests ( $n_s = 1.12$ ) .....	125
Table 4-6:	Juxtaposition of analytically and experimentally determined fatigue load cycles for M36 HV-bolt sets .....	131
Table 4-7:	Critical surface areas and corresponding notch sensitivity factors for expression of the statistical size effect .....	144

## 8 Appendix

<b>APPENDIX A – EXPERIMENTAL FATIGUE INVESTIGATIONS .....</b>	<b>190</b>
A.1 Calculation formulae of the staircase method .....	190
A.2 Test results of constant amplitude tests on M36 HV-bolt sets .....	191
A.3 Test results of constant amplitude tests on M64 HV-bolt sets .....	195
A.4 Additional result illustrations of variable amplitude tests on M36 HV-bolt .....	196
<b>APPENDIX B – MATERIAL TESTS .....</b>	<b>198</b>
B.1 Individual results of monotonic material tests .....	198
B.2 Stress evaluation of strain controlled material fatigue tests .....	200
<b>APPENDIX C – NUMERICAL CALCULATIONS .....</b>	<b>201</b>
C.1 Summary of mesh and contact parameters of finite element models .....	201
C.2 Results of path evaluations for HV-bolts M48, M64 and M72 .....	202
<b>APPENDIX D – DAMAGE PARAMETER EVALUATION .....</b>	<b>203</b>
D.1 Comparison of fatigue load cycles from material tests on material 32CrB4 at high mean strains, taken from <i>Oechsner et al. (2015)</i> , with damage parameter estimations ( $n_s = 1.0$ ) .....	203
D.2 Collocation of numerically calculated local loading conditions of a M36 HV-bolt set for different fatigue load levels .....	205
<b>APPENDIX E – TECHNICAL CRACK INITIATION .....</b>	<b>206</b>
E.1 Calculation of notch sensitivity factors .....	206
E.2 Fatigue curves with modified $P_M$ – damage parameter .....	207
E.3 Additional endurance limit calculation results .....	208
E.4 Additional analytical fatigue calculation results for hot-dip galvanized HV-bolts (M36) .....	209
E.5 Cyclic material data taken from the literature .....	210
<b>APPENDIX F – MACROSCOPIC CRACK PROPAGATION.....</b>	<b>211</b>
F.1 Fracture surfaces and crack depth measurements .....	211

## Appendix A – Experimental fatigue investigations

### A.1 Calculation formulae of the staircase method

Methodology of staircase method according to Dixon & Moods as given in DIN 969 (1997):

(1)	(2)													(3)	(4)	(5)	(6)	(7)	(8)		
F <sub>a</sub> [kN]	X = Rupture O = Run-out													X	O	z	f	z f	z <sup>2</sup> f		
F <sub>a,1</sub>																					
F <sub>a,2</sub>																					
F <sub>a,3</sub>																					
F <sub>a,4</sub>																					
...																					
Specimen No.	1	2	3	4	5	6	7	8	9	10	11	12	13	...	Σ	Σ(3)	Σ(4)	-	Σ(6)	Σ(7)	Σ(8)
																			<b>C</b>	<b>A</b>	<b>E</b>

$$F_{a,50\%} = F_{ao} + \Delta F_{all} \left[ \frac{A}{C} + x \right]$$

Endurance limit, survival probability Ps,50%

$$S(F_a) = 1.62 \cdot \Delta F_{all} \left[ \frac{C \cdot E - A^2}{C^2} \right] + 0.029$$

Standard deviation

where:

Columns:

$$\left[ \frac{C \cdot E - A^2}{C^2} \right] > 0.3$$

(1) Amplitude

(2) Test event (X or O)

x = +0.5 if DTE = O

(3) Sum of rupture per amplitude

x = -0.5 if DET = X

F<sub>ao</sub>: lowest amplitude of decisive test event

(4) Sum of run-outs per amplitude

ΔF<sub>all</sub>: load increment

(5) Index number, starting with 0 at F<sub>ao</sub>

Decisive test event / DTE (X or O):  
event with lower number of occurrences

(6) Sum of DTE per amplitude

C,A,E: Sums of columns (6),(7), (8)

(7) Product of (5) and (6)

(8) Product of (5) and (7)

## A.2 Test results of constant amplitude tests on M36 HV-bolt sets

### Uncoated, black:

#### Transition region to the endurance limit (TEL)

Test No. (chronological) [-]	Specimen No. (evaluation) [-]	Amplitude $F_a$ [kN]	Amplitude $S_a$ [N/mm <sup>2</sup> ]	Rupture/ run-out [R / RO] (RRO No.)	Failure location [Head / Thread]	Load cycles [-]
1	1	48.0	58.8	R	T	623 772
2	2	45.0	55.1	R	T	837 364
3	3	42.0	51.4	R	T	602 282
4	4	39.0	47.8	R	T	1 543 027
5	6	36.0	44.1	R	T	3 110 162
6	8	33.0	40.4	RO (RRO2)	-	5 000 014
7	10	36.0	44.1	R	T	2 491 435
8	14	33.0	40.4	RO (RRO1)	-	5 000 011
9	12	36.0	44.1	R	T	1 751 877
10	24	33.0	40.4	RO (RRO5)	-	5 000 014
11	16	36.0	44.1	RO (RRO6)	-	5 000 010
12	20	39.0	47.8	R	T	2 066 003
13	5	37.5	45.9	R	T	1 505 709
14	7	34.5	42.2	R	T	1 475 508
15	9	34.5	42.2	RO (RRO3)	-	5 000 015
16	11	34.5	42.2	RO (RRO4)	-	5 000 020
17	13	34.5	42.2	R	T	2 569 297
18	15	34.5	42.2	DL	-	5 000 010
19	17	37.5	45.9	R	T*	4 364 338
20	18	36.0	44.1	RO	-	5 000 013
21	19	37.5	45.9	RO	-	5 000 015
22	21	37.5	45.9	R	T	4 842 258
23	22	36.0	44.1	R	T	3 985 944
24	23	34.5	42.2	R	T	2 108 133

\* Crack initiation in the second load bearing turn of the thread:



**Upper high cycle fatigue range**

Specimen No.	Amplitude $F_a$	Amplitude $S_a$	Failure location	Load cycles
[-]	[kN]	[N/mm <sup>2</sup> ]	[Head / Thread]	[-]
1	56.0	68.6	T	282 947
2			T	293 013
3			T	320 665
4			T	327 651
5			T	329 612
<i>RRO1</i>			<i>T</i>	<i>476 382</i>
<i>RRO2</i>			<i>T</i>	<i>306 432</i>
6			84.0	102.9
7	T	94 864		
8	T	95 240		
9	T	119 644		
10	T	124 538		
<i>RRO3</i>	<i>T</i>	<i>107 508</i>		
<i>RRO4</i>	<i>T</i>	<i>116 236</i>		
<i>RRO5</i>	66.0	80.8		
<i>RRO6</i>			<i>T</i>	<i>201 194</i>

**Normal temperature hot-dip galvanized:****Transition region to the endurance limit (TEL)**

Test. No./ Specimen No. [-]	Amplitude $F_a$ [kN]	Amplitude $S_a$ [N/mm <sup>2</sup> ]	Rupture/ run-out [R / RO] (RRO No.)	Failure location [Head / Thread]	Load cycles [-]
1	36.0	44.1	R	T	542 157
2	34.0	41.6	R	T	642 385
3	32.0	39.2	R	T	818 503
4	30.0	36.7	R	T	1 251 035
5	28.0	34.3	R	T	1 077 581
6	26.0	31.8	RO (RRO3)	-	7 470 041
7	28.0	34.3	R	T	1 889 803
8	26.0	31.8	RO (RRO1)	-	10 682 531
9	28.0	34.3	RO (RRO2)	-	10 031 579
10	30.0	36.7	R	T	1 138 788
11	28.0	34.3	RO	-	5 237 323
12	30.0	36.7	R	T	1 461 350
13	28.0	34.3	RO (RRO4)	-	6 140 465
14	30.0	36.7	R	T	997 824
15	28.0	34.3	R	T	1 617 662
16	26.0	31.8	R	T	2 568 772
17	24.0	29.4	RO	-	5 111 123
18	26.0	31.8	RO	T	8 660 270
19	28.0	34.3	R	T	2 066 240

**Upper high cycle fatigue range**

Specimen No. [-]	Amplitude $F_a$ [kN]	Amplitude $S_a$ [N/mm <sup>2</sup> ]	Failure location [Head / Thread]	Load cycles [-]
1	44.0	53.9	T	242 071
2			T	243 785
3			T	247 640
4			T	269 469
5			T	291 094
RRO1			T	252 711
RRO2			T	240 238
6			66.0	80.8
7	T	107 078		
8	T	108 032		
9	T	110 374		
10	T	114 027		
RRO3	T	95 302		
RRO4	T	106 278		

**High temperature hot-dip galvanized:****Transition region to the endurance limit (TEL)**

Test No. (chronological)	Specimen No. (evaluation)	Amplitude $F_a$	Amplitude $S_a$	Rupture/ run-out	Failure location [Head / Shaft / Thread]	Load cycles
[-]	[-]	[kN]	[N/mm <sup>2</sup> ]	[R / RO] (RRO No.)		[-]
1	1/16	32.0	39.2	R	T	1 518 685
2	2/1	30.0	36.7	R	T	3 130 138
3	5/2	28.0	34.3	R/ RO	H	5 291 116
4	3/6	28.0	34.3	R	T	2 126 734
5	4/15	26.0	31.8	R/ RO	S	6 138 806
6	16/3	26.0	31.8	RO	-	9 558 587
7	7/14	28.0	34.3	R/ RO	T	8 731 405
8	17/7	26.0	31.8	RO ( RRO1)	-	11 500 831
9	15/4	28.0	34.3	RO ( RRO2)	-	18 020 964
10	6/5	30.0	36.7	R	T	1 535 633
11	18/8	28.0	34.3	RO ( RRO4)	-	11 154 910
12	8/9	30.0	36.7	R/ RO	H	5 918 444
13	9/17	32.0	39.2	R	T	789 717
14	10/11	30.0	36.7	R	T	3 616 310
15	11/10	28.0	34.3	RO	-	9 556 232
16	12/13	30.0	36.7	R	S	1 938 170
17	13/12	28.0	34.3	RO ( RRO3)	-	7 574 707
18	14/18	30.0	36.7	R	T	1 795 902

R/RO: Rupture, but after reaching  $5 \cdot 10^6$  load cycles**Upper high cycle fatigue range**

Specimen No.	Amplitude $F_a$	Amplitude $S_a$	Failure location	Load cycles
[-]	[kN]	[N/mm <sup>2</sup> ]	[Head / Thread]	[-]
1	44.0	53.9	T	299 143
2			T	308 280
3			T	319 775
4			T	320 893
5			T	340 462
RRO1			T	300 690
RRO2			T	338 181
6			66.0	80.8
7	T	107 442		
8	T	110 101		
9	T	115 048		
10	T	132 297		
RRO3	T	107 362		
RRO4	T	134 204		

### A.3 Test results of constant amplitude tests on M64 HV-bolt sets

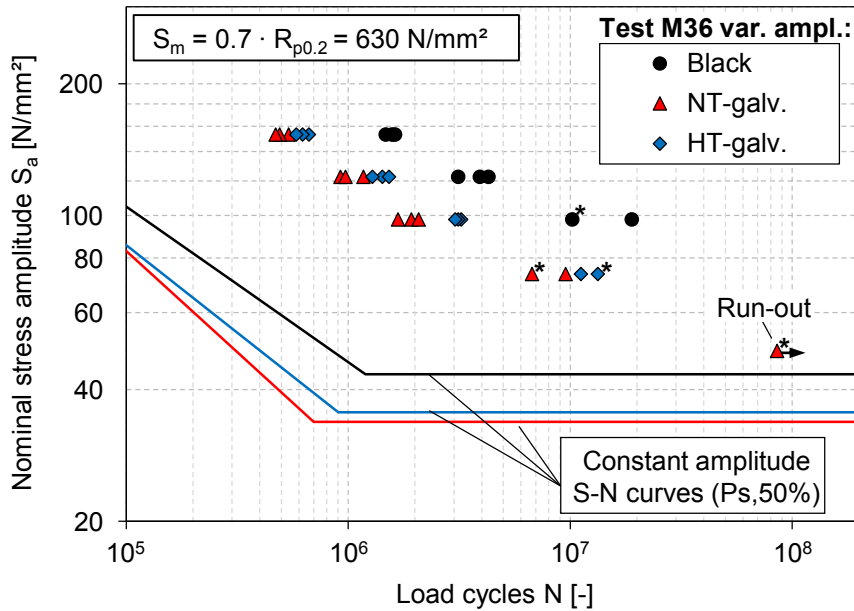
Specimen No.	Amplitude $F_a$	Amplitude $S_a$	Failure location	Load cycles
[-]	[kN]	[N/mm <sup>2</sup> ]	[Head / Thread]	[-]
<b>Uncoated, black:</b>				
1	350	130.79	T	24 200
2	300	112.11	T	38 547
3	250	93.42	T	50 438
4	225	84.08	T	68 009
5	200	74.74	T	86 469
6	150	56.05	T	191 247
7	125	46.71	T	331 530
8	105	39.24	T	1 006 998
9	90	33.63	-	2 357 301*
<b>Normal temperature hot-dip galvanized</b>				
1	300	112.11	T	32 207
2	250	93.42	T	56 072
3	225	84.08	T	63 183
4	200	74.74	T	82 222
5	175	65.40	T	135 399
6	150	56.05	T	172 660
7	125	46.71	T	291 091
8	100	37.37	T	707 122
9	85	31.76	T	1 355 440

\* Test ended manually without rupture



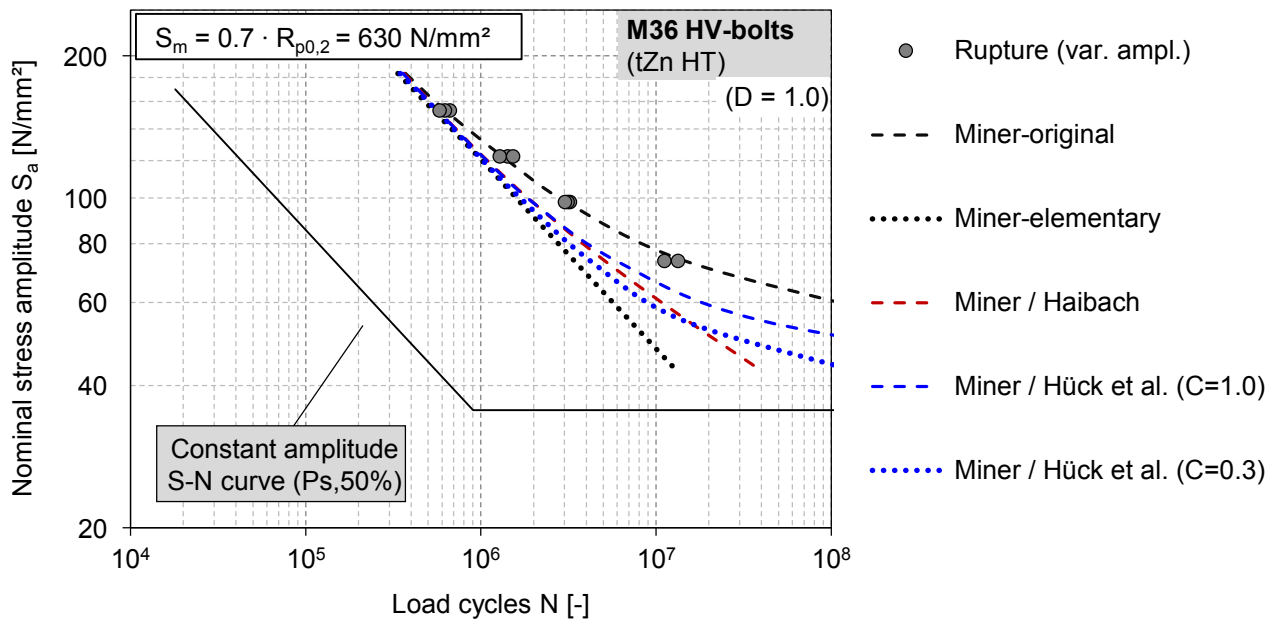
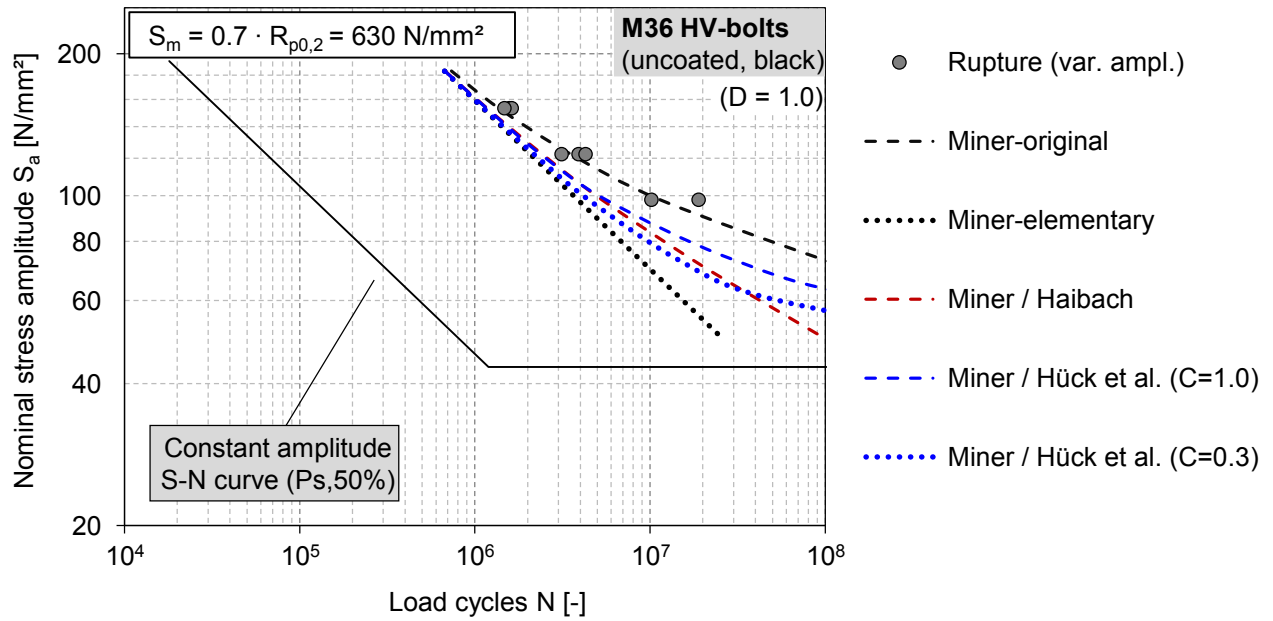
## A.4 Additional result illustrations of variable amplitude tests on M36 HV-bolt

### Close-up illustration of test results with different boundary layers



\*: Test-runs performed with reduced loading sequence due to omission of lowest loading blocks (see *Oechsner et al., 2015*)

**Evaluation of damage accumulation hypothesis based on constant amplitude S-N curves for uncoated, black and high-temperature (HT) hot-dip galvanized HV-bolt sets**



## Appendix B – Material Tests

### B.1 Individual results of monotonic material tests

#### Bolt size M36, 32CrB4, boundary layers B, NT, HT

Bolt No. Spec. No	M36 B1*				MEAN B	M36 NT1				MEAN NT
	1_1	1_2	1_3	1_4		2_4	2_2	2_3	2_4	
R <sub>p,0.2</sub> [N/mm <sup>2</sup> ]	1039	1045	1049	1043	<b>1044</b>	1074	1073	1073	1075	<b>1074</b>
R <sub>m</sub> [N/mm <sup>2</sup> ]	1114	1117	1118	1116	<b>1116</b>	1153	1152	1157	1160	<b>1156</b>
A [%]	-	-	-	-	-	14.79	14.76	14.50	14.87	<b>14.73</b>
A <sub>g</sub> [%]	-	4.40	-	4.43	<b>4.41</b>	4.81	4.80	4.77	4.78	<b>4.79</b>
E [N/mm <sup>2</sup> ]	-	213960	-	214620	<b>214290</b>	210142	218248	197383	204051	<b>207456</b>

Bolt No. Spec. No	M36 HT1				M36 HT2				MEAN HT
	1_1	1_2	1_3	1_4	2_1	2_2	2_3	2_4	
R <sub>p,0.2</sub> [N/mm <sup>2</sup> ]	1003.2	1012.8	1019.2	1010.8	1013.2	1008.1	1017.7	1005.8	<b>1011</b>
R <sub>m</sub> [N/mm <sup>2</sup> ]	1088	1095	1100	1095	1096	1089	1101	1087	<b>1094</b>
A [%]	15.16	15.36	15.39	15.33	15.55	15.39	15.09	15.44	<b>15.34</b>
A <sub>g</sub> [%]	5.16	5.06	5.12	5.06	5.10	4.86	5.10	5.07	<b>5.07</b>
E [N/mm <sup>2</sup> ]	245581	186660	241190	198979	214946	219982	222515	199524	<b>216173</b>

\*results from *Oechsner et al. (2015)*

#### Bolt size M48, 34CrNiMo6, boundary layers NT

Bolt No. Spec. No	M48 NT1		M48 NT2		MEAN NT
	1_1	1_2	2_2	2_2	
R <sub>p,0.2</sub> [N/mm <sup>2</sup> ]	1045	1040	1018	1017	1030
R <sub>m</sub> [N/mm <sup>2</sup> ]	1132	1129	1117	1113	1123
A [%]	15.60	15.40	15.55	15.86	15.60
A <sub>g</sub> [%]	5.06	5.07	5.05	5.07	5.06
E [N/mm <sup>2</sup> ]	205713	209212	204136	209982	207261

**Bolt size M64, 30CrNiMo8, boundary layers B, NT**

Bolt No. Spec. No	M64 B1							
	1_1	1_2	1_3	1_4	1_5	1_6	1_7	1_8
R <sub>p,0.2</sub> [N/mm <sup>2</sup> ]	1027	1024	1015	1012	1027	1018	1020	1016
R <sub>m</sub> [N/mm <sup>2</sup> ]	1145	1141	1130	1124	1147	1134	1134	1135
A [%]	16.11	15.86	15.90	15.59	16.12	15.85	16.21	15.64
A <sub>g</sub> [%]	5.30	5.29	5.32	5.31	5.29	5.31	5.29	5.29
E [N/mm <sup>2</sup> ]	200298	203398	203519	203787	205220	209496	204638	198198

Bolt No. Spec. No	M64 B2*		M64 NT1*		MEAN B1	MEAN B2	MEAN B	MEAN NT
	1_1	1_2	1_2	1_2				
R <sub>p,0.2</sub> [N/mm <sup>2</sup> ]	995	994	986	993	<b>1020</b>	<b>995</b>	<b>1015</b>	<b>990</b>
R <sub>m</sub> [N/mm <sup>2</sup> ]	1124	1121	1113	1119	<b>1136</b>	<b>1123</b>	<b>1134</b>	<b>1116</b>
A [%]	-	-	-	-	<b>15.91</b>	-	<b>15.91</b>	-
A <sub>g</sub> [%]	5.38	5.7	5.38	5.14	<b>5.30</b>	<b>5.54</b>	<b>5.35</b>	<b>5.26</b>
E [N/mm <sup>2</sup> ]	204200	204000	203300	203900	<b>203663</b>	<b>204100</b>	<b>203675</b>	<b>203600</b>

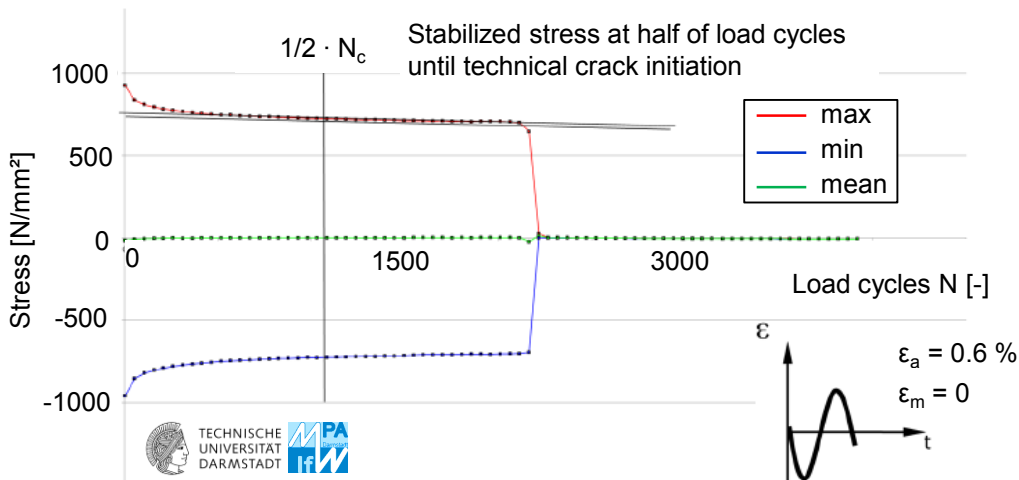
\*results from *Oechsner et al. (2015)*

## B.2 Stress evaluation of strain controlled material fatigue tests

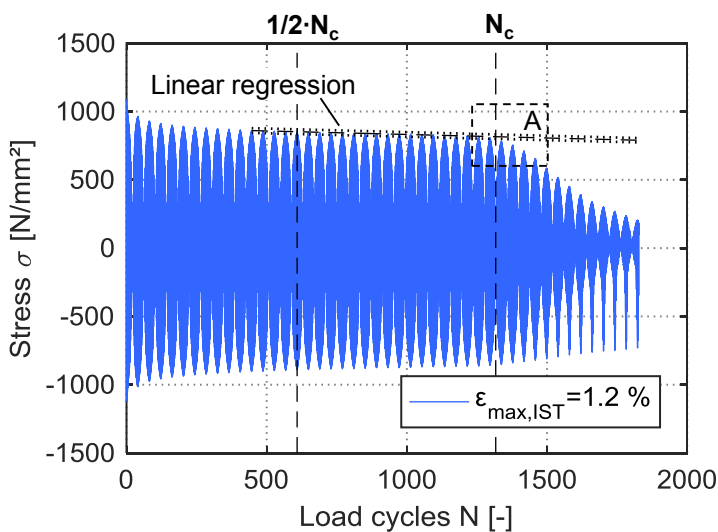
Stabilized stress level and load cycles until technical crack initiation  $N_c$  from strain controlled material tests are defined in dependence of the stress development throughout the test run. The two graphics depicted below illustrate the evaluation procedure that was analogously used in the test series with constant amplitudes by *Oechsner et al.* (2015) as well as for the Incremental-Step-Test (IST) evaluation.

After a notable mitigation of the stress decrease during the early test phase the stress level approximately stabilises. Based on the peak stress levels of the stabilized test phases a linear regression is defined. Technical crack initiation is assumed when the peak stress level falls below a parallel of the extrapolated regression line with a margin of more than  $\sim 2\%$ . Stress level or load block at  $1/2 \cdot N_c$  are used for determination of the Ramberg & Osgood relation.

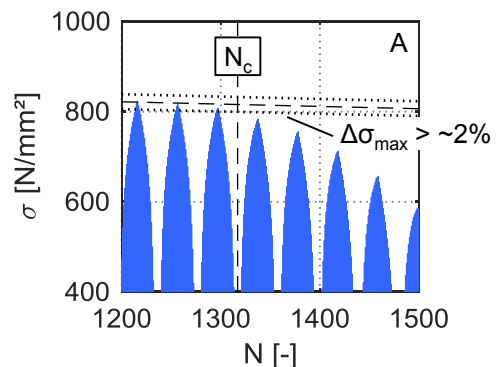
### Stress development during constant strain amplitude test (from Oechsner et al., 2015):



### Stress development during Incremental-Step-Test:

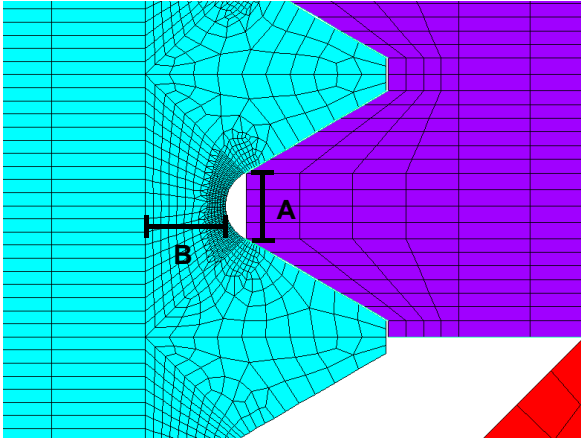
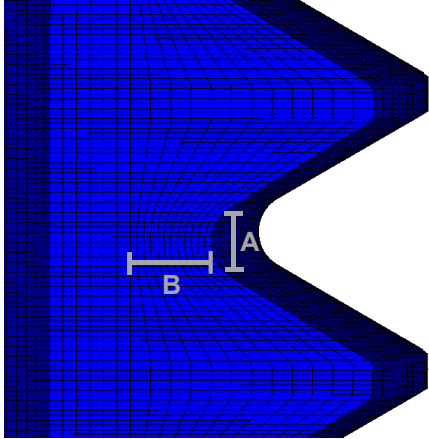


### Definition of crack initiation



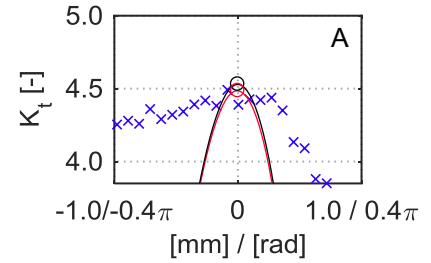
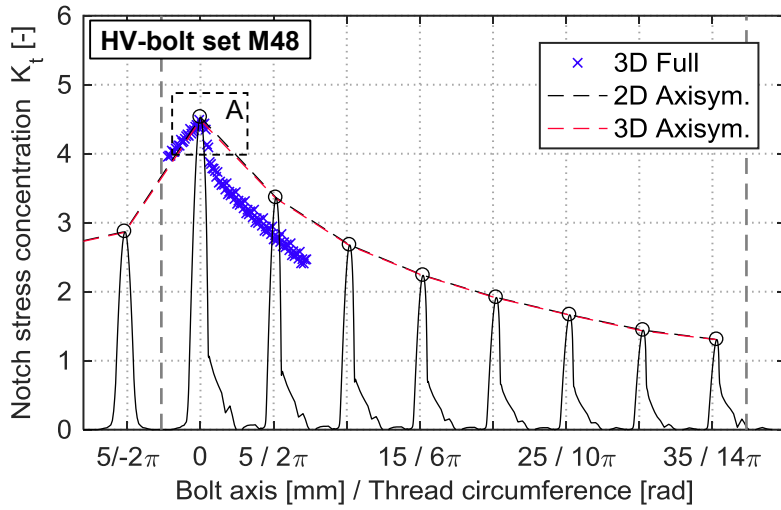
## Appendix C – Numerical calculations

### C.1 Summary of mesh and contact parameters of finite element models

	2D Axisymmetric	3D Axisymmetric	3D Full	
			Global	Sub
<b>Mesh</b>				
Element type <sup>1</sup>	Plane 182 (4 node struct. solid)	Solid 185 (8 node structural solid)		
Elements along notch root radius (A) (num. [-] / size [mm]) <sup>3</sup>	~60 / ~0.02		6 / ~0.17	14 / ~0.07
Elements in radial direction from notch root until 0.5 · thread depth (B) (num. [-] / size [mm]) <sup>3</sup>	15 / var. ~0.12 to ~0.05		4 / ~0.3	12 / ~0.1
Elements in circumferential direction (180°) (num. [-] / size [mm]) <sup>3</sup>	-	80 / ~0.6	48 / ~1.0	112 / ~0.4
Total number of nodes	13 730	994 478	491 781	480 928
<b>Contact</b> (Augmented <i>Lagrangian</i> / isotropic <i>Coulomb</i> friction)				
Normal contact stiffness factor FKN <sup>1,2</sup>	10 (10)	300 (20)	300 (20)	-
<sup>1</sup> acc. to ANSYS Inc. (2016) <sup>2</sup> value in brackets denotes contact stiffness factor applied in calculations with linear-elastic material definition <sup>3</sup> element size given for geometry M36				
<u>2D / 3D Axisymmetric Model</u>		<u>3D Full Model (Sub model)</u>		
				

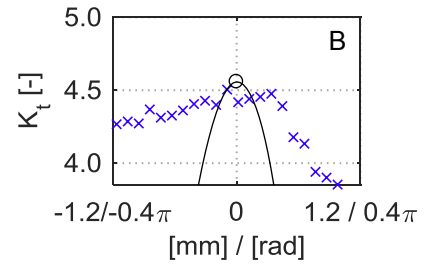
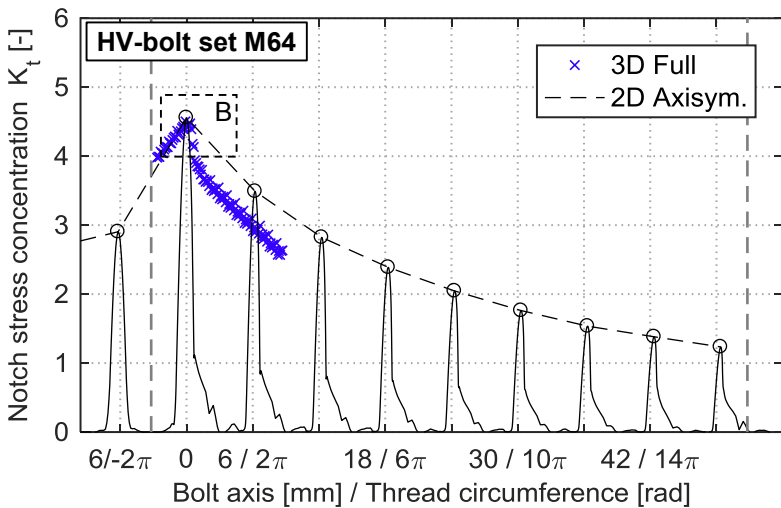
### C.2 Results of path evaluations for HV-bolts M48, M64 and M72

The depicted results are analogous to Figure 4-13 (bolt geometry M36) from FE calculations with linear-elastic material behavior and evaluation paths as shown in Figure 4-12.



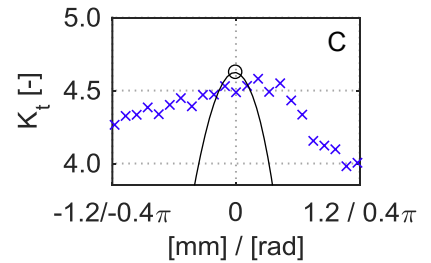
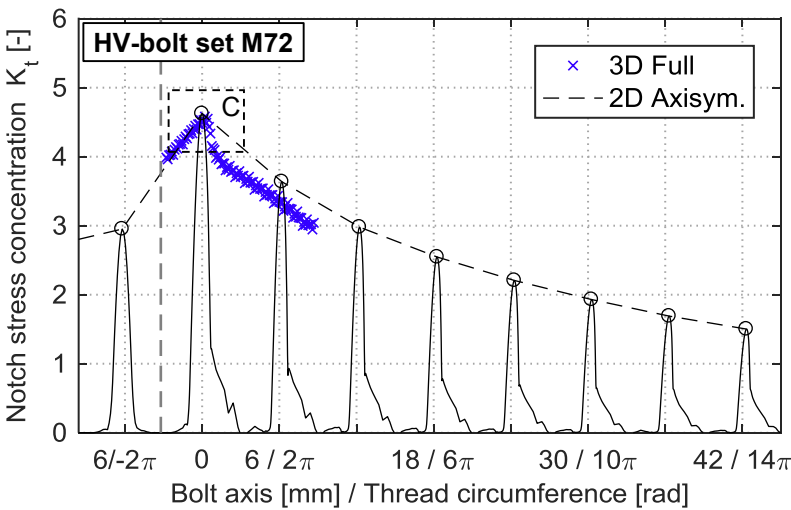
Max.  $K_t$ :

3D Full:	4.49
2D Axisym.:	4.53
3D Axisym.:	4.49



Max.  $K_t$ :

3D Full:	4.51
2D Axisym.:	4.56



Max.  $K_t$ :

3D Full:	4.58
2D Axisym.:	4.62

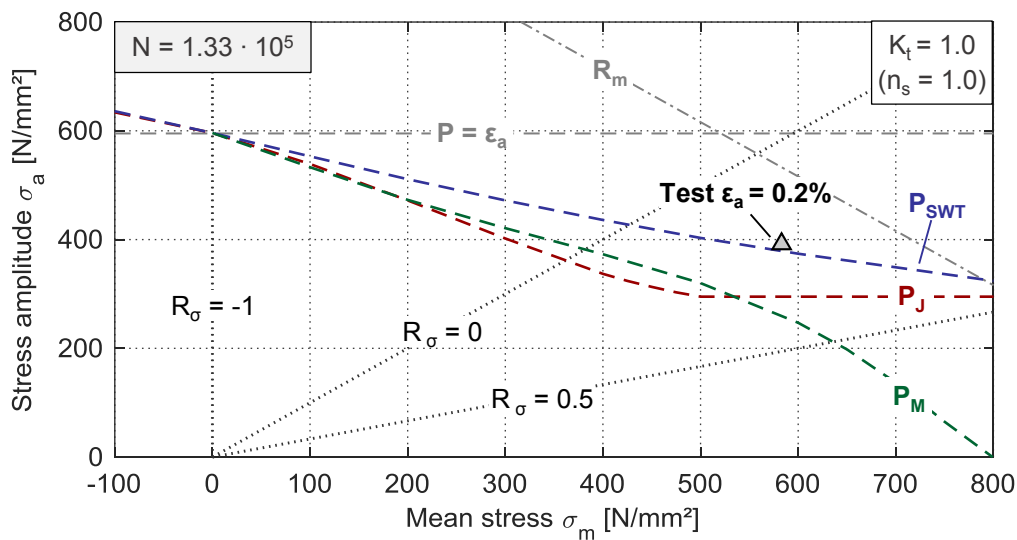
## Appendix D – Damage parameter evaluation

### D.1 Comparison of fatigue load cycles from material tests on material 32CrB4 at high mean strains, taken from *Oechsner et al. (2015)*, with damage parameter estimations ( $n_s = 1.0$ )

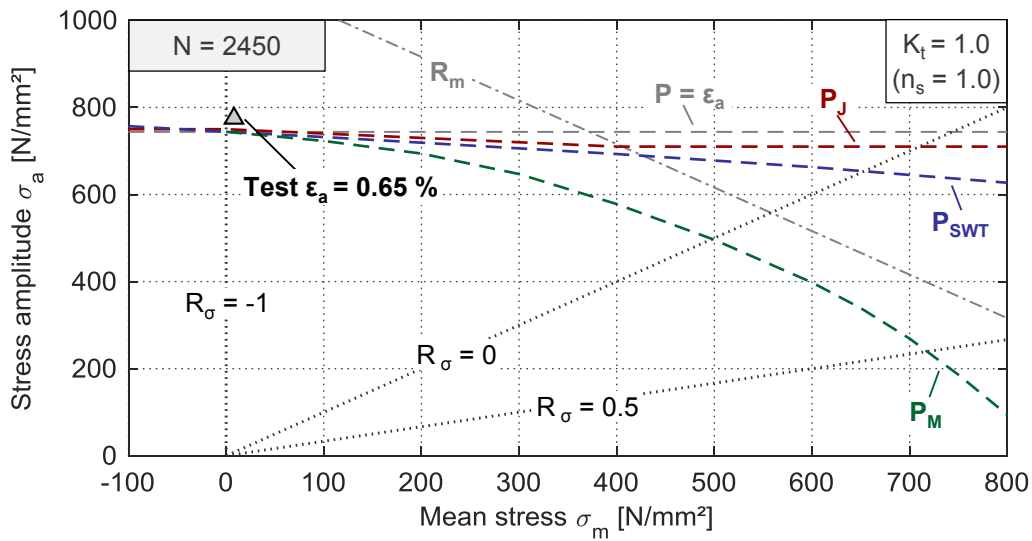
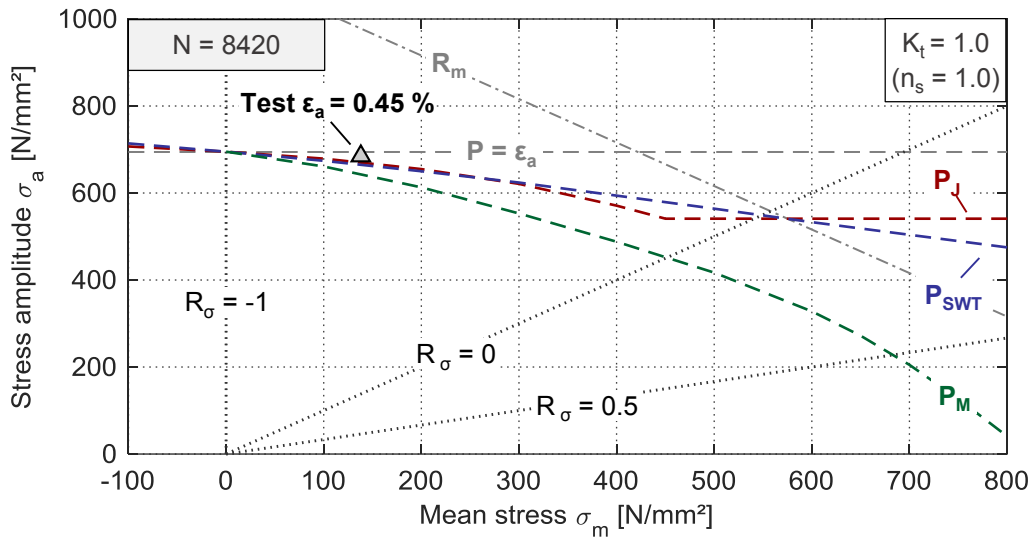
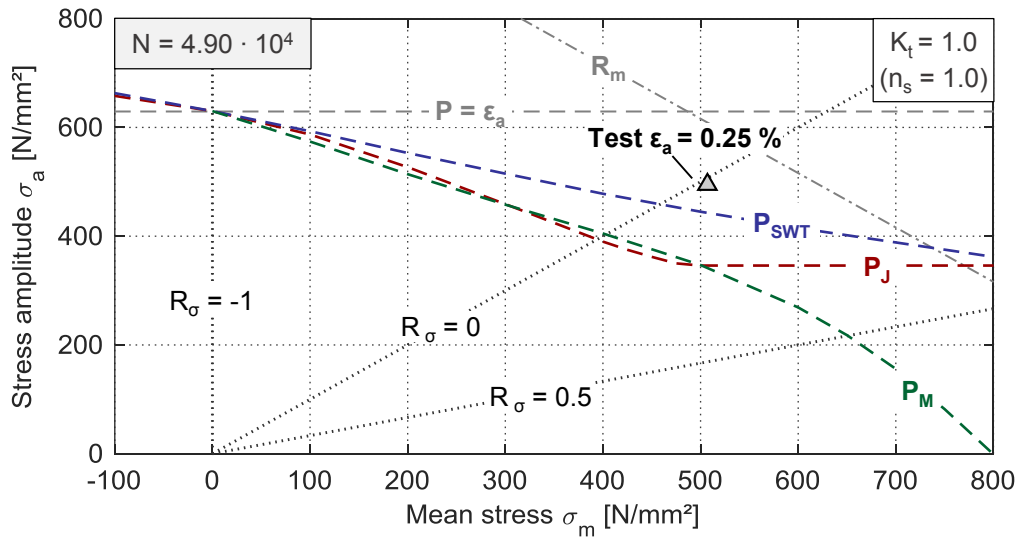
#### Calculation results:

Material tests under high mean strain ( $\epsilon_m = 1.1\%$ , $\sigma_o \approx R_m$ ):				
$\epsilon_a$	0.65%	0.40%	0.25%	0.20%
$R_\sigma = \sigma_u / \sigma_o$	-0.97	-0.66	0.01	0.20
Load cycles N	2450	8420	$4.90 \cdot 10^4$	$1.33 \cdot 10^5$
Deviation of calculated load cycles N:				
$P_{SWT}$	-527 (22%)	-2798 (33%)	$-3.4 \cdot 10^4$ (68%)	$-7.0 \cdot 10^4$ (53%)
$P_M$	-554 (23%)	-4318 (51%)	$-4.3 \cdot 10^4$ (88%)	$-1.2 \cdot 10^5$ (90%)
$P_J$	-341 (14%)	-1991 (24%)	$-3.7 \cdot 10^4$ (75%)	$-1.1 \cdot 10^5$ (80%)
Strain-life curve	-348 (-)	+2233 (x1.3)	$+1.6 \cdot 10^6$ (x33)	$(+\sim 10^8) \rightarrow \infty$

#### Haigh-diagrams:







## D.2 Collocation of numerically calculated local loading conditions of a M36 HV-bolt set for different fatigue load levels

The following exemplary given calculation results were obtained from numerical calculations using 32CrB4 material data for monotonic and cyclic loading (constant amplitude tests) and a 2D axisymmetric FE model. The cyclic material response was synthesized as described in Chapter 4.3.3.

$S_m$ [N/mm <sup>2</sup> ]	$S_a$ [N/mm <sup>2</sup> ]	$R_s$ [-]	$\sigma_{1,a}$ [N/mm <sup>2</sup> ]	$\sigma_{1,m}$ [N/mm <sup>2</sup> ]	$\varepsilon_{a,1}$ [%]	$\varepsilon_{m,1}$ [%]	$R_{\sigma 1}$ [-]	$R_{\varepsilon 1}$ [-]	$N (P_J)$ [-]
630	30.0	0.91	136.86	1194.25	0.071	1.958	0.79	0.93	7.37E+09
	45.0	0.87	205.00	1129.72	0.091	2.028	0.69	0.91	5.27E+06
	60.0	0.83	269.86	1068.43	0.119	2.114	0.60	0.89	3.81E+05
	75.0	0.79	335.81	1006.08	0.148	2.204	0.50	0.87	7.39E+04
	100.0	0.73	446.96	901.81	0.198	2.376	0.34	0.85	1.91E+04
	122.4	0.67	547.01	809.00	0.243	2.563	0.19	0.83	9.39E+03
	140.8	0.63	624.77	737.63	0.280	2.746	0.08	0.82	6.49E+03

## Appendix E – Technical crack initiation

### E.1 Calculation of notch sensitivity factors

The following notch sensitivity factors for different bolt sizes material data and loading conditions are calculated according to Equations 2-22 to 2-25. No statistical size effect is considered in the below calculations.

#### **Macroscopic notch sensitivity factor ( $N = 5 \cdot 10^5$ ):**

	$\epsilon_{pl}$	$\epsilon_{el}$	$n_p$
	[%]	[%]	[-]
32CrB4 Const. Ampl.	0.266	0.002	1.005
32CrB4 IST	0.202	0.014	1.033

#### **Stress mechanical and total notch sensitivity factor at purely axial loading conditions:**

	$\sigma_{1,max}$ [N/mm <sup>2</sup> ]	$dx$ [mm]	$d\sigma$ [N/mm <sup>2</sup> ]	$\chi^*$ [1/mm]	$R_m$ [N/mm <sup>2</sup> ]	$n_\chi$ [-]	$n_p$ [-]	$n$ [-]	
M36	2872.6	0.08063	614.9	2.655	1116	1.156	1.005	1.151	Const. Ampl.
							1.033	1.119	IST
M48	2859.5	0.104	615.1	2.066	1116	1.146	1.005	1.141	Const. Ampl.
M64	2861.1	0.124	609	1.713	1116	1.140	1.005	1.134	
M72	2910.5	0.125	621.5	1.711	1116	1.140	1.005	1.134	
M16	2699.0	0.042	576.6	5.109	1116	1.184	1.005	1.178	

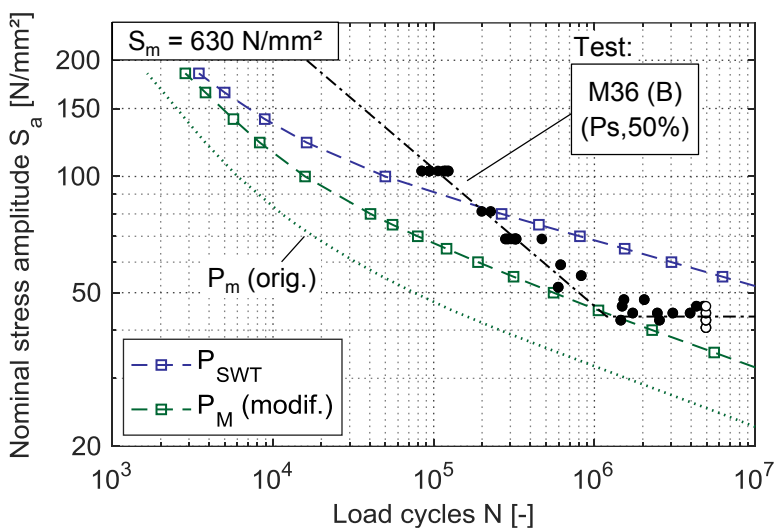
#### **Stress mechanical and total notch sensitivity factor at loading conditions with equally superimposes axial (50%) and bending loading (50%):**

	$\sigma_{1,max}$ [N/mm <sup>2</sup> ]	$dx$ [mm]	$d\sigma$ [N/mm <sup>2</sup> ]	$\chi^*$ [1/mm]	$R_m$ [N/mm <sup>2</sup> ]	$n_\chi$ [-]	$n_p$ [-]	$n$ [-]	
M36	2002.10	0.083	418.6	2.52	1116	1.154	1.005	1.149	Const. Ampl.

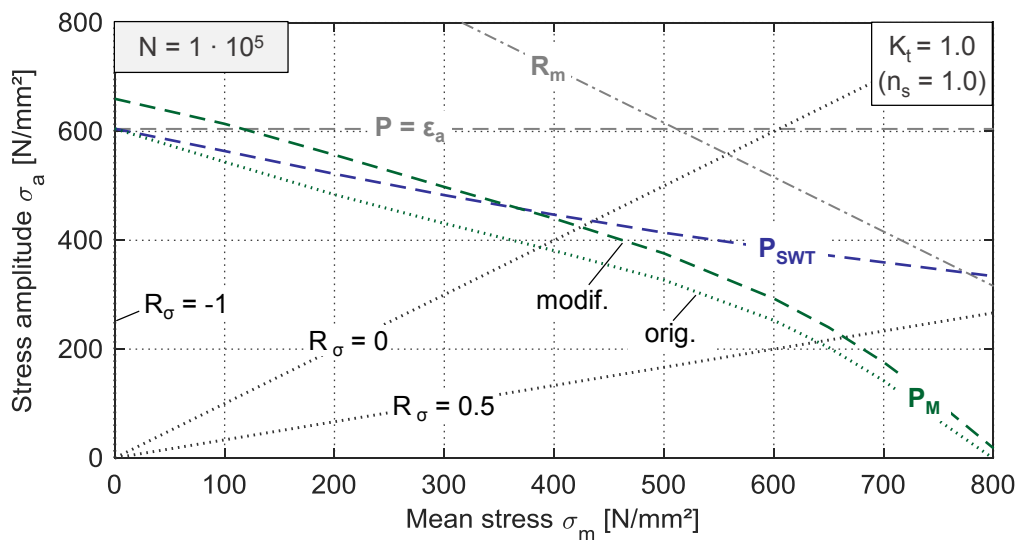
### E.2 Fatigue curves with modified $P_M$ – damage parameter

The below diagrams show the classification of calculation results with a ‘modified’  $P_M$  damage parameter, where the  $P_M$ -values, derived for the local loading condition of the bolt, are evaluated on the basis of the P-life curve for the  $P_{SWT}$  parameter, which establishes the basis of the  $P_M$ -parameter’s development. For reference the ‘original’  $P_M$  curves, applied in methodically consistency with the other investigated damage parameters, as well as the  $P_{SWT}$  parameter curves are plotted. Results are shown for cyclic material data for bolt material 32CrB4 from constant amplitude tests and FE calculations with a 2D axisymmetric model.

#### Results of analytical fatigue calculation for M36 HV-bolt:

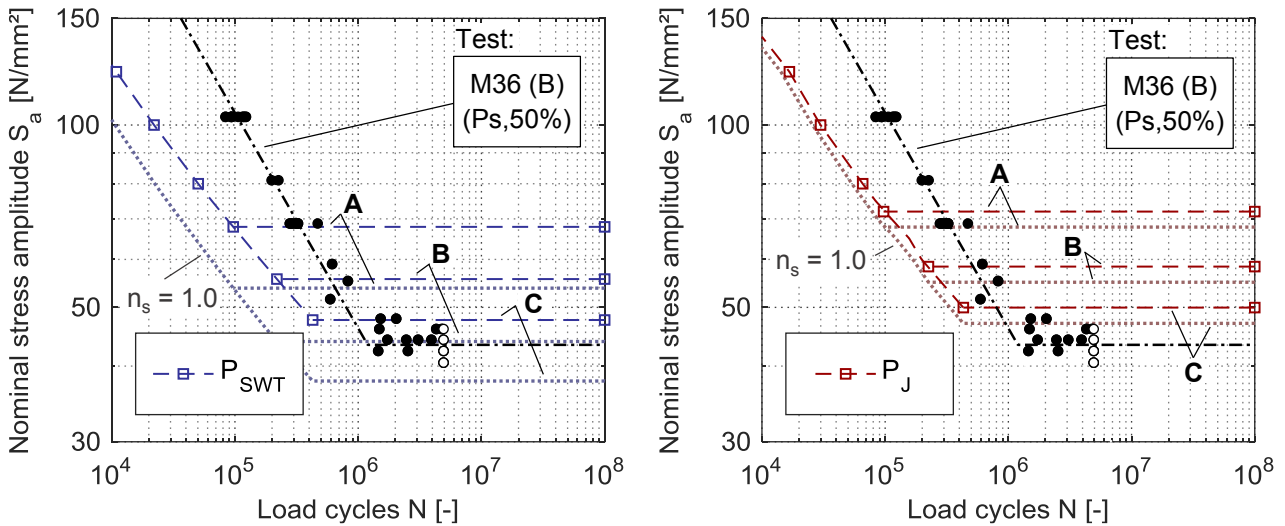


#### Damage parameter evaluation in Haigh-Diagram:



### E.3 Additional endurance limit calculation results

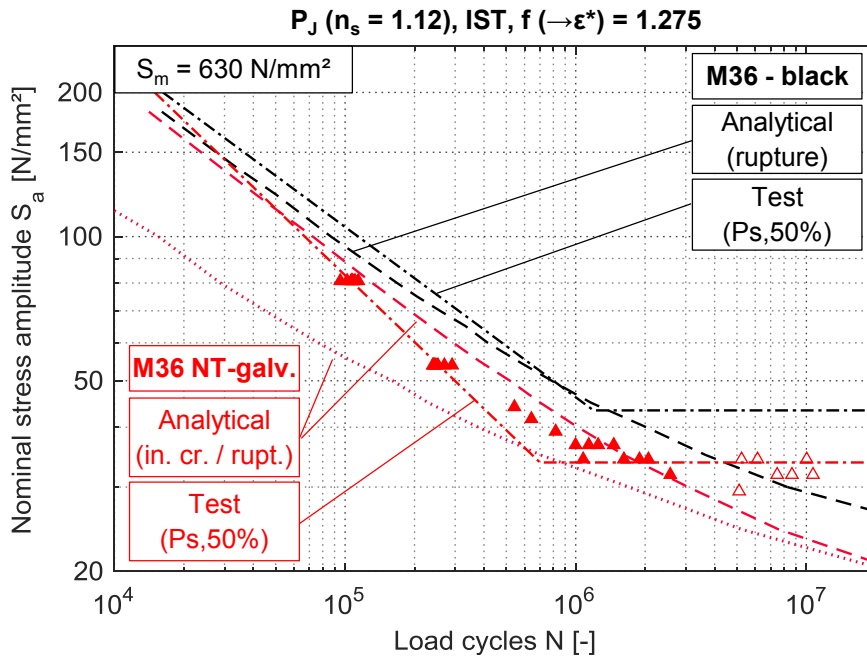
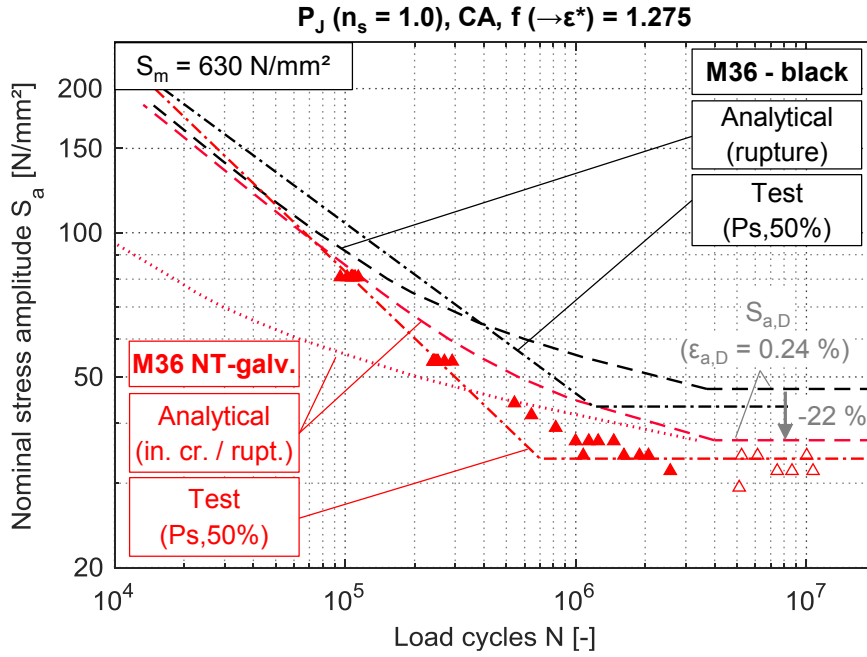
#### Graphical depiction of analytical calculated endurance limits for M36 bolts and base material 32CrB4 with material data from Incremental-Step-Tests:



#### Analytical calculated endurance limits for M36 bolts and base material 32CrB4 without consideration of the notch sensitivity factor ( $n_s = 1.0$ ):

	Material data from constant amplitude tests			Material data from Incremental-Step-Tests (IST)			Test result M36 (B) (Ps,50%)	
	(A)	(B)	(C)	(A)	(B)	(C)		
Estimated base material endurance limit $\epsilon_{a,D}$ [%]	0.27	0.24	0.22	0.27	0.24	0.22		
$S_{a,D}$ [N/mm <sup>2</sup> ]	$P_{SWT}$	56.1	44.01	37.14	53.79	43.92	37.79	<b>43.36</b>
	$P_J$	58.62	47.12	40.77	67.85	55.01	47.05	
$N_D$ [-]	$4.6 \cdot 10^5$	$3.3 \cdot 10^6$	$2 \cdot 10^7$	$9.7 \cdot 10^4$	$2.2 \cdot 10^5$	$4.3 \cdot 10^5$	<b><math>1.2 \cdot 10^6</math></b>	

**E.4 Additional analytical fatigue calculation results for hot-dip galvanized HV-bolts (M36)**



### E.5 Cyclic material data taken from the literature

Material	36CrB4	41Cr4	42CrMo4	41Cr4	30CrNiMo8	30CrNiMo8	UML <sup>2</sup>
Source	Schneider (2011)	Schneider (2011)	Boller et al. (1982) <sup>1</sup>	Ott & Nowack (1985) <sup>1</sup>	Boller & Seeger (1983) <sup>1</sup>	Boller & Seeger (1983) <sup>1</sup>	Bäumel & Seeger (1990)
R <sub>ε</sub> [-]	-1						
R <sub>m</sub> [N/mm <sup>2</sup> ]	1124	1121	1111	904	910	910	1116
E [N/mm <sup>2</sup> ]	206 630	205 120	211 400	200 000	206 000	206 000	214 290
σ <sub>f</sub> ' [N/mm <sup>2</sup> ]	1 208	1 037	1 555	1 288	1 106	643	1674
b [-]	-0.060	-0.043	-0.086	-0.093	-0.073	-0.025	-0.087
ε <sub>f</sub> ' [-]	0.8	3.432	1.447	0.221	0.549	0.190	0.427
c [-]	-0.71	-0.911	-0.710	-0.537	-0.611	-0.507	-0.58
K' [N/mm <sup>2</sup> ]	1 208	979	1 368	1 675	972	695	1841.4
n' [-]	0.086	0.047	0.104	0.174	0.085	0.049	0.15
ε <sub>a,D</sub> [%]	0.242	0.259	0.272	0.197	0.231	0.218	-
N <sub>D</sub> [-]	1.4·10 <sup>6</sup>	2.9·10 <sup>6</sup>	1.4·10 <sup>5</sup>	3.8·10 <sup>5</sup>	2.0·10 <sup>5</sup>	2.9·10 <sup>6</sup>	-
<sup>1</sup> taken from materials database <i>Boller et al.</i> (2008) <sup>2</sup> calculated with monotonic material properties from original M36 HV-bolt material 32CrB4							

## Appendix F – Macroscopic crack propagation

### F.1 Fracture surfaces and crack depth measurements

#### Results of crack depth measurements with digital microscope:

<b>M36 HV-bolts</b>	Upper higher cycle fatigue range				Transition region to endurance limit		
$S_a$ [N/mm <sup>2</sup> ]	103	81	69	54	44	37	34
Final crack depth [mm]:							
Black (B)	6.1	-	10.0	-	11.7	-	-
	4.9	-	12.1	-	13.3	-	-
	4.0	-	8.0	-	11.5	-	-
NT-galv.	-	6.5	-	11.0	-	-	12.9
	-	5.4	-	9.0	-	-	12.4
	-	8.0	-	9.3	-	-	11.4
HT-galv.	-	8.3	-	9.2	-	13.1	12.8
	-	8.7	-	8.7	-	12.5	-
	-	8.0	-	8.8	-	11.4	-
Mean	5	7.5	10.0	9.3	12.2	12.3	12.4
	<b>8.0</b>				<b>12.3</b>		

<b>M64 HV-bolts</b>	Upper higher cycle fatigue range						
$S_a$ [N/mm <sup>2</sup> ]	131	121	93	84	75	56	47
Final crack depth [mm]:							
Black (B)	9.5	9	11.3	10	11.1	12.5	13
NT-galv.	-	9.3	10.5	11.2	11.5	12	-
Mean	<b>11.0</b>						

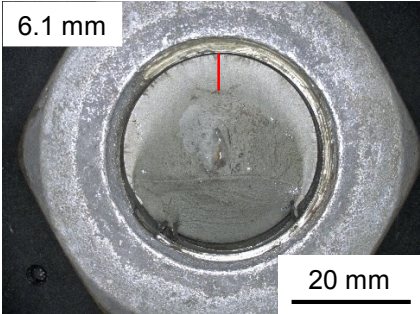
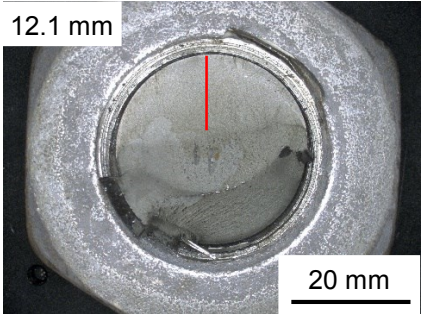
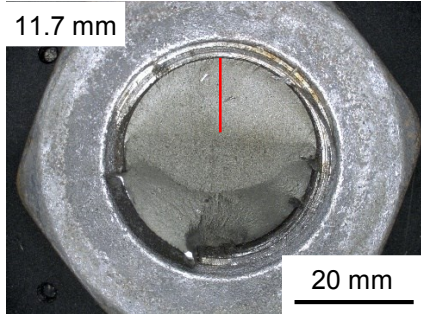
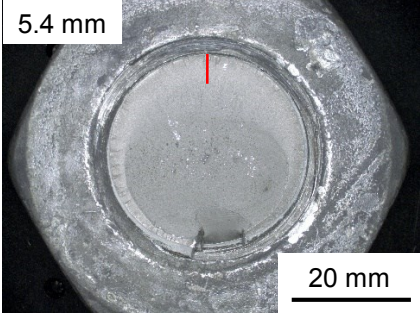
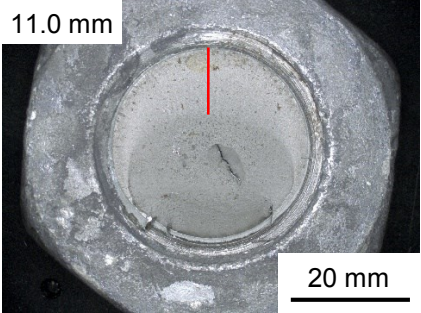
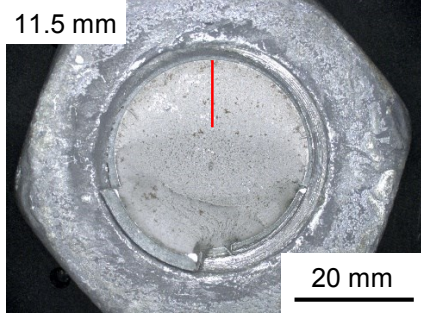
#### Applied final crack depth [mm] in macroscopic crack propagation calculation

Bolt	M36	M48	M64	M72
Upper HCF	8	9	11	11.5
TEL ( $S_a < 50$ N/mm <sup>2</sup> )	12	13.5	16.5	17.25

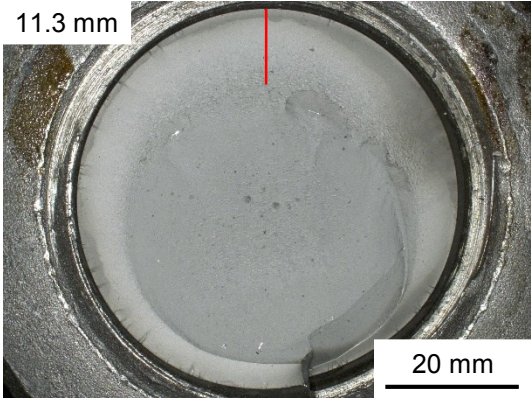
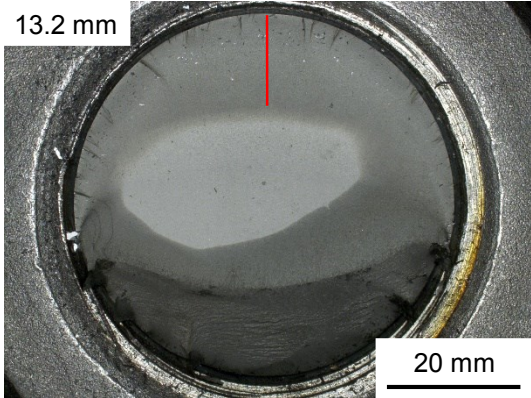
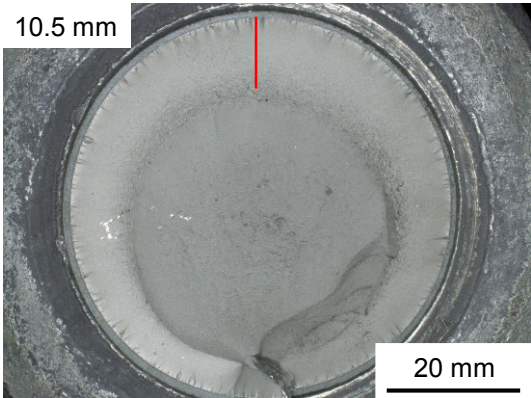
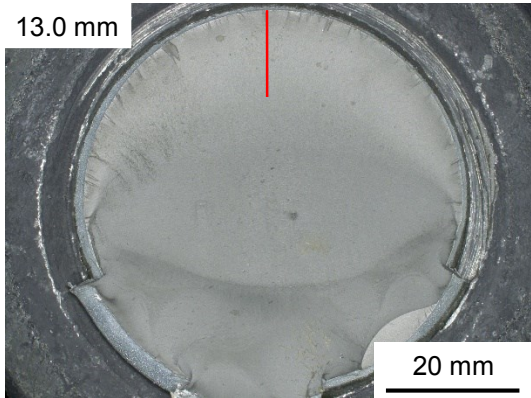




**Depiction of exemplary fracture surfaces of tested M36 HV-bots:**

	Upper higher cycle fatigue range 1	Upper higher cycle fatigue range 2	Transition region to endurance limit
<b>B</b>	 <p>6.1 mm</p> <p>20 mm</p> <p><math>S_m / S_a : 630 \text{ N/mm}^2 / 103 \text{ N/mm}^2</math></p> <p>Load cycles: <math>9 \cdot 10^4</math></p> <p>Crack shape: crescent</p>	 <p>12.1 mm</p> <p>20 mm</p> <p><math>S_m / S_a : 630 \text{ N/mm}^2 / 69 \text{ N/mm}^2</math></p> <p>Load cycles: <math>3 \cdot 10^5</math></p> <p>Crack shape: half-moon</p>	 <p>11.7 mm</p> <p>20 mm</p> <p><math>S_m / S_a : 630 \text{ N/mm}^2 / 44 \text{ N/mm}^2</math></p> <p>Load cycles: <math>3 \cdot 10^6</math></p> <p>Crack shape: half-moon</p>
<b>NT / HT</b>	 <p>5.4 mm</p> <p>20 mm</p> <p><math>S_m / S_a : 630 \text{ N/mm}^2 / 81 \text{ N/mm}^2</math></p> <p>Load cycles: <math>1 \cdot 10^5</math></p> <p>Crack shape: crescent / circumferential</p>	 <p>11.0 mm</p> <p>20 mm</p> <p><math>S_m / S_a : 630 \text{ N/mm}^2 / 54 \text{ N/mm}^2</math></p> <p>Load cycles: <math>3 \cdot 10^6</math></p> <p>Crack shape: crescent</p>	 <p>11.5 mm</p> <p>20 mm</p> <p><math>S_m / S_a : 630 \text{ N/mm}^2 / 34 \text{ N/mm}^2</math></p> <p>Load cycles: <math>1 \cdot 10^6</math></p> <p>Crack shape: half-moon</p>

**Depiction of exemplary fracture surfaces of tested M64 HV-bots:**

	Upper higher cycle fatigue range	Transition region to endurance limit
<b>B</b>	<p>11.3 mm</p>  <p>20 mm</p> <p><math>S_m / S_a : 630 \text{ N/mm}^2 / 93 \text{ N/mm}^2</math></p> <p>Load cycles: <math>5 \cdot 10^4</math></p> <p>Crack shape: crescent / circumferential</p>	<p>13.2 mm</p>  <p>20 mm</p> <p><math>S_m / S_a : 630 \text{ N/mm}^2 / 39 \text{ N/mm}^2</math></p> <p>Load cycles: <math>1 \cdot 10^6</math></p> <p>Crack shape: half-moon to crescent</p>
<b>NT</b>	<p>10.5 mm</p>  <p>20 mm</p> <p><math>S_m / S_a : 630 \text{ N/mm}^2 / 93 \text{ N/mm}^2</math></p> <p>Load cycles: <math>5 \cdot 10^4</math></p> <p>Shape: crescent / circumferential</p>	<p>13.0 mm</p>  <p>20 mm</p> <p><math>S_m / S_a : 630 \text{ N/mm}^2 / 37 \text{ N/mm}^2</math></p> <p>Load cycles: <math>7 \cdot 10^5</math></p> <p>Crack shape: half-moon to crescent</p>

---

## List of Publications

In accordance with the applicable doctoral regulations "Promotionsordnung der Fakultät für Bauingenieurwesen und Geodäsie der Leibniz Universität Hannover", partial results of this monograph have been pre-published by the author. These publications are listed hereinafter in chronological order.

**Schaumann, P.; Eichstädt, R.; Stang, A. (2018):** Advanced performance assessment methods for high-strength bolts in ring-flange connections. *Stahlbau* 87, No. 5, pp. 446-455.

**Eichstädt, R.; Schaumann, P. (2017):** Fatigue of very large high-strength bolting assemblies in wind turbines. Presentation at the Wind Energy Science Conference 2017, 26-29 June 2017, Lyngby/Copenhagen, Denmark.

**Eichstädt, R.; Schaumann, P. (2016):** Ermüdungsfestigkeit feuerverzinkter HV-Schrauben mit sehr großem Durchmesser [Fatigue strength of hot-dip galvanized HV-bolts with very large diameters]. Deutscher Ausschuss für Stahlbau DASt (Hrsg.): 20. DASt-Forschungskolloquium in Essen, Frehner Consulting, Füssen, Germany, pp.107-112 (in German).

**Schaumann, P.; Eichstädt, R. (2016):** Ermüdung sehr großer HV-Schraubengarnituren [Fatigue of very large HV-bolt sets]. *Stahlbau* 85, No. 9, pp. 604-611 (in German).

**Schaumann, P.; Eichstädt, R. (2016):** Fatigue Strength of Preloaded Hot-Dip Galvanized Bolt Assemblies with Very Large Diameters. *Insights and Innovations in Structural Engineering, Mechanics and Computation: Proceedings of the Sixth International Conference on Structural Engineering, Mechanics and Computation*, Taylor & Francis Group, Cape Town, South Africa, pp. 578-584.

**Oechsner, M.; Beyer, J.; Simonsen, F.; Schaumann, P.; Eichstädt, R. (2015):** Experimentelle und rechnerische Bewertung der Betriebsfestigkeit von Schrauben großer Abmessung im Stahlbau unter Berücksichtigung von Randschichteffekten [Experimental and analytical assessment of the fatigue strength of bolts with large dimensions under consideration of boundary layer effects]. Final report, Research project P925/IGF-Nr.486 ZN, Forschungsvereinigung Stahlanwendung FOSTA e.V. (in German).

**Oechsner, M.; Beyer, J.; Simonsen, F.; Schaumann, P.; Eichstädt, R. (2015):** Betriebsfestigkeit von Schrauben großer Abmessungen unter Berücksichtigung von Randschichteffekten [Fatigue strength of bolts with large dimensions under consideration of boundary layer effects]. Tagungsband der 11. Informations- und Diskussionsveranstaltung "Schraubenverbindungen - Neue Ergebnisse aus Forschung und Praxis", Darmstadt, Germany (in German).

**Oechsner, M.; Beyer, J.; Simonsen, F.; Schaumann, P.; Eichstädt, R. (2015):** Experimental and Analytical Assessment of the Fatigue Strength of Bolts with Large Dimensions under Consideration of Boundary Layer Effects. *Proceedings of the 2nd European Steel Technology and Application Days (ESTAD)*, Düsseldorf, Germany.

---

**Schaumann, P.; Eichstädt, R. (2015):** Fatigue Assessment of High-Strength Bolts with Very Large Diameters in Substructures for Offshore Wind Turbines. Proceedings of the 25th International Offshore and Polar Engineering Conference (ISOPE), Kona, USA, pp. 260-267.

**Schaumann, P.; Eichstädt, R.; Oechsner, M.; Simonsen, F. (2015):** Experimental Fatigue Assessment of High-Strength Bolts with Large Diameters in Consideration of Boundary Layer Effects. Proceedings of the 12th German Wind Energy Conference DEWEK 2015, Bremen, Germany.

**Schaumann, P.; Eichstädt, R.; Oechsner, M.; Simonsen, F. (2015):** Ermüdungsfestigkeit feuerverzinkter HV-Schrauben in Ringflanschverbindungen von Windenergieanlagen - Bewertung des Randschichteinflusses bei Schrauben mit sehr großen Durchmessern [Fatigue strength of hot-dip galvanized HV-bolts in ring-flange connections for wind turbines – Assessment of the boundary layer effect of bolts with very large diameters]. Stahlbau 84, No. 12, pp. 1010-1015.

---

## Supervised Student's works

The following Student's works, supervised by the author, were performed in the context of the research presented in this dissertation:

**Abe, H.:** Ermüdungsbewertung großer HV-Garnituren mit dem Kerbdehnungskonzept bei zyklischer Belastung mit variablen Amplituden [Fatigue assessment of very large HV assemblies with the strain-life approach for cyclic loading with variable amplitudes]. Master's thesis at the Institut for Steel Construction, Leibniz Universität Hannover, 2017.

**Gottlieb, G. E.:** Bewertung der Ermüdungsfestigkeit feuerverzinkter HV-Schrauben auf Grundlage örtlicher Beanspruchungen [Fatigue assessment of hot-dip galvanized HV-bolts based on local stresses and strains]. Master's thesis at the Institut for Steel Construction, Leibniz Universität Hannover, 2015.

**Hartmann, K.:** Analysis of advanced design methods for bolted ring-flange connections in wind turbines using FEM. Master's thesis at the Institut for Steel Construction, Leibniz Universität Hannover in cooperation with DNV GL, 2016.

**Hisir, M.:** Betriebsfestigkeitsanalyse geschraubter Ringflanschverbindungen in Offshore Windenergieanlagen unter Berücksichtigung von Vorspannkraftverlusten [Fatigue analysis of bolted ring-flange connections in offshore wind turbines under consideration of preload losses]. Master's thesis at the Institut for Steel Construction, Leibniz Universität Hannover, 2015.

**Kielbus, N.; Abe, H.:** Bewertung der Ermüdungsfestigkeit großer HV-Schrauben unter Betriebsbeanspruchung mit variablen Amplituden [Evaluation of the fatigue strength of large-size HV-bolts under service-loading conditions with variable amplitudes]. Seminar paper at the Institut for Steel Construction, Leibniz Universität Hannover, 2016.

**Kowalczyk, C.:** Herstellungsverfahren von Schrauben großer Abmessungen zur Anwendung in Stahlbauwerken [Manufacturing of bolts with large dimensions for the application in steel construction]. Project paper at the Institut for Steel Construction, Leibniz Universität Hannover, 2014.

**Wilms, L. J.:** Untersuchung zum Biegeeinfluss auf die Ermüdungsfestigkeit großer HV-Schrauben unter Anwendung der linear-elastischen Finite-Elemente-Methode [Examination of the effect of bending on the fatigue strength of large-size HV-bolts by application of the linear-elastic finite element method]. Bachelor's thesis at the Institut for Steel Construction, Leibniz Universität Hannover, 2017.

**Wilms, L. J.:** Studie zum Einfluss der FE-Modellierung auf die Berechnung der Ermüdungsfestigkeit von HV-Garnituren mit dem Kerbdehnungskonzept bei Axial- und Biegebeanspruchung [Study on the impact of the FE modelling approach on the calculation of the fatigue strength of HV assemblies with the strain-life approach under axial and bending loading]. Seminar paper at the Institut for Steel Construction, Leibniz Universität Hannover, 2017.

---

## **Statement of Authorship**

I hereby declare that I am the sole author of this dissertation. I have not used any text passages of third parties or own examination papers without declaration and I have stated all considered auxiliary sources and references used within this dissertation.

Rasmus Eichstädt, Hannover, 28.06.2019

---

## Curriculum Vitae

Rasmus Eichstädt

born on November, 26th 1984 in Bad Oldesloe, Germany

### Professional Career

- Since 2018 Expert for steel structures and load simulation for wind turbines at TÜV SÜD Industrie Service GmbH, München, Germany
- 2012 – 2018 Research engineer at the Institute for Steel Construction, Leibniz Universität Hannover, Germany
- 2012 – 2017 Freelance structural engineer for support structures of wind turbines

### Education

- 2011 Graduation as Diplomingenieur (Dipl.-Ing.)
- 2006 – 2011 University degree course in Civil Engineering, major in structural design and construction at the Leibniz Universität Hannover, Germany
- 2005 – 2006 Civil service at the Matthias-Leithoff School for children with disabilities in Lübeck, Germany
- 2005 Abitur at the Johanneum zu Lübeck, Germany

### Internships and stays abroad

- 2011 Internship and preparation of University degree final thesis at GL Garrad Hassan (today DNV GL) in Bristol, UK
- 2009 Semester abroad at the Universitat Politecnica de Catalunya in Barcelona, Spain
- 2007 – 2011 Student assistant at the Institute for Steel Construction, Leibniz Universität Hannover, Germany
- 2001 – 2002 Exchange year at the Colegio Alemán Medellín, Colombia